NASA TT F-67

TECHNICAL TRANSLATION

F-67

VARIATIONS OF COSMIC RAY INTENSITY

Yu. G. Shafer, Editor

Translation of the Issue 3, Physics Series, of Transactions of the Yakutsk Branch of the Siberian Division of the Academy of Sciences of the SSSR; published by the Academy of Sciences SSSR (Moscow), 1960.

NATIONAL AERONAUTICS AND SPACE ADMINISTRATION

WASHINGTON

August 1961

ERRATA

NASA Technical Translation F-67

Yu. G. Shafer, Editor
August 1961

Page 28, figure 4:

The value of R_3 should be "100 ohm" instead of "200 k."

L_3 - the plate load of the first half of the tube should have a 1 μf decoupling capacitor.

Page 57, line 3 up (in legend for fig. 1):

"c - rate of δlipN;" should be "c - rate of δI_{ipN};"

Page 57, figures 1c and 2c:

The ordinate scale "$\delta I_{ip}; \delta N_{\mu}, \%$" should be "$\delta I_{ipN}, \%$"

Page 63, line 20 up:

"Fig. 4" should be "Fig. 3."

Page 74, line 9 up:

"$\alpha, \epsilon^{\alpha}$" should read "$\alpha \cdot \epsilon^{\alpha}$"

NASA-Langley, 1961

Issued 8-30-1961

NATIONAL AERONAUTICS AND SPACE ADMINISTRATION

TECHNICAL TRANSLATION F-67

VARIATIONS OF COSMIC RAY INTENSITY*

Yu. G. Shafer, Editor

*Translation of the Issue 3, Physics Series, of Transactions of the Yakutsk Branch of the Siberian Division of the Academy of Sciences of the SSSR; published by the Academy of Sciences SSSR (Moscow), 1960.

PREFACE

The third issue of the Transactions (Trudy) of the Yakutsk Branch of the Siberian Division of the Academy of Sciences of the USSR (YBSDAS) deals with the first results of experimental and theoretical research carried out during the International Geophysical Year (IGY, 1957-58).

The collection consists of three sections. The first describes single-model automatic counter installations used to measure the frequency of extensive atmospheric showers and cosmic rays below ground, and apparatus which records the intensity aboard artificial earth satellites.

The second section deals with analysis of the role played by meteorological factors in cosmic-ray variations.

The third section, which is the fullest, describes experimental and theoretical investigations of extra-atmospheric cosmic-ray variations. It should be pointed out that these investigations were based on analysis of extensive recordings of cosmic rays over a wide energy range made in Yakutsk during the IGY.

The articles published in this book have been discussed at scientific seminars at the Physics Research Laboratory of the YBSDAS and at the Institute of Terrestrial Magnetism, Ionosphere and Radiowave Propagation of the Academy of Sciences (IZMIRAN). Some of the articles were delivered as reports, at meetings of the Physics-Mathematics section of the Scientific Session of the YBSDAS, on the results of basic scientific research for 1958 and on the Branch's tasks in the light of the resolutions of the XXI Party Congress (Communist Party of the Soviet Union) held in April, 1959.

The collection contains articles by L. I. Dorman (Academy of Sciences Magnetic Laboratory), and Ye. S. Glokova, N. S. Kaminer and Ya. L. Blokh (IZMIRAN), who used experimental material collected by YBSDAS for their research. These authors are thanked for their cooperation and coordination of the research.

Yu. G. Shafer

LIST OF SYMBOLS USED IN ARTICLES

I — Intensity of cosmic rays in pairs of ions per 1 cm^3 per 1 sec in air at 760 mm Hg;

I_0 — Compensated value of intensity of hard component in cosmic rays in paris of ions per sec inside chamber;

δI — Variation in intensity of cosmic rays in % of mean x value of I;

δI_{μ} — Variation in intensity of hard component in cosmic rays in % of I_0;

$\delta I_{\mu i}$ — Variation in intensity of hard component in cosmic rays taking into account ionization impacts in % I_0;

$\delta I_{\mu ip}$ — Variation in intensity of hard component taking into account ionization impacts with correction for variation in atmospheric pressure in % of I_0;

$\delta I_{\mu ipt}$ — Variation in intensity of hard component taking into account ionization impacts and corrections for variation in atmospheric pressure and temperature of atmosphere according to Feynberg-Dorman system in % of I_0;

$\delta I_{\mu ipW}$ — Variation in intensity of hard component taking into account ionization impacts and corrections for variation in atmospheric pressure and temperature of atmosphere according to Feynberg-Dorman system in % of I_0;

F 6 7

α_p — Barometric coefficient — variation in intensity of hard component during variation in atmospheric pressure by 1 mb in % of I_0;

α_t — Temperature coefficient — variation in intensity of hard component during variation in temperature of surface layer atmosphere by $1^{\circ}C$. in % of I_0;

δN_{μ} — Variation in intensity of μ-meson component due to meteorological factors and calculated from meteorological sounding data by the Feynberg-Dorman formula in % of the mean value of the theoretically expected intensity of the μ-mesons;

p — atmospheric pressure;

δ_p — Variation in pressure in mb;

ΔH — Difference between earth's magnetic field component H and mean value in γ (10^{-5} e);

h — Geometrical height of selected layer of atmosphere in m;

δ_h — Variation in geometric height of selected atmospheric layer in % of mean value in meters;

r — Correlation factor;

T_k — Temperature of atmosphere at k-th level in $^{\circ}C$.

δT_k — Variation in temperature of atmosphere at k-th level in $^{\circ}C$.

ε — Particle energy of cosmic rays.

*Translator's note: Where a comma appears in numbers in tables, etc., in this volume, it represents a decimal point.

CONTENTS

Preface ii

List of symbols used in articles iii

Section I. Experimental Apparatus and Methods 1

Yu. G. Shafer and A. V. Yarygin. Investigation of variations in primary cosmic radiation using artificial earth satellite 1

V. A. Belomestnykh, B. S. Nedzvedskiy and Yu. G. Shafer. Investigations of variations in cosmic ray intensity in stratosphere 9

D. D. Krasil'nikov. Apparatus for recording time dependence of frequency of extensive atmospheric showers with Geiger-Muller counter detectors 14

A. A. Danilov, S. N. Druzhinin, I. N. Kapustin, and G. V. Skripin. Counter telescope for measuring hard component of cosmic rays underground 27

S. V. Makarov. Some counter telescope calculations. Illumination of vertical telescope 31

B. S. Shalamov. Plotting an idealized volt-ampere characteristic for a two-terminal network containing a point-contact transistor with allowance for the temperature effect 35

Section II. Part Played by Meteorological Factors in Variations in Different Cosmic Ray Components 38

L. I. Dorman. Calculation of temperature effect of cosmic rays from isobar surface heights 38

A. I. Kuz'min and A. A. Danilov. Meteorological effects of cosmic rays at depths of less than 100 m w.e. underground 41

D. D. Krasil'nikov. Barometric effects of extensive atmospheric showers 46

Ya. L. Blokh, Ye. S. Glokova and N. S. Kaminer. Barometric effect of cosmic rays .. 53

N. P. Chirkov and Yu. G. Shafer. Effect of air mass fronts on cosmic ray intensity and role played by lower layers of stratosphere 56

Ye. S. Glokova. Annual variations in cosmic ray intensity and temperature corrections 60

N. S. Kaminer. Effect of small chromospheric flares on intensity of hard component in cosmic rays 66

Section III. Extra-atmospheric Variations in Cosmic Rays and Certain Theoretical Problems 71

A. I. Kuz'min. Basic features of solar-diurnal variations in cosmic rays 71

A. I. Kuz'min, V. D. Sokolov and G. V. Shafer. Twenty seven-day variations in cosmic ray intensity 80

G. I. Freydman and G. V. Shafer. Some results of comparing neutron and hard component variations during the period, August - October, 1957 84

A. I. Kuz'min and G. V. Skripin. Reduced intensity of cosmic rays during magnetic storms 88

T. M. Berdichevskaya and N. A. Zhukovskaya. On the problem of existence of sidereal-diurnal variations in meson intensity of cosmic rays 101

L. I. Dorman. Energy spectrum and duration of increase in cosmic ray intensity on earth due to corpuscular stream shock wave 105

N. S. Kaminer. Earth zones struck by solar particles (1 - 10 Bev) 108

L. I. Dorman. Determining primary variation in energy spectrum in region of very low energies from differences of effects in Europe and America 118

L. I. Dorman. Determining point at which earth enters corpuscular stream, nature of earth's motion within stream and stream velocity by means of detailed study of variation in cosmic ray intensity during magnetic storms 120

Layout of apparatus recording cosmic rays at physics laboratory of Yakutsk branch of Siberian Division of USSR Academy of Sciences 128

Section I

EXPERIMENTAL APPARATUS AND METHODS

Yu. G. Shafer and A. V. Yarygin

INVESTIGATION OF VARIATIONS IN PRIMARY COSMIC RADIATION USING ARTIFICIAL EARTH SATELLITE

Many of the publications produced in the USSR and other countries on the eve of the launching of the first artificial earth satellite, when discussing the most important tasks in studying cosmic radiation with artificial earth satellites, recognize the composition and variation in primary radiation [1] as subjects of prime importance.

The authors of these publications considered that as a first approximation of a single Geiger or scintillation counter aboard the artificial earth satellite could provide sufficient information regarding the geographical relationship and time variations in intensity of cosmic rays near the earth.

It was assumed that the interpretation of the expected experimental data would make it possible to describe all the known regular and irregular variations in primary radiation and to study the relationship between them and changes in solar activity, disturbances of the earth's magnetic field and variations in the intensity of various secondary components observed at sea level. Furthermore, the material obtained was to be used to study 11-year and other long-term variations in primary radiation.

This program was based on the results of earlier rocket measurements of cosmic ray intensity [2, 3] which showed the absence of any height dependence of the intensity, starting at about 50 km. The conclusion was drawn at the time that practically all charged particles at these heights were primary, that their intensity was constant and that the earth's albedo for cosmic rays was slight.

It was shown, however, that these views were incorrect. Experiments with geophysical rockets revealed a monotonic increase in intensity with height. From 70-210 km this increase amounted to approximately 17% [4].

Measurements made by Soviet earth satellites and cosmic rockets have shown convincingly that at a height of 500-1000 km around the earth there is, symmetrical about the earth, corpuscular radiation in the equatorial plane consisting of charged particles of secondary origin moving round the earth in a kind of "trap" formed by the earth's magnetic field [5].

As shown in publication [5], these charged particles form two high-intensity zones with a gap where the intensity is at least one order weaker (Figure 1).

In the external zone, limited by magnetic lines of force crossing the earth's surface at the geomagnetic latitudes 55 and 65°, most of the particles are electrons with energies of 20-100 kev.

In the internal zone, limited by magnetic lines of force of 30-40°, the data on the composition of the radiation is more vague, but it is known that it consists of high-energy particles and that it may contain protons with an energy of 100 Mev.

Measurements made by earth satellites have shown that the intensity increases along the lines of force when going from lower to greater heights. If we select points on the same line of

force of 60° at 300, 1800, 5600 and 14,000 km above the earth's surface, the measured intensities are in the ratio 1 : 20 : 200 : 700. This shows that the recorded charged particles do not come directly from interplanetary space, but oscillate along the lines of force, i.e., they are contained in a trap formed by the earth's magnetic field.

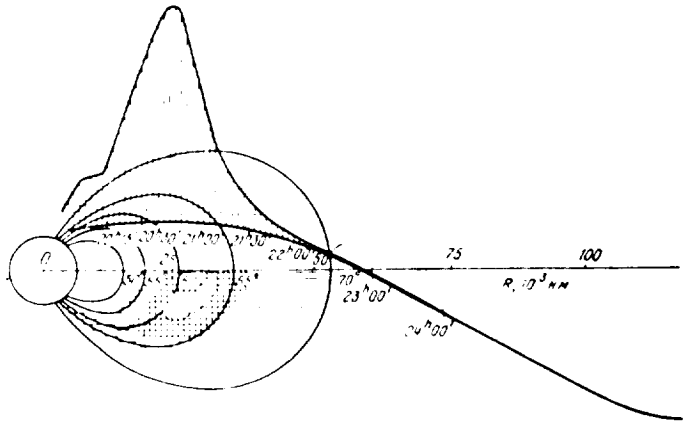

Fig. 1. Trajectory of rocket in geomagnetic coordinates. The flight time (Moscow) and intensity (vertical lines resting on the trajectory) are shown alongside the trajectory. The dots indicate the internal zone and the shading the external zone. The thickness of the shading gives a qualitative idea of the intensity distribution in the external zone [6]

It is known from artificial earth satellite measurements that the intensity of electrons with an energy up to 100 Kev, at a height of about 500 km between the latitudes 60-65° is 10^3 -10^4 particles $\cdot cm^{-2} \cdot sec^{-1} \cdot ster^{-1}$. When they enter the shell of a satellite or rocket, these electrons produce x-rays which are recorded by the counter.

The instruments aboard the cosmic rocket only recorded a constant intensity of 0.18 ± 0.008 particles $\cdot cm^{-2} \cdot sec^{-1} \cdot ster^{-1}$ above 65,000 km from the center of the earth. It is an important fact that this intensity of the prime radiation tallies with the results of stratospheric [6] and rocket [7] measurements in the region of the poles.

There has been a great deal of discussion of late with regard to the possible mechanism of the origin of the earth's corpuscular radiation [8]. Some people consider that the internal zone is caused by the injection into the earth's magnetic field of electrons and protons resulting from the decay of neutrons produced by the earth's atmosphere when acted upon by the primary cosmic rays.

The injection of particles into the external zone is apparently caused by the corpuscular streams emitted by the sun, in which solar-originating electrons with an energy of several tens of Kev are conveyed in magnetic traps "frozen" into these streams.

The intensity of the corpuscular radiation has proved to be many times greater than that of the primary cosmic rays. This fact at first sight creates insuperable difficulties in investigating variation in the primary radiation and the associated problems of the origin of cosmic rays.

Reliable observations of the variation in primary particle intensity are not possible in the sphere of the earth's corpuscular radiation where the background exceeds the measurable effect a thousand or more times. Such measurements are only possible outside the external zone or in the lower layers of the ionosphere, beneath the increased-intensity internal zone, where the secondary radiation background may be slight or entirely absent. To investigate the variations we require a satellite with a circular orbit having a radius 300 to 500 km greater than the radius of the earth, or an elliptical orbit, the points of which are at the same average height.

The single counters, double coincidence telescope and ionization chamber carried by the artificial earth satellite can provide fairly detailed and exact information on the intensity of the primary radiation. All these instruments should record radiation with a high degree of accuracy and over an extensive dynamic range.

An earth satellite of this kind, whose position is orientated with respect to the earth, can usefully carry scintillation counters and other devices which aid separate recording of the radiation from the upper and lower hemispheres. The earth's albedo for cosmic rays can be evaluated from the difference in the instrument readings.

The range of intensity should be calculated on the basis of data for the latitude effect, according to which the radiation stream at the equator is approximately 3.0 particles$\cdot$min$^{-1}\cdot$cm$^{-2}\cdot$ster^{-1}, and at the poles about 30 particles$\cdot$min$^{-1}\cdot$cm$^{-2}\cdot$ster^{-1} (including the albedo).

In experiments with earth satellites it is very important to provide for reliable measurement of the low intensity in the equatorial region over short intervals of time (at least once a minute). Otherwise the data will be unsuitable for determining the position of the geomagnetic equator and its variations.

F 67

The ionization chamber used by us in geophysical rockets [5] makes it possible for the collecting electrode to accumulate a potential of about 1.5 volts in one minute of chamber exposure above the equator. This potential can be measured with our apparatus with an accuracy of 7-10%.

The upper limit of the dynamic range of the ionization chamber should be several times greater than that due to the latitude effect. This is necessitated for recording the bursts and fluctuations in the primary radiation due to variation in solar activity, or geomagnetic storms. Furthermore, we have to be ready to measure the secondary radiation in the internal zone in case the lower boundary suddenly descends to heights monitorable by the earth satellite.

When determining the measurement range it must be kept in mind that the scale of the telemetric device aboard the satellite is usually limited. In this case the range can be extended either by making the scale rougher (using a divider) or by employing a self-adjusting electronic time programming device. The cybernetic principle of this method lies in automatic selection of optimum conditions under which we can measure any potential (within fairly wide limits) at the collecting electrode of the chamber, corresponding to the necessary exposure time, the resolving power and limited scale of the satellite's telemetric system.

The programming device suggested makes it possible to reduce, when the intensity increases, and to prolong, when it decreases, the chamber exposure time within the various limits within which the amplitude of the chamber signal (in volts) can be measured with a sufficient degree of accuracy on the voltmeter scale in the telemetric system.

Taking into account the conditions under which cosmic rays are recorded in the earth satellite, the following ionization chamber characteristics can be considered quite sufficient for the requirements of scientific research:

1) 600-fold range of cosmic ray measurement,
2) exposure-time range from 5 to 120 seconds,
3) amplitude range from 1.0 to 25 v, and
4) absolute accuracy of the electronic unit in the chamber circuit of not less than $\pm$ 0.1 v.

With regard to the counter units, we consider it advisable to attach single counters to the scale circuits with different multiplicities of conversion to increase the measurement range. In order to reduce the number of transmitter channels, it is necessary to make provision for an electronic commutating device which can in turn automatically plug the outputs of different counter scale circuits into the telemetric system.

The scaling multiplicity of the two single counters is the same.

We decided on the following characteristics for the counter devices:

1) a dead time of not more than 150 microseconds,
2) a resolving coincidence time of 10 microseconds,
3) a scaling factor of the coincidence unit of 16, and
4) a scaling factor for the single counters of 128.

The counter parameters are taken to be the same as in the apparatus we used for the geophysical rockets.

A block diagram of the apparatus intended for installation aboard a low earth satellite is shown in Figure 2.

As can be seen from the drawing the apparatus consists of two parts - the chamber channel and the counter channel.

The cosmic ray intensity in the chamber channel is measured by the amplitude-time method,

the essence of which is as follows:

The build-up time for the charge at the collecting electrode in the chamber (chamber exposure time) is set by the programming device.

This time is inversely proportional to the intensity of the radiation being measured.

We determine the potential accumulated at the central chamber electrode during the exposure time from the amplitude of the pulse at the measuring system output 1 with the aid of the calibration amplitude characteristic.

The electronic measuring circuit and the programming device provide signals at the output which can be broadcast to the earth. A sample of a recording of the signals at a ground receiving point is shown in Figure 3. It is clear from this drawing that the zero line, from which the pulses are counted off, is fixed two seconds before the end of the exposure. Then the full pulse (without divider) is recorded for one second, and, finally, the same pulse is recorded for a fourth second, but reduced by a factor of four (with divider). Thus, the measuring circuit has two scales - a 6-volt scale corresponding to the one in the telemetric device, and a 24-volt scale.

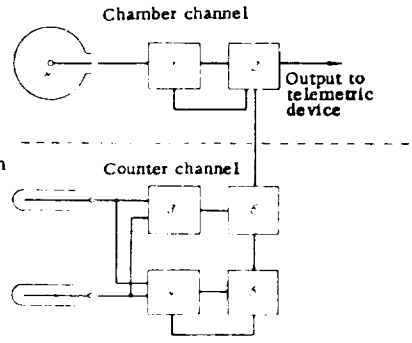

Fig. 2. Block diagram of instrument intended for measuring cosmic rays aboard artificial earth satellite: K) ionization chamber; 1) measuring circuit; 2) programming unit; 3) coincidence unit; 4) electronic commutator; 5) single counter unit; 6) coding unit.

During the gaps between recording the zero line and the chamber channel pulses, the programming device switches the telemetric device input to the counter channel.

In this channel, pulses from two STS-6 counters are fed simultaneously to the coincidence unit, 3 (Figure 2), and through the electronic commutator, 4, which makes certain they are interrogated in turn, to the single counter unit, 5.

The cosmic ray intensity (count rate) is determined from the time interval between voltage drops at the output of each scale unit, during which there are eight pulses in the coincidence unit and 64 pulses in the single-counter unit.

The electronic commutator switches the single counter block from one counter to another after there have been 64 pulses in the counter being interrogated.

The voltage drops from the end cells in the coincidence unit and the single counter unit are fed to the coding unit. When the counters are interrogated in turn at the coding unit output there is a voltage level of one volt for one counter and 1.5 volts for the second counter. Every eight coinciding pulses, these two levels either increase by 1.5 volts, i.e., become 2.5 and 3 volts respectively, or reacquire their former values. Thus, the coding unit provides for the transmission to the telemetric device input of four different voltage levels corresponding to a particular counter for a particular position of the coincidence unit output cell.

This system of coding, interrogating and programming makes it possible to transmit information from all four pickups along the same telemetric channel.

The ionization chamber K (Figure 4) is spherical, has a 240 mm diameter and is filled with argon. The time constant when the chamber is exposed is of the order of 10^4 seconds. The potential at the chamber electrodes is restored when the relay P_1 contacts are closed with a time constant of the order of 10^{-3} seconds.

The polarized relay P_1 makes it possible to produce a pulse of exponential shape without overshooting or breaking at the measuring circuit input.

The electronic measuring circuit consists of a pulse amplifier, a pulse stretcher and a cathode repeater.

The amplifier L_1 contains a 2P19B pentode with a screen feed-back circuit. The use of the circuit makes it possible to reduce the output resistance of the stage, which in turn has made it possible to increase the elongation factor and improve the stability of the system when the feed voltage oscillates. The amplification factor of the stage is approximately equal to 6.

The stretcher L_2 uses a 2S14B triode connected as a diode The stretcher circuit includes a "dosing" circuit C_3R_5, which is necessary for the normal operation of the programming device. The tube L_3 grid circuit has different time constants, when recording the zero line and when

recording the signal. The variation in the time constant is effected with the relay contacts P_2 and P_3, according to the programming device.

The end cathode repeater has a normal circuit with a 2S14B triode. The division factor of the output divider, required to expand the limits of measurement, is selected in such a way that the linear part of the amplitude characteristic of the entire channel fits into the 6-volt scale of the telemetric device.

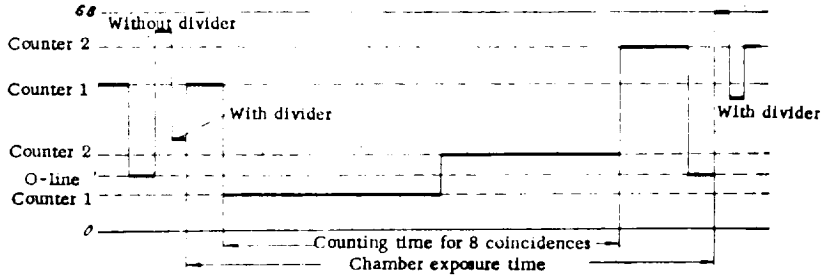

Fig. 3. Specimen of chamber and counter signal recording.

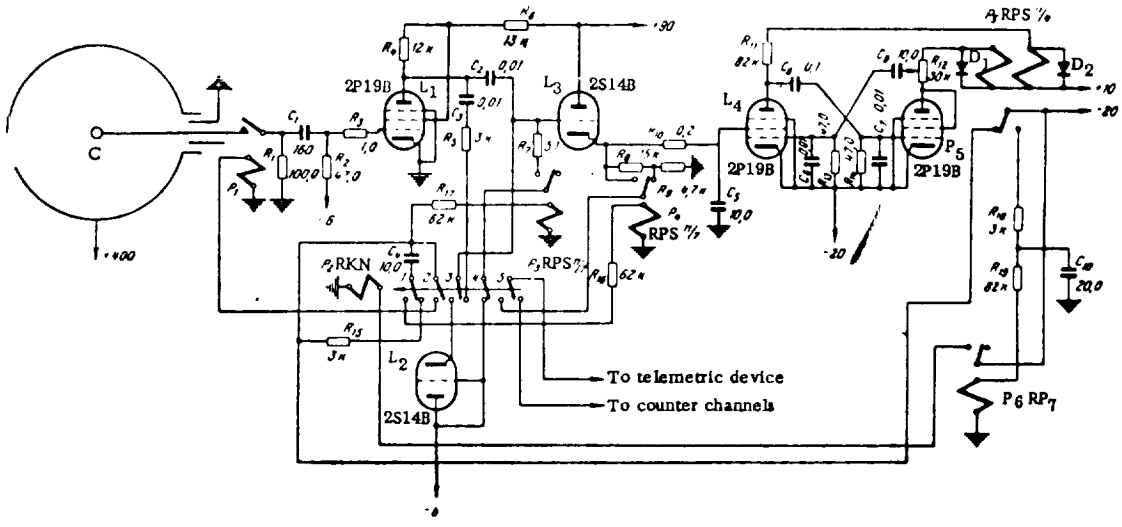

Fig. 4. Simplified chamber channel circuit.

The amplitude characteristic of the chamber channel is given in Figure 5.

The programming device ensures the necessary measurement range and is intended to control the operation of the chamber relay, stretcher, and divider, and to interconnect the channels. In our own apparatus we used the automatic programming method devised by A. V. Yarygin.

The position of the relay contacts in the circuit (see Figure 4) corresponds to the moment the chamber is exposed. At this moment the counter readings are being recorded. Only the relay P_3 is switched on. To increase the time constant in the L_3 tube grid circuit, the diode L_2 is disconnected and the dosing circuit is switched on in parallel to the capacitor of the stretcher C_2. The contacts, 5, of the relay P_2 disconnect the telemetric device from the chamber channel.

With the beginning of the two-second uncontrolled generation half-period in the multivibrator L_4L_5, the core of relay P_5 changes to the right hand position, which means that the relays P_6 and P_2 switch on and relay P_3 switches off. The diode L_2 connects to the grid of tube L_3, the dosing circuit disconnects, and the telemetric device switches over to recording the chamber channel signals. The relay contacts P_3 and P_2 "short" the stretcher, as a result of which the telemetric device records a zero line for two seconds.

When the half-period is over, the relay contacts P_3 and P_6 remain in their previous position for another two seconds, on account of the discharge of condenser C_{10}, during which the chamber pulse is recorded. When the P_5 relay core changes to the left-hand position, relay P_3 "opens" the stretcher, and the chamber relay P_1 removes the charge from the central electrode in the chamber. The pulse appearing at the R_1 load resistance is amplified, stretched and after the cathode repeater reaches the telemetric device. The divider relay P_4 controls the charge from condenser C_4 in such a way that the full value of the output pulse is recorded during the first second and a quarter of it during the second second.

When the condenser C_{10} is discharged, the chamber is again exposed and the signals from the counter channel are recorded. At this moment the multivibrator is in the position of the first controllable generation half-period.

The amplitude-time characteristic of the multivibrator is shown in Figure 6. The shape of this characteristic is selected with aview to receiving the greatest possible amount of information.

The dosing circuit increases the stability of the programming device and reduces its "inert quality" (hysteresis) when there is a great degree of oscillation in the cosmic-ray intensity. For this purpose the screen grid circuit for tube L_4 in the multivibrator includes the circuit R_6C_5, which sets a lower limit on the exposure time range. The dosing circuit only reports part of the output pulse voltage during the first cycle for control of the multivibrator. If the intensity of the radiation remains unchanged after this, the exposure time and the output pulse will not achieve a stable value until after the third cycle, but there will be no loss of information involved.

A simplified counter channel circuit is shown in Figure 7. At the input of this channel there are compensating dividers for each counter and matching emitter repeaters 1 and 3, which make it possible to create conditions for the counters close to those rated. Pulses from the emitter repeaters are fed to both the coincidence unit and a single-counter unit.

In the coincidence block the pulses are formed by the single flip-flop multivibrators, 2 and 4, assembled with resistance-capacity coupling. Rectangular-shaped pulses lasting 10 microseconds are fed from the single multivibrator output to the coincidence circuit, 5, containing two transistors with a total load in the collector circuit. The coinciding pulses are scaled by the counting circuit which consists of one stage of the emitter repeater-amplifier, 6, and four binary scaling units, 7-10, with a total scaling factor of 16. The output voltage level changes after every eighth coinciding pulse.

In the single counter unit pulses from the emitter repeater inputs are fed to the electronic commutator circuit, 11-12, and are then scaled by a similar circuit, 13-19, with a scaling factor of 64.

The electronic commutator which is based on the coincidence principle consists of two matching emitter repeaters, 20, and two coincidence circuits, 11-12. The counters are interrogated in turn by the commutator in the following way. Voltages from different arms of the end stage in the counting circuit, after the emitter repeaters, are applied to the corresponding coincidence circuits, opening and closing the triode in the circuit in turn. Only those pulses reaching

an occupied (conducting) triode arrive at the output. The voltages in the end stage arms change every 32 pulses, hence after the same number of pulses the counting circuit will be switched into action to interrogate the next counter.

Apart from pulses from the counter, the counting circuit input of the single counter unit also receives "brightening" pulses with a frequency of 0.5 cycles per second. The use of brightening speeds up the interrogation of the counters, which is important when the intensity of the cosmic rays is low.

The coding unit contains two transistors with an overall emitter load. The transistors are controlled by voltage drops coming from the scaling cell outputs of the coincidence unit and the single counter unit. In this way various currents determined by the resistances R_1 and R_2 are commutated. Combinations of these currents produce different voltage drops at the load (levels), each of which corresponds to the operation of a definite counter for a particular position of the coincidence unit output cell. To make the absolute value of these levels positive, a 5.2 volt battery is placed in series with the output.

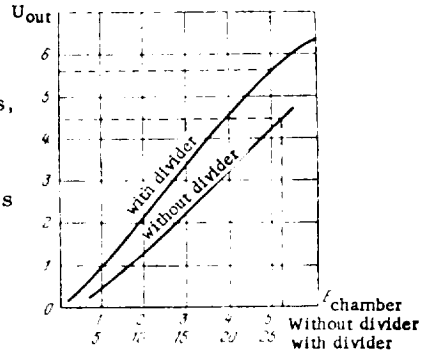

Fig. 5. Amplitude characteristic of chamber channel.

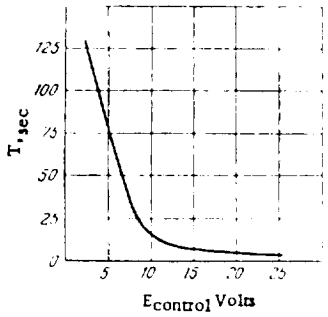

Fig. 6. Amplitude-time characteristic of multivibrator.

In conclusion the authors express profound gratitude to Professor N. L. Grigorov, Doctor of Physico-Mathematical Sciences, whose advice and practical assistance was instrumental in designing the apparatus. The authors are also grateful to N. N. Goryunov, scientific worker, and I. N. Kapustin, radio technician, for assistance in designing, assembling and testing the transistor systems.

Bibliography

1. Vernov, S.N., Yu. I. Logachev, A. Ye. Chudakov, and Yu. G. Shafer. "Investigation of the variation in cosmic radiation", Uspekhi Fizicheskikh Nauk, Vol. 13, Issue 1b, 1957.
2. Meredith, L.H., J. A. Van Allen, and M. B. Gottlieb. Phys. Rev., vol. 99, p. 198, 1955.
3. Vernov, S. N., and A. Ye. Chudakov. Study of cosmic rays using rockets and earth satellites in the USSR. Report given at Fifth Assembly of IGY, 1958.
4. Shafer, Yu. G. and A. V. Yarygin. Investigation of cosmic rays with geophysical rockets. Contained in "Artificial Earth Satellites", 1960, issue 4.
5. Vernov, S. N., A. Ye. Chudakov, P. V. Vakulov, and Yu. I. Logachev, Study of terrestrial corpuscular radiation and cosmic rays during space rocket flights. Doklady Akad. Nauk SSSR, 125, No. 2, 1959.
6. Charakhch'yan, A. N., "Zh. eksperim. i teor. fiz.", vol. 35, issue 5 (11), 1955.
7. Meredith, L. H., M. B. Gottlieb, and J. A. Van Allen. Phys. Rev., 97, p. 201, 1955.
8. Vernov, S. N., A. Ye. Chudakov, A. I. Lebedinskiy, and I. P. Ivanenko. Composition of terrestrial corpuscular radiation and possible mechanisms of its origin. Report given at International Conference on Cosmic Rays, Moscow, July 6-11, 1959.

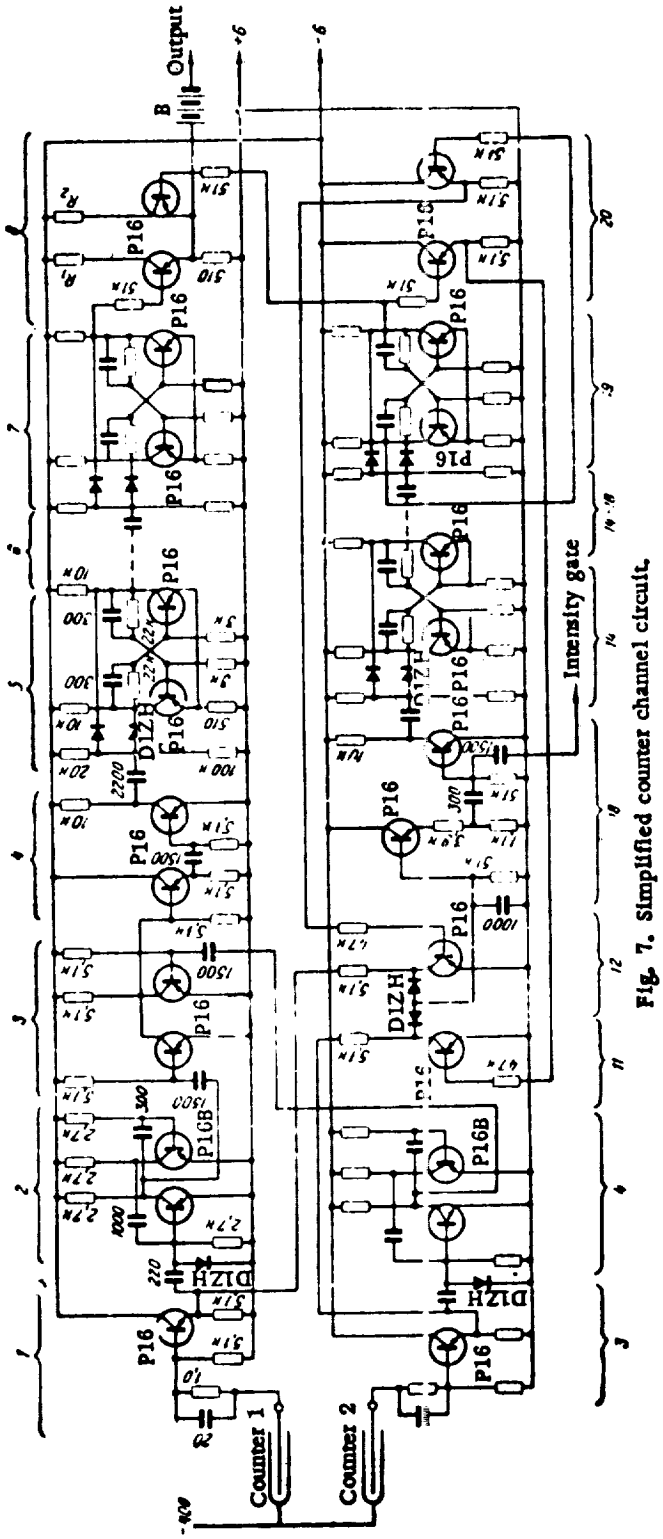

Fig. 7. Simplified counter channel circuit.

V. A. Belomestnykh, B. S. Nedzvedskiy and Yu. G. Shafer

INVESTIGATIONS OF VARIATIONS IN COSMIC RAY INTENSITY IN STRATOSPHERE

Investigation of the cosmic rays in the stratosphere is being conducted in Yakutsk with a counter telescope and a single counter carried aloft into the stratosphere by sounding balloons and with special recording apparatus on the ground.

The first version of this apparatus is described in [1]. Extensive tests have shown the criticality of the circuit in the original version with respect to the feed voltages and the unsatisfactory conditions selected for certain parts of the apparatus.

This article describes the second version of the apparatus. Numerous measurements of cosmic rays in the stratosphere made with this new apparatus enabled us to obtain reliable experimental material during the International Geophysical Year. Some of the results of the analysis of the stratospheric measurements are considered in this article.

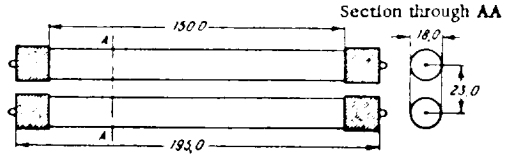

Fig. 1. Diagram showing arrangement of Geiger counters (type STS-6) in double coincidence telescope aboard balloon.

The apparatus consists of a double-coincidence counter telescope (Figure 1) and a single counter. Halogen counters of the STS-6 type are used to record the intensity of the cosmic radiation in two channels.

The coincidence circuit is made with D1Zh crystal diodes and is connected to the counters by a differentiating circuit R = 10 kilohms and C = 1000 micromicrofarads with a time constant $\tau = 10^{-5}$ sec. (see Figure 3).

The selected system provides a coincidence-circuit resolving time of less than 10 microseconds and a selection factor of about 4, and is non-critical with respect to the feed voltages. At the same time, this system brings about a reduction in the input resistance and increases the counter dead time. Partial elimination of these shortcomings is afforded by careful choice of the crystal diodes with respect to inverse current, the lower limit of which should be 12 microamps at a voltage of 25 volts.

Use of this system gives rise to certain apprehension with regard to the normal functioning of the counters, which at first sight are not being used under conditions for which they were designed. However, comparison of simultaneous measurements of cosmic rays with two telescopes, one of which was joined to the input of the crystal diode coincidence circuit, and the other to the normal Rossi tube circuit, showed promising results. Data obtained over more than a year of simultaneous operation of the two instruments are compared in the table.

It can be concluded from analysis of the table that counters attached to the input of our coincidence circuit mounted on semiconductor diodes do work normally.

Among the other important parts of the apparatus we should mention the single flip-flop multivibrator mounted on one 1A2P multigrid tube.

The multivibrator has two functions: it shapes the coincidence pulses and works as a generator when its input receives barographic signals from the positive-polarity relaxer.

These signals are divided into short, medium and long, according to their duration. Their periods are set by the relaxer according to the position of the aneroid contact within the limits 550 microseconds to 0.003 seconds.

The barographic signals make the multivibrator oscillate by acting on the blocked grid. The oscillation period of the multivibrator is about 150 microseconds. Asymmetry is expressed by a

Table. Results of Comparison of Number of Telescope Readings for Same Time Intervals*

June-August 1958			October 1958-March 1959			June - July 1959		
A	B	A/B	A	B	A/B	A	B	A/B
707	626	1,13	677	636	1,11	721	657	1,09
739	655	1,13	676	607	1,11	829	734	1,12
723	659	1,08	690	643	1,07	611	576	1,06
686	611	1,12	729	671	1,13	668	604	1,11
637	594	1,07	692	645	1,07	2031	1835	1,09
1064	951	1,11	719	657	1,09	2072	1927	1,08
1060	960	1,12	1382	1267	1,09	6074	5515	1,10
679	628	1,09	685	618	1,11	3147	2782	1,13
707	621	1,13	730	677	1,00	5538	5089	1,09
667	609	1,09	693	638	1,09	3958	3503	1,13

* A - Data from telescope attached to input of coincidence circuit with crystal diodes;

B - Data from telescope attached to Rossi coincidence circuit input.

pulse length of about 15 microseconds, and by a reciprocal of the pulse duty factor of the order of 100 microseconds.

Barographic signals are transmitted from the single flip-flop multivibrator output to the modulator in the form of three types of pulse trains consisting of 3, 8 and 20 pulses.

To avoid mutual induction of the sensitive elements in the circuit, both multivibrator grid circuits contain filters R = 33 kilohms and C = 10-20 micromicrofarads.

The relaxer mounted on a MTKh-90 three-electrode neon tube is intended to send signals indicating barometric pressure and air temperature.

As can be seen from the circuit (see Figure 3), the relaxation period varies with the position of the contact of the bimetallic temperature pickup. The length of the pulse picked off the cathode resistance varies according to the position of the aneroid pressure pickup contact. An integrating (shaping) circuit, $\tau = 3.10^{-3}$ sec, is coupled to the relaxer output and this converts sawtooth pulses into bell-shaped ones, which are better for triggering the signal vibrator.

The MTKh-90 neon tube is chosen to match the ignition potential within the limits 140 volts ± 2%. This is essential to make it easier to adjust the instruments and identify them.

A 1A2P heptode or a 1B2P pentode in a triode regime may be used as the modulator tube.

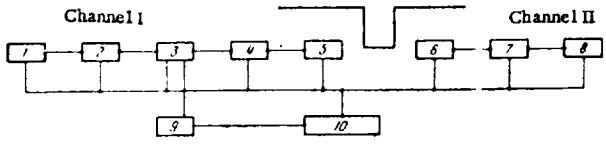

Fig. 2. Block diagram of airborne apparatus: 1) counter telescope; 2) coincidence circuit; 3) single flip-flop oscillator; 4) channel I modulator; 5) channel I radio transmitter; 6) channel II radio-transmitter; 7) channel II modulator; 8) single counter; 9) relaxer; 10) power supply unit.

Normally the modulator tube is blocked. A positive pulse coming from the single multivibrator unblocks it, and a pulse with a 60-70 volt amplitude is then formed at the modulator resistance, R = 10 kilohms. This pulse reduces the potential at the transmitter tube cathode to the value which can act as the generation threshhold.

The resistance in the modulator tube anode R = 5.1 kilohms is auxiliary. When the apparatus is being adjusted to it, an oscillograph or input stand can be attached to calibrate the telescope. When the apparatus is being used, this resistance switches off. The USW radio transmitter contains a 2P1P tube. Because of the high anode voltage, the transmitter is able to provide signals sufficiently powerful for reliable reception over large distances.

The second apparatus channel (Figures 2 and 3) consists of a single STS-6 counter, modulator

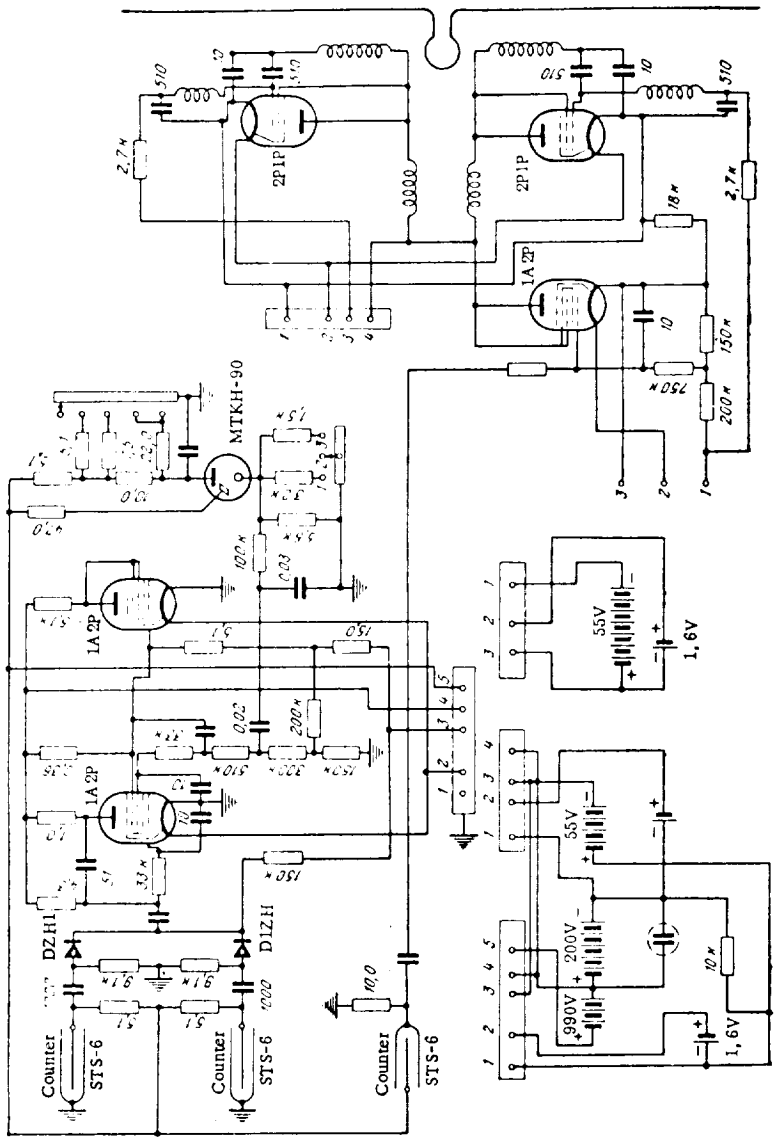

Fig. 3. Simplified circuit of airborne apparatus.

and radio transmitter. The last two of these are similar to those described above in the first channel; the only difference is that the modulator resistance in the second channel is double the first.

The transmitters in the first and second channels are spaced at a frequency of 2 to 10 megacycles.

The power supply unit consists of batteries of the following types and ratings.

1. A 390-volt battery with a + 220-volt tap (anode voltage) to power the counter and relaxer. The circuit normally functions at 390 volts ± 8%. Criticality with respect to this voltage is

determined by the amplitude of the counter pulse, which decreases as the voltage fed to the counter drops.

2. A bias battery for the first channel circuit of 55 volts, with a voltage criticality of 20%.

3. A bias battery for the second channel circuit of 55 volts, with a criticality of 20%.

4. Three filament batteries: a) to feed the single vibrator and modulator in the first channel, b) to feed both transmitters, and 3) to feed the first channel modulator. The voltage criticality ranges from 1.65 to 1.0 volts.

The batteries feeding the counters, anode circuits and bias are made up of disc batteries type 105-PMGU-0.05. The filament batteries are type 1-KSU-[illegible]. The structure of the power supply ensures that the apparatus functions normally for three hours.

To obtain the necessary power from the anode battery at the moment of the pulse it is shunted with a 30 microfarad capacitance.

Before being launched the apparatus is usually checked and adjusted. In particular, the necessary number of pulses in the barographic signal trains is selected by adjusting the resistances in the MTKh-90 tube cathode. The relaxation intervals are also selected by varying the resistances in the anode circuit.

The STS-6 counters are selected in accordance with the standard on the basis of the beginning of the count, length and inclination of the plateau. Furthermore, the single counters are calibrated from a γ-preparation and the telescope from a natural background. A deviation from the standard instruments of more than 2-3% is not tolerated.

When the apparatus is being prepared, the pressure pickup in the barograph chamber is graduated at the control points 900, 800, 700, 600, 500, 400, 300, 200, 100, 50 and 25 mb. A calibration curve for the aneroid is plotted from these data.

Before the flight the power supply unit is packed with cotton wool and placed in a cardboard box painted black. Except for the temperature pickup, the whole apparatus is enclosed in a cellophane bag to avoid convective heat exchange with the surrounding sphere.

To receive the signals sent out by the transmitters aboard the balloon, the two sets of equipment (one set for each channel) are set up at a point on the ground. Each set includes a highly sensitive ultrashortwave receiver, coder, scaling circuit and undulator. Figure 4 shows a diagram of the ground installation described in [1]. The tape winder and monitoring oscillograph are the same. Signals received and processed by the decoder and scaling circuits are recorded by the undulator on telegraphic tape on two lines corresponding to the channels in the airborne apparatus. Accurate time markings every thirty seconds are marked on the tape.

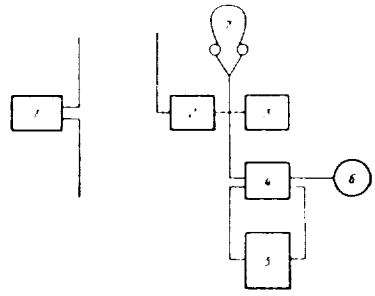

Fig. 4. Block diagram of airbone apparatus and apparatus on ground: 1) airborne apparatus; 2) USW radio receiver; 3) oscillograph for visual observation; 4) decoder; 5) PS-64 scaling circuit; 6) telegraphic tape undulator; 7) telephone for check up.

The apparatus weighs 2150 g; it can easily be carried aloft on two standard No. 150 radio sounding balloons. The maximum ceiling achieved corresponds to a pressure of 5-10 mb. The ceiling, however, depends considerably on the quality of the balloon envelopes and preliminary treatment. The duration of the ascent averages 70 minutes. It is usually possible to receive normal signals during the ascent and descent to a pressure level of 300-400 mb.

In Yakutsk the cosmic-ray intensity of the stratosphere is measured regularly every other day. During magnetic storms the number of ascents is increased (two each day).

A considerable amount of experimental material has been acquired by the laboratory since October, 1957. Of measurements relating to different heights the main ones processed are those during which a pressure level of 100 mb or more was achieved

Processing has made it possible to plot height-dependence graphs, in which the intensity is averaged according to pressure levels or for 5-minute intervals. The statistical accuracy of the telescope measurements at the Pfotzer maximum is 1.5 to 3.0%.

Analysis of the experimental material has enabled us to obtain data on the decline in solar

activity in cosmic ray intensity from measurements in the stratosphere [2].

It was shown during this research that the intensity of the ionizing component in the stratosphere from 1958 to 1959 increased to such a degree, compared with 1957-1958, that a level of 150 mb it amounted to 3.5 ± 2% and at 50 mb to 16 ± 8% (Figure 5).

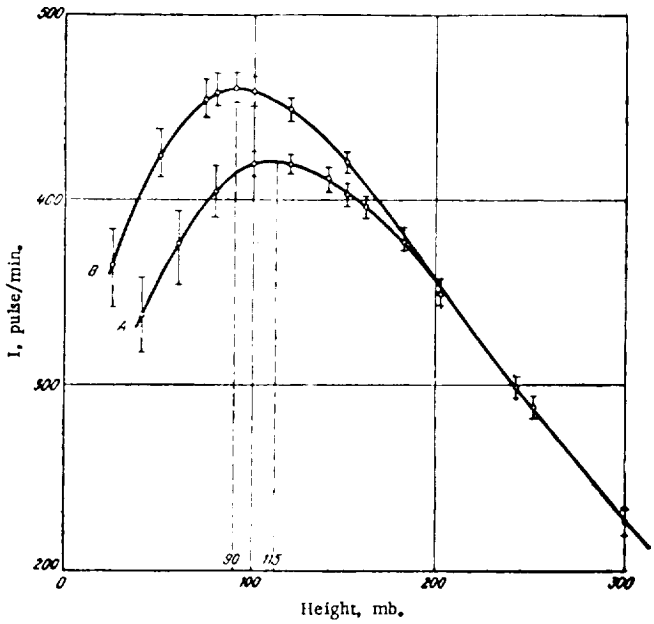

Fig. 5. Curves showing intensity versus height of ionizing component of cosmic rays obtained from averaged data for stratospheric measurements made in Yakutsk:

A - during period from December, 1957 to April, 1958; B - during period from December, 1958 to May, 1959.

The considerable errors are apparently due to the small amount of data for great heights used and to instrument errors, chiefly radiation errors, due to the apparatus being heated by the sun.

Comparison of the results obtained with ground data on variation in the intensity of the hard and neutron components in cosmic rays, obtained over the periods in question at Yakutsk, and with the results of calculations using coupling factors has made it possible to conclude that the increase in cosmic ray intensity during the decreasing solar activity (from 1957 through 1959) was due to an additional flow of particles with energies up to 10 ± 2 Bev, and that the variation is not accompanied by substantial transformation of the energy spectrum and is therefore due to primary radiation scattering by magnetic fields.

The experimental material obtained does not clash with views on a reduction of the number of corpuscular streams carrying frozen magnetic fields associated with the fall off in solar activity [3].

Bibliography

1. Belomestnykh, V. A. and Yu. G. Shafer. "Variation in Cosmic-Ray Intensity in the Stratosphere and Methods of Recording and Investigation". Transactions of Yakutsk Branch of Academy of Sciences of USSR, Physics series. Issue 2, p. 47, 1958.
2. Shafer, Yu. G., "Effect of Fall-Off in Solar Activity on Intensity of Cosmic Rays from Measurements in Stratosphere". Report given at International Conference on Cosmic Rays, Moscow, 1959.
3. Dorman, L. I., Cosmic-ray variations, Moscow, Gostekhizdat, 1957.

D. D. Krasil'nikov

APPARATUS FOR RECORDING TIME DEPENDENCE OF FREQUENCY OF EXTENSIVE ATMOSPHERIC SHOWERS WITH GEIGER-MULLER COUNTER DETECTORS

Introduction

The development of techniques for the acceleration of particles up to 10 Bev under laboratory conditions, the need to obtain further information on the interaction of particles with still higher energies, the desire to ascertain the origin of cosmic rays and various astrophysical problems associated with them are at present the incentive for investigation of cosmic radiation particles in the sphere of superhigh energies (greater than 10^{13} ev) and make the investigation particularly topical. The investigation of temporal variation in cosmic-ray intensity in this energy region is, among other things, of very great interest.

Temporal variation in the intensity of cosmic rays with superhigh energy was little studied until recently because of the experimental difficulties involved.

These difficulties are due first and foremost to the extremely small intensity. For instance, to judge from recent measurements and evaluations [1,2], 1 cm^2 of surface at the boundary of the atmosphere is crossed by particles with energy E_0 greater than 10^{13} ev once in twenty eight days, by particles with energy E_0 greater than 10^{15} ev once in approximately 240 years, and particles with energy E_0 greater than 10^{17} once in $(7\text{-}8) \cdot 10^5$ years.

At the present time we only know of one way of effectively studying variations in the intensity of particles with energy above 10^{13} ev, and this is by prolonged and continuous recording of the frequency of extensive atmospheric showers. The latter are produced in the atmosphere by superhigh-energy cosmic rays. Due to the fact that every such shower covers a large area S (up to several square kilometers in the case of giant showers) at the depth of the atmosphere, it is possible to record, over an area S considerably greater than the area σ of the detector itself, instances of the incidence of superhigh energy particles., that is there is in principle a possibility of collecting sufficient statistics of instances to perform an analysis of the various types of time dependence in superhigh energy cosmic rays in spite of the very, very slight intensity. However, at the present level of techniques employed the practical task of continuous and prolonged recording of the frequency of these showers involves great difficulties. From the viewpoint of the variety of conditions (the very great spread of size) of the showers, and the rate at which statistical data can be collected which have to be covered by the shower recording apparatus, the latter becomes cumbersome, and the large scale use of such short-lived parts as electronic tubes and self-quenched counters as detectors means that the work of the apparatus is interrupted, that a large number of additional links have to be provided and that the apparatus has to be carefully tended and checked during operation.

Basically, it is the difficulties involved in arranging the experiment which have resulted in comparatively poor study of the time dependence. For example, only a few points in the world are at present engaged in recording them.

It should be pointed out that the variations in the frequency of these showers observed in the depths of the atmosphere (near sea level) are not only due to variations in the intensity of primary particles of corresponding energies, but are also due, as shown by experience [3-5], first and foremost to variations in the state of the atmosphere above the observation point. By forcing us to make corrections for atmospheric effects this fact hampers direct consideration of the variation in intensity of primary particles with superhigh energies, but at the same time, it provides

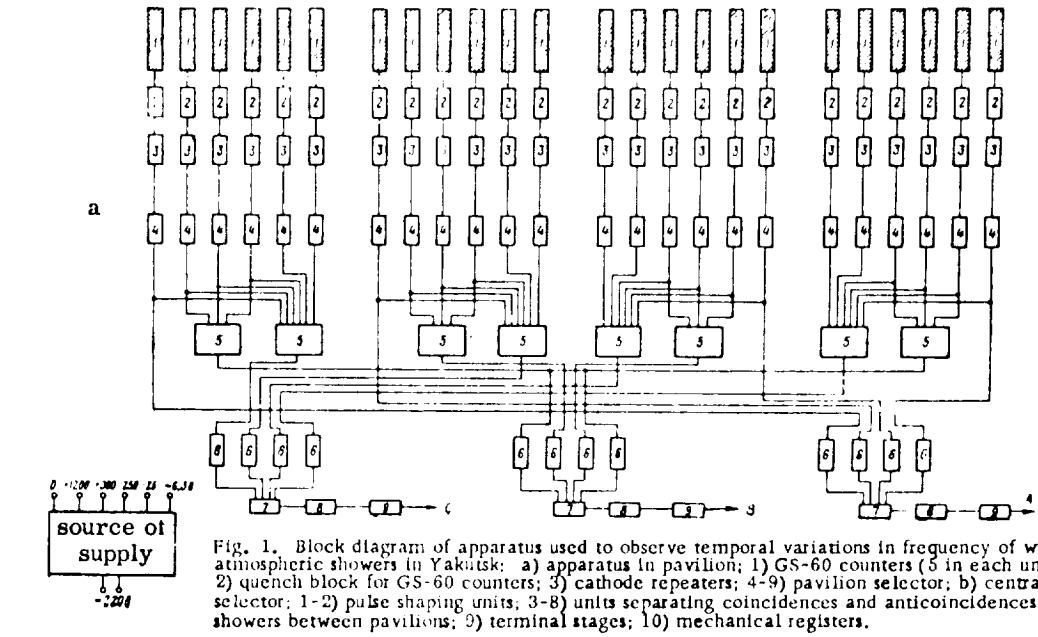

Fig. 1. Block diagram of apparatus used to observe temporal variations in frequency of wide atmospheric showers in Yakutsk: a) apparatus in pavilion; 1) GS-60 counters (5 in each unit); 2) quench block for GS-60 counters; 3) cathode repeaters; 4-9) pavilion selector; b) central selector; 1-2) pulse shaping units; 3-8) units separating coincidences and anticoincidences of showers between pavilions; 9) terminal stages; 10) mechanical registers.

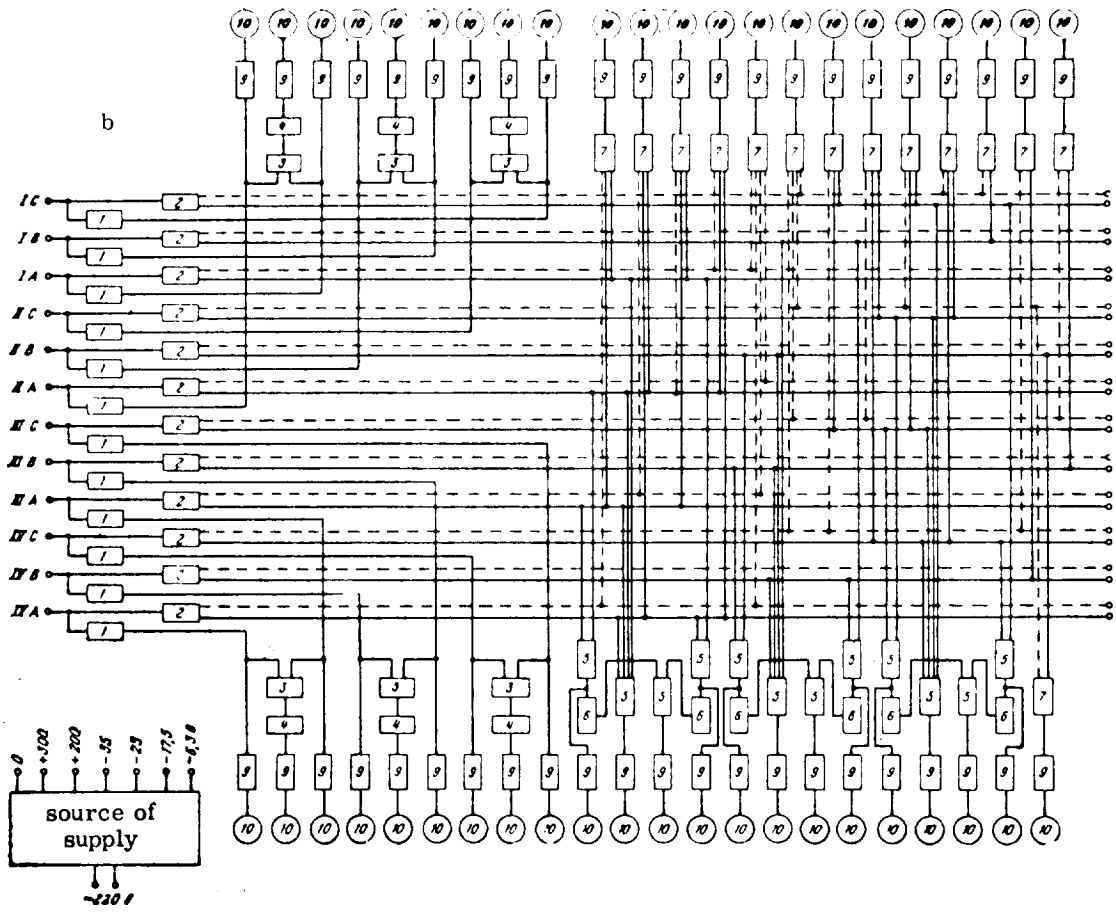

an opportunity to study and extend the data on certain important characteristics of the primary interaction at superhigh energies. This information concerns such characteristics of the primary event as the interaction cross section, multiplicity of nascent particles, fraction of unstable particles and so on. Indeed, the very genesis and development of the extensive atmospheric showers is accompanied by a large number of primary events [6], and the observed effects of the atmosphere on their frequency depend in the long run on the characteristics of these primary events.

Thus, when recording variations in the frequency of the showers, the investigation of time dependence of the intensity of cosmic rays of corresponding energies, which is carried out in order to ascertain the origin of cosmic rays and to throw light on certain related astrophysical problems, is combined with the acquisition of further data on the characteristics of the primary event at superhigh energies of the interacting particles.

The systematic recording of variations in shower frequency near sea level in Yakutsk (100 m above sea level) was begun by the author in 1954 in order to study the associated meteorological phenomena [5]. There could be no question of studying any other aspects when it was considered that the incidence of cases obtained with the use of low-powered apparatus was comparatively small. Thus, during the first series of observations (1954-1955), recordings in a normal building with a roofing thickness of 60 g · cm^{-2} produced a frequency of about 10-12 per hour for atmospheric showers selected by the triple coincidence apparatus, at a counter group area of $\sigma_1 = \sigma_2 = \sigma_3 = 0.1$ m^2. When a doubling unit had been constructed and a special pavilion built with a simpler ceiling (2.5 g · cm^{-2}), the frequency of the recorded showers went up to 30 per hour (1955-1956). During the first series of observations the author used a self-quenched Geiger-Muller counter, type GS-9, with a working area of about 100 cm^2 each, and during the second series GS-60 counters, each with an area of 330 cm^2. As the experiment showed, when the electronic circuit for processing the Geiger-Muller counter pulses was simple, and the number of counters was comparatively small (20-30), it was possible in both series of observations to record for about 85% of the total possible observation time; 15% of the time was wasted on interruptions involving replacing counters and tubes and daily checks to assure the proper operation of the apparatus, interruptions in the power supply and time taken to deal with various types of malfunctions.

On the basis of a certain amount of experience, at the beginning of 1956 the Working Group for Cosmic Rays of the Soviet Inter-Departmental Committee of the International Geophysical Year instructed the Cosmic Ray Laboratory in Yakutsk to construct a substantially enlarged installation, within a comparatively short time, for effective recording of variations in the frequency of extensive atmospheric showers in accordance with the International Committee's draft program for USSR research during the International Geophysical Year.

A draft of the basic parameters and a block diagram of the electronic circuits for this apparatus, designed by the author on the basis of the Working Group's recommendations, were discussed by the Cosmic Ray Laboratory staff after checking with the work supervisor, S. I. Nikol'skiy, and at the end of 1956 the design was approved and used in development and assembly of the apparatus.

The design took into account the following requirements in the new apparatus for effective observation of variations in the shower frequency:

1. Sufficient frequency in collecting statistical data; for most of the shower ranges selected, the data recorded over one year had to be adequate for clarification of all the salient effects of frequency of the showers with an amplitude greater than 1%.

2. The greatest possible differentiation between the separately recorded shower sectors of the region, and a large total area coverage of the region of mean showers (from $\bar{N} \sim 10^4$ to $\bar{N} \sim 10^7$).

3. The detectors used were self-quenched GS-60 Geiger-Muller counters, each with an effective area of about 330 cm^2, made in this country.

4. Simplicity in controlling the operation and convenience in operating the equipment; two operators should be sufficient to ensure normal functioning.

5. Cross-checking of the recorded data from all channels, and "cross linking" of a number of recorded data when replacing the counters.

6. Minimum interruptions in observation; in any case, the interruptions should not exceed 10-15% of the total possible recording time.

7. Simplicity of design in the main parts of the apparatus, for easy assembly on the spot without expert assistance.

Work on the construction of the apparatus did not begin until the second quarter of 1956. By necessity the designing and assembly work proceeded almost concurrently. The first units (more or less half the apparatus) were put into operation at the end of 1957, and the remainder in May, 1958, while the main work on the unit as a whole was completed by July 1, 1958.

A block diagram of the apparatus used to observe the extensive atmospheric showers is shown in Figure 1.

The first results of processed material are available [7,8]. The apparatus continues to function normally. Below we describe the basic characteristics of the apparatus and its principal parts, including a brief description of some of the results observed.

Receiving Apparatus

1. Detectors. Geiger-Muller counters are used as detectors of charged particles. The use of scintillation counters, Cherenkov radiation in the air or special Cherenkov counters for this purpose, which is possible in principle, seemed to us to involve greater difficulties than the use of ordinary Geiger-Muller counters, to judge by the state of the development of Cherenkov counters [9-11] at the time this apparatus was designed.

Taking into account the temperature variation from +30 to - 60°C. at the observation point, and the fact that at the time the only available counter was the GS-60 (filled with argon and ethyl alcohol vapor), we were forced, unlike the British [12], to construct powerful local installations concentrated in several separate insulated pavilions. In selecting the site for the pavilions and the areas for counter groups in separate local recording installations, we were guided, apart from other things, by considerations of differentiating between the sectors of recorded showers and identifying them in order to cross check the data obtained.

As already pointed out, we used GS-60 counters as detectors. They are glass cylinders with a wall thickness of 2 mm, covered on the inside with a thin graphite layer (cathode), having a central tungsten filament 0.1 mm in diameter (anode). The counters are filled with argon under a pressure of 80 mm Hg and ethyl alcohol vapor at 20 mm Hg, providing a mean effective thickness of the sensitive volume for shower particles of about 10^{-3} g · cm^{-2}.

The mean dimensions of the effective working area of the counter are: diameter 60 mm, length 550 mm, i.e., the effective cross-section area is 330 cm^2. The "ignition" voltage is about 1200 volts. The plateau length is > 150 volts, and the plateau tilt is < 0.1% per volt. In Figure 1 each block, 1, consists of 5 GS-60 counters in parallel with respect to the output signal.

2. Pavilions. Four pavilions constructed of wood (6 X 6 X 2.5) m^3 were set up. They constitute one cell of the network scheduled to be spread out over a wide area in the future. Their arrangement is shown in Figure 2.

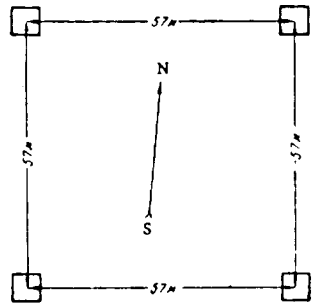

Fig. 2. Arrangement of pavilions.

The distance between the pavilions is 57 m, which is approximately equal to the mean square radius R, of the shower near sea level. If R is actually a function of the temperature T of the ground layer of air, in the form of $R(T) \sim r_0 T$, where r_0 is constant [13], then at such distances we can expect the local temperature effect of the ground layer of air for showers recorded simultaneously in two pavilions to be close to zero as an average, or to change its sign to posivite, as distinct from the negative local temperature effect for showers recorded by only one local installation. The roofing over the counters (Figure 3) was made of a material similar in composition to air (moss and plywood) 3 g · cm^{-2} thick to avoid the screening effect of normal ceilings and to avoid considerable transition effects as well. A subsequent check confirmed that the roofing had been successfully chosen. It was also satisfactory from the point of view of heat insulation. The temperature inside the pavilions is kept at +20 ± 5°C.

3. Local installations; layout of the detectors. In effect there are three separate triple-

coincidence installations in each pavilion with counter group areas of $\sigma_1 = 1/6\ m^2$, $\sigma_2 = 1/2\ m^2$ and $\sigma_3 = 1.0\ m^2$, or 5, 15 and 30 GS-60 counters in parallel, respectively.

The positioning of the installation is shown in Figure 4. We decided to place two counters next to each other mainly for reasons of assembly, but partly because we doubted that there was any gain in working area if they were separated from each other. The fourth counter stand is a spare one intended to reduce interruptions due to part failure. When the installation is in operation, the spares are in a state of readiness, and when parts that have ceased working properly have to be replaced they can be switched into operation with a plug connection and four rotary switches. As can be seen from Figures 1 and 4, each stand contains 30 GS-60 counters and is serviced by 6 quenching units mounted together with the counters. All counter stands can be easily disassembled; the power supply and signal leads are of the plug-in type.

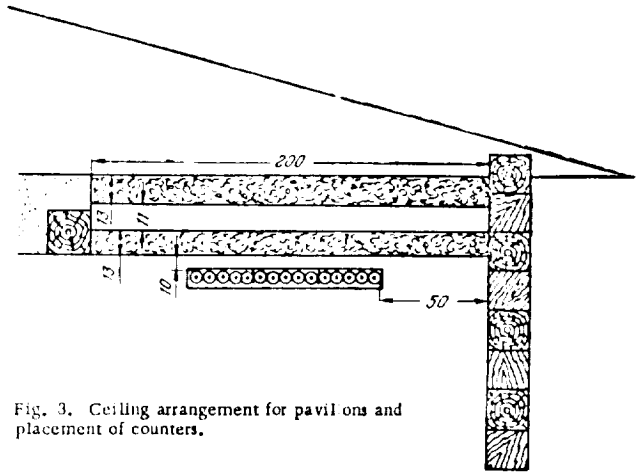

Fig. 3. Ceiling arrangement for pavilions and placement of counters.

4. Feed and counter voltage control circuit. As can be seen from Figure 5, the voltage supply and its control are sufficiently independent of one another in the case of each counter. The counters are only joined in parallel with respect to the output pulses. Apart from convenience in replacing counters, this is done to establish for each counter conditions which reduce the end effects and which allow a maximum gain in effect from enforced quenching of the counter charge (see below).

For an exact check on the voltage fed to the operating counters we use a monitoring control counter, which does not affect or interfere with the operating counters (it is difficult to follow the overvoltage from indicating instruments at the power supply). The monitoring counter receives voltage only during the actual check. Otherwise it is switched off. The overvoltage in all the counters is regulated on the basis of the monitor counter readings. Each stand has a potentiometer for this purpose. Experience shows that this kind of check is rarely required.

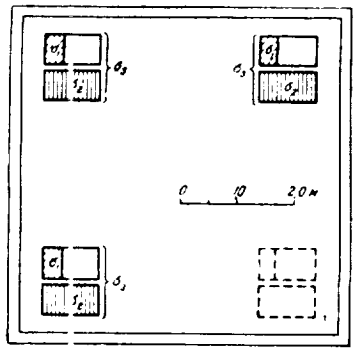

Fig. 4. Arrangement of GS-60 counter -- receiving unit in pavilion (cross-section).

Electronic Circuits

1. Units for quenching charge in GS-60 counters (block 2 in Figure 1). Although they are the most suitable in size and from the point of view of certain other characteristics for the given shower installation, GS-60 counters made in the Soviet Union have a substantial defect. This is the limited operating lifetime and wide distribution (with a flat maximum) of this lifetime within the same batch of counters.

In the usual simple circuits for GS-60 counters, without external enforced charge quenching, the lifetime of most of the counters ranges from 10^7 to $3 \cdot 10^8$ discharges, with an average of 10^8 discharges for the whole batch. When observing near sea level this corresponds to one week and eight months of continuous recording. It is extremely difficult in practice to predict in advance

which counters will have a short life.

This shortcoming, which can be ignored if the number of counters used is small and the observations are brief, is intolerable when operating several hundred counters at the same time to record long time variations in the frequency of atmospheric showers. For this use we require uninterrupted recording and invariant parameters in the receiving apparatus over a very long period of time.

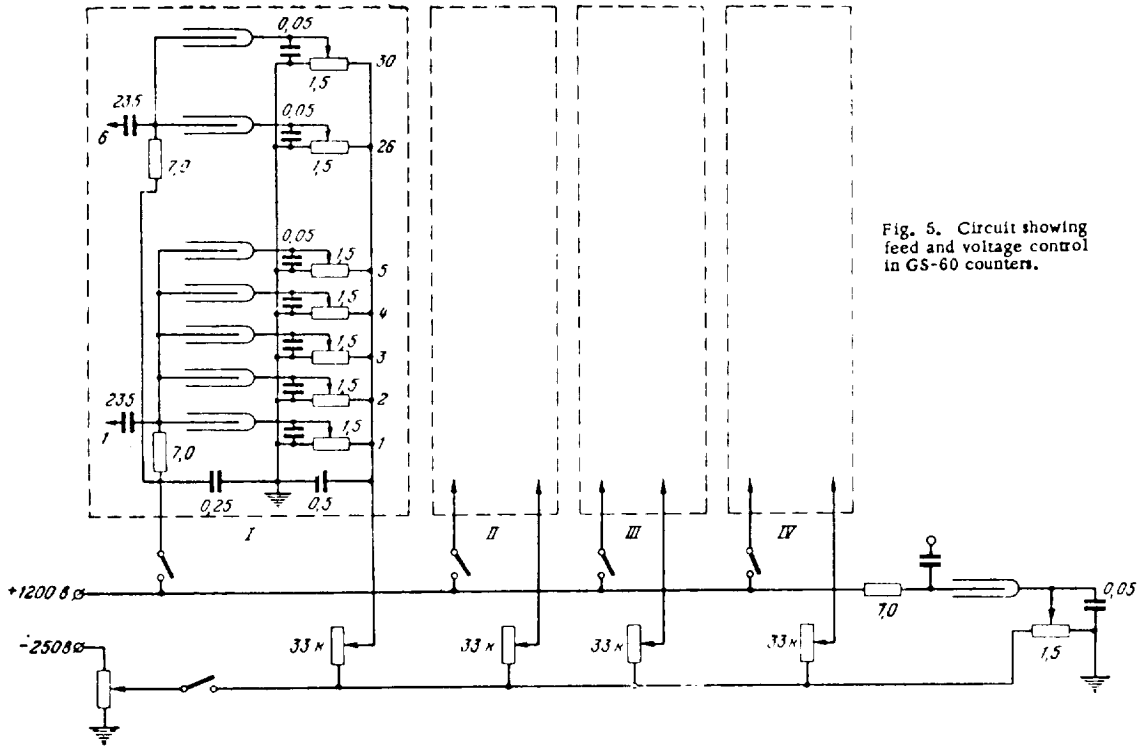

Fig. 5. Circuit showing feed and voltage control in GS-60 counters.

To ensure effective recording of these time variations, the first thing was to correct, at least to some extent, this defect in the GS-60 counters, i.e., to prolong their life, if only to a slight extent, by using an electronic circuit for forced external quenching of the discharge in the counters.

As it is known, the life of counters of the self-quenched type is connected with the expenditure (by dissociation) of the quenched component - ethyl alcohol vapor. The degree of dissociation of the alcohol molecules is approximately proportional to the electric charge passed through the counter when it discharges [14]. Hence by using the voltage pulse from a corresponding electronic circuit to interrupt the discharge current each time it begins to increase, we can reduce the dissociation of the molecules, i.e., we can prolong the life of the counter.

Consideration of the two discharge-quenching circuits which have become common of late [15,16] showed that the use of them in our apparatus was neither advisable nor possible. The first circuit is only applicable to a single counter, and therefore, in our 480-counter installation this would have meant making the same number of quenching units with a corresponding complication in the commutation system. Both circuits require a high degree of stability in the negative bias voltage from the supply battery (± 0.1 volts). This makes them inconvenient and capricious when used for prolonged and continuous recording.

Hence, we avoided using these circuits and decided to work out a new quenching circuit which would satisfy the requirements and operating conditions of the described installation. The

quenching circuit had to rely on five GS-60 counters in parallel, had to trigger reliably, be only slightly sensitive to the oscillations in the supply voltage, and had to produce a maximum quenching effect. It seemed advisable to include in the circuit a preamplifier (such that it would discontinue the counter discharge as soon as possible), an electronic potentiometer and a single flip-flop vibrator. A circuit of this kind was worked out by engineer A. V. Yarygin [17]; the circuit, together with the cathode repeater, is shown in Figure 6, where L_1 is the pre-amplifier, L_2 and L_3 are the single vibrators, L_4 and L_5 are the electronic potentiometers and L_6 is the cathode repeater for the output pulse to the cable.

As can be seen from Figure 6, the entire quenching unit with the cathode repeater contains three tubes, 6N15P and 6N1P. This circuit differs from the one described in [16] in the presence of the pre-amplifier, a different electronic potentiometer tube connection and the absence of an inductive circuit in the single vibrator anode circuit. The quenching circuit and the cathode repeater (blocks 2 and 3 in Figure 1) make up one assembly unit, which is plugged into the counter stand.

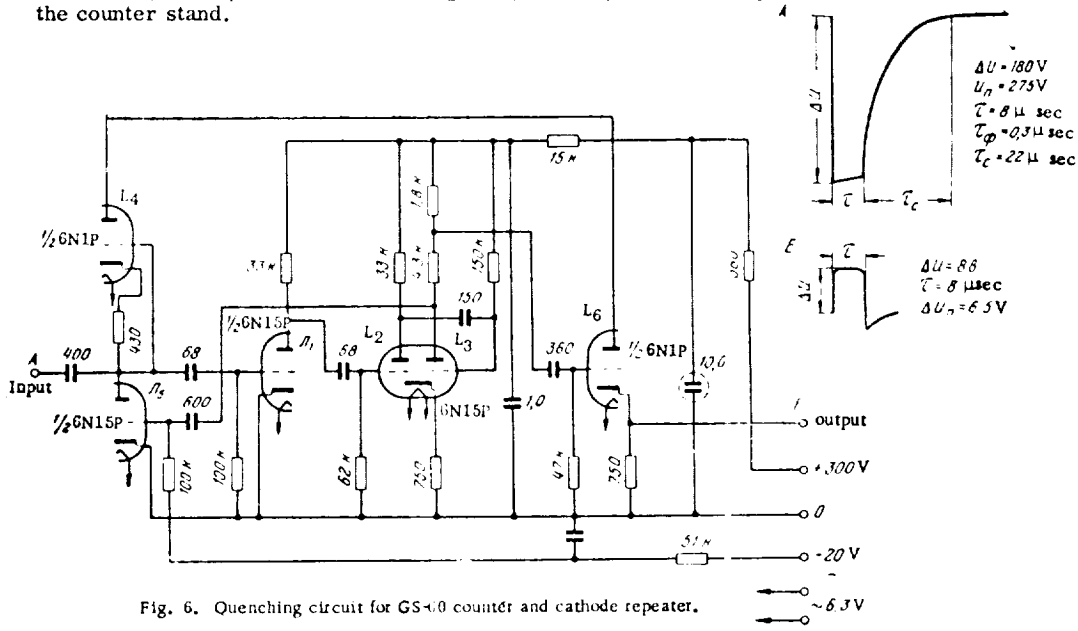

Fig. 6. Quenching circuit for GS-60 counter and cathode repeater.

Using the method of measuring the discharge rate of the condenser [16], it has been found that if the voltage feeding a GS-60 counter is slightly higher than the beginning of the Trost zone, the electric charge Q_q passing through the counter using the given quenching circuit during discharge is smaller by a factor of 8 or 9 than the charge Q_o without this circuit, i.e.,

$$\frac{Q_o}{Q_q} = \text{from 8 to 9.}$$

By reducing the cathode tilt, the quenching circuit expands the plateau by a factor of 2.5 - 3.

2. The pavilion selector consists of the blocks 4-9 (see Figure 1).

The pulses are fed from the cathode repeater (block 3) to block 4 through a RK-2 coaxial cable 6-8 m long. Through the screen circuit of tube 6P9 in block 4 the pulses reaching block 3 are shortened to $2.5 \cdot 10^{-6}$ sec and are fed to the mixing circuits (block 5), and being amplified in amplitude and power, pass through the anode circuit into the cell signalling the abnormality of the GS-60 counter background. The latter, with the aid of two neon MTKh-90 tubes, sends a

signal when the deviations are ± 20% from the normal background. The mixing circuits (block 5) consist of D2-Ye. separator diodes.

In block 6, containing a 6N8S tube, the pulses are shaped again and at the output have an amplitude of 18 volts (negative polarity) and a length of $1.0 \cdot 10^{-6}$ sec. It is this length which determines the coincidence resolving time, which is also $1.0 \cdot 10^{-6}$ sec.

The coincidence circuit uses the Rossi system (block 7); the discriminator and single vibrator (block 8) contain 6N15P tubes; they provide a good selectivity factor and ensure reliable recordings.

For some of the recording channels the functions of blocks 6-8 are fulfilled by "apple-tree type" instruments (with certain changes).*

Three types of treble coincidences are selected in each pavilion in accordance with the three different areas of the counter groups (1.0, 0.5 and 1/6 m^2). Spurious coincidences here do not amount to more than 1.5% (for an area of 1.0 m^2).

Pulses from block 8, lengthened to $8 \cdot 10^{-5}$ sec, proceed to the matching stage with the cable (block 9), from where they reach the central selector via the coaxial cable 80 m long.

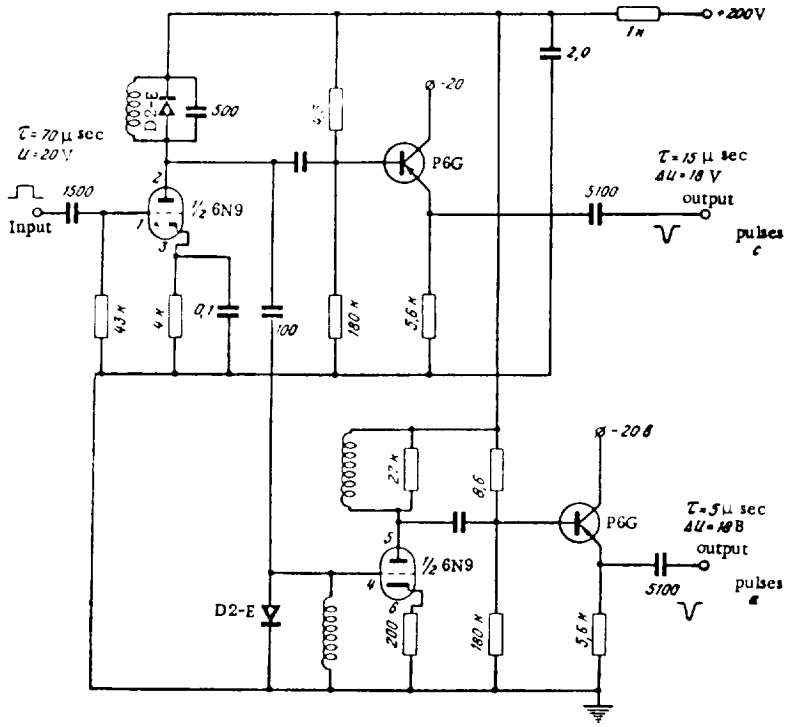

Fig. 7. Shaping stage (blocks 1 and 2 in Figure 1b).

3. Central selector. Twelve different types of triple-coincidence pulses reach the central selector from 4 pavilions. The selector consists of three parts.

In the first two parts a partial selection of the triple and sextuple coincidences takes place, i.e., simultaneous instances of triple coincidences in two pavilions. In these, blocks 3 and 4 are similar to blocsk 7 and 8 in the pavilion selectors, with the exception of the coincidence

* "Apple-tree" is a literal translation of the Russian word which also appears in quotation marks in the original book.

resolving time which in the given case is $10 \cdot 10^{-6}$ sec.

The third part of tl central selector samples all the recorded combinations of the coincidence (large multiples) and anticoincidence of the shower pulses betv een pavilions. The most important part of this installation, the pulse-shaping unit, is shown in Figure 7. Pulse c has a minus polarity an amplitude of 15v and $15 \cdot 10^{-6}$ sec interval; pulse a having th e same polarity and amplitude as that of pulse c is shorter by $5 \cdot 10^{-6}$ with an interval of only $5 \cdot 10^{-6}$. Pulses c are used as selectors of various types of combinations of pulse coincidence between p avilions and as pulse filters for anticoincidences; pulses a are used for interrogation for anticoincidence. This splitting of a pulse into two and shift of the beginning of one, is done to discriminate cases of anticoincidence reliability, i.e., to prevent false cases of anticoincidence due to fluctuation of the beginning of the excitation of the following circuits.

This is vital when using transistors in the anticoincidence separating circuit.

All the coincidence separating circuits (blocks 3, 4, 5 and 6 in Figure 1 b) contain D2-Ye semiconductor diodes. The anticoincidences (blocks 7 in Figure 1 b) are separated with the aid of P6V and P6G transistors. The end stages contain 6N8S tubes.

4. Recording. All the separated coincidence and anticoincidence pulses are recorded by mechanical annunciators. These are ordinary telephone message registers, but with tougher mechanical parts and increased inductance. Regular checking has shown that they work satisfactorily. The counter readings are photographed every hour u sing a FR-2 photographic recorder. F 6 7

In all there are 44 recording chennels, four of which are used t) record the background in the pavilions.

5. Power supply. The observation apparatus is practically entirely powered from the mains using VS-16, VS-12 and VS-11 rectifiers with electronic stabilization of the output voltage. The exception to this rule is in the P6V and P6G transistors, which are fed from batteries. The apparatus consumes approximately 8 kilowatts.

6. Control of apparatus operation. A duty technician (one for the whole laboratory) makes an hourly check of the background signal readings and out-of-action indicators for each power supply. Furthermore, a careful check is made each day of the following: 1) counter background on all stands using a PS-54 scaling device; 2(readings of all mechanical recorders for four-hour recordings made during the previous day.

All work involving preventive inspection and repair, replacement of tubes and counters proceeds according to set schedules.

7. Calculation of mean values of recorded showers. For subsequent analysis of the observed variations in the shower frequency it is important to know the mean values of the showers recorded through all the channels. We made the relevant calculations with the follow ng assumptions as regards the spectrum and spatial distribution of the atmospheric showers at sea level:

1) in accordance with measurements [18 - 20 and other publications] the spatial distribution function is the same for extensive atmospheric showers with different numbers of particles N and takes the form of

$$\varphi(r) = \begin{cases} \frac{a}{r} & \text{when} \quad r < 10 \text{ м}, \\ b \cdot r^{-1,6} e^{-\frac{r}{88}} & \text{when} \quad 10 < r < 100 \text{ м}, \\ c \cdot r^{-2,6} & \text{when} \quad r > 100 \text{ м}, \end{cases}$$

where r is the distance of the shower axis in meters, $a = 1.84 \cdot 10^{-3}$, $b = 2.21 \times 10^{-3}$ and $c = 0.568$.

2) The differential shower spectrum with respect to the nu nber of particles takes the form

$$K(N)\,dN = A \cdot N^{-\varkappa-1} dN$$

and according to [2 and 21]

$$\varkappa = \begin{cases} 1,32 & \text{for} \quad 10^3 < N < 10^5, \\ 1,55 & \text{for} \quad 10^5 < N < 10^6, \\ 1,80 & \text{for} \quad N > 10^6. \end{cases}$$

The frequency of the showers recorded by an n-fold coincidence counter installation between counter groups of equal area σ is determined by an expression with the form

$$C(n,\ \sigma)=\int_0^{\infty}k(N)dN\iint_{(S)}W[n,\ \sigma,\ N,\ \varphi(r_1),\ \ldots,\ \varphi(r_n)]dS,$$

where r_i is the distance from the shower axis to the i-th counter group (i = 1, 2,...n), **S** is the area of incidence of the shower axis, W[n, σ ,N, $\varphi(r_n)$] is the probability of recording a shower with N particles with the given installation, if its axis strikes the area element dS located at a distance r_1, r_2,...r_n, from the counter groups 1, 2...n, respectively.

Since all showers, irrespective of their size, take an equal part in causing the observed variation in the shower frequency $\delta C(n, \sigma)/C(n,\sigma)$, it is convenient to take the mean value N determined from the following condition as the mean.

$$\int_0^{N}k(N)dN\iint_{(S)}W[n,\ \sigma,\ N,\ \varphi(r_1),\ \ldots,\ \varphi(r_n)]\,dS=$$
$$=\int_N^{\infty}k(N)dN\iint_{(S)}W[n,\ \sigma,\ N,\ \varphi(r_1),\ \ldots,\ \varphi(r_n)]\,dS=\frac{1}{2}C(n,\ \sigma).$$

A similar approach may be taken in calculating the cases in which anticoincidences are recorded. The integrals are not taken in their finite form, hence they were calculated by approximate methods of numerical integration.

The mean values of the showers calculated by this method are given in Table 1, where C(n, σ) is a coincidence of multiplicity, n over the counter area σ (for example, multiplicity n = 6 and n = 12, denote coincidences in two and four pavilions simultaneously); $A_3(1/2, \sigma)$ denotes the anticoincidences, i.e., three-fold coincidences over the area σ in one pavilion, unaccompanied by these coincidences for the same area in any of the other pavilions.

Table 1

Type of selection	$\bar{N}$	Type of selection	$\bar{N}$
$A_3(1/2; 1,0)$	$1,5\cdot10^4$	$C(6; 0,5)$	$3,1\cdot10^5$
$C(3, 1,0)$	$2,3\cdot10^4$	$C(12; 1,0)$	$3,9\cdot10^5$
$C(3; 0,5)$	$4,0\cdot10^4$	$C(12; 0,5)$	$7,4\cdot10^5$
$A_3(1/2; 0,17)$	$6,7\cdot10^4$	$C(6; 0,17)$	$7,7\cdot10^5$
$C(3; 0,17)$	$1,1\cdot10^5$	$C(12; 0,17)$	$2,0\cdot10^6$
$C(6; 1,0)$	$2,0\cdot10^5$		

Preliminary results of operation of atmospheric shower installations

Since the time it was started, the installation has been working satisfactorily. During 1958 it recorded about 10^7 cases of showers of different sizes. Interruptions in observation in the recording units have mainly been due to defects in and the need to replace the 6N15P and 6N1P tubes, and interruptions in recording for the installation as a whole have only been due to the power supply failure.

The counter discharge quenching circuit has proved its worth. All 360 GS-60 counters now need replacement only after six months of continuous operation. The semiconductor coincidence and anticoincidence circuits have also shown themselves to be worthwhile.

The mean recorded frequencies for various types of selection of the showers are shown in Figure 2. For some types of selection, Figure 8 gives frequency variation curves together with variation curves for the atmosphere at the observation point.

Meteorological effects of shower frequency

Analysis of the recorded material shows that the barometric effect of the extensive showers (for more detail see the author's article in this issue) remains constant up to mean values

Table 2

Type of selection	Expected frequency, hr.$^{-1}$	Experimental frequency, hr.$^{-1}$
A_3 (1/2, 1,0)	306	330
C (3; 1,0)	413	411
C (3, 0,5)	161	154
A_3 (1/2, 0,17)	27	29
C (3, 0,17)	32	34
C (6; 1,0)	63,8	50,0
C (6; 0,5)	23,3	16,5
C (12; 1,0)	21,3	13,0
C (12; 0,5)	7,0	4,1
C (6, 0,17)	4,0	2,9
C (12, 0,17)	1,0	0,62

$\bar{N} \approx 10^5$, but beginning at $\bar{N} \geqslant 10^5$ particles it begin to increase considerably. This effect cannot be explained by variation (within sensible limits) in the exponent x of the shower spectrum.

On the basis of the seasonal effect, the temperature effect for showers of type C (3, 1.0) is of the nature of α_t = -0.20% per 1°C, which tallies with results obtained by other authors [22]; for type C (6, 1.0) showers, α_t = +0.05% per 1°C. At the same time, for some strange reason this effect cannot be followed during brief variations in temperature in the ground layer of air. It is therefore doubtful whether this effect is entirely due to ground conditions, as asserted in [22,23]. It is most probable that it is comprised of two effects - a local and an upper-layer effect.

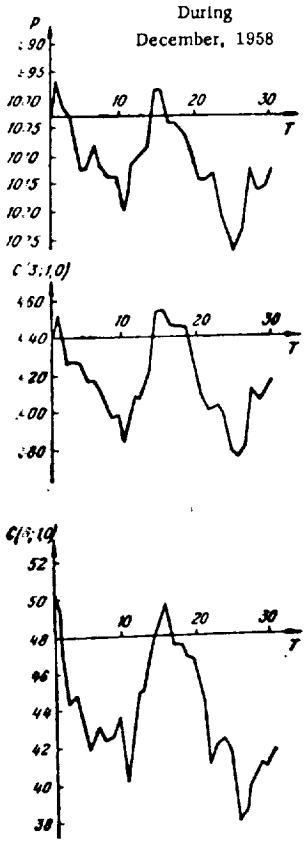

Fig. 8. Frequency variation of showers C (3; 1.0) and C (6; 1.0) variation of pressure, p, at observation point.

Atmospheric shower spectrum at sea level

The data in Table 2 show that the shower spectrum used in the calculation of $C(n,\sigma)$ is too high in the region of large values of N. Hence in this area we attempted to use the spectrum obtained by Kulikov and Khristiansen [24] and recalculate $C(n, \sigma)$. In doing so we further took $\varkappa$ = 1.36 for $N < 10^5$. The results of the comparison of the expected values of $C(n, \sigma)$ for both versions of the calculation with experimental data are given in Figure 9.

We consider that in the region of showers, $N = 10^5 - 5 \cdot 10^5$, the spectrum usually taken is too high and that, beginning with $N > 10^5$ the spectrum probably has only one exponent $\varkappa \approx 1.7$.

The diurnal curve of the frequency of extensive atmospheric showers with $N = 2 \cdot 10^4$ is given in Figure 10. A semi-diurnal frequency wave with an amplitude of the order of 1% and a maximum at 4 - 5 A.M. and 4 - 5 P.M. is fairly pronounced. This wave may be due to corresponding diurnal variations in the mass of the atmospheric column above the observation point.

Data from the observations are still being processed, and we hope to be able to communicate the results in the near future.

Conclusion

The construction and start-up and operation of the

apparatus for observing variations in the frequency of extensive atmospheric showers are the result of the efforts of a considerable number of people.

A large part in building the apparatus was played by the overall support, advice and personal participation of S. I. Nikol'skiy. Support and assistance were given by G. T. Zatsepin, Yu. G. Shafer and L. I. Dorman. The following contributed a great deal in designing the circuits and assembling the equipment: A. V. Yarygin, V. V. Kotkin, V. A. Belomestnykh, N. N. Yefimov, M. A. Nifontov, V. A. Orlov, and B. S. Nedzvedskiy.

In processing the observation material great assistance was rendered by F. K. Shamsutdinova and T. F. Panfilova. I take this opportunity of thanking all those concerned.

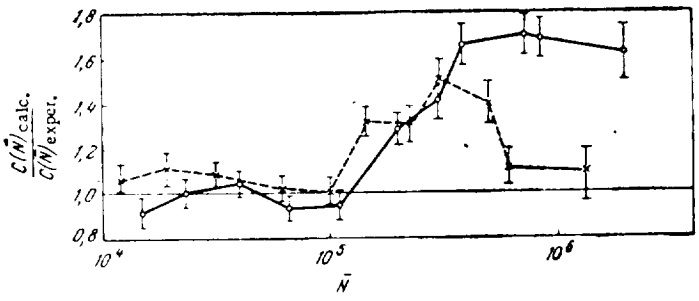

Fig. 9. $C(n, \sigma)_{calc.}$ and $C(n, \sigma)_{exper.}$; X - denotes calculated values, data of reference [24]; 0 - from data of reference [2, 21].

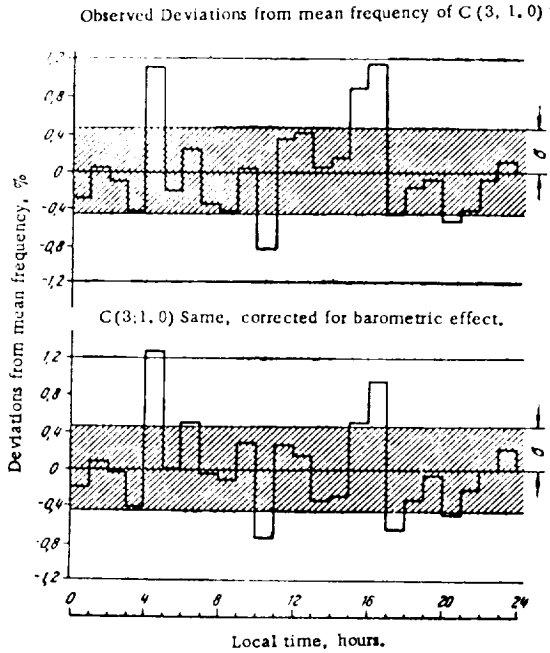

Fig. 10. Diurnal variation of extensive atmospheric shower frequency with $N = 2 \cdot 10^4$ particles.

Bibliography

1. Greisen, K., Progress in cosmic ray physics, III, 1957.
2. Clark, G., J. Earl, J. Kraushaar, J. Kinsley, B. Rossi and F. Scherb. "Nature", 180, p. 406, 1957.

3. Daudin, A. and S. Daudin. J. Atm. Terr. Phys., 3, p. 245, 1933.
4. Cranshaw, T. E. Proc. Oxford Conference, p. 90, April 1956.
5. Koval'skaya, A. I., D. D. Krasil'nikov, and S. I. Nikol'skiy. Trudy Yakutskogo Filsala, AN, SSSR, Physics series, Issue 2, 1957.
6. Dobrotin, N. A., G. T. Zatsepin, I. L. Rozental', L. I. Sarycheva, G. B. Khristiansen, and L. Kh. Eyus. Uspekhi fizicheskikh nauk, 49, p. 195, 1953.
7. Krasil'nikov, D. D. ZHETF, 35, p. 295, 1958.
8. Krasil'nikov, D. D. Present collection, p. 65.
9. Krauskopf, W., Proc. Oxford Conference, April, 1956.
10. Gol'danskiy, V. I., G. B. Zhdanov, N. N. Nesterova, and A. Ye. Chudakov. Izvestiya AN, SSSR, Physics series, 19, p. 747, 1955.
11. Anderson, K. and S. R. Winckler. "Physical Review", 91. p. 431, 1953.
12. Cranshaw, T. E. Proc. Oxford Conference, April, 1956, p. 32.
13. Zatsepin, G. T. Personal communication.
14. Veksler, V., L. Groshev, and B. Isayev. Ionization methods of studying radiation. Moscow-Leningrad, 1950. In Russian.
15. Cranshaw, T. E. and W. Galbraith. "Phil. Mag.", 45, p. 1109, 1954.
16. Blokh, Ya. L., N. N. Dubrovin, and A. A. Sanin, "Pribory i tekhnika eksperimenta", 2, Issue 1, 1957.
17. Yarygin, A. V. Nauchnyye soobshcheniya YaFSOAN SSSR, Issue 1, p. 74, 1958.
18. Zatsepin, V. I., ZHETP, 33, p. 190, 1957.
19. Dobrovol'skiy, S. P., S. I. Nikol'skiy, Ye. N. Tukish, and V. I. Yakovlev. ZHETP, 31, p. 939, 1956.
20. Dobrotin, N. A. Cosmic rays, Gotsekhizdat, 1955. In Russian.
21. Cocconi, G. Handbook Der Physik, 1958.
22. Janossy, L., T. Sandor, Somogyi. Suppl. Nuovo cimento, 8, serie X, p. 701, 1958.
23. Hodson, A. L. Proc. Phys. Soc., A66, p. 49, 1953.
24. Kulikov, G. V., and G. B. Khristiansen. ZHETP, 55, p. 635, 1958.

A. A. Danilov, S. N. Druzhinin, I. N. Kapustin, and G. V. Skripin

COUNTER TELESCOPE FOR MEASURING HARD COMPONENT OF COSMIC RAYS UNDERGROUND

In order to improve the reliability and accuracy of data from continuous observations of the intensity of the μ-meson component in cosmic rays at a level of 60 m w.e., the Yakutsk cosmic ray laboratory added two identical counter telescopes to the existing equipment at the beginning of 1958. Thus the recording statistics for cosmic ray intensity at this level, compared with previous years, were increased by a factor of 1.7. This improves chances of detecting small periodic and non-periodic variations in cosmic-ray intensity at the given depth, and provides further opportunity for checking the operation of individual installations.

The experience in operating the installations described earlier [1,2], and techniques since developed have made it possible, when designing the new installation to take a number of steps to increase the stability and efficiency.

Among the steps are the following:

1) the addition of quench circuits prolonging the life of the counters;

2) automatic control of the stability of the high voltage for feeding the counters;

3) improvement of the parameters of the radio-circuit for triple coincidence selection using semiconductor devices;

4) exclusion of the end effect in the GS-60 counters.

The latter fact makes it possible to take into account the possible contribution of the end effect to various variations in cosmic-ray intensity (by comparing data obtained with the new and old installations). The given installation was mounted on a "cube telescope" manufactured by the Fizpribor Plant. This article describes the blocks and units which were either completely or partially altered; a description of the blocks and units which were left unchanged can be found in [2]. A block diagram of the installation is shown in Figure 1.

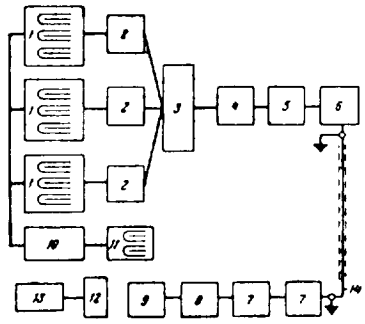

Fig. 1. Block diagram of counter telescope; 1 - Geiger-Muller counter units; 2 - quench circuits; 3 - tripple coincidence radio circuit; 4 - signal amplifier; 5 - scaling cell; 6 - cathode repeater; 7 - scaling cells; 8 - output device; 9 - mechanical counter; 10 - high-voltage rectifier; 11 - monitor counter unit; 12 - control and signalling unit; 13 - register; 14 - 60 m multiconnector cable.

Counter telescope

The counter telescope (Figure 2) consists of three identical blocks of GS-60 working counters placed in three rows in a welded steel, parallelipiped-shaped casing. There is a 10-cm lead screen consisting of 64 lead plates 200 X 100 X 50 mm^3 between the second and third counter blocks.

The counter blocks are placed underneath each other in the telescope stand. The distance from the upper cradle to the lower one is 34 cm. Each block contains 11 GS-60 counters, 9 of which are in one plane and form a telescopic array more or less square in shape and 540 X 550 mm^2 in area. There are two other counters along the edges of these nine counters for exclusion of the end effect.

The principal characteristics of the installation are as follows:

1. Cosmic-ray intensity is recorded vertically and restricted by aperture angles of 120° in the north-south plane and 125° in the east-west plane.

2. The amount of ground above the telescope in a vertical direction is 60 m w.e. The mean energy of the primary particles recorded by the instrument is about 450 Bev.

3. The mean hourly number of readings for two telescopes is 9400 pulse/hour. The statistical accuracy of the measurements over one hour is 1.4%.

4. The directivity pattern expressing the intensity of the particles measured by this apparatus as a function of the angle of their direction of motion with the vertical is given in Figure 3.

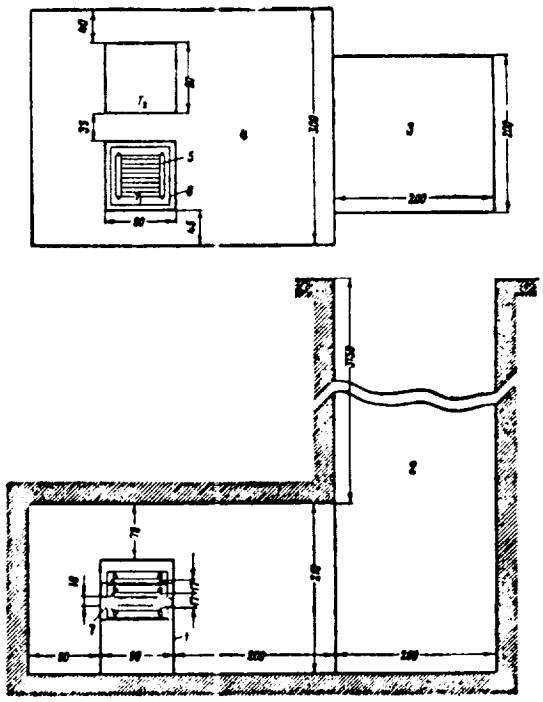

Fig. 2. Geometry of counter telescope. 1 - side view of counter telescope in underground passage; 2 - section of shaft; 3 - view of shaft from above; 4 - view of counter telescopes in passage from above; 5 - counters used to exclude end effect; 6 - welded frame for counter units; 7 - lead screen.

High-voltage rectifier block

The high-voltage rectifier, which is part of the "cube telescope" [2], did not work reliably. There were periodic oscillations in the high voltage on account of insufficient filtration and lagging of the pulses. Hence the first four stages of the rectifier were altered, as shown in Figure 4. The fifth and sixth stages were left unchanged. Pulses from the monitoring counter are fed to the amplifier input. When amplified they pass onto the delay circuit R_5C_2 composed of half a 6Kh2P tube. The time constant is 900 microseconds. The capacitor C_2 is selected in such a way that during the impulse it manages to charge up to the amplitude value and discharge much more slowly through R_5.

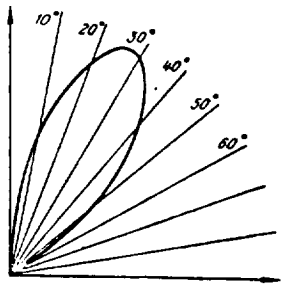

Fig. 3. Radiation pattern.

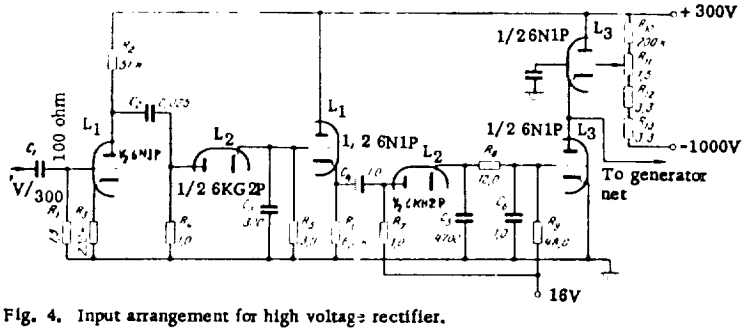

Fig. 4. Input arrangement for high voltage rectifier.

The pulse, elongated by the first pulse stretcher, is amplified by the cathode repeater (half L_1, R_4) and fed to the second stretcher (1/2 L_2, R_7, R_8, C_4), the time constant of which is 300 microseconds. The capacitor C_4 is also charged up to the amplitude value.

The two pulse stretchers used in series in the circuit made it possible to obtain a voltage at the condenser C_4 which is solely a function of the pulse amplitude and not a function of their frequency. The voltage, smoothed out by the filter R_7C_5 is then fed to the voltage divider tube L_3. The second half of this tube receives a rectified negative voltage (-1000 volts) from the generator through the divider $R_9R_{10}R_{11}R_{21}$.

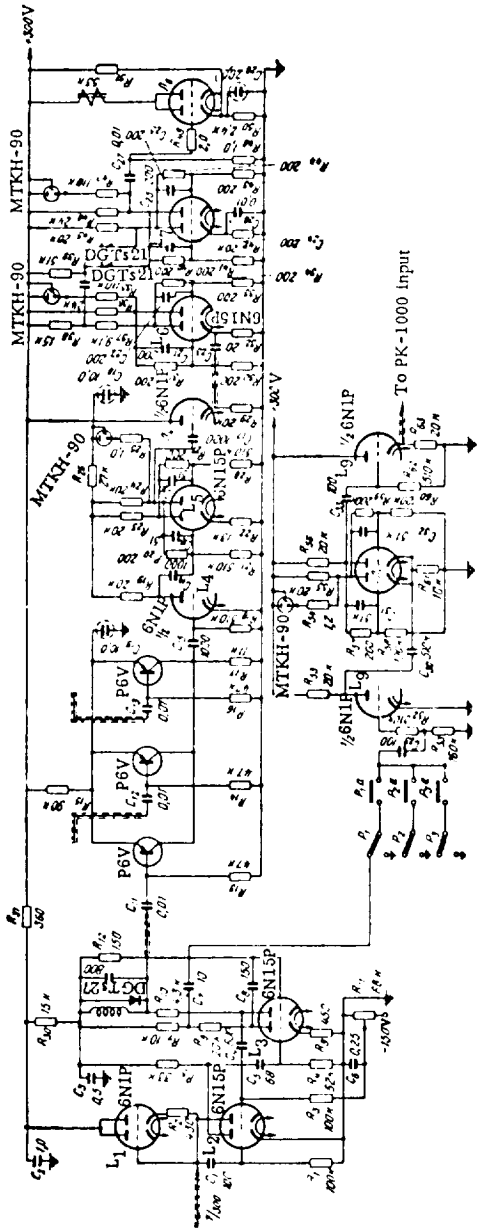

Figure 5. Radio measuring device circuit.

The voltage passes from the divider L_3 to the generator screen grid. Thus, the high voltage generator is controlled along two channels by the screen grid. When the amplitude of the monitoring counter pulse varies, the voltage fed to the generator grid does as well. This causes a variation in the voltage at the generator output; the output voltage varies in such a way that the pulse amplitude remains constant in all the counters. The application of this circuit halted periodic variation ("breathing") of the high voltage.

The circuit is stable during variation in the supply voltage to the anode within 40% and to the filament within 20%.

Quench circuit and triple-coincidence selection

The quench circuit is intended to increase the life of the counters. Experience showed that the quench circuits in the "cube telescope" installation [3] do not meet the requirements of continuous recording; they are unstable, they often oscillate, and the quench factor is too small for practical purposes. Hence we chose one of the tested quench circuits worked out by A. V. Yarygin [4].

Having made some small alterations to his version, we produced the quench circuit shown in Figure 5. It has the following characteristics:

1) quench pulse 250 volts; 2)duration 10 microseconds; 3) rise time 1 microsecond; 4) the counter life is 3-5 times as long. The triple coincidence selection circuit contains P6V transistors connected on Rossi's principle. The voltage at the load R varies whenever positive pulses with an amplitude 2 to 10 v and a duration of at least 1.5 microsec are impressed upon all three transistor bases simultaneously. The circuit functions reliably and is not sensitive to the supply voltage within 15%.

Recording apparatus

The tripe-coincidence pulses as well as those from the single background channels are amplified, scaled to two in the scaling circuits and fed to the cathode repeaters. The triple coincidence and single-channel output pulses taken from the cathode repeater are fed 60 m along the cable. Practice in operating the PK-1000T showed that it worked unreliably (blurred picture, pulses skip the next triggers in turn). We therefore assembled the

triple-coincidence channels in a separate scale unit, leaving it at the same time as a duplicate for the PK-1000T.

The output scaling block consists of two scaling tubes L_6L_7 and an output tube L_8 (Figure 5). A mechanical register is attached to the anode circuit of L_8.

The front panel of the recording device is fitted with four PK-1000T scaling circuits which record signals from the single channels and triple coincidences after scaling by two for each telescope separately, two mechanical triple-coincidence counters after scaling by 8, about 80 small-size mechanical counters which record readings from the neutron monitor, underground units and extensive atmospheric shower units. The recording apparatus also includes a RSK-1G reversible counter which is coupled to the flare recording circuit. The RSK-1G counter is joined by one input to the local pulse generator while the other input is attached to the triple coincidences of the ground-level telescopic unit. The RSK-1G is not photographed.

A FR-2 photorecorder photographs the front panel every 15 minutes. The PK-1000T readings are taken every two hours in the case of the triple coincidences, every 15 minutes in the case of the single-counter monitor and every hour in the case of the RSK-1G. In case of a sharp increase in cosmic ray intensity (10%), the frequency of the photographing is increased automatically. The recording of a burst of activity does not disturb the normal functioning of the recorder.

The above described apparatus has been working since February 1, 1958, and recorded data are being sent to a world center under the IGY agreement.

The efficiency of the installations can be seen from the following data for operation from February 1 - December 31, 1958.

Causes of interruption in operation of installation	Stoppage time as % of total operating time
Through the fault of servicing personnel...	3,0
Malfunction in main power supply	1,5
Precautionary measures...	1,0
Break-down of apparatus...	2,5
TOTAL...	8,0

It will be clear from these data that given good organization of the operation of the installation, stoppages can be reduced to 3.5% of the entire operating time.

We should point out in conclusion that all work on designing, assembling and adjusting the installation was carried out under the guidance of A. I. Kuz'min, to whom the authors of the article wish to express their appreciation.

Bibliography

1. Kuz'min, A. I., G. V. Skripin, and A. V. Yarygin, Trudy YaFAN SSSR, Physics Series, Issue 2, 1958.
2. Kuz'min, A. I. and A. V. Yarygin, Ibid.
3. Description of and instructions for adjusting "cube telescope" unit made by "Fizpribor" Plant. Moscow, 1957.
4. Yarygin, A. V., Informatsionnoye soobshcheniye YaFAN SSSR, Issue 1, 1958.

F
6
7

S. V. Makarov

SOME COUNTER TELESCOPE CALCULATIONS. ILLUMINATION OF VERTICAL TELESCOPE

The parallelepiped $A_1B_1C_1D_1$ $A_2B_2C_2D_2$ is a schematic representation of a telescope aimed at the zenith (Figure 1). The bases $A_1B_1C_1D_1$ and $A_2B_2C_2D_2$ consist of cosmic ray particle detectors and represent the telescope's sensitive planes. Let us adopt the following designations: T is the vertical counter telescope $A_1B_1C_1D_1$ $A_2B_2C_2D_2$, a is A_1B_1, b is A_1D_1, l is A_1A_2, P_1 is the base $A_1B_1C_1D_1$, and P_2 is the base $A_2B_2C_2D_2$.

The telescope T works on the basis of coincidences; the ionizing particle is recorded by the telescope if, and only if, it passes through both P_2 and P_1.

The angular distribution of the total ionizing component in the cosmic rays is given in the form

$$J = (\theta, A) = J_0 \cos^{\gamma}\theta, \qquad (1)$$

where θ is the zenith angle, A is the azimuth, $J(\theta A)$ is the intensity in the direction (θ, A), i.e., the number of particles in the direction (θ, A) in a unit of solid angle per unit area normal to the direction (θ, A) per unit of time ($cm^{-2} \cdot sec^{-1} \cdot ster^{-1}$); J_0 is the verticle intensity; γ is the angular distribution parameter which mainly depends on the thickness h of the layer of matter expressed in meters of water equivalent which the particle can pass through prior to being recorded. On the basis of numerous experiments it can be taken (see, for example, [1,2]) that

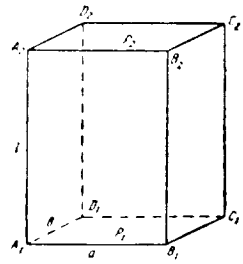

Fig. 1. Vertical counter telescope

$$0 \leqslant \gamma \leqslant 4. \qquad (2)$$

Let us solve the following problem. How many particles will the telescope T record in a unit of time if the angular distribution of the intensity takes the form of (1)?

Let us introduce the coordinate systems $x_1y_1z_1$ and $x_2y_2z_2$ (Figure 2). The axes z_1 and z_2 coincide both with each other and with the edge A_1A_2, and are parallel to the vertical. Let us separate out in the plane P_1 the elementary area

$$dS_1 = dx_1 \cdot dy_1,$$

and in the plane P_2 the area

$$dS_2 = dx_2 \cdot dy_2.$$

It follows from (1) that the number of particles dN passing through dS_1 and dS_2 per unit of time can be expressed by the formula

$$dN = J_0 \frac{l^{2+\gamma} \cdot dS_1 \cdot dS_2}{[l^2 + (x_2 - x_1)^2 + (y_2 - y_1)^2]^{\left(2+\frac{\gamma}{2}\right)}}. \qquad (3)$$

Consequently, the entire telescope will record per unit of time N particles:

$$N = J_0 \int_0^a \int_0^a \int_0^b \int_0^b \frac{l^{3+\gamma} \cdot dx_1\, dx_2 \cdot dy_1\, dy_2}{[l^2 + (x_2 - x_1)^2 + (y_2 - y_1)^2]^{\left(\frac{3}{2} + \frac{\gamma}{2}\right)}} =$$

$$= J_0 \frac{a^2 b^2}{l^3} \int_0^1 \int_0^1 \int_0^1 \int_0^1 \frac{dx_1\, dx_2\, dy_1\, dy_2}{[1 + \alpha^2 (x_2 - x_1)^2 + \beta^2 (y_2 - y_1)^2]^{\left(\frac{3}{2} + \frac{\gamma}{2}\right)}}, \tag{4}$$

where

$$\alpha = \frac{a}{l}, \quad \beta = \frac{b}{l}. \tag{5}$$

Let us substitute the variables

$$\left.\begin{aligned} x_2 - x_1 &= u_1, \\ x_2 &= v_1, \\ y_2 - y_1 &= u_2, \\ y_2 &= v_2 \end{aligned}\right\} \tag{6}$$

Then (4) is easily transformed into

$$N = J_0 \frac{4a^2 b^2}{l^3} \int_0^1 \int_0^1 \frac{(1-x)(1-y)}{(1 + \alpha^2 x^2 + \beta^2 y^2)^{\frac{3}{2} + \frac{\gamma}{2}}}\, dx\, dy. \tag{7}$$

The expression

$$L = \frac{4a^2 b^2}{l^3} \int_0^1 \int_0^1 \frac{(1-x)(1-y)}{(1 + \alpha^2 x^2 + \beta^2 y^2)^{\frac{3}{2} + \frac{\gamma}{2}}}\, dx\, dy \tag{8}$$

will be termed the illumination of the telescope T.

Let us rewrite (7) in the form

$$N = J_0 L. \tag{9}$$

The equality (9) can be regarded as the definition of illumination for a telescope of arbitrary configuration. If a, b, l, and γ are known, the values of N can be found by using one of the iterated quadrature formulae (for example, Simpson's 2-dimensional formula [3]).

Inverse problem. It is intended to use equation (9) to solve the inverse problem, i.e., to find J_0 and γ from measurement of the N_1 and N_2 with two vertical telescopes.

At a certain level h let there be two vertical telescopes T_1 and T_2 with the dimensions a_1, b_1, l_1 and a_2, b_2, l_2. For T_1 we have the relationship

$$L_1 = L_1(\gamma) \tag{10}$$

and for T_2 a similar relationship

$$L_2 = L_2(\gamma). \tag{11}$$

Let us assume that $L_1(\gamma)$ and $L_2(\gamma)$ are tabulated for $\gamma \subset (0.4)$. We can then write the following set of equations on the basis of (7).

$$\left.\begin{aligned} N_1 &= J_0(h) \cdot L_1[\gamma(h)], \\ N_2 &= J_0(h) \cdot L_2[\gamma(h)]. \end{aligned}\right\} \tag{12}$$

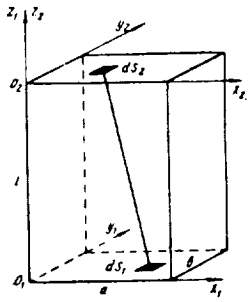

Fig. 2. Coordinate systems.

The values N_1 and N_2 are measured with the telescopes T_1 and T_2. We are required to find J_0 and γ. It follows from (12)

$$\frac{L_1(\gamma)}{L_2(\gamma)} = \frac{l'_1}{l'_2}. \tag{13}$$

Let us define

$$\frac{N_1}{N_2} = q. \tag{14}$$

Finally we have

$$L_1(\gamma) = q \cdot L_2(\gamma). \qquad (15)$$

The factor q is known from observations. Provided $L_1(\gamma)$ and $L_2(\gamma)$ are tabulated, (15) can easily be solved with respect to γ. Knowing γ, we find J_0 from equation (12).

In this way we find γ (h) and J_0 (h) from data from two stationary installations at the level h on the ground or beneath it. The use of this method for investigations in the atmosphere is also possible. If two radiosounding balloons are sent up into the atmosphere at the same time, carrying counter telescopes differing in geometrical parameters, it is possible in principle to obtain γ(h) and J_0 (h) for the entire section of the atmosphere, right up to the sounding ceiling. Admittedly, in this case it would be difficult to ensure sufficient accuracy in the result on account of the balloons rocking during the ascent.

Similar problems can be solved for telescopes of any shape and orientation.

Example of numerical calculation. Directivity pattern of counter telescope.

Figure 3 shows a schematic representation of the counter telescope at the Cosmic Ray Laboratory of the Yakutsk Branch of the Siberian Division of the Academy of Sciences at the bottom of a shaft 20 m deep.

The planes P_1P_2 and P_3 consist of counters. The telescope works on triple coincidences, i.e., the ionizing particle is recorded by the telescope only if it passes through all three sensitive planes P_1, P_2 and P_3.

We are given the angular distribution function (1). The telescope is pointed towards the zenith, and, consequently, the planes P_1, P_2, and P_3 are perpendicular to the vertical.

We are required to calculate the telescope's directivity pattern, i.e.,

$$b(\theta, A) = \frac{dN}{d\omega} = \frac{dN}{\sin\theta d\theta dA}, \qquad (16)$$

where b (θ, A) is the density of the cosmic particle stream referred to a unit of solid angle $d\omega$ in the direction (θ, A).

Using (1), we find the number of particles dN going in the direction (θ, A) and recorded by the telescope:

$$dN = J(\theta, A)\cos\theta \cdot d\omega \cdot S(\theta, A) = J_0 \cos^{\gamma+1}\theta \cdot \sin\theta \cdot d\theta \cdot dA \cdot S(\theta, A) \quad (17),$$

where S (θ, A) is the part of the plane P_1 illuminated by those cosmic rays moving in the direction (θ, A) and providing triple coincidences.

The exact meaning of S (θ, A) will become clear after consideration of the following geometrical problem.

Let us remove the planes P_2 and P_3 from the counter installation depicted in Figure 3. Let the figure thus obtained be illuminated by a parallel pencil of light, the direction of which is given by the angular coordinates θ, A. We are required to determine the area of the illuminated part of the plane P_1. The unknown area is equal to S(θ, A) in the right hand side of (17). The numerical value of S(θ, A) can be found using a geometrical construction, the description of which will be left out on account of its simplicity.

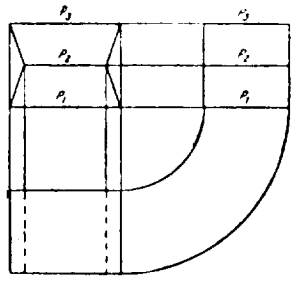

Fig. 3. Schematic drawing of telescope set up in shaft.

From (16) and (17) it follows that

$$b(\theta, A) = J_0 \cos^{\gamma+1}\theta \cdot S(\theta, A). \quad (18)$$

The proposed method of calculating the directivity pattern {b (θ, A)} could naturally be called the "light-spot method", since we have used the analogy of a spot of light.

The table {b, (θ, A)} can be used to calculate the effective screen of the installation from the formula

$$T = \frac{1}{N}\iint r(\theta, A)\sin\theta\, b(\theta, A)\, d\theta\, dA, \qquad (19)$$

where r (θ, A) is the path (in meters of water equivalent) traversed by the particle prior to

being recorded. By making a numerical integration, we can find the illumination L of the given installation (Figure 3) from the direction pattern.

$$L = \frac{N}{J_0}. \qquad (20)$$

Conclusion

The term "illumination of a counter telescope" has been suggested by A. I. Kuz'min, a junior staff member of the Cosmic Ray Laboratory attached to the Yakutsk Branch of the Siberian Division of the Academy of Sciences. All the computations which we have discussed in this article were made on his advice. A. P. Shapiro, a teacher at the Yakutsk State University, has pointed out the advisibility of the transformation (6). This article was written at the suggestion of the Scientific Council of the Cosmic Ray Laboratory.

Bibliography

1. Wilson, J., (ed.), Cosmic Ray Physics, vol. I, Moscow, 1954.
2. Dobrotin, N. A., Cosmic Rays, Moscow, 1954, In Russian.
3. Mikeladze, Sh. Ye., Numerical methods of mathematical analysis. Gostekhizdat, 1953.

B. S. Shalamov

PLOTTING AN IDEALIZED VOLT-AMPERE CHARACTERISTIC FOR A TWO-TERMINAL NETWORK CONTAINING A POINT-CONTACT TRANSISTOR WITH ALLOWANCE FOR THE TEMPERATURE EFFECT

On the basis of static output characteristics of a point-contact transistor obtained at temperatures of 0, 20 and 50° C, we analytically calculate and plot the volt-ampere characteristic of a circuit containing a unit with negative dynamic resistance. The conductivity of the electronic semiconductors is highly dependent on temperature:

$$\alpha = \alpha_0 e^{-\frac{\Delta E}{2kT}},$$

where ΔE is the activation energy of the current carriers in electron volts, T is the temperature in absolute degrees, and $k = 1.38 \cdot 10^{-16}$ erg/deg is the Boltzmann constant.

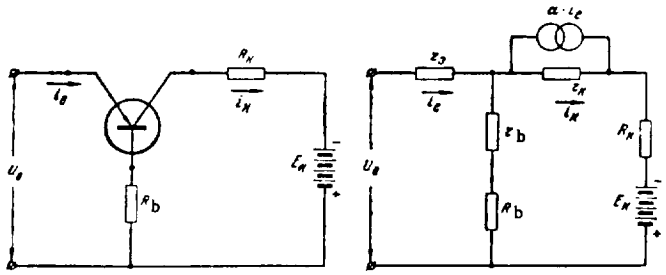

Fig. 1. a - two-terminal network including point-contact transistor; b - its equivalent circuit.

A variation of several tens of degrees in the temperature of a semiconductor considerably alters its electric characteristics. Hence, when calculating circuits containing transistors, we must definitely take the temperature effect into account. It has been given on many occasions for amplifying circuits using junction transistors, but for pulse circuits the problem has not been investigated sufficiently fully as yet.

Figure 1a shows a conventional two-terminal circuit with input to the transistor emitter. In [1] the volt-ampere characteristic $u_e = f(i_e)$ is plotted graphically for this circuit, and a true volt-ampere characteristic is obtained as a result, i.e., the method does not necessitate any assumptions. But it is laborious to plot. For engineering purposes satisfactory accuracy is provided by an analytically calculated idealized volt-ampere characteristic. Hence, in our case we use an idealized characteristic to evaluate the temperature effect.

Setting up a Kirchoff equation, we have from Fig. 1b

$$u_e = i_e(r_e + r_b + R_b) + i_н(r_b + R_b), \quad (1)$$

$$-E_н = i_e(r_b + R_b + \alpha r_к) + i_н(r_b + r_к + R_b + R_н). \quad (2)$$

From which we can obtain an analytical expression for the volt-ampere characteristic

$$u_e = \left[r_e + \frac{(R_b + r_b)[R_н + r_к(1-\alpha)]}{R_b + r_b + R_н + r_к}\right] i_e - \frac{(R_b + r_b)E_н}{R_b + r_b + R_н + r_к}. \quad (3)$$

The characteristic is shown in Figure 2. In a normally functioning circuit the currents and voltages vary over a wide range. To plot the characteristic we clearly only need to know the coordinates of the bending points for the cut-off areas, active area and saturation area. Taking into account the parameters in these three areas, we obtain

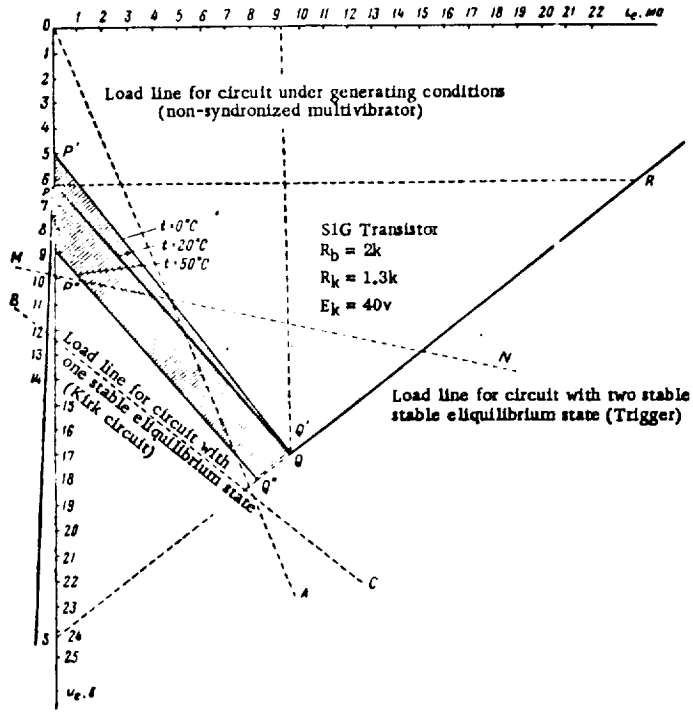

Fig. 2. Volt-ampere characteristic $u_e = f(i_e)$.

$$P:\ i_e = 0,\quad u_e = -\frac{R_b}{R_b + R_k + r_k} E_k; \tag{4}$$

$$Q:\ i_e = \frac{E_k}{\alpha(R_b + R_k) - R_b},\quad u_e = \frac{R_k(1-\alpha)}{\alpha(R_b + R_k) - R_b}; \tag{5}$$

$$S:\ i_e = 0,\quad u_e = -\frac{E_k R_b}{R_b + R_k}. \tag{6}$$

When the surrounding temperature varies, the two parameters of the point contact transistor r_k and α vary to the greatest extent.

As can be seen from expressions (4), (5) and (6), these parameters are part of the formulae for calculating the volt-ampere characteristic. r_e and r_b also vary, but we shall not take them into account since they do not come into the calculation. To plot the volt-ampere characteristic of the two-terminal network all we need is a set of static output characteristics for the transistor. Figure 3 shows the output characteristics of a SIG point-contact transistor obtained with the use of the described graph [2] for temperatures of 0, 20 and 50° C.

The sequence for plotting $u_e = f(i_e)$ is as follows: we select E_k.

Usually $E_k = (1.5 + 2)\ V_k$, where V_k is the pulse amplitude. As shown in Figure 3, the load line should pass through the points E_k and A. The resistance of the collector junction to direct current is

$$r_{\text{пост}} = \frac{V_k}{i_{k0}}.$$

To find α, we must extend the load line into the area where $i_e \neq 0$.

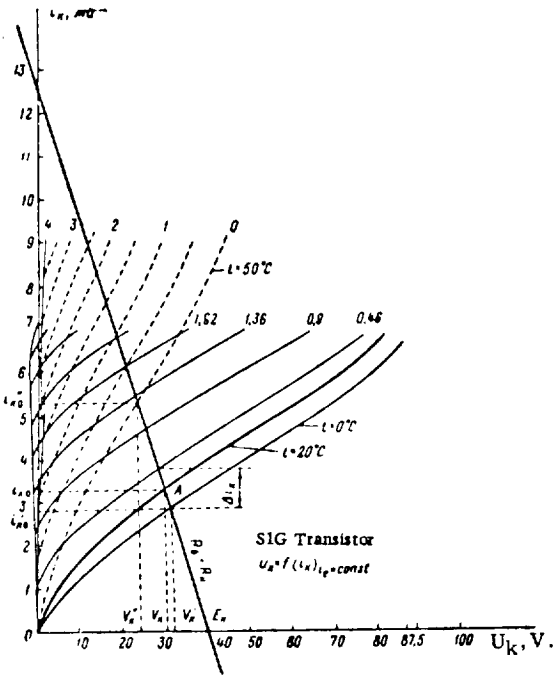

Fig. 3. Output characteristics of SIG triode taken at t = 50°C.

$$\alpha = \frac{\sum_{1}^{n} \left(\frac{\Delta i_k}{\Delta i_e} \right)}{n}.$$

We calculate r_k and α at T_1, T_2, and T_3, and for each T we find the bending point coordinates.

From this data we plot an idealized volt-ampere characteristic taking temperature into account. In Figure 2 the shaded area represents the shift in the volt-ampere characteristic during variation in temperature.

The effect of the temperature on the shape of the volt-ampere curve can conveniently be studied with an oscillograph circuit. A practical circuit for this is given in Figure 4.

In conclusion I would like to express my appreciation to Yu. G. Shafer for his assistance in carrying out this research.

Bibliography

1. Brodovich, N. I., Graphical method of plotting volt-ampere characteristic for two-terminal network containing transistor, Avtomatika i telemekhanika, XVII, No. 4, 1956.
2. Shalamov, B. S., Experimental characteristic curve for transistors, Izv. Sibirskogo otd. AN SSSR, (in print).

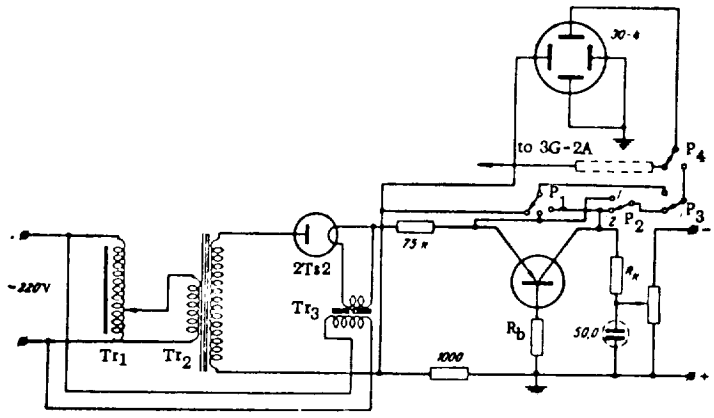

Fig. 4. Circuit for oscilligraphing dynamic characteristics $u_e = f(i_e)$ and $i_k = f(i_e)$.

Section II

PART PLAYED BY METEOROLOGICAL FACTORS IN VARIATIONS IN DIFFERENT COSMIC RAY COMPONENTS

L. I. Dorman

CALCULATION OF TEMPERATURE EFFECT OF COSMIC RAYS FROM ISOBAR SURFACE HEIGHTS

At the present time the Soviet Cosmic Ray station network is calculating the temperature effect from the formula (see [1], chapter 5)

$$\frac{\delta N}{N} = \int_0^{h_0} W_T(h)\,\delta T(h)\,dh, \tag{1}$$

where $\delta N/N$ is the variation in cosmic ray intensity reduced to the constant pressure, h_0, $W_T(h)$ is the density of the temperature coefficient, and $\delta T(h)$ is the variation in temperature at corresponding isobar levels. This method has been recommended at the present time by the Cosmic Ray Working Group of the Special Committee for the International Geophysical Year as one of the main ways of calculating temperature corrections. Nevertheless, many world stations do not send in their meteorological data in the form of a temperature cross section for the basic isobars, as required for this method, but rather in the form of the heights of different isobars, as required for Duperier's method [2] (which is inaccurate, as shown in [3]). Here we would like to show how these meteorological data can be used for our method. Their use also makes it possible to exclude radiation errors.

The height H of the isobaric surface with a pressure h is

$$H = \int_h^{h_0} \frac{dh'}{\rho(h')}, \tag{2}$$

where $\rho(h')$ is the air density at the level h'. The variation in this height is

$$\delta H = \frac{\delta h_0}{\rho(h_0)} - \int_h^{h_0} \frac{\delta\rho(h')\,dh'}{\rho^2(h')} = \frac{\delta h_0}{\rho(h_0)} + \int_h^{h_0} \frac{R}{h'}\,\delta T(h')\,dh', \tag{3}$$

in which it is taken into account that $\rho(h) = h/RT$. Differentiating expression (3) with respect to h, we find

$$\frac{d\delta H}{dh} = -\frac{R}{h}\,\delta T(h), \tag{4}$$

from which

$$\delta T(h) = -\frac{h}{R}\,\frac{d\delta H}{dh}. \tag{5}$$

Substituting expression (5) into Formula (1) we obtain:

$$\frac{\delta N}{N} = -\int_0^{h_0} \frac{h}{R}\,W_T(h)\,\frac{d\delta H}{dh}\,dh. \tag{6}$$

The integral in the right hand side of (6) will be integrated by parts:

$$\frac{\delta N}{N} = -\frac{hW_T(h)\,\delta H}{R}\Bigg|_0^{h_0} + \int_0^{h_0}\left[\frac{W_T(h)}{R} + \frac{hW'_T(h)}{R}\right]\delta H\,dh. \qquad (7)$$

Here the first term becomes zero (provided $W_t(O)\,\delta H(O) < \infty$), and we will represent the second term in the form of a sum, breaking down the area of pressures $0 - h_o$ into n intervals $h_i = h_o, \ldots h_{n+1}, 0$:

$$\frac{\delta N}{N} = \sum_{i=1}^{n}\int_{h_{i+1}}^{h_i}\frac{1}{R}\left[W_T(h) + hW'_T(h)\right]\delta H\,dh. \qquad (8)$$

If $h_i - h_{i+1}$ is sufficiently small, by placing $\delta H_{i+1/2}$ lying between δH_i and δH_{i+1} before the integral sign, we obtain

$$\frac{\delta N}{N} = \sum_{i=1}^{n}\frac{\delta H_{i+1/2}}{R}\int_{h_{i+1}}^{h_i}\left[W_T(h) + hW'_T(h)\right]dh =$$

$$\sum_{i=1}^{n}\frac{\delta H_{i+1/2}}{R}\left[\int_{h_{i+1}}^{h_i} W_T(h)\,dh + hW_T(h)\Big|_{h_{i+1}}^{h_i} - \int_{h_{i+1}}^{h_i} W_T(h)\,dh\right] =$$

$$= \sum_{i=1}^{n}\frac{\delta H_{i+1/2}}{R}\left[h_i W_T(h_i) - h_{i+1}W_T(h_{i+1})\right] = \sum_{i=1}^{n}\varkappa_{i+1/2}\delta H_{i+1/2}, \qquad (9)$$

where

$$\varkappa_{i+1/2} = \frac{1}{R}\left[h_i W_T(h_i) - h_{i+1}W_T(h_{i+1})\right]. \qquad (10)$$

From (10) it is clear that if

$$W_T(h) = \frac{a}{h}, \qquad (11)$$

where a is a constant, then all $\varkappa_{i+1/2} = 0$. It is easy to see that if (11) is the case, the second term in the right hand part of expression (7) identically becomes zero. For practical purposes the state of the atmosphere is determined from the level h_o to a level $\bar{h}$ at a height still within reach of the radiosondes. Then, if (11) is satisfied, we obtain from (7)

$$\frac{\delta N}{N} = \frac{a\delta H(\bar{h})}{R} = \beta\delta H(\bar{h}). \qquad (12)$$

where $\beta = a/R$ is the "decay" coefficient found by Duperier [2]. It is clear from this (as pointed out in [3]) that the method of calculating the temperature effect from Formula 912) is only valid if expression (11) is chosen as $W_T(h)$ which generally speaking is untrue.

If $W_T(h)$ found from analysis of generation and propogation of the μ-meson component through the atmosphere differs substantially from (11), then Formula (12) is not valid and the following formula should be used

$$\frac{\delta N}{N} = \frac{\bar{h}W_T(\bar{h})}{R}\delta H(\bar{h}) + \sum_{i=1}^{n}\varkappa_{i+1/2}\delta H_{i+1/2}, \qquad (13)$$

where $\varkappa_{i+1/2}$ is determined by expression (10), and the layer from $h_o - \bar{h}$ is divided into n intervals (here we ignore the effect of the layer from $\bar{h} - 0$). The results of calculation of $W_T(h)$ are given in [1] for different recordings. If h is measured in atmospheres and $W_T(h)$ is measured in %/atm. °C., then R = 0.029 km/°C. The values $\bar{h}W_T(\bar{h})/R$ and $\varkappa_{i+1/2}$ will be in %/km (the values of δH are measured in km).

The factors $\bar{h}W_T(\bar{h})/R$ and $\varkappa_{i+1/2}$ can easily be calculated from known $W_T(h)$ for any case of recording and any break-down of the atmosphere. An example of this calculation is given in Table 1 (where it is assumed that $\bar{h} = 0.05$).

It should be pointed out that use of Formula (13) is of a certain advantage over the error calculation in [4]. First of all, according to (3), the differences in height variation determine certain effective temperatures of layers, whereas in [4] use is made of the temperature of certain levels measured, naturally enough, less accurately. Second, if δH_i is measured by some other independent means rather than temperature cross-section, Formula (13) makes it possible to avoid errors involved in radiation heating of the temperature pick-ups in the sondes, which is

Table 1. Values of factors (in %/km) for isobaric level of height corrections form Formula (13) for screened ionization chamber at the sea level.

$\varkappa_{0.85}$	$\varkappa_{0.60}$	$\varkappa_{0.45}$	$\varkappa_{0.35}$	$\varkappa_{0.25}$	$\varkappa_{0.175}$	$\varkappa_{0.125}$	$\varkappa_{0.085}$	$\varkappa_{0.06}$	$\frac{\overline{hW}_1(\bar{h})}{R}$
−2,03	−1,00	−0,55	−0,60	−0,83	−0,44	−0,47	−0,26	−0,26	−0,66

particularly important when excluding the meteorological effect of the upper layers of the atmosphere, where these errors are usually very large and make it very difficult to study many types of cosmic ray variation (solar-diurnal, sidereal-diurnal, and so on).

Bibliography

1. Dorman, L. I., Cosmic-ray variations, Gostekhizdat, 1957
2. Duperier, A., J. Atm. Terr. Phys., 1, p. 296, 1951.
3. Dorman, L. I., Doklady AN SSSR, 95, p. 443, 1954.
4. Glokova, Ye. S., L. I. Dorman, and N. S. Kaminer. Instructions on meteorological corrections to cosmic-ray data. Moscow, NIIZMIR, 1948.

A. I. Kuz'min and A. A. Danilov

METEOROLOGICAL EFFECTS OF COSMIC RAYS AT DEPTHS OF LESS THAN 100 m w.e. UNDERGROUND

The study of the meteorological effects of the cosmic ray intensity underground makes it possible to obtain information on the competitive processes of absorption and decay of particles generating μ-mesons, on the number of μ-mesons generated by particles differing from π-mesons, on the dynamics of the meteorological state of the lower stratosphere, and on the part played by radiation effects in measuring the atmosphere's temperature. Evaluation and calculation of these effects are also needed for study of time variations in cosmic-ray intensity which can provide important information on cosmic rays from the cosmological point of view.

The meteorological effects of cosmic-ray intensity I underground have been studied to some extent [1-4]. One such publication [2] relates to a depth of 60 m w.e., while the rest deal with depths greater than 800 m w.e. This article concerns meteorological effects of cosmic rays at depths of 7, 20 and 60 m w.e.

In 1957, using standard counter apparatus [7] synchronous measurements [6] of I were begun at three levels, 7, 20 and 60 m w.e., below ground, in addition to measurements on the earth's surface itself, in order to obtain information on the energy characteristics of the variations in I and to test the theory of them [5]. The radio engineering installations [7] at 7 and 20 m w.e., were augmented with quench circuits [8,9], and at 60 m w.e., two extra standard semi-cube telescopes were put into operation [9].

As initial material for consideration of the meteorological effects of I we took the mean daily values of cosmic ray intensity at each level and the corresponding barometric pressures and free atmosphere temperatures.

The latter information is supplied by the Yakutsk Meteorological Service. The mean diurnal I are taken as the mean two-hourly values $\sum_{12}^{24} I_i$, where I_i is the intensity over the i-th hour. In the installations which have duplicating channels, I_i designates the sum of the readings for the i-th hour. For instance, for the 20 m w.e. level $I_i = I_i^1 + I_i^2$, and for 60 m w.e. $I_i = I_i^1 + I_i^2 + I_i^3 + I_i^4$, where the superscripts 1, 2, 3 and 4 show the number of the duplicating units.

The mean diurnal statistical accuracy of the measurement of I on the earth's surface and at 7, 20 and 60 m w.e. is equal to 0.07, 0.09, 0.10 and 0.14%, respectively. This accuracy is sufficient to obtain reliable results at all levels $I_\odot$

When compiling correlation equations to segregate the barometric temperature effects, we discarded cases of possible systematic variations which were not due to temperature or barometric effects.

In particular, we discarded cases of effective magnetic storms and took steps to exclude long-periodic variations in I which might accidentally correlate with meteorological factors.

In investigating meteorological factors, it is important to take proper account of the distributed temperature effect of the free atmosphere, which in the case of an actual non-equilibrium atmosphere, as shown by Feynberg [10], cannot be reduced to the concept of a single-temperature effect.

Later on, this probelm was considered by Dorman for the case of a "two-meson" system of hard component generation in a series of studies, the chief results of which are given in his monograph [5].

In considering the theory of the meteorological effect of the hard component in cosmic rays,

V. Dorman [5] proceeded from the conventional view that the μ -meson component is generated by π -mesons throughout the atmosphere on the basis of a law corresponding to the law of absorption of μ -meson generating components. The conclusions from this theory, just as those from the single meson theory [10], can be shown in the form

$$\frac{\delta N_\mu}{N_\mu} = \beta_0 \delta h_0 + \int_0^{h_0} W(h)\,\delta(h)\,dh. \qquad (1)$$

Here β_0 is the barometric factor, W(h) is the temperature coefficient density characterizing the role played by different atmospheric layers in causing the temperature effect. In this formula $W(h) = W^{\pi}(h) + W^{\mu}(h)$, where $W^{\pi}(h)$ is the positive temperature effect due to the competition between decay and absorption of π -mesons, while $W^{\mu}(h)$ is the negative temperature effect due to the decay of μ-mesons.

Figure 1 shows the densities of the temperature effect W(h) which we calculated for our experimental recordings of μ-mesons by approximate formulae which provide, according to Dorman [11], sufficient accuracy when observing at sea level and to a certain depth underground.

It is clear from Figure 1 that the negative μ -meson effect declines sharply with depth (it is approximately inversely proportional to the depth), whereas the positive temperature effect increases, and is predominant at 60 m w.e. These calculations tally closely with Dorman's [5] for other recording depths (25, 55, 150, 300, 550, and 100 m w.e.).

Using these curves we calculated the expected temperature effects $\delta N_\mu / N_\mu$ for each depth, and from then on used them to compile correlation equations. The mean diurnal values of $\delta N_\mu / N_\mu$ were calculated from three daily sets of data obtained by readings in Yakutsk at 0206 hours, 0806 hours, and 2006 hours, local time.

The $\delta N_\mu / N_\mu = \int_0^{h_0} W(h)\,\delta T\,\delta h$ was calculated up to a height h = 50 mb. The mean daily barometric pressure was calculated from hourly barograph readings $\bar{h} = \frac{1}{12}\sum_1^{24} h_i$.

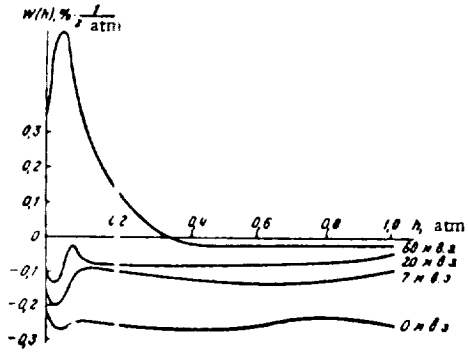

Fig. 1. Total density of temperature coefficient for semi-cubic telescope on earth's surface and at 7, 20 and 60 m w.e. underground.

For this study we used observational data obtained from Dec. 1, 1957 to October 30, 1958. Evaluation of meteorological effects of I underground is carried out by examining the variation in the number of coincidences N as a function of the cahnge in the barometric pressure h and the temperature at the observation point. Instead of the temperature of a particular layer, we take the expected effect calculated by Formula (1).

It is assumed that the variations can be described by the equation

$$I - \bar{I} = \beta(h - \bar{h}) + \alpha(W - \bar{W}), \qquad (2)$$

where I, h and W are the mean diurnal μ-meson intensities at the given depth, the barometric pressure of the earth's surface and the expected intensity, respectively, while $\bar{I}$, $\bar{h}$ and $\bar{W}$ are the corresponding mean values over the period under consideration.

The table gives the results of the calculation. The following symbols are used:

$r_{Ip(W)}$ — Is the partial correlation factor between intensity and barometric pressure p for constant W.

$r_{IW(p)}$ — Is the partial correlation factor of the intensity I and W at for constant p.

β — Is the barometric factor determined experimentally.

Δr — Is the mean square error for the correlation factor $\left(\Delta r = \pm 0{,}67\frac{1-r^2}{\sqrt{N}}\right)$.

$\Delta\beta$ — Is the mean square error for the regression factor $\left(\Delta\beta = \pm\frac{\sigma_I}{\sigma_p}\sqrt{\frac{1-r^2}{N-3}}\right)$.

ρ — Is the correlation ratio $\left(\rho = \sqrt{\frac{r_{1p}^2 + r_{1W}^2 - 2r_{1p}r_{Wp}}{1 - r_{1W}^2}}\right)$,

γ — Is the exponent in the μ-meson integral spectrum.

Furthermore, the table gives the theoretical barometric factor α_T for all recording levels and is calculated from an approximate formula [5].

$$\alpha_T = +\int_0^1 \left\{ -\frac{xe^{-\nu_1(Lx)}}{\varphi_\gamma[S(Lx),\ \nu(Lx)][1+S(Lx)](h_0 - Lx + \Delta\varepsilon)} - \right.$$
$$\left. - \frac{b_\mu(h_0)\chi_\gamma[S(Lx),\ K_0(Lx),\ \nu(Lx)]}{h_0(h_0 - Lx + \Delta\varepsilon)\varphi_\gamma[S(Lx),\ \nu(Lx)]} \right\} I(x)\,dx \Big/ \int_0^1 I(x)\,dx. \qquad (3)$$

The first item describes the absorption effect (α_a), and the second describes the μ-meson decay effect (α_p). In this formula we have ignored the term describing the generation effect. It is extremely small at sea level and underground [5].

In Formula (3) x = cos Θ, where Θ is the zenith angle, $b\mu$ is a parameter depending on the experimental conditions and properties of the μ-mesons, $\varphi_\gamma[S(Lx),\ \nu(Lx)]$ is a function of the μ-meson energy spectrum and parameters χ (Lx) and S(Lx) depending on the experimental conditions and π-meson properties, $\varkappa_\gamma[S(Lx),\ K_0(Lx)]\ \nu(Lx)]$ is a function depending on the μ-meson spectrum and the parameters $S(Lx),\ \nu(Lx)$ and K(Lx), h_0 is the observation level pressure, L is the path of the meson-generating component, and $\Delta\epsilon$ is the minimum effective screen.

The calculations shown in the table demonstrate that the barometric factor must decrease as the observation depth increases, and that at 60 m w.e. it must be less than at sea level by a factor of approximately 4.

It should be pointed out that the quantitative ratio between the absorption and decay effects also varies extremely rapidly with depth. For instance, while at sea level the decay effect is approximately three times greater than the absorption effect, at 7 m w.e. the decay effect is approximately half the other, smaller by a factor of 4 at 20 m w.e. and by a factor of 10 at 60 m w.e. This relationship between the effects hardly depends on the exponent of the μ-meson spectrum when n varies from 2 to 3. Thus, it can be said that the barometric effect at 60 m w.e. is almost entirely due to absorption.

Comparison of the theoretical barometric factors with mean experimental values show that they tally closely. They tally best of all when the integral μ-meson spectrum is

at sea level 1.3
at 7 m w.e. 1.45
at 20 m w.e. 1.7
at 60 m w.e. 2

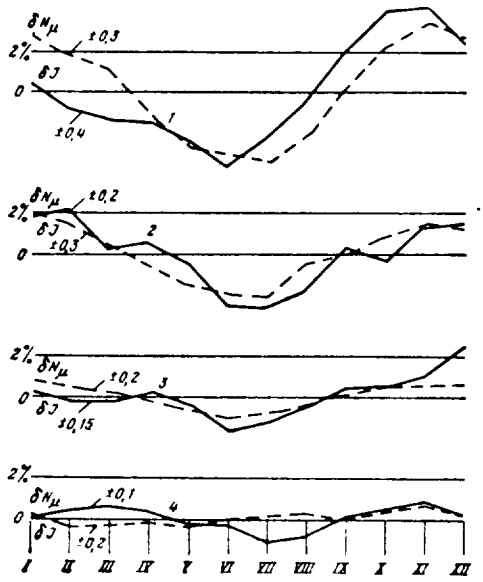

Fig. 2. Seasonal variations in intensity of hard component in cosmic rays at Yakutsk from 1957 to 1958. 1, 2, 3, & 4 - hard component measured with semi-cubic telescope on earth's surface and at 7, 20 and 60 m w.e., respectively, underground.

These effective values of the exponent in the energy spectrum accord well with the exponents determined for each of the installations from the intensity-depth relationship [11].

Apart from the mean correlation and regression factors determined from a great deal of observation material, the table gives values from a brief observation period. The breakdown into short periods was made to avoid the effect of possible random systematic deviations of the

No. in order	Date	Level	n	$r_{Ip(W)}$	Δr_1	$r_{JW(p)}$	Δr_2	ρ	β	$\Delta\beta$	Theoretically calculated barometric factor γ	e_a	e_p	e_T
1	1.XII—19.I 1958	At earth's surface	36	−0.92	±0.02	−0.67	±0.06	0.92	−0.13	±0.01				
2	6.II—23.II	"	42	−0.83	±0.03	−0.73	±0.05	0.84	−0.155	±0.02				
3	1.IV—13.V	"	40	−0.79	±0.04	−0.65	±0.11	0.79	−0.135	±0.02				
4	7.VI—14.VIII	"	47	−0.80	±0.03	−0.45	±0.04	0.86	−0.11	±0.03	0.45	−0.035	−0.105	−0.14
						Mean weight		$\beta = -0.13 \pm 0.01$			0.3	−0.03	−0.09	−0.12
1	12.XII—3.II	7 m w.e. below ground	50	−0.90	±0.02	−0.71	±0.05	0.94	−0.10	±0.01				
2	20.II—17.III	"	26	−0.95	±0.01	−0.91	±0.02	0.95	−0.09	±0.01				
3	1.IV—26.IV	"	28	−0.79	±0.05	−0.28	±0.12	0.81	−0.11	±0.02				
4	IV—29.V	"	29	−0.78	±0.05	−0.49	±0.09	0.90	−0.10	±0.01				
5	14.VII—6.XII	"	24	−0.60	±0.03	−0.21	±0.13	0.57	−0.11	±0.02	0.45	−0.034	−0.065	−0.10
						Mean weight		$\beta = -0.10 \pm 0.01$						
1	XII 1957	20 m w.e. below ground	30	−0.78	±0.06	−0.59	±0.06	0.86	−0.07	±0.01				
2	I 1958	"	31	−0.94	±0.03	−0.32	±0.13	0.96	−0.07	±0.01				
3	II	"	20	−0.81	±0.10	−0.53	±0.10	0.86	−0.07	±0.01				
4	III	"	22	−0.87	±0.04	−0.67	±0.04	0.88	−0.07	±0.01				
5	IV	"												
6	V	"	24	−0.82	±0.11	0.04	±0.11	0.93	−0.08	±0.01				
7	VI	"	25	−0.87	±0.12	0.24	±0.12	0.88	−0.06	±0.01				
8	VII	"	22	−0.72	±0.12	0.46	±0.12	0.80	−0.09	±0.02	0.45	−0.062	−0.017	−0.08
9	VIII	"	21	−0.82	±0.12	−0.43	±0.12	0.88	−0.12	±0.02	0.8	−0.072	−0.018	−0.09
						Mean weight		$\beta = -0.08 \pm 0.01$						
1	1 1958	60 m w.e. below ground	23	−0.80	±0.05	−0.22	±0.13	0.81	−0.03	±0.01				
2	II	"	23	−0.56	±0.09	−0.51	±0.16	0.65	−0.02	±0.01				
3	III	"	21	−0.79	±0.06	−0.36	±0.10	0.81	−0.07	±0.01				
4	IV	"	22	−0.80	±0.05	−0.46	±0.11	0.85	−0.06	±0.01				
5	V	"	27	−0.82	±0.04	−0.31	±0.12	0.83	−0.07	±0.01				
6	VI	"	27	−0.49	±0.10	−0.42	±0.11	0.78	−0.04	±0.02				
7	VII	"	19	−0.68	±0.08	−0.08	±0.15	0.75	−0.07	±0.02			−0.03	
8	VIII	"	28	−0.58	±0.08	0.21	±0.12	0.59	−0.04	±0.01	0.45			
9	IX	"	30	−0.59	±0.05	−0.10	±0.12	0.61	−0.05	±0.01	1.0		−0.04	
						Mean weight		$\beta = -0.05 \pm 0.01$						

measured I due to replacement of the counters, and also to avoid long periodic oscillations in I which might accidentally correlate with meteorological factors.

Comparison of barometric factors determined from short observation periods shows that the barometric factor is not a function of the season. This also accords with the theory [5].

The partial correlation factors $I_{JW(p)}$ are comparatively small; this is evidently due to the fact that in view of the short processing periods a large part is played by statistical errors and effects of non-atmospheric origin (magnetic storms), which cannot be completely avoided.

Taking these facts into account, it can be seen that the data given here on the temperature effect of cosmic rays fit in with theoretical views of the nature of the effect.

The validity as a first approximation of the temperature effect density curves used (see Figure 1) can be checked from data for the seasonal effect of cosmic rays.

Figure 2 shows curves for the seasonal intensity of cosmic rays I on the earth's surface and at 60 m w.e., corrected for barometric effect, and the expected seasonal variations N calculated by means of the curves in Figure 1.

It is clear from Figure 2 that the seasonal variations δI at a depth of 60 m w.e. are less than on the surface, while the maximum time shifts from winter to spring months. This shift in the seasonal variation tallies with a shift in the maximum temperature of the upper layers to the spring months [12] and qualitatively accords with the great part played by the upper atmospheric layers in underground measurements.

Comparison of the expected seasonal variations δN due to seasonal changes in temperatures

in the free atmosphere with observed seasonal variations in δ I reveals coincidence within the limits of the accuracy of the calculation and measurements.

In this way we can speak of the semi-quantitative agreement between theory and practice. More accurate and convincing results in testing the theory can be obtained from an analysis of air-mass effects [13]. At the present time material for this analysis is being collected and processed.

Bibliography

1. Farro. Phys. Rev., 72, p. 868, 1947.
2. Makonatx. Thesis. London, 1950.
3. Greizen et al., Rev. Mod. Phys., 24, p. 133, 1952.
4. Sherman, N., Phys. Rev., 93, p. 208, 1954.
5. Dorman, L. I., Variations in cosmic rays, Moscow, Gostekhizdat, 1957.
6. Kuz'min, A. I., G. V. Skripin, and A. V. Yarygin. Trudy YaFAN SSSR, Physics series, Issue 2, p. 334, 1958.
7. Kuz'min, A. I. and A. V. Yarygin, Trudy YaFAN SSSR, Physics series, Issue 2, p. 36, 1958.
8. Yarygin, A. V., Nauchnyye Soobshcheniya YAFSO AN SSSR, Issue 1, p. 74, 1958.
9. Danilov, A. A., S. N. Druzhinin, I. N. Kapustin, and G. V. Skripin. This issue, p. 40.
10. Feynberg, Ye. L., Doklady AN SSSR, 53, p. 421, 1946.
11. Wilson, Cosmic Ray Physics, vol. 1, Moscow, Foreign literature press, 1954.
12. Belinskiy, Dynamic meteorology, Gidrometelizdat, 1950.
13. Krasil'nikov, D. D., ZHETF, 28, p. 618, 1958; D. D. Krasil'nikov and Yu. G. Shafer, Trudy YaFAN SSSR, Physics Series, Issue 1, p. 44, 1956.

D. D. Krasil'nikov

BAROMETRIC EFFECTS OF EXTENSIVE ATMOSPHERIC SHOWERS

According to the earlier theory that extensive atmospheric showers were purely electron-photon avalanches originating through electromagnetic interaction of high-speed charged particles and photons with matter in the atmosphere, extensive atmospheric showers with a large number of particles should achieve their maximum development, on the average, at a greater depth in the atmosphere than showers with a smaller number of particles. It was therefore expected that there would be a decrease in the barometric coefficient (or factor) of the shower frequencies, α_h, with increasing number of particles in the shower near sea level (affecting the absorption of showers in the atmosphere) [1].

Qualitatively speaking, similar behavior of α_h is expected according to the new, comparatively recently developed theory, which states that nuclear processes are the basis of the development of extensive atmospheric showers [2, 3]. This expectation is based on the hypothesis that the fraction of energy transmitted to the secondary particles during the primary interaction between particles of high and altrahigh energy is constant, i.e., the fraction is not a function of the energy [4]. Admittedly, according to the nuclear-cascade theory, the barometric coefficient α_h may vary with the size of the shower to a lesser extent than predicted according to the electromagnetic cascade theory.

Direct measurements of the barometric effect of extensive atmospheric showers [5-7], and the closely associated behavior with various particle densities [9, 10] as a function of altitude [8] have shown that the barometric effect is practically identical for showers of different sizes and that the $\alpha_h = -0.10$ per 1 cm Hg of pressure change. The latter corresponds to a mean path of shower absorption $L = 136\ g \cdot cm^{-2}$. The practical constancy of α_h for showers of different sizes was explained by an assumed corresponding increase in the exponent γ in the spectrum of primary ultrahigh energy particles, and consequently also in $\varkappa = \gamma/s$ - the exponent of the shower spectrum with respect to the number of particles (s is the age parameter which is equal to 1.2 - 1.3 at sea level) [4]. The constancy of α_h was also used at one time as one of the basic facts for substantiating the considerable part played by nuclear-cascade processes in the development of these showers [2].

Results of earlier recordings of temporal variations in frequency of showers with various energies in Yakutsk [1954-1957] showed a tendency towards an increase in α_h with an increase in the shower energy [11, 12]. There were substantial defects in the geometry of the experiment, however, the errors in calculating α_h were still too great because of the scarsity of data. Moreover, the effect of the variation in the exponent $\varkappa$ in the shower spectrum (with respect to the number of particles) on the observed value of α_h was not evaluated.

In the Handbook [3], $\varkappa$ is assumed to vary between 1.32 and 1.80. The value of the exponent $\varkappa$ in various sectors of the shower spectrum with respect to the number of particles has been determined more precisely by recent measurement of the differential shower spectrum near sea level [13, 14]. The results of recent measurement of the barometric coefficient, α_h, at sea level [15] show a possible increase in α_h with an increase in the number of particles N in the shower.

Keeping in mind the present obscurity regarding the behavior of α_h with the increase in the number of particles N in the shower, we give below the results of calculation of α_h for showers with different mean N, on the basis of the new series of observations made in Yakutsk in 1958 and taking into account the variation in $\varkappa$.

To obtain α_h we used recorded data for the variations in shower frequency with six different mean particle numbers $\bar{N}$ obtained over the period January to April, 1958, using the apparatus

described earlier [16,17].

The recorded data taken into account were obtained by:

a) two local triple-coincidence installations with a counter group area of $\sim$1.0, $\sim$0.5 and $\sim$1/6 m^2, respectively;

b) six-fold coincidences, i.e., coinciding shower pulses from two local installations with identical counter group areas.

The layout of the counters for cases of C(3; 1.0 m^2) - triple coincidences with a counter area 1.0 m^2 - and C(6; 1.0 m^2) - six-fold coincidences with the same counter area - are given in Figures 1 and 2. The layout of the groups of counters for triple and six-fold coincidences for a counter area of 1/2 and 1/6 m^2 was the same as that given in Figures 1 and 2.

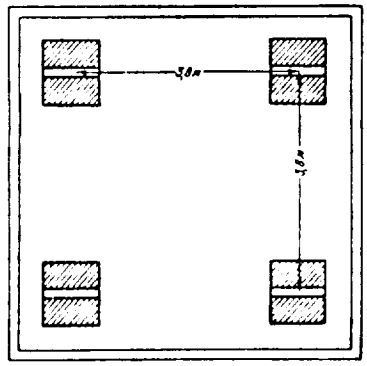

Fig. 1. Layout of counters for a case of selection C(3; 1.0 m^2).

The observation data were processed, as before [11], by three-factor correlation analysis: the regression factors δC with respect to δh and δC with respect to δT were calculated from the variation plane of the shower frequency δC during variations in atmospheric pressure δh and temperature of the ground air layer δT at the observation point.

The results of calculation of α_h and α_t for various combinations of shower coincidences are given in Table 1, where C is the shower recorded by the coincidence method, the first figure in parentheses is the multiplicity of coincidence, the second figure is the area of the counter groups in parallel, A is the anticoincidence, i.e., incidences of showers in one local installation unaccompanied by simultaneous recordings in the other local installation with the same counter area; the frequency of the latter in the given case was not recorded separately, but determined from the frequency of other combinations:

$$A(3; 1.0) = C(3; 1.0)_I + C(3; 1.0)_{II} - 2C(6; 1.0).$$

The data in Table 1 show the poor correlation between variations in the frequency of showers δC and the variations in the temperature of the ground air layer δT, but, nevertheless, a trend is detectable showing that for a local installation, $\frac{\partial C}{\partial T} < 0$, and for the the system of two local installations spaced 57 m apart, $\frac{\partial C}{\partial T} > 0$.

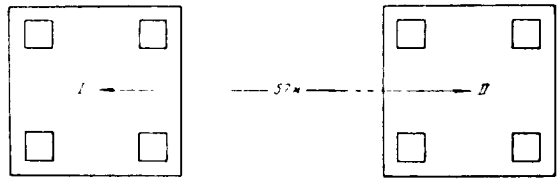

Fig. 2. Layout of a group of counters for a case of selection C (6; 1.0 m^2).

This result agrees qualitatively with views on the relationship between the spatial distribution function for particles in the extensive atmospheric showers and the ground temperature T of the type cited by [18].

$$R(T) \sim T,$$

where R(T) is the mean square shower radius as a function of temperature T.

At the same time, as is clear from Table 1, the barometric coefficient α_h begin to increase considerably for showers with $\bar{N} > 10^5$ particles, i.e., beginning at C(6; 1.0 m^2).

Let us consider to what extent the observed increase in the barometric factor α_h with the increase in size of the shower can be explained by an increase in the exponent of the shower spectrum $\varkappa$ with an increasing number of particles in the shower.

The frequency of the showers recorded with an n-fold coincidence counter unit between groups of counters with an equal area σ is determined by an expression of the following type

$$C(n,\ \sigma) = \int_{N=0}^{N=\infty} K(N)dN \iint_{(S)} W[n,\ \sigma,\ N,\ \varphi(r_1),\ \ldots\ \varphi(r_n)]\,dN, \qquad (1)$$

where $K(N)dN = AN^{-\kappa-1}dN$ is the differential distribution of the showers with respect to the number of particles, $\varphi(r_i)$ is the spatial distribution function in the shower, r_i is the distance between the shower axis and the i-th group of counters (i = 1, 2...n), S is the area encompassed by the shower axes, $W[n, \sigma, N, \varphi(r_1), \ldots \varphi(r_n)]$ is the probability of the installation recording a shower with N particles, providing its axis strikes the area element dS, located at a distance $r_1, r_2, \ldots r_n$ from the counter groups 1, 2...n, respectively

Table 1

	Barometric effect		Temperature effect	
	α_h, % per 1 cm Hg	r_{cm} (m)	α_m, % per 1° C.	r_{cm} (h)
C (6; 1.0 m²)	9.75 ± 0.37	0.95 ± 0.01	−0.08 ± 0.05	−0.44 ± 0.10
C (6; 1.0 m²)	9.90 ± 0.35	0.96 ± 0.01	0.05 ± 0.06	0.33 ± 0.11
C (6; 1.0 m²)	10.07 ± 0.81	0.82 ± 0.03	0.03 ± 0.05	0.08 ± 0.04
C (6; 1.0 m²)	11.74 ± 0.66	0.92 ± 0.02	0.15 ± 0.08	0.52 ± 0.09
C (6; 0.5 m²)	12.61 ± 0.90	0.86 ± 0.03	0.10 ± 0.09	0.27 ± 0.11
C (6; 1.0 m²)	10.8 ± 2.0			

In order to find a formula for the expected barometric factor of the variation in shower frequency α_h, which is equal to the relative variation in shower frequency when the pressure h_0 varies by one unit of measurement at the observation point, expression (1) has to be varied with respect to h_0 (separately for each type of coincidence recorded):

$$\alpha_h = \frac{1}{C(n,\ \sigma)}\frac{\partial C(n,\ \sigma)}{\partial h_0} = \frac{1}{C(n,\ \sigma)}\left\{\int_0^{\infty}\frac{\partial}{\partial h_0}K(N)dN\iint_{(S)}W[n,\ \sigma,\ N, \varphi(r_1), \ldots,\right.$$

$$\left.\varphi(r_n)]\,dS + \int_0^{\infty}K(N)dN\iint_{(S)}\frac{\partial}{\partial h_0}W[n,\ \sigma,\ N,\ \varphi(r_1),\ \ldots,\ \varphi(r_n)]\,dS\right\}, \qquad (2)$$

The right-hand side in expression (2) consists of two terms. The first represents variation in the frequency of the observed showers due to variation in the spectrum at the observation level, while the second is associated with variation in the effective radius of the shower, R, in the function $\varphi(r_i)$ when the observation level h_0 varies, and is classed as the geometry effect of the installation. For the sake of brevity we will represent expression (2) as follows:

$$\alpha_h = \alpha_h(K) + \alpha_h(R). \qquad (3)$$

The values $\alpha_h(K)$ and $\alpha_h(R)$ can be evaluated in the following way. The integral spectrum of the showers with respect to the number of particles, N is

$$F(>N) = BN^{-\kappa}, \qquad (4)$$

$$\frac{\partial F(>N)}{\partial h} = \frac{\partial F(>N)}{\partial N}\frac{\partial N}{\partial h} = -\kappa \cdot BN^{-\kappa}\ \frac{\partial \lg N}{\partial h} = -\kappa\mu_N \cdot F(>N), \qquad (5)$$

where $\mu_N = \frac{\partial \lg N}{\partial h}$ is the particle absorption factor in the shower and is equal, according to equation (3), to $\mu_N = 0.56\%$ per one millibar, which corresponds to $1/\mu_N = 180$ g/cm^2.

Assuming that the above is applicable, the behavior of the integral shower spectrum as a function of altitude with respect to the number of particles near sea level can be represented as

follows: $$F(>N, h) = B(h_0) \cdot e^{-\varkappa\mu_N \cdot (h-h_0)} \cdot N^{-\varkappa} = B(h) \cdot N^{-\varkappa}. \quad (6)$$

Hence

$$\frac{\partial K(N)}{\partial h} = \frac{\partial^2 F(>N, h)}{\partial N\, \partial h} = -\varkappa\mu_N \cdot AN^{-\varkappa-1} = -\varkappa\mu_N \cdot K(N). \quad (7)$$

It follows from Equation (7) that

$$\varkappa_h(K) = -\varkappa\mu_N. \quad (8)$$

The second term in the barometric factor $\alpha_h(R)$ describes the effect of the geometry of the experimental apparatus. It can be determined by direct differentiation of the second term in Equation (2) (under the double integral sign) and by subsequent integration. If the exponent d of the spacing function

$$C(D) \sim D^{-d}$$

for the given type of shower C(n, σ) is known, the approximate Equation (6) can be used.

$$\alpha_h(R) = \frac{2(\varkappa-1)-d}{h_0}, \quad (9)$$

where h_0 is the pressure at the observation level, $D \approx 0.1$ to 0.2 for moderate spacings (D < 10 m).

As the experiment shows, near sea level the contribution made by $\alpha_h(R)$ to α_h is small compared with $\alpha_h(K)$ [less than 0.1 $\alpha_h(K)$].

It is clear from Equations (8) and (9) that both $\alpha_h(K)$ and $\alpha_h(R)$ depend on the exponent $\varkappa$ of the shower spectrum with respect to the number of particles. If $\varkappa$ is a variable for the recorded showers, we will have to use the following average values for the entire recorded spectrum instead of $\varkappa$, in order to evaluate α_h in Formulae (8) and (9).

$$\bar{\varkappa} = \sum_{i=1}^{i=n} P_i \varkappa_i, \quad (10)$$

where P_i is the weight of the i-th sector of the shower spectrum with respect to the number of particles with the exponent $\varkappa$ in producing the observed shower frequency C(n, σ).

It has been shown [19] on the basis of data obtained in measuring the shower density spectrum (taking into account that the exponents of the density spectrum and shower spectrum with respect to the number of particles at sea level coincide within 2% [20] that $\varkappa$ is not a constant, but, generally speaking, is a function of the shower size:

$$\varkappa = \varkappa(N),$$

whence it can be concluded that

$$\alpha_h = \alpha_h(N). \quad (11)$$

On the basis of experimental data from recent direct measurements of the extensive atmospheric shower spectrum (see [13] and other publications) quoted in Cocconi's latest review [3], the shower spectrum with respect to the number of particles at sea level can be broken down into three ranges, within which the value of $\varkappa$ remains constant:

$$\left.\begin{array}{ll} \varkappa_1 = 1{,}36 & \text{for the number of particles in the shower } 10^3 < N < 10^4 \\ \varkappa_2 = 1{,}55 & \text{for the number of particles in the shower } 10^5 < N < 10^6 \\ \varkappa_3 = 1{,}84 & \text{for the number of particles in the shower } N > 10^6 \end{array}\right\} \quad (12)$$

The value of $\varkappa$ adopted in the range $N > 10^6$ does not correspond to the approximate value quoted in [3] (it is larger), and merely satisfies measurement data [13].

The weight P_i (i = 1, 2 and 3) in Equation (10) can be determined separately in each case from the recording spectrum for the given type of shower coincidence C(n, σ) in the following way:

$$\left.\begin{aligned} P_1 &= \frac{1}{C(n,\sigma)_{\text{pred.}}}\int_0^{N=10^4} A_1 \cdot N^{-\gamma_1+1}\,dN \iint_{(s)} W[n,\sigma,r_1,r_2,\ldots,r_n,\varphi(r),N]\,dS, \\ P_2 &= \frac{1}{C(n,\sigma)_{\text{pred.}}}\int_{N=10^4}^{N=10^5} A_2 \cdot N^{-\gamma_2+1}\,dN \iint_{(s)} W[n,\sigma,r_1,r_2,\ldots,r_n,\varphi(r),N]\,dS, \\ P_3 &= \frac{1}{C(n,\sigma)_{\text{pred.}}}\int_{N=10^5}^{\infty} A_3 \cdot N^{-\gamma_3+1}\,dN \iint_{(s)} W[n,\sigma,r_1,r_2,\ldots,r_n,\varphi(r),N]\,dS, \end{aligned}\right\} \quad (13)$$

where $C(n, \sigma)_{\text{pred.}}$ is the predicted number of shower coincidences of the given type per unit of time:

$$\begin{aligned} C(n,\sigma) = &\int_0^{N=10^4} A_1 \cdot N^{-2.36}\,dN \iint_{(s)} W[n,\sigma,r_1,r_2,\ldots,r_n,\varphi(r),N]\,dS + \\ &+ \int_{N=10^4}^{N=10^5} A_2 \cdot N^{-2.55}\,dN \iint_{(s)} W[n,\sigma,r_1,r_2,\ldots,r_n,\varphi(r),N]\,dS + \\ &+ \int_{N=10^5}^{\infty} A_3 \cdot N^{-2.80}\,dN \iint_{(s)} W[n,\sigma,r_1,r_2,\ldots,r_n,\varphi(r),N]\,dS. \end{aligned} \quad (14)$$

In the double integral with respect to the area S the expression

$$W[n,\sigma,r_1,r_2,\ldots,r_n,\varphi(r),N] = \begin{cases} \prod_{i=1}^{i=4}\left[1-e^{-N\varphi(r_i)\,\sigma}\right] & \text{for a shower of the type } C(n=3,\sigma), \\ \prod_{i=1}^{i=2}\left[1-e^{-N\varphi(r_i)\,\sigma}\right] & \text{for a shower of the type } C(n=6,\sigma), \end{cases} \quad (15)$$

$\varphi(r_i)$ is the function of spatial particle distribution in the shower; r_i is the distance in meters between the shower axis and the counter group, and A_1, A_2 and A_3 are constants.

On the basis of measurements near sea level [21], the function $\varphi(r)$ is taken for these calculations in the form of

$$\varphi(r) = \begin{cases} a \cdot r^{-1} & \text{at } r < 10\ m \\ b \cdot r^{-1-\frac{r}{55}} & \text{at } 10 < r < 100\ m, \\ c \cdot r^{-2.5} & \text{at } r > 100\ m, \end{cases} \quad (16)$$

where $a = 1.84 \cdot 10^{-3}$, $b = 2.21 \cdot 10^{-3}$ and $c = 0.568$.

The constants of the differential particle-number spectrum for the showers near sea level A_1, A_2 and A_3 are taken from Cocconi's publication [3] and from measurements made by Rossi, Clark, and others [13]. All the integrals were calculated by approximate numerical integration methods.

The differential spectrum for extensive atmospheric showers recorded with the given type of selection $C(n, \sigma)$, i.e., the recording spectrum, can be represented in the form

$$R[n,\sigma,N] = K(N) \iint_{(s)} W[n,\sigma,\varphi(r_1),\ldots,\varphi(r_n),N]\,dS, \quad (17)$$

where K(N)dN is the differential spectrum for the number of particles in the shower at sea level.

The shower recording spectra calculated by the above method for the types $C(n, \sigma)$ are given in Figure 3. The number of coincidences per unit of time for the type of selection $C(n, \sigma)$ is determined by the area under the curve for the recording spectrum function (17), i.e.,

$$C(n, \sigma) \int_0^\infty R[n, \sigma, N]\,dN. \qquad (18)$$

Figure 4 gives the results of calculations, using Equations (2), (8), (9) and (10), of the predicted barometric factor as a function of the mean shower size $\alpha_h(\bar{N})_{pred.}$ and the corresponding observed values of $\alpha_h(\bar{N})_{exper.}$

As the mean size of the shower we do not take the average arithmetic value,

$$\bar{N}_{arith.} = \frac{\int_0^\infty N\,R[n, \sigma, N, \varkappa, \varphi(r_1), \ldots, \varphi(r_n)]\,dN}{\int_0^\infty R[n, \sigma, N, \varkappa, \varphi(r_1), \ldots, \varphi(r_n)]\,dN}, \qquad (19)$$

but the median value $\bar{N}_{eff.}$, determined from the condition

$$\int_0^{N_{eff.}} R[n, \sigma, N]\,dN = \int_{N_{eff.}}^\infty R[n, \sigma, N]\,dN = \frac{1}{2} C(n, \sigma)_{pred.} \qquad (20)$$

This is due to and justified by the fact that in producing the observed variation in frequency $\delta C(n, \sigma)/C(n, \sigma)$ all showers, irrespective of their size, take part with an equal weight, i.e., they are equivalent in this sense.

A comparison of the corresponding $\alpha_h(\bar{N})_{pred.}$ and $\alpha_h(\bar{N})_{exper.}$ in Figure 4 throughout the range under consideration of mean $\bar{N}$ in the showers shows the following:

1) The increase in $\alpha_h(\bar{N})_{pred.}$ with the increase of $\bar{N}$ in the shower is comparatively slight. This is due to the fact that the increase in $\varkappa_i$ with the increase in the shower N_i from the viewpoint of an effect on $\alpha_h(\bar{N})_{pred.}$ is compensated to a considerable extent by the corresponding decrease in the weight P_i of the given sector of shower magnitudes N_i in the recording spectrum.

We should recall that when calculating $\alpha_h(\bar{N})_{pred.}$ the maximum effect of $\varkappa$ was assumed: instead of $\partial \log N/\partial h$ decreasing with an increase in N, we took a constant equal to 0.56% for one millibar, according to [3], which is greater than in Equation (2); and the greatest of the measured x over the range $N > 10^6$ was selected [13].

2) A substantial discrepancy is observed between $\alpha_h(\bar{N})_{pred.}$ and $\alpha_h(\bar{N})_{exper.}$ We can conclude from this that for showers with $N \geqslant 10^5$, the absorption of the particles in the shower $\mu_N = \partial \log N/\partial h$ with an increase in N does not only not decrease, or even stay constant, but increases.

An explanation for the increase in $\partial \log N/\partial h$ with an increase in N should be sought in the corresponding substantial variation in some, possibly all, principal factors (interaction cross section, multiplicity of nascent particles, fraction of energy passed on to secondary particles, etc.) of the elementary act at primary particle energies of $E_0 \geqslant 10^{15}$ ev.

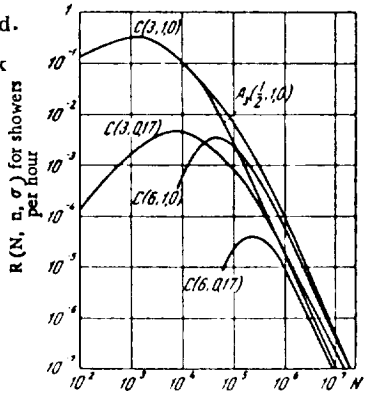

Fig. 3. Recording spectra of extensive atmospheric showers R (N, n, σ) in Yakutsk.

In particular, the results obtained here correspond with S. I. Nikol'skiy's hypothesis [22] that at $E_0 \geqslant 10^{15}$ ev, the multiplicity of the separated particles, over the given energy range, among the large number of nascent secondary particles must be greater than one.

Furthermore, it should be pointed out that the changes in the slope of the curves (increase of $\varkappa$), beginning from $N \geqslant 10^5$ particles in the shower spectrum at sea level, are probably due to an increase in μ_N for showers with $N \geqslant 10^5$ [23], and are not caused by corresponding variations in the exponent γ in the spectrum for ultrahigh energy primary particles, as assumed by certain investigators [24].

In conclusion the author considers it his pleasant duty to express profound apprcciation to S. I. Nikol'skiy, under whose guidance and with whose active assistance the research was carried out, and also to Comrades N. N. Yefimov, M. A. Nifontov, F. K. Shamsutdinova, V. A. Orlov and T. F. Panfilova, who helped to assemble and operate the installations and process the data.

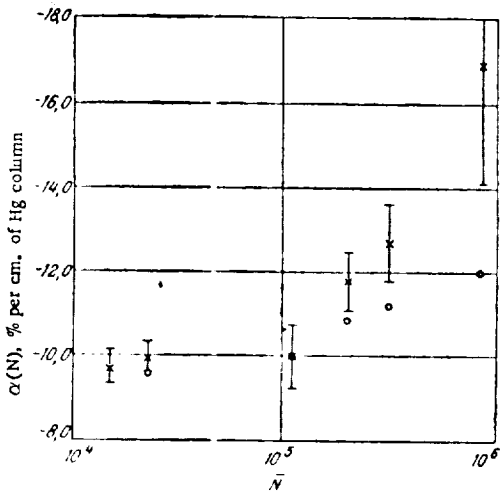

Fig. 4. X - denote $\alpha_h(N)_{exp.}$, O - denote $\alpha_h(N)_{pred.}$ assuming that $\frac{1}{\mu_N}\frac{\partial \ln N}{\partial h} = \text{const} = \frac{1}{|N|}\,g^{-1}\,cm^2$, independently of the number of particles, N, in the showers.

Bibliography

1. Yanossi, L. Cosmic rays. Moscow. Foreign Literature Press, 1949. In Russian.
2. Dobrotin, N. A., G. T. Zatsepin, I. L. Rozental', L. I. Sarycheva, G. B. Khristiansen, and L. Kh. Eydus, Uspekhi Fizicheskikh Nauk, 49, p. 185, 1953.
3. Cocconi, G. Handbook der Physik, 1958.
4. Zatsepin, G. T., Doctoral dissertation, FIAN, 1954.
5. Citron, A. Z. Naturforsch, 7a, p. 712, 1952.
6. Daudin, A. and J. Daudin. "J. Atm. Terr. Phys." 3, p. 245, 1953.
7. Hodson, A. L., Proc. Phys. Soc., A66, 49, 1953.
8. Zatsepin, G. T. and L. I. Sarycheva, Dokl. Ak. Nauk SSSR, 99, 1951 (1954).
9. Cocconi, G., Phys. Rev., 75, 1058, 1949.
10. Zatsepin, G. T., Dissertation for the degree of Candidate of Sciences, FIAN, 1950.
11. Koval'skaya, A. I., et al., Trudy YaFAN, SSSR, Phys. series, Issue 2, 88, 1958.
12. Krasil'nikov, D. D., ZHETF, 35, 295, 1958.
13. Clark, G., J. Earl, J. Kraushaar, J. Linsley, B. Rossi, F. Scherb. Nature, 1957, 180, 406.
14. Khristiansen, G. B., Personal communication.
15. Cranshaw, T. E., Proc. Oxford Conference, April 1956.
16. Krasil'nikov, D. D. and S. I. Nikol'skiy, Nauchnyye soobshcheniya YaFSO AN, SSSR, Issue 1, 65, 1958.
17. Krasil'nikov, D. D., This symposium, p. 22.
18. Zatsepin, G. T., Personal communication.
19. Eydus, L. Kh. et al, Dokl. Ak. Nauk SSSR, 75, 669, 1950.
20. Greisen, K., Progress in Cosmic-Ray Physics, v. III, Amsterdam, 1956.
21. Nikol'skiy, S. I, Personal communication.
22. Nikol'skiy, S. I., et al., Dokl. Ak. Nauk SSSR, III, 71, 1956.
23. Vernov, S. N. and G. T. Zatsepin, Report at Conference in Tbilisi, 1956.
24. Kulikov, G. V. and G. B. Khristiansen, ZHETF, 35, 635, 1958.

Ya. L. Blokh, Ye. S. Glokova and N. S. Kaminer

BAROMETRIC EFFECT OF COSMIC RAYS

1. When a stream of cosmic rays passes through the atmosphere, it is weakened because of absorption. The stream is not parallel or monoenergetic, but it can be considered that the weakening in a layer of matter dp (mb) is described with sufficient accuracy by the expression:

$$dI = -\mu I\, dp, \tag{1}$$

where μ is a coefficient describing the weakening of the stream.

Let us use I_{p_0} to denote the intensity at a certain constant depth $p = p_0$ in mb. Integration of (1) then gives

$$\ln I = \ln I_{p_0} = -\mu (p - p_0), \tag{2}$$

or

$$I = I_{p_0} e^{-\mu (p - p_0)}. \tag{2}$$

Let I and p be the cosmic-ray intensity and barometric pressure, respectively recorded by the station. The variations in cosmic-ray intensity due to changes in pressure can be excluded by introducing barometric corrections. This is the same as determining the intensity at the depth p_0, if the intensity at p is known at the given moment of time. According to equation (2),

$$\ln I_{p_0} = \ln I + \mu (p - p_0), \tag{3}$$

or

$$I_{p_0} = I e^{\mu (p - p_0)}. \tag{3'}$$

2. Variations is cosmic-ray intensity are conventionally expressed in relative units. It follows from equation (2) that the relative variation in cosmic-ray intensity due to changes in pressure can be expressed by the formula

$$\frac{I - I_{p_0}}{I_{p_0}} \cdot 100 = 100 \left[e^{-\mu (p - p_0)} - 1 \right] = B, \tag{4}$$

where B is the barometric correction. Expanding $e^{-\mu (p-p_0)}$ into a series, we obtain

$$B = 100 \left[e^{-\mu (p - p_0)} - 1 \right] =$$

$$= 100 \left[-\frac{\mu (p - p_0)}{1!} + \frac{\mu^2 (p - p_0)^2}{2!} - \frac{\mu^3 (p - p_0)^3}{3!} + \ldots \right]. \tag{5}$$

However, equation (4) cannot be used in this form because I_{p_0} is an unknown which varies continuously with time. For practical purposes the relative variation is expressed in percent of a constant value of I_0 which has been adopted as the standard ($I_0 \approx \bar{I}_{p_0}$).

Let us transform equation (4) by separating the variable term I_{p_0} in the denominator. Assuming $I_{p_0} = I_0 + (I_{p_0} - I_0)$ in the denominator on the left-hand side and multiplying both sides of equation (4) by $\frac{I_0 + (I_{p_0} - I_0)}{I_0}$, we obtain*

* This formula can be directly derived from Formula (2') by substituting the expressions for I and I_{p_0} in terms of ΔI and ΔI_{p_0}. Formula (6) can also be represented in the form

$$\Delta I - \Delta I_{p_0} = -\left[B + \frac{I - I_0}{I_0} B \right],$$

$$\frac{I - I_{p_0}}{I_0} 100 - \Delta I = \Delta I_{p_0} = B + \frac{I_{p_0} - I_0}{I_0} B. \qquad (6)$$

Where

$$\Delta I = \frac{I - I_0}{I_0} 100\ (\%) \text{ and } \Delta I_{p_0} = \frac{I_{p_0} - I_0}{I_0} 100\ (\%),$$

i.e., all the data before and after barometric corrections are expressed in percent of I_0. The term $\frac{I_{p_0} - I_0}{I_0} B$, which occurs here in the right hand side of equation (6), takes into account the effect of deviation in I_{p_0} from the standard I_0 on the barometric correction. If these deviations are small, the additional term is small, and at $I_{p_0} = I_0$ it is equal to zero.

Disregarding this additional term and limiting ourselves to the first term in the series (5), we obtain the formula which is usually employed to make the barometric correction of data for the hard component in cosmic rays,

$$\Delta I - \Delta I_{p_0} = \beta (p - p_0), \qquad (7)$$

where $\beta = 100\mu$ is the barometric coefficient (factor) expressed in %/mb. Clearly, equation (7) is an approximate one.

Table

Errors made in calculation of the barometric correction by using equation (7) [in percent of I_0]

$p - p_0$, mb	$\beta (p - p_0) - B$		$\frac{I_{p_0} - I_0}{I_0}$	$\frac{I_{p_0} - I_0}{I_0} B$	
	$\beta = -0.75\%$/mb	$\beta = -0.15\%$/mb		$\beta = -0.75\%$/mb	$\beta = -0.15\%$/mb
1	0,003	0,0001	0,01	0,01	0,0015
			0,10	0,08	0,02
			0,50	0,38	0,08
10	0,27	0,01	0,01	0,07	0,01
			0,10	0,72	0,15
			0,50	3,60	0,74
20	1,07	0,04	0,01	0,16	0,03
			0,10	1,52	0,30
			0,50	8,09	1,48
40	4,08	0,18	0,01	0,26	0,06
			0,10	2,59	0,58
			0,50	12,96	2,91

3. Equation (7) enables us to calculate the barometric effect fairly accurately provided that $\beta (p - p_0)$ is small. It is known, however, that the neutron component in cosmic rays reacts to a much greater degree (4 - 6 times) to the variation in barometric pressure than the hard

---

where

$$B' = 100 \left[e^{\mu (p - p_0)} - 1 \right] = 100 \left[\mu (p - p_0) + \frac{\mu^2 (p - p_0)^2}{2!} + \frac{\mu^3 (p - p_0)^3}{3!} + \ldots \right], \qquad (6')$$

or

$$\Delta I_{p_0} = \Delta I \left[\beta (p - p_0) - \frac{\beta^2 (p - p_0)^2}{200} \right] \left[1 + \frac{\Delta I}{100} \right]. \qquad (6'')$$

component. Furthermore, we often observe deviations in the diurnal means of the barometric pressure of 20 to 30 mb (or even more) from the average pressure at the given station. The deviations of I_{p_0} from I_0 are also large and comparable to the value of I_0. All this suggests that in a number of cases equation (7) provides too rough an approximation.

The table shows some values of the errors which are made when making barometric corrections from equation (7): 1) due to the use of the linear approximation for B, and 2) due to disregarding the term $\frac{I_{p_0} - I_0}{I_0} B$. The errors have been calculated for the neutron component ($\beta = -0.75\%/mb$) and the hard component ($\beta = 0.15\%/mb$) in cosmic rays for certain values of $(p - p_0)$ and $\frac{I_{p_0} - I_0}{I_0}$.

It is clear from the table that

a) for the hard component in cosmic rays the linear approximation can always be used, even when the barometric pressure variations are very large, up to 40 mb (the error does not exceed 0.2% of I_0).

b) for the hard component, in practically all cases, we can disregard the term $\frac{I_{p_0} - I_0}{I_0} B$.

This value is only high when the hard component variations are very great and correspond to "bursts". During a burst, however, the intensity grows so rapidly (10 - 20 minutes) that the barometric pressure hardly has time to change appreciably. Even when the intensity goes up by 200% and the pressure changes by 1 mb, the error due to disregarding this term will not be more than 0.3% of I_0, and can be completely ignored.

c) for the neutron component in cosmic rays, when the decreased pressure variations are 15-20 mb., the linear approximation will not suffice. In this case the error will amount to 0.6 - 1.1% which is beyond precision for reporting.

d) for neutron component, when the pressure change is 10 - 15 mb and the deviation of I_{p_0} from I_0 is 10%, the error due to disregarding the term $\frac{I_{p_0} - I_0}{I_0}$ is 1 - 1.5%.

The following conclusions can be drawn:

1. For the hard component in cosmic rays, equation (7) gives a fairly good approximation and can be used in all cases.

2. For the neutron component in cosmic rays, equation (7) can lead to considerable errors in many cases. Since the more exact equation (6") is inconvenient, it is preferable not to convert data for the neutron component, expressed in terms of the number of pulses, into percentage of I_0 before barometric corrections are made. The reduction of data for the neutron component to a constant barometric pressure should be made on the basis of equation (3).* In equation (3) [$\ln I_{p_0} = \ln I + \mu (p - p_0)$] the intensity of the cosmic rays is expressed in terms of the number of pulses and the calculation of the barometric correction does not involve the use of the standard I_0.

3. As has been shown, the barometric correction to data for the neutron component should be made by equation (3), i.e., the logarithmic relationship between variations in I and p should be taken into account. In this case the method of determining the barometric coefficient β or the coefficient μ is also varied. The conventional method of linear correlation between cosmic-ray intensity and barometric pressure should be replaced by linear correlation between the logarithm of the neutron component intensity and the barometric pressure.

---

* M. Wada. "J. Scient. Res." 1957, v. 51, p. 201.

N. P. Chirkov and Yu. G. Shafer

EFFECT OF AIR MASS FRONTS ON COSMIC RAY INTENSITY AND ROLE PLAYED BY LOWER LAYERS OF STRATOSPHERE

The meteorological nature of the effect of replacement of air masses on cosmic-ray intensity has been explained fairly clearly in the publications of the Yakutsk laboratory [1,2], which refer to a possible reduction in the effect through redistribution of the air masses in the lower stratosphere.

This article endeavors to analyze experimental material with a view to evaluating this effect, and, using meteorological effect calculations devised by Feynberg-Dorman [3], to ascertain the frontal situation in the lower stratosphere when pronounced tropospheric warm and cold meteorological fronts pass over the cosmic ray recorder. For the investigation we used material from continuous measurements of the global intensity of the hard component made in Moscow at the Institute of Terrestial Magnetism, Ionosphere and the Propagation of Radio Waves of the Academy of Sciences of the USSR (IZMIRAN) using the ASK-1 apparatus.

The data on the temperature radio-sounding of the atmosphere, when the meteorological fronts passed over Moscow, were obtained from the Central Aerological Observatory (CAO).

In all, 49 warm and 48 cold fronts passing over Moscow between 1953 and 1957 were studied. All the fronts were selected by specialists from the Central Weather Forecasting Institute (after examination of ground weather charts). The fronts were required to meet the following specifications:

a) they had to be well pronounced in the meteorological field at the earth's surface and at an isobaric surface level of 850 mb;

b) before the moment the selected front passed over the observation point, Moscow had to be in a homogeneous air mass, i.e., neither at ground level nor at any height had there to be any other meteorological fronts during this period;

c) after the selected front had passed over Moscow, no other frontal divisions were to be noted until the front had passed over at all altitudes.

The frontal divisions of the air masses and their upper boundaries were fixed from data of four radiosondes every 24 hours and from aircraft sounding, and also from temperature field analysis at isobaric surface levels of 850, 700, 500, 300 and 200 mb, and in certain cases at 100, 50 mb, or higher.

When the warm fronts passed over, seven moderate and three strong magnetic storms were recorded, and three moderate and one strong one when the cold front passed over.

The experimental material was processed in the following way. Just as in other research work [1,2], the frontal division projection onto the earth's surface was divided into seven zones in the case of the warm, and six zones in the case of cold fronts. Moreover, an analysis was made of material from two zones, corresponding in pairs to "pure" cold and warm air masses passing over the observation point before and after the front, regardless of the type. Each zone was given a number (, 2, ... k) which was used to mark its other relevant characteristics. The zones were not included in the analysis unless there were radio sondes or aircraft sounding while they were overhead.

In accordance with the time of passage of the fronts over the Moscow Cosmic Ray Station, we collected δI_{nip} data for each hour following the radio sounding. The values of the intensity for each front type obtained in this way were then averaged. The derived deviations ΔI_n^k (where k is the zone number and n is the number of fronts of the given type) were processed by the Cri method (superimposition of epochs). We thus derived mean deviations of δI^k for each type (Figures 1b and 2b).

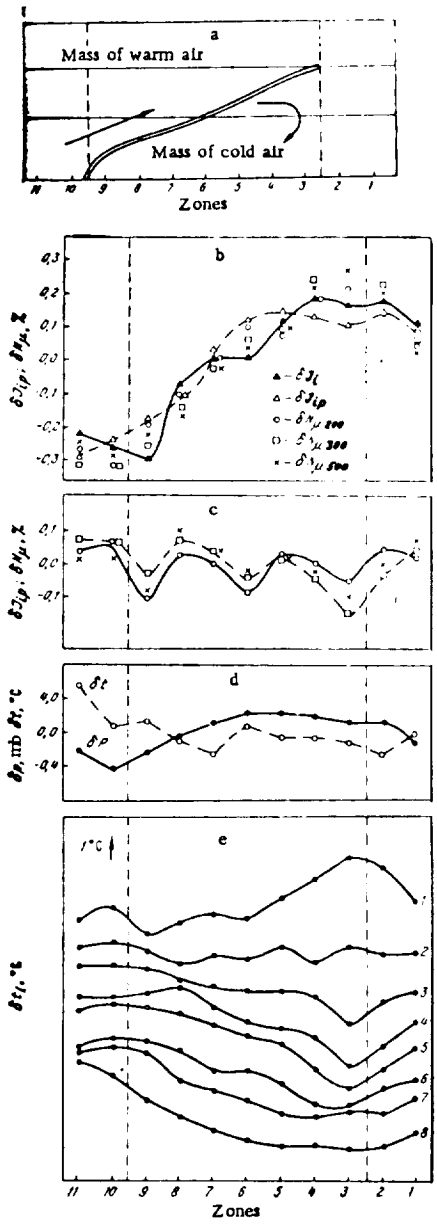

Fig. 1

Observed and theoretically predicted intensity variations of μ-meson component and atmospheric temperature, on standard levels at the time the warm fronts pass over the point of observation (mean of 35 cases).

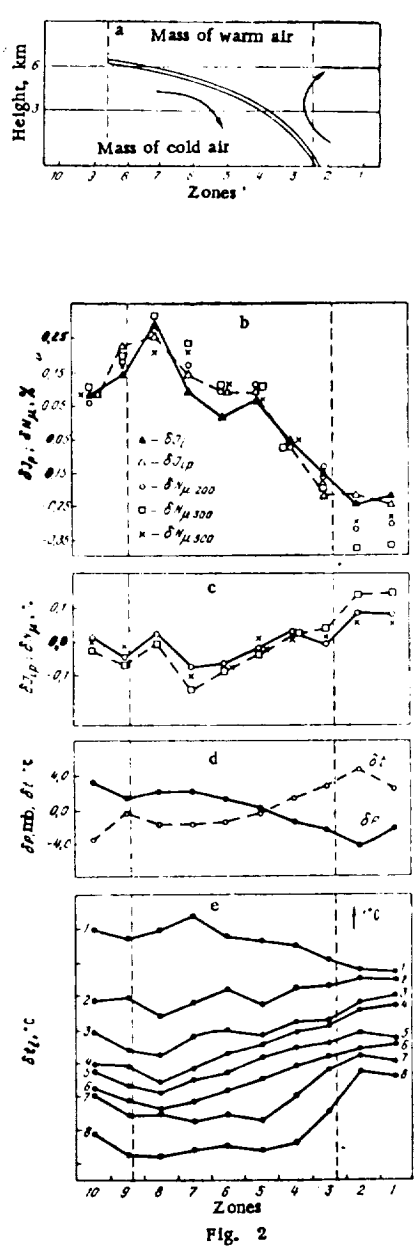

Fig. 2

Same as Fig. 1. Observed for cold fronts (mean of 31 cases)

a - typical profile of a warm front; b - rate of slip and $\delta N\mu$; c - rate of δ lipN; d - rate of the terrestrial δ p and temperature (δt, ter); 3 - rate of the atmospheric temperature on standard levels; 1 - 200 mb; 2 - 300 mb, 3 - 400 mb; 4 - 500 mb; 5 - 600 mb; 6 - 700 mb; 7-800 mb; 8 - 900 mb.

The results of the temperature sounding for each standard pressure level were processed in similar fashion. The averaged curve for temperature variation at different levels is shown in Figures 1e, 2e, 3b and 4b.

Variations in intensity, in percent of the theoretical mean, due to meteorological factors were calculated from data for the temperature cross section of the atmosphere by the Feynberg-Dorman system. These results and the experimental curves for the μ-meson component intensity are given in Figures 1b and 2b. Figures 1c and 2c show curves for the μ-meson intensity variation taking the temperature of the atmosphere, collisions and barometric pressure into account. It is clear from these curves that the hard component intensity freed, in a first approximation, from the effect of the layer of atmosphere between the earth's surface and a height of 200 mb, undergoes variations of particular interest in the case of the warm front.

Analysis of the material suggests the following:

1. When the warm front passes over (Figure 1b), the intensity of the hard component is reduced by 0.48 ± 0.10%. The reduction begins a short time after the projection of the upper boundary of the frontal section reaches the point and ends approximately one hour before the ground line of the front passes over.

The correlation factors for the meson intensity variations and theoretically expected intensity are very great: $r_1 = 0.98 \pm 0.01$ between δI_{ip} and δN_{500}, $r_2 = 0.96 \pm 0.02$ between δI_{ip} and δN_{300} and $r_3 = 0.93 \pm 0.04$ between δI_{ip} and δN_{200}.

2. In the case of the cold front the effect is 0.53 ±0.10%. The intensity increase begins when the ground line of the front passes over the observation point. Maximum intensity is observed just before passage of the projection of the upper boundary of the frontal section.

The correlation coefficient between δI_{ip} and δN_{μ} is very high for the cold front, as well.

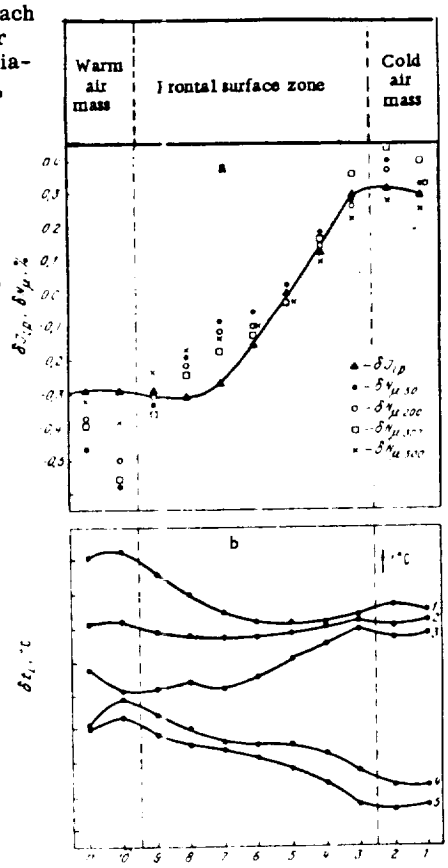

Fig. 3.

a - the values of δI_{ip} and δN_u during passage of a warm front, considering the effect of lower stratosphere (average of 14 instances); b - variation of temperature on levels, 1-50 mb, 2 - 100 mb, 3 - 200 mb, 4 - 300 mb and 5 - tropospheric average.

3. In order to be able to assess the possible effect of redistribution of air masses in the lower stratosphere on the front effect in cosmic-ray intensity to any extent at all, we had to make use of additional experimental material from 1955 - 1957 during which there was higher temperature sounding of the atmosphere than in preceeding years.

Figures 3a and 4a show curves for δI and δt for warm and cold fronts obtained from the processing of this additional material. It is not difficult to note from study of these graphs that the contribution made by the lower stratosphere steps up the meteorological front effect in I. The appearance of the curves for δI and δW changes as well.

To some extent this conclusion confirms G. D. Zubyan's hypothesis regarding the participation of the lower stratosphere in the formation and development of meteorological fronts [4]. Unfortunately, we do not yet have sufficient experimental material for any more definite conclusions.

A feature which stands out when looking at Figures 3a and 4a is the divergence between the

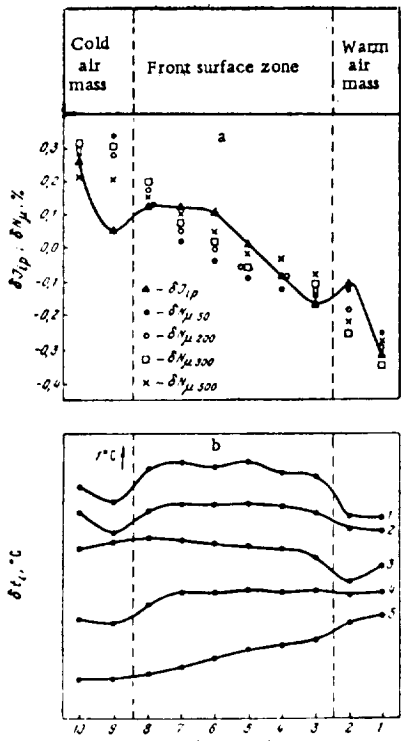

Fig. 4. Same as Fig. 3, for a cold front (average of 12 instances).

μ-meson intensity obtained experimentally and the values calculated by the Dorman-Feynberg system which takes into account $\gamma = 0.5$ adopted in [5]. Rough calculation shows that these discrepancies become minimal if we take $\gamma \simeq 0.35$ when calculating δW.

Figures 1e, 2e, 3b and 4b clearly show a reversal of the temperature distribution of the air in the stratosphere compared with variation in temperature in the troposphere. This fact shows up particularly in the case of the warm front and coincides with L. R. Rakipova's views [6]. We consider that these processes mutually compensate for the effects in I when the fronts pass over.

4. Using 1949 - 1952 material [2] and the results of our own research, we were able to trace the relationship between the variation in the meteorological front effect and the state of solar activity for a number of years.

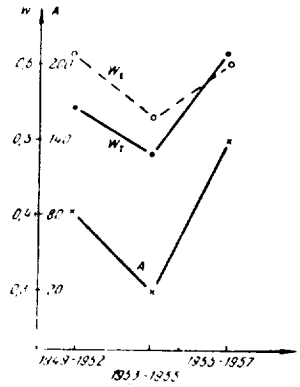

Fig. 5. Variation of temperature effect on the Wolf number in 1949-1952, 1953-1955, and 1955-1957. W_x - temperature effect in cold front; Wm - temperature effect in warm front; A - Wolf number.

The curves given in Fig. 5 for A (Wulf number) and W (temperature contribution to front effect) reveal considerable correlation. This fact suggests that as the sun's activity increases, so do the processes in the atmosphere leading to an increase in W.

Bibliography

1. Krasil'nikov, D. D., ZHETF, 28, Issue 5, 1955.
2. Krasil'nikov, D. D. and Yu. G. Shafer. Trudy YaFAN, SSSR, Physics series, Issue 1, Moscow, Academy of Sciences Press, 1955.
3. Dorman, L. I. and Ye. L. Feynberg. Uspekhi fizicheskikh Nauk, 59, p. 189, 1956.
4. Zubyan, G. D., Meteorology and Hydrology, no. 9, 1956; no. 5, 1957.
5. Dorman, L. I., Cosmic-ray variations, Moscow, Gostekhizdat, p. 119, 1957.
6. Rakipova, L. R., Physics of solar corpuscular streams and their effect on earth's upper atmosphere. Moscow, Academy of Sciences Press, p. 273, 1957.

Ye. S. Glokova

ANNUAL VARIATIONS IN COSMIC RAY INTENSITY AND TEMPERATURE CORRECTIONS

There is no longer any doubt that the regular annual variations in the intensity of the hard component in cosmic rays I, reduced to a constant barometric pressure, are produced by a temperature effect. It is not yet entirely clear, however, whether there are residual annual variations in I of non-meteorological origin, or how regular they are.

When the meteorological corrections W calculated by Dupcrier's method had been made, there was discovered in Manchester [1] a residual annual wave I - W of opposite phase, i.e., with a maximum in the summer and minimum in the winter. The total amplitude of this inverse wave was almost equal to that of the annual wave I observed and amounted to more than 1% of the mean intensity I_0. As Dorman has shown [2], this inverse wave might have been the result of inaccurate meteorological corrections which had been determined using regression coefficients obtained from correlation of mean diurnal I with barometric pressure and isobar height of 100 mb.

At the Freiburg station [3], at which a large cylindrical ionization chamber was used for recording, the meteorological factors were determined by multiple correlation of four variables: the intensity I, barometric pressure, isobar height of 96 mb, and difference in height between isobars 96 mb and 225 mb. When the data for I had been reduced to constant values for the said variables, no further inverse annual wave was detected in Freiburg. Neither is there one in Cheltenham, according to Forbush, [8].

The author determines temperature corrections by Dorman's method [2] from aerological temperature data from the Cheltenham station from 1939 to 1946, and for Soviet stations over the period 1953 to 1957. After temperature corrections had been made, no appreciable inverse annual wave was observed at Cheltenham from 1939 to 1946. The variations in the mean monthly values of I - W were easily correlated with magnetic activity. In the mean annual variation a clearly marked reduction in intensity was noticed during the equinoxes, corresponding to the Corty effect in magnetic activity [4].

Both at Cheltenham and at the USSR stations I was recorded with ionization chambers of similar design. The temperature corrections were calculated by the same method using the same temperature coefficients. However, at the USSR stations the mean monthly values I - W showed inverse annual variations from 0.5 - 1.5% of I_0 [5]. These variations are a smaller percentage of the observed annual wave I than in [1], since the yearly variations in I observed at USSR stations were considerably greater than in Manchester. But the inverse-phase variation in I - W is regular in nature, recurring from year to year. Figures 1 and 2 show variations in mean monthly I - W at the Moscow and Yakutsk stations from 1953 to 1957, at the Freiberg station from 1953 to 1954, and at Cheltenham from 1942 - 1946 (Figure 2) and 1953 - 1957 [8] (Figure 1)*. From the curves in Figures 1 and 2 it is clear that:

1. The mean monthly I - W for Moscow and Yakutsk show regular annual variations with a maximum in summer (Figure 1, curves 1 and 2).

2. The amplitude of the inverse annual variations is greater for Yakutsk than for Moscow (Figure 1, curves 1 and 2).

---

* The data in Figure 2 were corrected for non-cyclic variations by subtracting the smoothed curve. The smoothing was done by averaging for 12 consecutive months using sliding means. Fig. 1 gives data without non-cyclic correction. Data for I and W from Yakutsk were provided by YBSDAS. Data from Freiberg were generously supplied by A. I. Ol'.

3. The inverse annual variation in I - W does not occur in the case of Freiburg or Cheltenham, according to Forbush's data (Figure 1, curves 4 and 5).

4. The spread of the mean monthly I - W for Moscow and Yakutsk (through inverse annual variations) is considerably greater than for Freiburg or Cheltenham.

5. The mean monthly I - W for Cheltenham from 1942 - 1946 do not show appreciable inverse annual variations even when W is calculated by Dorman's formula, and correlate closely with the variation in magnetic activity (Figure 2).

As will be shown below, the different results obtained by Cheltenham and the Soviet stations using Dorman's method for determining the temperature corrections can be explained by the inaccuracy of the temperature coefficients used to compute the corrections at different stations. Because of very great annual oscillations in temperature at the Soviet stations, only a small error in the temperature coefficients is required for appreciable distortion of the residual variations in I - W. A slight increase in the temperature coefficients in comparison with the true ones should produce a regular inverse annual wave I - W.

Effect of Screen

As has already been pointed out, the temperature corrections at the Moscow, Yakutsk and Cheltenham stations (1940 - 1946) were calculated with the use of the same temperature coefficients. Despite the more or less identical thickness of the lead shot surrounding the chamber, however, the instruments at these stations were actually working with different screens, as is clear from Table 1.

Ionization chamber screens consist of their own lead screen and the building screen. The former can be calculated fairly accurately, on the basis of the chamber's dimensions. As shown by Dorman [6], the effective screen for spherical ionization chambers increases with the chamber size, at the same thickness of the lead shot layer. The building screens could only be calculated approximately, particularly before July, 1954, in Moscow, where the screen provided by the building was extensive and unsymmetrical. It can be taken as a rough estimate that in light materials used for roofing (stone, clay, sand, concrete, tar paper, wood), losses in meson energy on ionization are the same as in aluminum. For particles with a kinetic energy 0.3 Bev, energy losses in lead per 1 g/cm^2 amount to 1.15 Mev, and in aluminum 1.65 Mev. To obtain the equivalent screening, the building screen in g/cm^2 was multiplied by 1.5 and added to the chamber screen.

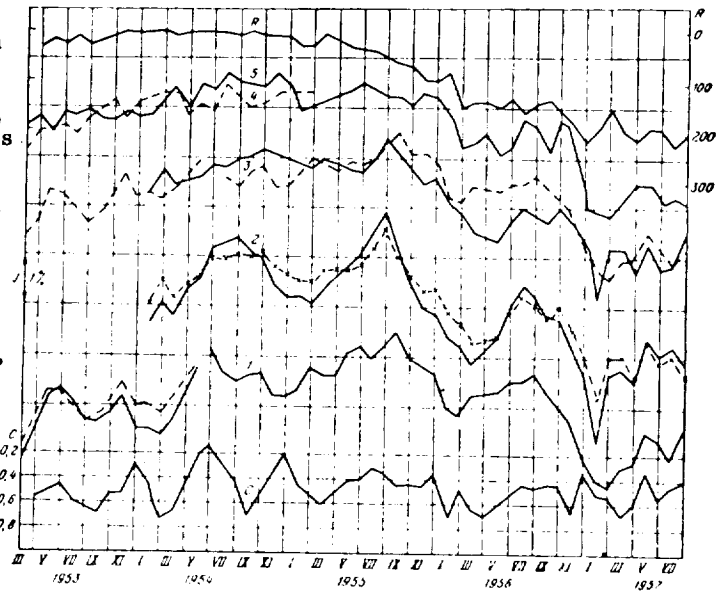

Fig. 1. Variation of average monthly values of I - W. 1 - I - W, Moscow, solid line - W not corrected for screen; 2 - I - W, Yakutsk, dashed line - W corrected for screen, 3 - I - W, Moscow and Yakutsk, corrected for screen and gamma (solid line - Yakutsk, dashed line - Moscow), 4 - I - W, Freiburg; 5 - I - W, Cheltenham, from ref. 8. R - relative number of sun spots; C - index of magnetic activity, average for USSR stations.

The temperature coefficients used for calculating the corrections were derived for minimum total energy of the recorded meson 0.4 Bev, or kinetic energy 0.3 Bev, which corresponds to a screen of 240 g/cm^2 Pb. Table 1 shows that since August, 1954, the screen in Moscow has

Table 1

Station	Recording period	Instrument	Chamber screen, g/cm^2 Pb	Roofing screen, g/cm^2	Total equivalent screen, g/cm^2 Pb	No. of screen
Moscow.....	from July 1954	ASK-1	175	120±20	355	2
Moscow.....	to August 1954	ASK-1	175	40±2	235	1
Yakutsk.....	1953-1957	ASK-1	175	120±5	355	2
Cheltenham.....	1939-1945	C-2	155	>20	>135	3

changed little from that value. It is designated No. 1. The screens in the ASK-1 apparatus in Moscow up to July, 1954, and in Yakutsk for the whole of the period under consideration, were identical (No. 2), and greater than screen No. 1 by 120 g/cm^2 Pb. Screen No. 3 in Cheltenham is smaller than screen No. 1 by at least 50 g/cm^2 Pb.

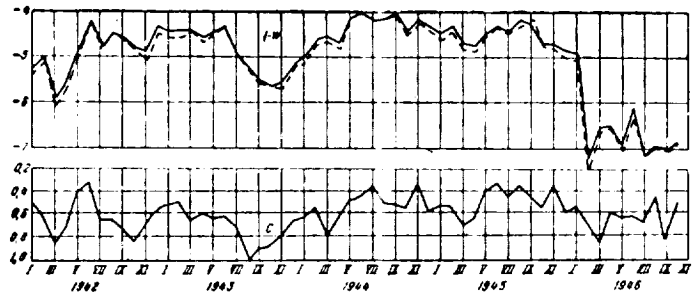

Fig. 2. Variation of average monthly values I - W in Cheltenham. Solid line, without screen correction; dashed line, corrected for screen (W as determined by the Dorman method); C - planetary index of magnetic activity.

To investigate the part played by the screen in producing the inverse annual wave I - W as a value describing the extent of the annual variation in the temperature correction W, we took the difference between the maximum and minimum W_0. This difference will be called ΔW_0. The symbols W_0 and ΔW_0 designate corrections calculated using the same temperature coefficients, regardless of the screen. It can be taken that W_0 describes the extent of yearly temperature oscillations at the stations. Let us use ΔI to designate the difference in I over the same months; $\Delta I - \Delta W_0$ is the extent of the inverse annual wave using temperature corrections W_0. To determine ΔI we selected I from extreme values of W_0, since other factors might have had an effect on the variation in cosmic ray intensity, while we were interested in the inverse wave $\Delta I - \Delta W$ in terms of the temperature corrections.

Table 2

Station	No. of Screen	Months of Extremes in W_0	ΔW_0	ΔI	$\Delta I - \Delta W_0$	$\frac{\Delta I - \Delta W_0}{\Delta W_0}$, %
Moscow.....	1	Feb. and July	4,5	3,9	—0,6	13
Moscow.....	2	Feb. and July	5,2	4,0	—1,2	23
Yakutsk.....	3	Dec. and July	6,3	5,0	—1,3	21
Cheltenham.....	4	Jan. and August	3,0	2,8	—0,2	7

ΔI and ΔW_0 were determined for Moscow for the mean annual variation over the period August 1954 - July 1956 (screen No. 1), and for the annual variation from June 1953 to May 1954 (screen No. 2). In the case of Yakutsk ΔI and ΔW_0 were determined for the mean annual variation from August 1954 to July 1956 (screen No. 2); for Cheltenham we took the mean annual variation from 1940 - 1945. Dorman [2] has given approximate formulae for evaluating the relative variation in temperature coefficients $\delta W - W$ with variation in the screen (see Dorman's

book [2], p. 115):

$$\frac{\delta W_\mu}{W_\mu} = -\frac{\delta\Delta\epsilon}{h_0 - Lx + \Delta\epsilon} \quad \text{for } \mu\text{-mesons},$$
$$\frac{\delta W_\pi}{W_\pi} = \delta\Delta\epsilon \quad \text{for } \pi\text{-mesons}; \qquad (1)$$

here h_0 is the depth of the atmosphere at which I is recorded, (h_0 = 1000 g/cm^2 is taken as equal to unity), L is the path of the meson-generating component (in the units selected it is taken as L = 0.12), $\Delta\epsilon$ is the minimum meson energy for which the temperature coefficients were calculated ($\Delta\epsilon$ = 0.24), x = cos z, where z is the zenith angle of the incident particles. For our purpose, considering the approximate nature of Equation (1) and the inaccuracy of the equivalent screen, we can assume that z = 0 and x = 1.

Substituting numerical values into (1), we obtain

$$\frac{\delta W_\mu}{W_\mu} = -\frac{\delta\Delta\epsilon}{1.12} \quad \& \quad \frac{\delta W_\pi}{W_\pi} = \delta\Delta\epsilon \qquad (2)$$

The variation in the total effect $\left(\frac{\delta W_\mu}{W_\mu} + \frac{\delta W_\pi}{W_\pi}\right)$ will depend on the traction contributed by the μ-meson and π-meson effects to the total temperature correction. W_π is only substantial at great heights, and for $\Delta\epsilon$ = 0.24 the part played by W_π is eight times smaller than W_μ. For a specific case of annual variation, the relative part played by W_π is still smaller, since the annual variations in temperature decrease with height. As a result of the difference in the height distribution of the annual temperature variations, the effect of the change of the screen in ΔW may be somewhat different at different stations.

Fig. 3 shows the variation, calculated from Equation (2), in annual variations of the total temperature correction as a function of the variation in screen for Moscow, Yakutsk and Cheltenham (1942 - 1946). The changes in annual variation are expressed in % of ΔW_0 at the given station (Table 2).

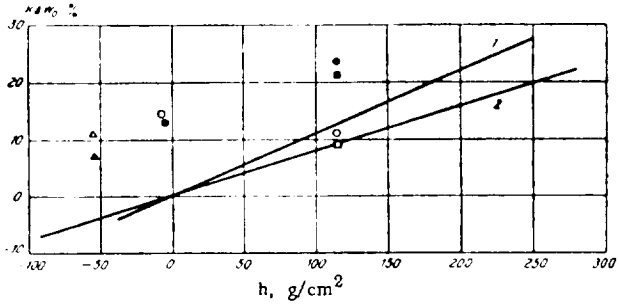

Fig. 3. Changes in annual variation of the temperatue correction as a function of screen. Straight lines calculated by equation (2); 1 - for Moscow and Yakutsk; 2 - for Cheltenham. The plotted data points -- are experimental values of the annual variation $\frac{\Delta I - \Delta W}{\Delta W_0}$, in %; solid points -- without screen correction, open points - with screen corrections; squares -- Yakutsk; circles - Moscow; triangles - Cheltenham.

Fig. 4 shows the experimental values of the inverse annual variation ($\Delta I - \Delta W_0$) ΔW_0 and ($\Delta I - \Delta W_0$)/ ΔW_0 after ΔW has been corrected for the variation in the screen. The values ($\Delta I - \Delta W_0$)/ ΔW_0 increase with the increase in the screen and lie nicely along a straight line parallel to the theoretical one. After correcting W for the screen variation, the inverse annual variation ($\Delta I - \Delta W_0$)/ ΔW_0 does not show any regular dependence on the screen, and it can be taken that its value, within the limits of errors, coincides for all stations. Thus, the difference in the relative inverse annual variation in I - W in Moscow, Yakutsk and Cheltenham can be explained by the use of the same temperature coefficients for calculation of temperature corrections with different screens.

Origin of inverse annual variations with screen 240 g/cm^2

In Moscow, the screen over the apparatus has corresponded fairly closely, since August, 1954, to $\Delta\epsilon$ = 240 g/cm^2, but an inverse wave I - W has been observed (Curve 1 in Figure 1). In Yakutsk the screen correction of W has reduced the inverse wave I - W, but has not eliminated

it completely (dotted curve 2 in Figure 1).

The shape of the I - W curve for Cheltenham, however, has hardly changed after correction for the screen. The relative variation in $(\Delta I - \Delta W_0)/\Delta W_0$ by 4% of ΔW_0 for Cheltenham, where ΔW_0 is small, gives too small a figure in % of I_0 to have any appreciable effect on the shape of the I - W curve in Figure 2.

It seems fairly probably that the inverse seasonal wave at a screen thickness of 240 g/cm^2 is also the result of inaccuracy in the temperature corrections.

The temperature coefficients which were used for calculating W when the screen was 240 g/cm^2 are evidently too high. Indeed, if the inverse wave I - W is a function of the increased temperature coefficients, it must be a function of the annual temperature variation and have the same value in % of W_0 at all stations, which is approximately the actual case (Figure 3). The variation in I expressing the changes in the intensity of primary cosmic rays evidently ought to be the same in percentages of I_0 for Moscow, Yakutsk and Cheltenham, since the geomagnetic latitudes of these stations are close (Yakutsk 51° N, Moscow, 50° 8' N, Cheltenham 50° 1' N) and the instruments used are identical. However, in % of I_0, the variation at Cheltenham is definitely less than in Moscow or Yakutsk. The increase in the temperature coefficients is most likely the result of inaccuracy of the exponent taken in the formula for the differential spectrum of the meson-generating component.

Dorman took $dN/d\epsilon \sim \epsilon^{-(2+\gamma)}$ and $\gamma = 0.5$. At the present time $\gamma = 0.35$ is usually taken for the primary particle differential spectrum in the energy region lower than 30 Bev [7]. Temperature coefficient density curves were calculated for $\gamma = 0$ and $\gamma = 1$. It was assumed that within this range the increase in temperature coefficients is proportional to the variation in γ. The temperature corrections are significantly affected by the value of γ, whereas they vary little when the other constants in the theoretical formulae vary.

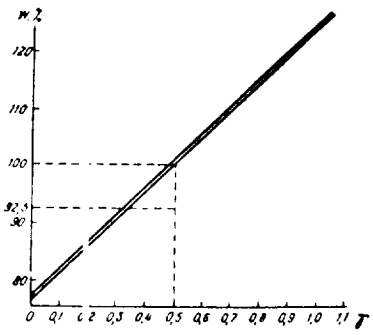

Fig. 4. The Depence of the area under the curve of the density of temperature coefficient, W on the value of gamma.

Figure 4 shows the variation in area under the temperature coefficient density curve during variations in γ from 0 - 1, assuming a linear dependence of the coefficient increment on γ. The area under the curve shows the intensity of variation in percent of the mean, when the temperature varies by 1° C throughout the atmosphere, or the temperature correction W_0. At $\gamma = 0.5$, W_0 is taken in Figure 4 as 100%. Figure 5 shows the relationship between W_0 and actual annual variation ΔW for various stations. In Yakutsk the distribution of annual variations in temperature with altitude, as a first approximation, can be considered the same as in Moscow. It is quite clear from Figures 4 and 5 that when $\gamma = 0.35$, the annual variation in Moscow and Yakutsk should be reduced by approximately 7%, and in Cheltenham by 5%. For Yakutsk, the correction due to the reduction in γ is added to the correction for the screen. In Cheltenham the correction due to γ is opposite in sign to the screen correction and they cancel themselves out. If we use the temperature coefficients corresponding to $\gamma = 0.35$, then as is clear from the curves 3 in Figure 1, the regular inverse annual wave I - W in Moscow and Yakutsk disappear almost entirely. The wide spread of the mean monthly I - W for Moscow and Yakutsk, after the correction for the screen and for γ have been made, is not substantially different from the one for the mean monthly values at Freiburg and Cheltenham. Curve 5 for Cheltenham and curves 3 for Moscow and Yakutsk, are, generally speaking, similar. Slight differences may be due to the observation conditions not being sufficiently constant (for example in Moscow) and to the inaccuracy of meteorological corrections.

Thus, there are no grounds for assuming that there definitely is an inverse seasonal wave in cosmic-ray intensity.

Conclusion

Investigation of the annual variations of nonmeteorological origin in the intensity of the hard

component in cosmic rays, at stations with high annual variation in temperature, requires very careful calculation of temperature corrections. The following conclusions may be drawn from the research carried out:

1. The regular inverse annual wave which is found to exist at USSR stations, after the data has been corrected for temperature by Dorman's method, can be chiefly explained by the insufficient accuracy of the temperature coefficients used.

2. When calculating temperature corrections by Dorman's method, the difference between the actual screen over the instrument and the screen for which the temperature coefficient density curves have been computed must be taken into account. This is particularly important when the temperature variation is great.

3. The value of $\gamma = 0.35$, in the formula for the π-meson-generation spectrum $dN/d\epsilon \sim \epsilon^{-(2+\gamma)}$, seems more probable in the energy region less than 30 Bev rather than the value of $\gamma = 0.5$.

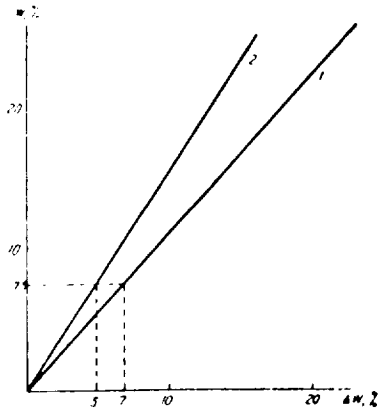

Fig. 5. W_0 in %, as a function of ΔW, in % with a screen of 240 g/cm^2 and $\gamma = 0.5$. 1 - for Moscow and Yakutsk, 2 - for Cheltenham.

Bibliography

1. Dolbear, D. W. and H. Elliot, J. Atm. Terr. Phys., 1, 215, 1951.
2. Dorman, L. I., Cosmic-ray variation, Moscow, Gostekhizdat, 1957, pp. 97-131.
3. Sittkus, A., J. Atm. Terr. Phys., 7, p. 80, 1955.
4. Glokova, Ye. S., Izvestiya AN SSSR, Physics Series, 20, p. 47, 1956.
5. Glokova, Ye. S., L. I. Dorman, N. S. Kaminer, and G. V. Tyanutova. NIIZM Report, 1955.
6. Dorman, L. I., Dissertation, Moscow, NIIZMIR-FIAN, 1955, p. 304.
7. Simpson, J. A., F. Jory, and M. Ryka. J. Geoph. Res., 61, p. 11, 1956.
8. Forbush, S. Variations in cosmic ray intensity during two solar cycles. Report at Fifth General Assembly of CSAGI, Moscow, 30, VII-9.VIII, 1958.

N. S. Kaminer

EFFECT OF SMALL CHROMOSPHERIC FLARES ON INTENSITY OF HARD COMPONENT IN COSMIC RAYS

Introduction

One of the most interesting problems arising in the study of variations in cosmic-ray intensity is the generation of high-energy charged particles on the sun. The great increases in cosmic-ray intensity observed from time to time show that the acceleration of charged particles is due to the processes accompanying the origination and development of chromospheric flares. Since such events, however, are observed very rarely, and chromospheric flares occur on the sun fairly often, it is most probable that the majority of the flares are accompanied by increases in cosmic ray intensity.

Indeed, this effect ("small flare" effect) has been discovered in the neutron [1] and hard [2] components of cosmic rays.

Comparison and analysis of the results of [1] and [2] has led to the rather unexpected conclusion [3] that the small flare effect in the hard component is of a complex nature and is not only due to the influx of additional particles, but also to meteorological factors: the additional stream of short wave radiation leads to variation in the temperature of the atmosphere's upper layers, resulting in variation of the hard component intensity. It appears that the contribution made by the meteorological effect is so substantial that it is mainly responsible for the increase in the small flare effect discovered in [2].

This conclusion, which has been arrived at on the basis of Dorman's coupling factor method [4] is a point of departure for special investigation of the meteorological origin of the small flare effect in the hard component. Below we give the results of this investigation for the hard component of cosmic rays recorded at a number of points in the Soviet Union.

Small flare effect

The effect of chromospheric flares on the intensity of the hard component [2] was studied by the epoch superimposition method. The appearance of a chromospheric flare was indicated by the cessation of short wave radio contact, i.e., cases of very powerful, geophysically effective flares were purposely chosen.

A separate analysis of the data for daytime (9 AM - 4 PM, local time) and night time (4 PM - 9 AM) showed the following:

a) At the moment radio contact ceases on the side of the earth lit by the sun, there is a sharp increase in the hard component intensity by $0.3 \pm 0.06\%$, which gradually fades during the next twelve hours.

b) The effect is totally absent on the unlit side of the earth

Firor [1] has investigated the small flare effect in the neutron component and discovered an appreciable increase in intensity of $0.6 \pm 0.15\%$. The intensity returns to its normal level within two hours. It is characteristic that a relationship was also discovered between the power of the chromospheric flares and the increase in the neutron component with a correlation factor $+0.6 \pm 0.2$.

The results of [2] might have been considered confirmation of the fact that chromospheric flares generate high-energy particles, and that the slow fall in the intensity might have indicated that the generation lasted many hours after the flare began, or that in the regions nearest the sun

there were some kind of scattering centers. The diffusion on these centers made it possible for particles to impinge upon the earth for a long period after they had left the sun.

It was shown in [3], however, that the results obtained in [1] and [2] were incompatible. The amplitude ratio of the neutron effect and hard component should not be 2:1, as was observed, but 40 (50):1. The hypothesis is being put forward that the increase in hard component intensity during cessation of radio communication in the daytime is a meteorological effect: an additional stream of ultraviolet radiation during the flare may cause appreciable temperature variations in the ozone layer and produce the effect observed. This explanation also throws light on such phenomena as the absence of any effect in the hard component when it is dark, and the slow decrease in intensity after the maximu, whose duration is considerably greater than the time that the chromospheric flare lasts.

It should be pointed out at the same time that a direct comparison of the results of [1] and [2] can only be made qualitatively, and even then with great circumspection.

During the research [1] there was discovered a marked relationship between the power of the flares and the amplitude of the neutron component increase. Most of the flares used for the analysis in this research, however, had a power of 1+ or 2. As opposed to this, the small flare effect in the hard component involves exceptionally powerful chromospheric flares causing cessation of short wave radio communication, i.e., flares obviously effective in the geophysical sense. When comparing results this fact should be taken into account. Furthermore, it should not be forgotten that the amplitude of the effect is different for different years [1].

All this suggests that the slight difference in the increases in the neutron and hard components in [1] and [2] may be to a considerable extent the result of a difference (nonuniformity) between experimental data and analytical methods. And if the effect in the hard component cannot be completely explained by the influx of additional streams of cosmic-ray particles, it can be assumed with fair validity that the additional stream and meteorological effects may, under certain circumstances (as, for example, in [2]) make a considerable contribution to the observed increase in the intensity of the hard component.

Experimental data and analytical methods

As had already been pointed out, the expected small flare effect in the hard component is very slight -- considerably less than the accuracy with which the data is recorded. Hence, in order to obtain a statistically significant result, we have to make use of a large amount of experimental data. This can be done by analyzing data from several cosmic-ray stations and selecting a time period over which a large number of flares were recorded on the sun.

During the minimum solar activity in 1954 there were no chromospheric flares on the sun. Some were recorded in the second half of 1955, and then in 1956 solar activity sharply increased and the number of recorded flares reached several hundreds. Hence, for our research we used data for intensity of the hard component during 1956, corrected for the barometric effect. Names of the recording points and their locations are given in the following table.

Cosmic ray recording points

POINT	Geographical		Geomagnetic latitude
	Latitude	Longitude	
Tbilisi	41,7	44,8	36,3
Irkutsk	52,5	104,0	40,8
Moscow	55,5	37,3	50,8
Sverdlovsk	56,2	61,1	48,1
Yakutsk	62,0	129,7	51,0

To obtain reliable results, it is vital to select the correct analytical method. Since the solar-diurnal variation may greatly distort and mask the effect, in earlier research [1,2] it was excluded by subtracting the first harmonic of the mean diurnal variation from the hourly intensity

values. We also used this method, although one of its great disadvantages is that the analytical results may be appreciably influenced by semi-diurnal variation, which during some years is comparable with the actual effect under investigation [5].

Hence, in addition to the above-mentioned method of correcting the data, we used another method which makes it possible to eliminate all regular variations in cosmic rays within the diurnal period. For this, the mean monthly hourly values for intensity are subtracted from the intensities recorded every hour. It is easy to see that in this case we exclude all variations arising in the mean monthly diurnal variation. Admittedly, this method has its disadvantages as well. For instance, if the number of chromospheric flares during the period under analysis is considerable, or if there is a stable (in a diurnal respect) flare effect for the month, it may be considerably weakened under this method.

We therefore used both methods, and were able to compare the results directly.

The analysis was made by the epoch superimposition method. As zero-hour we took the time when a chromospheric flare was observed (or originated). On the left and right of the intensity at zero-hour we note the values for the 6 preceeding and 10 or 18 subsequent hours.

For the research we used data on chromospheric flares from observations carried out by astronomical observatories in the USSR, which network covers the interval from 4 AM to 2 PM world time. Thus, the very important interval between 3 PM and 3 AM is left out.

During observations, the moment of occurrence of a chromospheric flare is recorded comparatively rarely, whereas it is actually the beginning of the flare which it is important to compare with the cosmic-ray data. Taking the consequent uncertainty into account, and striving to improve the statistical accuracy of the data, we arranged our material into sets in such a way that each set contained information on flares observed over a two-hour period. In this way we had six sets of data in which the zero hours related to 7 - 8, 9 - 10, 11 - 12 AM and 5 - 6 PM local time at each recording point. As can be seen from Figures 6 - 14 in the reference [6], during these hours the observation points are outside the impact zones, excluding Moscow and Sverdlovsk, which are in the 9-hour impact zone for only a short period of time. It is clear from this that during the analysis we have to limit ourselves to finding the only possible meteorological effect of the flares in the hard components. This greatly hampers the solution of the task and in effect leaves unsolved the question of the effect of small flares in the hard component due to the influx of additional particles from the sun.

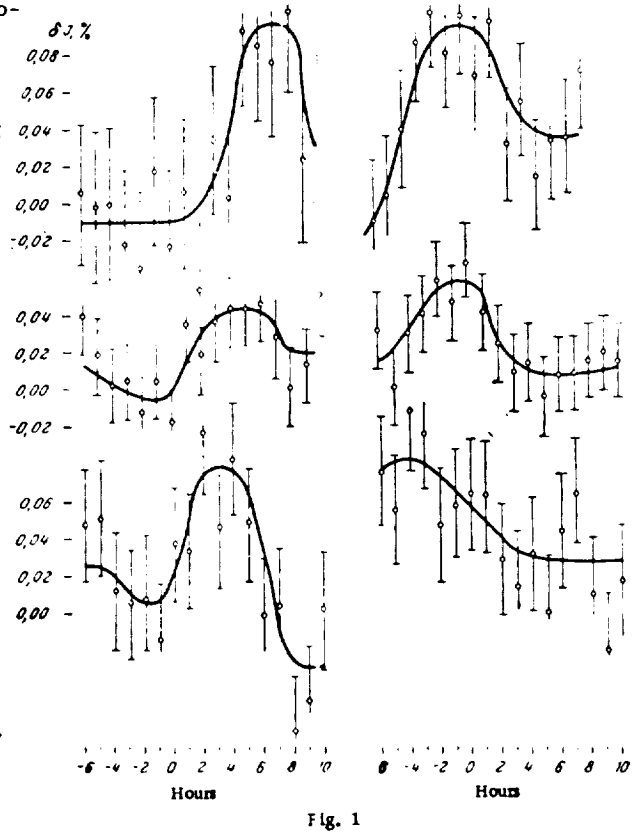

Fig. 1

Results

Let us take a look at the results of the analysis. Investigation of the effect from data for all the points from which the first diurnal variation harmonic has been excluded produces the results shown in Figure 1. The graphs in Figure 1 reveal a characteristic detail: when there are chromospheric flares on the sun, there is a maximum of 0.04 - 0.08% in the intensity of the hard component, and the position of the maximum is hardly dependent at all on the time of observation of the flare on the sun and is recorded at 1 - 3 PM local time. We will now attempt to explain this fact.

The appearance of a maximum in hard component intensity during the afternoon leads to a curious consequence. As pointed out above, it was shown in [2] that chromospheric flares causing cessation of short wave radio communication observed during the part of the day when it is light (9 AM - 4 PM local time) leads to a sharp increase in the hard component intensity of 0.3% with a subsequent gradual decrease. On the basis of data in Figure 1 we plotted a graph for the intensity of flares observed from 9 AM to 4 PM local time. The result shown in Figure 2 looks very much like the result in [2], although the magnitude of the effect is almost one order of magnitude smaller. The reason for this may be that in [2] the chromospheric flares used for analysis were exceptionally strong in their geophysical effect, while most of ours had a power of 1 and 1+. Hence, taking into account the positive correlation between the flare power and the magnitude of the effect in cosmic rays [1], we should not wonder at the difference in the effects in Figure 2 and in [2].

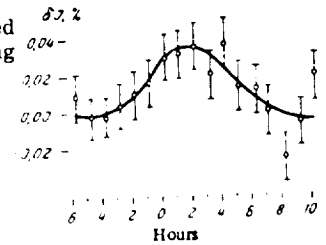

Fig. 2

The gentler increase in intensity shown in Figure 2 compared with the sharp increase reported in [2] is due to the fact that it is only in rare cases that the actual moment of origin of the flare is noted; in most cases flares are observed after they have occurred. Furthermore, there are often several flares in the active region, and the superimposition of these flares must also lead to a diffused "leading front" in the curve, when analyzing it by the epoch superimposition method.

Let us now take a look at results obtained from data for which the mean monthly variations have been excluded. They are shown in Figures 3 and 4.

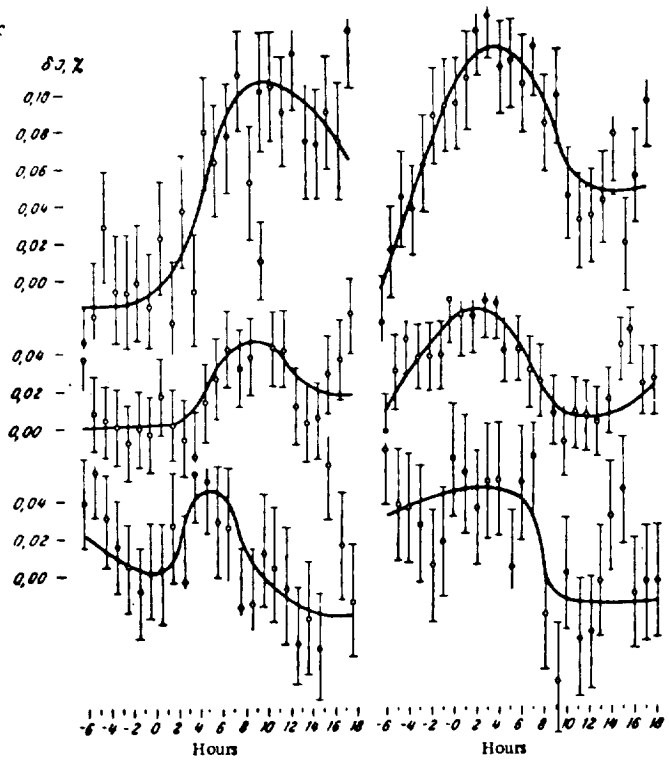

Fig. 3

Figure 3, just as Figure 1, shows an appreciable maximum in the afternoon, although the quality of the results is much poorer. The intensity maximum for flares observed from 9 AM to 4 PM (Figure 4) is also less pronounced.

The poorer quality of the results by the second method and the very fact of a stable intensity

maximum in the hard component in the afternoon, regardless of the time the flares are observed, can apparently be explained from a single standpoint.

The flares are closely associated with active regions on the sun. Hence, the number of flares is determined by the active regions on the visible hemisphere of the sun and the degree of activity of these regions. The time taken by the active regions to pass across the visible hemisphere and the period over which their activity develops are extensive. It may therefore be considered that the probability of a flare appearing at any moment of time during 24 hours is constant. In effect, if it is assumed that the activity of the chromospheric flares is proportional to the energy radiated by them per unit of time during the day in the hydrogen line H_δ, it turns out that this flare activity index is a slowly varying function of time (7). Consequently, if flares are observed during the evening, the probability of them occurring earlier is considerable. This conclusion also follows from our data. That is why it is possible to have a stable maximum in hard component intensity in the daytime during the active periods, provided, of course, it is assumed that the observed effect is of meteorological origin. As confirmation of this it can be added that publication [1] shows the existence of a close connection between the flare activity index and the nuetron intensity increase in impact zones.

The reduction in the clear-cut nature of the effect in Figures 3 and 4 is explained at the same time. If the flare activity index is a slowly varying function of time, the effect of chromospheric flares may even manifest itself in the value of mean monthly hours. When using the second method, we weaken this effect to a considerable extent, which means that the results are not so reliable.

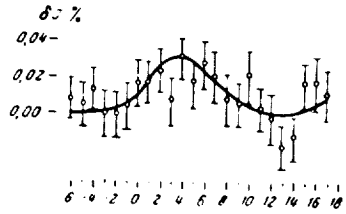

Fig. 4

Let us take it that the observed increase in the hard component by 0.04 - 0.08% is the result of the action of an additional ultraviolet stream of radiation emitted by the chromospheric flares in the upper layers of the atmosphere, most probably in the ozone layer. If it is roughly assumed that the ozone layer is 20 km higher, i.e., that it lies in the layer 0 - 25 mb, the increase in hard component intensity may be explained by a temperature decrease in this layer by (0.04 - 0.08) %: 0.01% ≈ 4-8°C [3, 4].

It is rather difficult to detect this temperature variation directly from radiosounding data for the following reasons:

a) radiosounds are sent out only occasionally - 2 - 4 times in 24 hours;

b) the relative number of radio sounds reaching heights of 25 - 30 km is very small;

c) dispersion of the temperature at these heights due to instrument errors in the radio sondes and advective-dynamic processes in the atmosphere.

Bibliography

1. Firor, J. Phys. Rev., 94, p. 1017, 1954.
2. Dolbear, D., H. Elliot, and D. Danton. J. Atm. Terr. Phys., 1, p. 187, 1951.
3. Dorman, L. I., A. I. Kuz'min, G. V. Tyanutova, Ye. L. Feynberg, and Yu. G. Shafer. 26, p. 537, 1954.
4. Dorman, L. I. Variations in cosmic rays. Gostekhizdat, 1957.
5. Sarabhai, V., V. Desai, and D. Venkatesan. Phys. Rev., 99, p. 1490, 1955.
6. Kaminer, N. S., this issue, p. 149.
7. Trotter, Roberts. Flare activity index, Report NHAO-NBS:0, High Altitude Observatory, Boulder, Colo., 1953.

Section III

EXTRAATMOSPHERIC VARIATIONS IN COSMIC RAYS AND CERTAIN THEORETICAL PROBLEMS

A. I. Kuz'min

BASIC FEATURES OF SOLAR-DIURNAL VARIATIONS IN COSMIC RAYS

Study of diurnal variations in cosmic ray intensity, I, using crossed telescopes [1], investigation of the meteorological contribution of the troposphere to the diurnal effect [2] and correlation of the variations with diurnal and geomagnetic activities [1, 3-8] point equally to the extraterrestrial origin of the greater part of these variations. So far, however, there is no reliable information on the effect of diurnal variation in the temperature of the upper layers of the atmosphere on the diurnal effect of I. Hence, the magnitude of the effect on the earth's surface and at various levels in the atmosphere is not known.

The determination of the chief characteristics of the diurnal variations in I made by Dorman [9] suffers from a number of substantial shortcomings. First, it is assumed in the analysis that the primary variations $\delta D(\epsilon)/D(\epsilon)$ are the same at different points on the globe. When they approach the earth, however, primary cosmic rays redistribute themselves as a result of the influence of the geomagnetic field. Hence, diurnal variations $\delta D(\epsilon)/D(\epsilon)$ may be different in different parts of the world, as qas quite rightly pointed out by the author of [9].

Second, Dorman has assumed that the diurnal variations in I do not vary with time (or if they do, then only slightly). Hence, when determining energy characteristics, he compares experimental data relating to different observation periods (1938-1944 and 1950-1954). However, detailed investigation [3, 5] has shown considerable variations in the diurnal variations in I with the solar activity cycle.

Third, it is assumed without reason [9] that the meteorological contribution does not vary with the latitude of the observation point. It is therefore both desirable and of interest to check the results of earlier research on the chief properties of the diurnal variations in I from synchronous observations in various sectors of the cosmic-ray energy spectrum carried out at a single point.

This article describes the results of processing synchronous cosmic-ray intensity measurements over a wide range of energies from $2 \cdot 10^9$ to $200 \cdot 10^9$ ev recorded by the installations in Yakutsk (λ = 51° North, φ = 193°8' East) over 1957/1958.*

The hard component in I at the earth's surface is recorded in Yakutsk with ASK-1 and S-2 ionization chambers [10] and semicubic triple-coincidence telescope identical to the telescopes set up underground at 7, 20 and 60 m water equivalent (w.e.) [11]. The neutron component in I is measured with a local-generation neutron monitor [12] developed at NIZMIR [13] and later improved at the Yakutsk laboratory [14].

Figure 1 shows solar-diurnal variations obtained by averaging annual observation material from July 1957 to July 1958, making allowance for the barometric effect for each unit separately (crosses). In order to make the data comparable, the readings for different units have been averaged for the period over which they were all working at the same time and over which data was available for complete 24-hour periods.

* The layout of the installations recording the cosmic-ray intensity at the YBSDAS cosmic-ray laboratory will be found at the end of this book.

The barometric effect was calculated with the aid of the following factors: 0.65%/mb for the neutron components [16], 0.11%/mb for the hard component at the earth's surface measured from ionization [21], 0.13%/mb for the hard component on the earth's surface measured from the number of particles [15], and 0.10, 0.08 and 0.04%/mb at 7, 20 and 60 m water equivalent, respectively underground. During the observation period there occurred a large number (about 14) of effective magnetic storms with a pronounced Forbush effect (17), which might have appreciably distorted the true solar-diurnal variations in I, hence the day the storm began and the next day were discarded from the averaged material. The diurnal curves for I obtained in this way are given in Figure 1 (continuous line).

Table 1 gives the amplitude and time of the first two harmonic components of the diurnal variations in I_n measured in different sectors of the cosmic ray energy spectrum. Furthermore, the diurnal variation in I is shown in Figures 2a and 2b which relate to diurnal variations in Ih before and after correction for temperature effect, respectively. The temperature effect correction is made by the standard method [9] using temperature coefficient density curves [9, 15] from data of four soundings of the atmosphere. The errors shown in Figures 1 and 2 and contained in Tables 1 and 2 have been calculated from mean square deviations and represent average errors.

The following designations are used in Table 1 and below: A_{h1} A_{h2} t_{h1} and t_{h2} are the amplitude and time of the maximum of the first and second harmonics for diurnal cosmic-ray variations taking into account the barometric effect; A_{hw} and t_{hw} are the amplitude and time of maximum of the first harmonic taking into account the barometric and temperature effects.

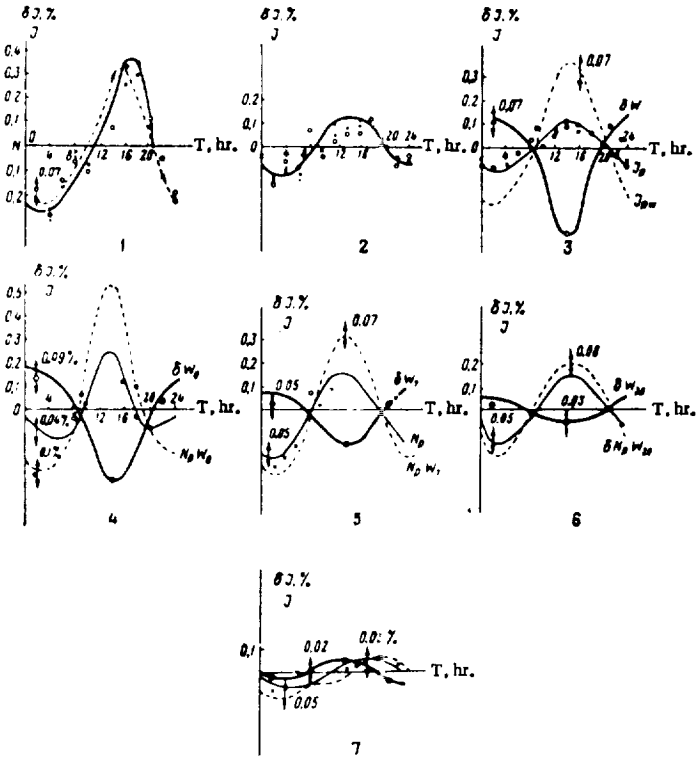

Fig. 1. Diurnal intensity of various components of cosmic rays in 1957-1958.

1 - neutron component; 2 - hard component, measured by ionization under a "thin" shield; 3 - hard component, measured by ionization under a "thick" shield; 4, 5, 6 and 7 - hard component, measured from the number of particles on the earth's surface and underground at a depth of 7, 20, and 60 meters (water equivalent). Thin solid line - intensity, corrected for the barometric effect. Thick solid line - predicted behavior due to diurnal variations of temperature in the atmosphere. Dashed line - intensity corrected for barometric and temperature effects.

If the diurnal variations in I obtained from observations with different installations are compared, the following characteristics can be observed:

1) The diurnal variations in I obtained by averaging annual material before and after exclusion of the Forbush effect [17] differ appreciably one from the other. It is therefore essential to take the Forbush effect into account when studying these variations.

2) The nature of the diurnal variations in I with an increase in energy of the recorded particles does not vary to any appreciable extent. Nevertheless, the amplitude of the variations before the temperature effect is taken into account is not greater than the corresponding value measured

underground at 7 and 20 m.w.e., while the time of the maximum with an increase in recorded particle energy shifts to later hours.

3) The correction for temperature effect substantially increases the amplitude of diurnal variations in the hard component measured at the earth's surface and at 7 m.w.e., but does not alter the nature of the shift in the time of the maximum with the increase in energy. The amplitude of diurnal δI_{pW} after barometric and temperature effects have been taken into account decreases considerably with an increase in the energy of the recorded particles.

4) The amplitude of the diurnal component of the diurnal variations in the hard component of I, measured from the number of particles, is approximately double the corresponding variations in intensity by ionization before the temperature effect is taken into account, and approximately 1.3 larger after it has been taken into account.

5) The amplitude and time of maximum of the semidiurnal component in the diurnal variations in I does not undergo any appreciable change with an increase in recorded particle energy.

The substantial difference between the amplitude of the diurnal variations in the hard component measured at the earth's surface from ionization and the amplitude measured from the number of particles maybe due to the following facts. First, the ionization chamber collects radiation with a solid angle $\omega = 2\pi$, whereas for the semicubic telescope the angle is $\omega \sim \pi$. Second, an ionization chamber screened with 10 cm Pb records the total ionization produced by μ-mesons and equilibrium particles in the soft component [18], and, possibly, also by particles of another nature (neutrons), whereas the telescope does not record "accompanying" particles or neutrons. Since the equilibrium soft component increases with an increase in μ-meson energy [22], the mean energy $\bar{E}$ of the particles recorded by the ionization chamber may be greater than the corresponding mean energy for particles recorded with the telescope.

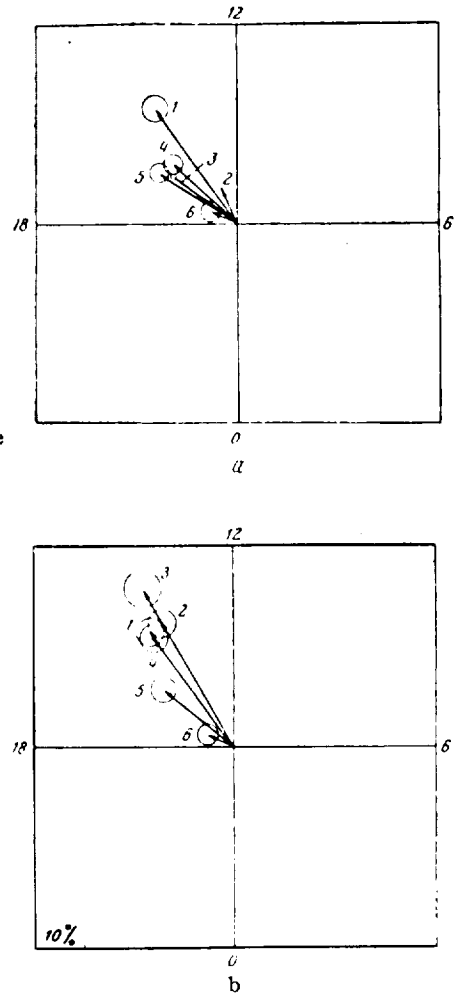

Fig. 2. Harmonic dial of diurnal variations. a - accounted for the barometric effect; b - accounted for the barometric and temperature effects. 1 - neutron component; 2 - hard component, measured by ionization; 3, 4, 5 and 6 - hard component measured from the number of particles on the earth's surface and underground at a depth of 7, 20 and 60 meters (water equivalent).

It is clear from the general trend in the change of the diurnal variations in hard component with depth, after correction for meteorological effects, that the ionization chamber located on the earth's surface at a latitude $\lambda = 51°$, corresponds, on the average, to a semicubic telescope at a depth of 7 m.w.e. below ground at the same latitude. Thus, the difference in the mean particle energies for the hard component at the earth's surface recorded with an ionization chamber and a counter telescope is from 2 to 3 Bev. Clearly, this difference in mean μ-meson energies is due to the difference between the μ-meson energy spectrum at sea level and the corresponding ionization spectrum. The ionization spectrum is considerably harder than the true μ-meson energy spectrum.

It should be pointed out that the diurnal variations in the hard component (prior to correction for temperature effect) on the earth's surface are not greater than the corresponding variations

Table 1

Amplitude and time of maximum for first two harmonics in diurnal variations of I measured by different installations

Meteorological effects taken into account	Harmonic parameters	Neutron component at sea level	Hard component on earth's surface		Hard component at depth of		
			Ionization chamber	Semicubic telescope	7 m w.e.	20 m w.e.	60 m w.e.
Taking barometric effect into account	A_{h_1}, %	0,28± ±0,03	0,080± ±0,002	0,160± ±0,015	0,17± ±0,02	0,18± ±0,02	0,05± ±0,02
	t_{h_1}, hr.	14,4± ±0,5	13,6± ±0,1	15,5± ±0,5	15,2± ±0,6	15,7± ±0,6	16,2± ±1,2
	A_{h_2}, %			0,09± ±0,015	0,03± ±0,02	0,05± ±0,02	0,03± ±0,02
	t_{h_2}, hr.			7± ±0,5	9,6± ±2,0	7,3± ±1,2	8,0± ±2,0
Taking barometric and temperature effects into account	A_{hW}, %	0,28± ±0,03	0,28± ±0,03	0,36± ±0,04	0,27± ±0,0.	0,180± ±0,025	0,05± ±0,02
	t_{hW}, hr.	14,4± ±0,5	14,0± ±0,5	14± ±0,5	14,4± ±0,6	15,4± ±0,7	16,2± ±1,2

7 and 20 m.w.e. below ground. It follows directly from this that the diurnal variations in I are not due to a temperature effect. Indeed, if they had been due to the temperature effect of the μ -mesons, the greatest variations would have been observed on the earth's surface, and as their mean energy increased, they would have decreased proportionally to $1/\epsilon$. In actual fact, the experimental data in Table 1 show that hard diurnal variations on the earth's surface before the temperature correction are not greater than the corresponding variations at 7 and 20 m.w.e. below ground. This relationship between these diurnal variations in I and the μ -meson energy shows that the atmospheric part of these variations due to a negative temperature effect decreases with depth at a much faster rate than the part of the diurnal variations which are not due to atmospheric factors, and that in actual fact there is merely "masking" of the true diurnal variations. In this way, despite what has been assumed [23], the diurnal variations in the μ -meson component of I on the earth's surface are masked to a high degree by the diurnal changes in temperature of the free atmosphere [2] and are not of atmospheric origin.

The reduction in the amplitude of the diurnal variations of the μ -meson component in I with an increase in the mean energy of the particles recorded tallies with out earlier results [20] and shows that the primary particle spectrum responsible for these variations in considerably softer than the spectrum for the whole stream. Since diurnal variations in I are observed at 60 m.w.e. underground, their spectrum stretches at least as far as 200 Bev More detailed information on the spectrum of primary diurnal variations in I can only be obtained with the aid of coupling factors [9] which are given for our installation in [19]. These factors were used to calculate the expected diurnal variations in I for some trial spectra.

$$\frac{\delta D(\epsilon)}{D(\epsilon)} = \begin{cases} a, \epsilon^{\alpha}, & \text{when } \epsilon > \epsilon_1 \\ 0, & \text{when } \epsilon < \epsilon_1 \end{cases}$$

where $\alpha < 0$. It is obvious that in a spectrum of the type $\epsilon^{\alpha} \alpha \leqslant 0$, because the diurnal variations in I decrease with an increase in energy of the recorded particles.

The results of the calculation and the experimental values are given in Table 2. It is clear from this table that the material does not contradict the assumption with regard to the spectrum that

$$\frac{\delta D(\epsilon)}{D(\epsilon)} = \begin{cases} a\epsilon^{-(1\pm 0.2)}, & \text{when } \epsilon > \epsilon_1 \\ 0, & \text{when } \epsilon < \epsilon_1 \end{cases}$$

reduced at ϵ_1 = 10 to 15 Bev. The best agreement (with a more symmetrical distribution of the experimental errors) is found for α = -0.7 at a = 0.050 and ϵ_1 = 12 Bev. The certain discrepancy between the experimental and predicted values cannot be eliminated by a further assumption regarding reduction of upper spectrum or other modification of the spectrum. Indeed, since the diurnal variations in I decrease with an increase in energy, their energy spectrum must decrease. Spectra of the type $\frac{\delta D(\epsilon)}{D(\epsilon)}$ = const or $\frac{\delta D(\epsilon)}{D(\epsilon)} = a\epsilon^{-0.8}$ contradict observations at any ϵ_1 because of the impossibility of agreement with the neutron or hard components at the earth's surface or with data from underground measurements at 20 and 60 m.w.e. Hence, it can be considered as a first approximation that the diurnal variations in I are described by a spectrum of the type

$$\frac{\delta D(\epsilon)}{D(\epsilon)} = \begin{cases} a\epsilon^{-1.0}, & \text{when } \epsilon > \epsilon_1, \\ 0, & \text{when } \epsilon < \epsilon_1. \end{cases}$$

Table 2

Predicted and experimental values of amplitude of diurnal variations in I (in %) at geomagnetic latitude. λ = 51 North.

Assumption regarding nature of energy spectrum		Neutron component at sea level	Hard component: Sea level, From ioniz.	Hard component: Sea level, From partic no.	Hard component: Below ground at (m w.e.), 7	Hard component: Below ground at (m w.e.), 20	Hard component: Below ground at (m w.e.), 60
$\frac{\delta D(\epsilon)}{D(\epsilon)} = \begin{cases} a\epsilon^{-0.7}, \text{when } \epsilon > \epsilon_1 \\ 0, \text{when } \epsilon < \epsilon_1 \end{cases}$	ϵ_1 = 5 Bev; a = 0,0406	0,51	0,28	0,34	0,22	0,15	0,078
	ϵ_1 = 7,5; a = 0,0430	0,42	0,28	0,35	0,23	0,16	0,084
	ϵ_1 = 10; a = 0,0452	0,36	0,28	0,36	0,24	0,165	0,087
	ϵ_1 = 15, a = 0,052	0,50	0,28	0,36	0,270	0,19	0,104
$\frac{\delta D(\epsilon)}{D(\epsilon)} = \begin{cases} a\epsilon^{-}, \text{when } \epsilon > \epsilon_1 \\ 0, \text{when } \epsilon < \epsilon_1 \end{cases}$	ϵ_1 = 5; a = 0,113	0,650	0,28	0,35	0,174	0,160	0,044
	ϵ_1 = 7,5; a = 0,12	0,49	0,28	0,36	0,184	0,120	0,047
	ϵ_1 = 10, a = 0,13	0,40	0,28	0,38	0,20	0,13	0,05
	ϵ_1 = 15, a = 0,155	0,304	0,28	0,38	0,23	0,15	0,06
$\frac{\delta D(\epsilon)}{D(\epsilon)} = \begin{cases} a\epsilon^{-1.2}, \text{when } \epsilon > \epsilon_1 \\ 0, \text{when } \epsilon < \epsilon_1 \end{cases}$	ϵ_1 = 15; a = 0,21	0,7	0,28	0,33	0,15	0,084	0,037
	ϵ_1 = 7,5, a = 0,237	0,53	0,28	0,37	0,165	0,095	0,043
	ϵ_1 = 10; a = 0,259	0,415	0,28	0,39	0,18	0,103	0,047
	ϵ_1 = 15, a = 0,31	0,34	0,28	0,37	0,21	0,12	0,056
Experiment		0,28± ±0,03	0,28± ±0,03	0,36± ±0,04	0,27± ±0,03	0,18± 0,025	0,05± ±0,02

At α = -1.0 the best values are a = 0.155 and ϵ = 15 Bev.

Thus, the variations are due to particles of fairly high energies, which is in agreement with the lack of any appreciable relationship between the diurnal variations and latitude.

It is clear from Table 2 that at a = 0.155 the predicted results agree well with the experiment in the case of cosmic rays on the earth's surface or at only 7 m. w. e. below ground. At 20 and 60 m.w.e. we observe a systematic discrepancy between experimental and predicted effects. This may be due to the fact that the strength of the source a has a tendency to vary with energy, firstly, because of the variation in the effective exponent in the differential energy spectrum of the undisturbed primary cosmic-ray stream with an increase in energy, and, secondly, because of the energy relationship between the angular dimensions of the source in a plane perpendicular to the plane of the ecliptic.

In order to consider these possibilities, however, the direction of the effective source of the

variations has to be determined. The direction of the motion of particles outside the earth's magnetic field is determined by the angles Φ (the angle between the direction of the particle motion in infinity and the plane of the geomagnetic equator) and φ (angle between projection of direction of particle motion in infinity onto geomagnetic equator plane and projection onto same plane of a radius-vector drawn through center of earth to the point on its surface where the particle must strike). These angles are a function of ϵ. In view of the fact that the earth's magnetic field in some way redistributes the anisotropic particle stream, according to Dorman [9] we will only calculate the effective Φ and φ;

Table 3. Location of source of diurnal variations in cosmic rays

Component and observation level	Function	ϵ 12	15	25	35
Neutron component Sea level	$\varphi(\epsilon)$	45	44	41	37
	$\Phi(\epsilon)$	+0	12	26	39
	$W_n(\epsilon, h_0)\frac{1}{\epsilon}$	$0{,}2\cdot10^{1}$	$3\cdot10^{-3}$	$1{,}7\cdot10^{-4}$	$0{,}9\cdot10^{-4}$
	$\varphi(\epsilon)W_n(\epsilon, h_0)\frac{1}{\epsilon}$	9,0	132	70	33
	$\Phi(\epsilon)W_n(\epsilon, h_0)\frac{1}{\epsilon}$	0,0	36,0	44,0	35,0
Hard component. From ionization. Sea level.	$W_\mu^H(\epsilon, h_0)\frac{1}{\epsilon}$	0,45	0,45	1,22	0,90
	$\varphi(\epsilon)W_\mu^H(\epsilon, h_0)\frac{1}{\epsilon}$	20	33	50	33
	$\Phi(\epsilon)W_\mu^H(\epsilon, h_0)\frac{1}{\epsilon}$	0,0	9,0	32,0	35,0
Hard component. From particle number. Sea level.	$W_\mu^T(\epsilon, h_0)\frac{1}{\epsilon}$	0,6	1,0	1,98	1,46
	$\varphi(\epsilon)W_\mu^T(\epsilon, h_0)\frac{1}{\epsilon}$	27	44	81,0	54,0
	$\Phi(\epsilon)W_\mu^T(\epsilon, h_0)\frac{1}{\epsilon}$	0,0	12	53,0	57,0
Hard component. From number of particles. 7 m w.e.	$W_\mu(\epsilon, h_0, 7)\frac{1}{\epsilon}$		0,08	0,28	0,62
	$\varphi(\epsilon)W_\mu(\epsilon, h_0, 7)\frac{1}{\epsilon}$		3,5	11,5	23,0
	$\Phi(\epsilon)W_\mu(\epsilon, h_0, 7)\frac{1}{\epsilon}$		0,96	7,7	24,0
Hard component. From number of particles 20 m w.e.	$W_\mu(\epsilon, h_0, 20)\frac{1}{\epsilon}$		0,02	0,06	0,13
	$\varphi(\epsilon)W_\mu(\epsilon, h_0, 20)\frac{1}{\epsilon}$			0,8	2,2
	$\Phi(\epsilon)W_\mu(\epsilon, h_0, 20)\frac{1}{\epsilon}$			0,5	2,3
Hard component. From number of particles 60 m w.e.	$W_\mu(\epsilon, h_0, 60)\frac{1}{\epsilon}$				
	$\varphi(\epsilon)W_\mu(\epsilon, h_0, 60)\frac{1}{\epsilon}$				
	$\Phi(\epsilon)W_\mu(\epsilon, h_0, 60)\frac{1}{\epsilon}$				

$$\bar{\Phi} = \frac{\int_{\varepsilon_1}^{\infty} \frac{W_1(\varepsilon, h_0)}{\varepsilon} \Phi(\varepsilon)\, d\varepsilon}{\int_{\varepsilon_1}^{\infty} \frac{W_1(\varepsilon, h)}{\varepsilon}\, d\varepsilon},$$

$$\bar{\varphi} = \frac{\int_{\varepsilon_1}^{\infty} \frac{W_1(\varepsilon, h_0)}{\varepsilon} \varphi(\varepsilon)\, d\varepsilon}{\int_{\varepsilon_1}^{\infty} \frac{W_1(\varepsilon, h_0)}{\varepsilon}\, d\varepsilon}.$$

Table 3. (Continuation)

Bev									
45	100	200	$\delta \int \frac{W_1(\varepsilon)}{\varepsilon} d\varepsilon$	$\delta \int \frac{\varphi(\varepsilon) W_1(\varepsilon)}{\varepsilon} d\varepsilon$	$\delta \int \frac{\Phi(\varepsilon) W_1(\varepsilon)}{\varepsilon} d\varepsilon$	φ, deg	$\bar{\Phi}$, deg	t_{max}, hr	$\varkappa$, deg
35	18	10							
41	49	50							
$0,4 \cdot 10^{1}$	$0,25 \cdot 10^{-1}$	$0,25 \cdot 10^{-3}$	6,6						
14	4,5	1,5		264		40		14,5±0,5	7,5±8
16,0	12,0	7,5			150,5		23		
0,62	1,22	0,69	5,87						
20	22	6,9		186,9		32		14,0±0,5	62±8
25,0	60	34,5			195,5		33		
0,91	1,0	0,65	7,60						
32,0	18,0	6,5		262,5		34,0		14,0±0,5	64±8
37,0	49,0	32,5			240,5		32		
0,89	2,31	2,15	5,33						
31,0	41,6	11,5		122,1		23		14,4±0,6	59±9
36,0	106,0	58,0			232,6		44		
3,0	0,46	3,67							
4,6	54,0	4,6		66,2		18		15,4±0,7	69±10
5,3	147	23,0			178,1		48		
	0,2	1,74	1,94						
	3,6	17,4		21,0		10,5		16,2±1,2	73±18
	9,8	87,0			96,8		49,7		

The direction of the diurnal variation source is then determined with the aid of these values $\bar{\varphi}$ and $\bar{\Phi}$. The direction of the source is determined [9] from the formula

$$\varkappa = \bar{\varphi} + (t_m - 12) \cdot 15^\circ,$$

where t_m is the moment of the diurnal variation maximum in local time, and $\bar{\varphi}$ is the effective drift (projection) angle.

When calculating $\bar{\varphi}$ and $\bar{\Phi}$ we used the experimental values of $\varphi(\epsilon)$ and $\Phi(\epsilon)$ [24]. The results are given in Table 3.

It is clear from this table that the entire set of experimental data for the period July 1957 to July 1958 for diurnal variations in cosmic rays at one point with an energy range from 2 to 200 Bev results in approximately the same value of $\varkappa$. The mean for all data is $\varkappa = (66 \pm 11)^\circ$. The effective value of the angle $\bar{\Phi}$ increases with the energy of the recorded particles, reaching 50° at 60 m.w.e. It is clear from this that the source has considerable angular dimensions in a plane perpendicular to the plane of the ecliptic.

Table 2 shows the predicted amplitudes of diurnal variations on the assumption that the strength and the source are the same for the entire energy range. Comparison of experimental data with expected values at $\alpha = -1.0$ shows that despite the agreement within the limits of experimental errors, the observed variations in δI, beginning at a level of 7 m.w.e. are systematically smaller than expected. Hence the strength of the source remains unchanged within Φ angles from 20 to 30°, and constitutes

$$a(20 \div 30^\circ) = 0{,}155 \quad \text{Bev.}$$

On the other hand, Table 2 shows that during measurements at 20 and 60 m.w.e., the predicted variations in δI are greater than the experimental data by a factor of 1.3 - 1.5. It ensures from this that the strength of the source in the region $\Phi = 45$ to 50°, which is mainly responsible for particles causing diurnal variations in I underground at latitude $\lambda = 51^\circ$, should be approximately 1.5 times smaller than in the region $\Phi = 20 - 30^\circ$. Consequently, the coefficient a in the region $\Phi = 45$ to 50° should be $a(50) = 0.11$.

The diurnal variation spectrum

$$\frac{\delta D(\epsilon)}{D(\epsilon)} = \begin{cases} a\epsilon^{-1.0}, & \text{when } \epsilon > \epsilon_1, \\ 0, & \text{when } \epsilon < \epsilon_1 \end{cases}$$

does not differ from the variation spectrum, which is due to electric fields of a solar corpuscular stream. Dorman [9] has shown that the spectrum due both to retardation and acceleration of primary stream particles as well as reflection by electric fields takes the same form.

$$\frac{\delta D(\epsilon)}{D(\epsilon)} = \frac{a}{\epsilon}.$$

If the diurnal variations are really due to the electric fields of the stream, the slight difference in the source strength a(50°) determined from the neutron component and a(50°) determined from underground data, may be evidence of the fact that the strength of the source may increase considerably with energy. Indeed, the total relative variation in the energy spectrum for particles when passing through a stream, taking into account the stream's size and its effectiveness [9], is

$$\frac{\delta D(\epsilon)}{D(\epsilon)} = \frac{\Omega}{2\pi} r(\gamma + 1) \frac{\Delta\epsilon}{\epsilon},$$

where Ω is the solid angle covered by the stream, γ is the exponent in the exponential prime stream energy spectrum, $\Delta\epsilon$ is the maximum possible variation when intersecting the stream, and $r \lesssim 1$. It is known from a number of experiments [25] that the exponent γ increases with an increased energy. Thus, according to [25], the effective value of γ for a region of several tens of Bev is ~ 2, and ~ 3 for several hundred Bev.

It is clear from this that when going from ground measurements to underground measurements, the strength of the source must somehow be increased by a factor of 1.3. If we take this into account, the slight discrepancy in the amplitude of the predicted and observed diurnal variations in the neutron component on Heiss Island is eliminated, and the strength of the source in the region

$\Phi = 45 - 50°$ will be less than in $\Phi = 20 - 30°$ by a factor of approximately 1.8 [a(50°) = 0.08].

Thus, the basic properties of the diurnal variations derived from experimental data obtained with a recording apparatus at one point do not clash with views regarding modulation of the primary stream by solar corpuscular streams [9].

The results can be summed up in the following way:

1. Solar-diurnal variations in the hard component of I are masked to a high degree by temperature variations in the atmosphere.

2. The principal properties of the diurnal variations in I from 1957 to 1958 do not contradict the views regarding the modulation of cosmic rays by solar corpuscular streams carrying a frozen magnetic field [9], where $1H = 5 \cdot 10^7$ cm · gauss.

Bibliography

1. Elliot, H., and D. W. N. Dolbear, J. Atm. Ter. Phys., 1, p. 205, 1951.
2. Kuz'min, A. I., ZHETF, 28, p. 537, 1935, Trudy YaFAN SSSR, Physics Series, Issue 1, p. 11, 1956; K. K. Fedchenko. Arctic, 1957; Ye. S. Glokova, N. S. Kaminer and others. Trudy YaFAN SSSR, Physics Series, Issue 2, p. 82, 1958; Fuks, Shvartsman, Trudy YaFAN SSSR, Physics Series, Issue 2, p. 118, 1958.
3. Sarabhai, V., V. D. Desai, and D. Venkatesen, Phys. Rev., 96, p. 469, 1954.
4. Elliot, H. and T. Tambeapillai, Nature, 171, p. 918, 1953.
5. Glokova, Ye. S., Izvestiya of the AN SSSR, Physics Series, 20, p. 47, 1956.
6. Sekido, J. and S. Ioshida. Rep. Ion. Res. Japan, 4, p. 37, 1950.
7. Kuz'min, A. I. and G. V. Skripin. Trudy YaFAN SSSR, Physics Series, Issue 2, p. 107, 1958.
8. Ioshida, S., I. Kondo Geomagn Geoelectr., 6, p. 15, 1954.
9. Dorman, L. I., Variations in cosmic rays, Moscow, Gostekhizdat, 1957.
10. Shafer, Yu. G., Trudy YaFAN SSSR, Physics Series, Issue 2, p. 7, 1958.
11. Kuz'min, A. I., G. V. Skripin, and A. V. Yarygin. Op. cit. p. 34.
12. Kuz'min, A. I. and A. V. Yarygin. Ibid, p. 36; J. A. Simpson, W. H. Fonger, and S. B. Treiman. Phys. Rev., 90, p. 934, 1950.
13. Kopylov, Yu. N., Instructions and description of neutron monitor, Moscow, NIIZMIR, 1957.
14. Shafer, Yu. G., G. I. Freydman, I. I. Kapustin. Report at Eighth Session of YaFAN SSSR, 1957.
15. Kuz'min, A. I. and A. A. Danilov, Present issue, p. 58.
16. Shafer, G. V., Report at Eighth Session of YaFAN SSSR, 1957.
17. Forbush, J. E., Terr. Magn. Atmos. Electr., 43, p. 207, 1938.
18. Krasil'nikov, D. D., Nauchnyye Soobshcheniya YaFAN SSSR, 1, p. 80, 1959.
19. Kuz'min, A. I. and G. V. Skripin, present issue, p. 121.
20. Kuz'min, A. I., On absorption of diurnal variations in global intensity of hard component of cosmic rays at sea level (in printing).
21. Koval'skaya, A. I., Trudy YaFAN SSSR, Physics Series, Issue 2, p. 85, 1958.
22. Dzhordzh, Ye. (E. George ?), Cosmic-ray physics, edited by G. Wilson, v. 1, ch. VII, Moscow, 1954.
23. Sarabhai, V., Report at Fifth Assembly of IGY, 1958.
24. Dattner, A. and Ye. A. Brunberg, Tellus, 5, p. 269, 1953.
25. Charakhch'yai, A. A. and G. A. Charakhch'yai, ZHETF, 35, p. 5, 1088, 1958.

A. I. Kuz'min, V. D. Sokolov and G. V. Shafer

TWENTY SEVEN-DAY VARIATIONS IN COSMIC RAY INTENSITY

When studying twenty seven-day variations in cosmic ray intensity it is important to take proper note of the effect of the corresponding variations in meteorological factors, which evidently play a considerable role, particularly when the solar activity is at a minimum [1]. In previous publications [2-6] the effect of meteorological factors on twenty-seven-day variations was either not taken into account at all, or not correctly calculated, while in [1] the temperature effect was only calculated for a limited layer of atmosphere. This latter fact is due to the fact that radio sounding of the atmosphere can only be carried out fairly reliably and systematically to a certain ceiling (12 - 15 km). Hence the part played by the upper layers of the atmosphere is still obscure. There are indications, however, [7] that twenty seven-day variations in temperature are possible in the ozonosphere and that they may cause the observed effects. Both to check this hypothesis put forward by Roka [7] as well as to calculate the primary variations in δ I in addition to data for I at the earth's surface, we have to have data on cosmic ray measurements at a depth of at least 40 m. w.e. below ground [8].

This communication gives the results of synchronous measurements of 27-day variations in cosmic rays at one point (Yakutsk) at the earth's surface and below ground over the years 1957-1958, and an attempt is made to determine the primary 27-day variations in I.

Experimental data for δ I were obtained with a standard neutron monitor [9] an ASK-1 ionization chamber [9] and semi-cubic telescopes set up at different levels below ground [11]. For the analysis we used measurements of I from July 1957 through July 1958 in the form of mean diurnal δI_p. The expected variations in intensity δN_μ, conditioned by variations in temperature of the free atmosphere according to Feynberg-Dorman [8], were calculated for the same period from temperature soundings of the atmosphere over Yakutsk. The radio sounding was made by the Yakutsk Weather Service three times in 24 hours; the mean δN_μ was taken as the mean diurnal. The expected variations in δN_μ are calculated taking into account a temperature section of the atmosphere from the earth's surface to a pressure level of 50 mb.

The barometric effect in δI was taken into account with the aid of constant coefficients; for the neutron monitor α_p = -0.68%/mb [12]; for the hard component at the earth's surface α_p = -0.11%/mb [13]; for the hard component at 20 m w.e. underground α_p = -0.08%/mb and at 60 m w.e. = 0.04%/mb [14].

Figure 1 shows the results worked out in the form of difference curves by the epoch superimposition method on the basis of the continous recording of different cosmic ray components in Yakutsk. It follows from these curves that the mean amplitude mean for 3 first peaks) of the 27-day variations in I is (1.35 ± 0.05)% at sea level for neutrons. and (0.52 ± 0.05)% and (0.33 ± 0.05)% for μ-mesons with barometric correction and corrections for barometric and temperature effects, respectively. The 27-day variations were also traced underground at depths of 20 and 60 m.w.e., where the mean amplitude was (0.24 ± 0.06)% and (0 13 ± 0.03)%, respectively.

All the curves are of the nature of damped oscillations: each succeeding peak is approximately half the previous one.

It follows directly from Figure 1 that the 27-day variations in I over the period July 1958 through July 1958 cannot be reduced to atmospheric effects. Indeed, making allowance for temperature variations from the earth's surface to a 50 mb level only reduces the hard component amplitude at the earth's surface by 0.2%, and does not make any contribution to the observed variations at 20 and 60 m.w.e., either.

If we agree with Roka [7] that there are considerable 27-day temperature variations in the ozone layer (0 - 25 mb), and that they completely are responsible for 27-day variations at 60 m. w.e., in accordance with the temperature coefficient density at this depth, ± 0.014% per 1°C,

we should expect an increase in temperature during the peak periods of the 27-day wave by 20 - 30°C.

Variation of this kind in temperature would cause variation in the hard component intensity I on the earth's surface of not more than 0.2 - 0.3%, and not more than 0.06 - 0.1% at a depth of 20 m w.e., but with a phase opposite to that observed. At the same time, the presence of similar temperature variations would not have a marked influence on the intensity of the neutron component [8]. Thus we are unable to explain the 27-day variations in I by changes in temperature in the upper layers of the atmosphere. We can only assume that they are basically of non-atmospheric origin.

It is clear from Figure 2, which shows the mean diurnal intensities of the neutron and hard component at the earth's surface, that the zero days selected with minimal I coincide with effective magnetic storm periods. This shows the possibility that the 27-day variations in I and the tendency towards a 27-day repetition of the effective magnetic storms [16] have a common source of disturbance. Whether this assumption is right or not can be checked by comparing the experimental ratios of the 27-day variations for different components in I with the ratio of the mean reduction in intensity of these components during effective magnetic storms. They can be found in Table 1.

It is quite clear from Table 1 that the ratios of the amplitudes of the 27-day variations for different I components are really very close to the ratios of the mean reduction in the corresponding I components during effective magnetic storms. Within the limits of experimental error it can be asserted that the 27-day variations and the reduction effect during magnetic storms are of the same nature.

The following should also be pointed out at this juncture. Since the 27-day variations in I have a marked amplitude below ground at least to a depth of 20 m w.e., it follows directly that the spectrum of the primary variations in I certainly stretches beyond an energy of 80 Bev.

Table 2 gives the results of the calculation of

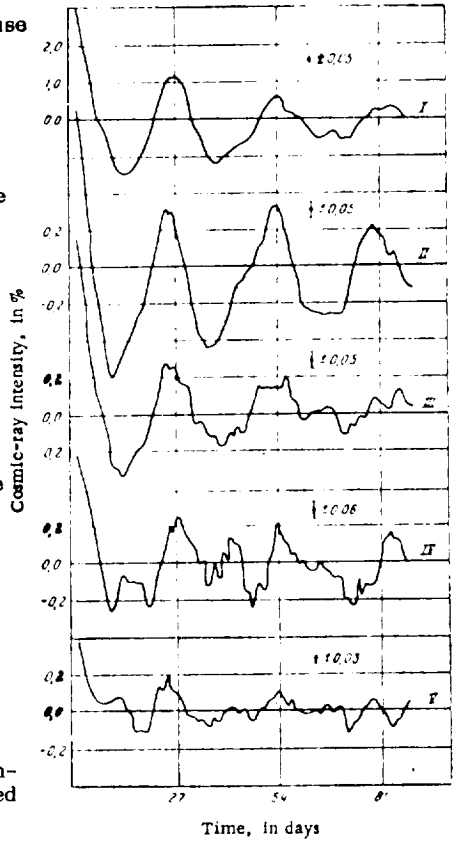

Fig. 1. Difference curves of 27-day variations in cosmic ray intensity from July, 1957 to May, 1958, in Yakutsk. I - neutron component corrected for barometric pressure, II - hard component on the surface of the earth, corrected for pressure, III - hard component on the surface of the earth, corrected for pressure and temperature, IV - hard component, underground, at a depth of 20 m w.e., corrected for pressure; V - hard component underground, at a depth of 60 m w.e., corrected for pressure.

Table 1

	Neutron monitor ASK-1 (δI_{pN})	Telescope 20 m w.e. ASK-1	Telescope 60 m w.e. ASK-1
From data for 27-day variations.....	4±0,8	0,73±0,3	0,4±0,15
From data for effect during magnetic storm....	3,5	0,69	0,27

predicted relationships between the variations in I with different assumptions with regard to the primary variation spectrum.

Since the 27-day variations decrease as the mean particle energy increases, the variation in the primary spectrum $\delta D(\epsilon)/D(\epsilon)$ can only be satisfied by those exponential spectra of the type ϵ^{α} for which $\alpha < 0$. The calculations were made on the basis of a coupling factors [8] for the installations described in [16].

It is clear from Table 2 that the experimental results (mean for first three

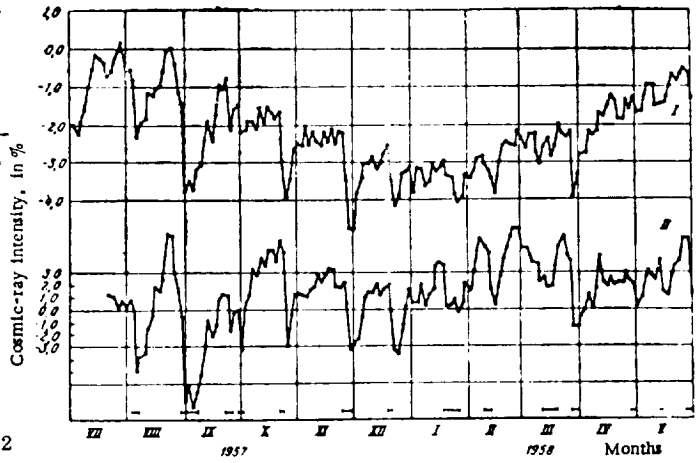

Fig. 2. Mean diurnal values of cosmic-ray intensity. I - hard component on the surface of the earth, corrected for pressure and temperature; II - neutron component, corrected for pressure.

Table 2. Predicted and experimental results of twenty-seven-day variations in I.

Test spectrum	ϵ_1, Bev.	I_0 (ASK-1)	I_{20} (ASK-1)	I_{60} (ASK-1)
$\frac{\delta D(\epsilon)}{D(\epsilon)} = \begin{cases} -a, \text{ when } \epsilon < \epsilon_1 \\ 0, \text{ when } \epsilon > \epsilon_1 \end{cases}$	30	2,9	0,02	0,00
	60	1,83	0,21	0,00
	100	1,46	0,57	0,01
	140	1,33	0,86	0,05
	180	1,26	0,97	0,14
	220	1,21	0,99	0,31
	260	1,20	0,99	0,43
	∞	1,00	1,00	1,00
$\frac{\delta D(\epsilon)}{D(\epsilon)} = \begin{cases} a\epsilon^{-1}, \text{when } \epsilon < \epsilon_1 \\ 0, \text{ when } \epsilon > \epsilon_1 \end{cases}$	60	3,8	0,05	0,00
	100	3,50	0,21	0,00
	140	3,48	0,31	0,02
	180	3,48	0,36	0,04
	220	3,48	0,37	0,06
	260	3,48	0,37	0,09
	∞	3,30	0,38	0,15
$\frac{\delta D(\epsilon)}{D(\epsilon)} = \begin{cases} a\epsilon^{-0.5}, \text{when } \epsilon > \epsilon_1 \\ a, \text{ when } \epsilon < \epsilon_1 \end{cases}$	3,0	2,02	0,74	0,42
	5,0	2,28	0,73	0,42
	7,0	2,53	0,71	0,41
	9,0	2,74	0,69	0,39
	11,0	2,83	0,65	0,37
	13,0	2,86	0,60	0,34
	15,0	2,87	0,56	0,31
	20,0	2,70	0,50	0,28
$\frac{\delta D(\epsilon)}{D(\epsilon)} = \begin{cases} a\epsilon^{0.7}, \text{when } \epsilon > \epsilon_1 \\ a, \text{ when } \epsilon < \epsilon_1 \end{cases}$	3	2,62	0,61	0,28
	5	3,25	0,59	0,27
	7	3,75	0,55	0,25
	9	4,10	0,50	0,23
	11	4,10	0,44	0,20
	13	4,01	0,37	0,17
	15	3,85	0,33	0,15
	20	3,36	0,30	0,13
Experiment.....		4,0±0,8	0,7±0,3	0,4±0,15

periods) do not agree with the assumption that $\delta D(\epsilon)/D(\epsilon)$ = const with a reduction at ϵ_1 = 40 to 600 Bev, but do not belie the spectrum

$$\delta D(\epsilon) \quad D_{(\epsilon)} = \begin{cases} a \\ a\varepsilon^{-(0.6 \div 0.7)}. \end{cases}$$

More accurate data for α can be obtained by increasing the accuracy of the experiment. It should be pointed out this spectrum does not agree quantitatively, but qualitatively it does not contradict the assumptions with regard to the nature of the 27-day variations in I expressed in [8].

Bibliography

1. Sokolov, V. D., Papers of YBAS, Physics Series, Issue 2, p. 123, 1958; Ye. S. Glokova, G. V. Tyanutova. NIIZMIR Report, 1955; A. I. Kuz'min, G. V. Skripin, Papers of YBAS, Physics Series, Issue 1, 1956.
2. Hess, V. F., Terr. Magn. Atm. Elektr., 41, p. 345, 1936.
3. Monk, A. T., and A. N. Compton, Rev. Mod. Phys., 11, p. 175, 1939.
4. Broxon, J.W., Phys. Rev., 62, p. 508, 1942.
5. Cheri, H. and R. Steinmaurer, Acta. Phys. Austriaca, 1, p. 42, 1957.
6. Hogg, A. R., J. Atm. Terr. Phys., 1, p. 56, 1950.
7. Roka, E. G., Zs. Maturforsch., 5a, p. 157, 1950.
8. Dorman, L. I., Cosmic ray variations, Gostekhizdat, 1957.
9. Kopylov, Yu. M., IGY Papers, Cosmic Ray Series, Issue i, 1959.
10. Shafter, Yu. G., Papers of YBAS, Physics Series, 2, p. 7, 1958.
11. Kuz'min, A. I., G. V. Skripin, and A. V. Yarygin, Ibid, p. 34.
12. Shafer, G. V., Ye. S. Glokova, and L. I. Dorman, NIIZMIR Report for 1955.
13. Koval'skaya, A. I., Papers of YBAS, Physics Series, Issue 2, p. 85, 1958.
14. Kuz'min, A. I. and A. A. Danilov, Present collection, p. 58.
15. Sekido, Y., M. Wada, Report Ionos. Res. Japan, 9, p. 174, 1955.
16. Kuz'min, A. I., and G. V. Skripin, Present issue, p. 121.

G. I. Freydman and G. V. Shafer

SOME RESULTS OF COMPARING NEUTRON AND HARD COMPONENT VARIATIONS DURING THE PERIOD, AUGUST - OCTOBER, 1957

Considerable variations in cosmic ray intensity were observed during the period from August to October, 1957. During this time two ionization chambers (ASK-1 with a volume of 950 liters at 10 atmospheres of pressure, with a lead screen 10 cm thick and roofing ~120 g/cm^2; and a S-2 with a 20 liter volume at 50 atm, with a 10 cm lead screen and roofing ~20 g/cm^2) and a standard neutron monitor were operating continuously under a roofing of 50 - 100 g/cm^2.

Graphs of the mean diurnal readings for these instruments corrected for atmospheric effects are shown in Figure 1. Magnetic storms with a sudden beginning are also shown. The storm data was received from the Yakutsk magnetic station.

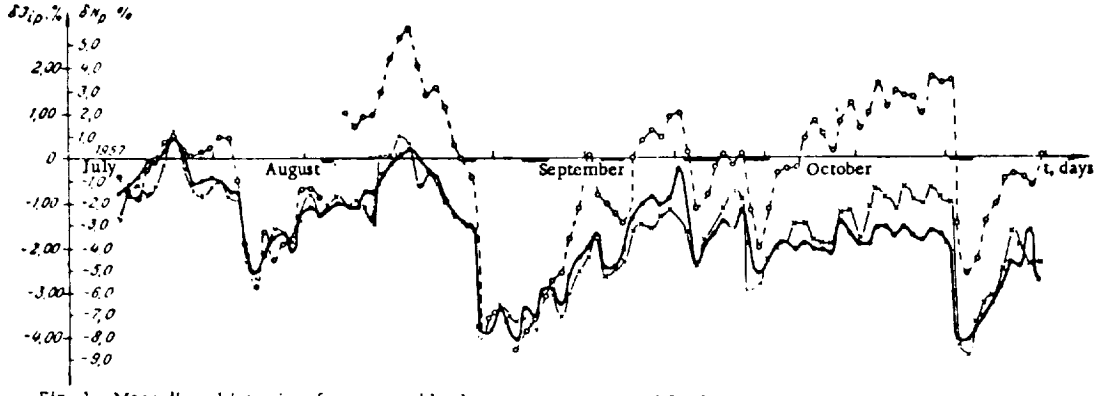

Fig. 1. Mean diurnal intensity of neutron and hard components, corrected for the barometric effect, during July - October, 1957. –○–○–○– neutron monitor, ···●—●—●··· ASK-1 chamber, ···×–×–× S-2 chamber, - periods of magnetic storms.

It is clear from the graphs that from August to October, 1957, except for three, all the storms with a sudden beginning were accompanied by a more or less sharp reduction in cosmic ray intensity. Furthermore, from August 16 - 29 there was a slow variation in intensity, apparently due to a variation in the intensity of the primary spectrum. The smooth rise in the readings shown by the neutron monitor and S-2 chamber from the beginning of October to October 20 were not accompanied by any such change in the ASK-readings. The reason for this discrepancy is not clear. It may be due to instrument errors, although they worked perfectly during this period.

Table 1 gives the basic characteristics of the cosmic ray intensity reductions and accompanying magnetic storms. Column 3 shows the time of the beginning and end of the steepest decrease in ASK-1 readings, corrected for collisions and barometric effect and column 4 shows the rate of this decrease. For the storms on August 3, September 29 and October 21 the rate at which the intensity was reduced is of the same nature, while it is greater by a factor of 4 or 5 in the case of the storm on August 29. It should be pointed out, however, that the figures given in the third and fourth columns do not describe the rate and continuity of the initial phase in the intensity drop completely objectively, since it was not possible to separate the total drop in intensity from

diurnal variations which were probably growing at that time on the basis of data from one station.

Table 1

Time of beginning and end of magnetic storm	Character of magnetic storm	Time of linear decrease	Rate of decrease during this period, %/hr	Decrease in intensity of mean diurnal values		$\frac{\delta N_p}{\delta I_{p,W}}$	ϵ_{max}, Bev	Time to reestablish one half of the maximum value
				δN_p, %	$\delta I_{p,W}$, %			
3.VIII, 16.00—4.VIII, 4 hrs	Small	4.VIII, 8—18 hrs	0.25	4.8±0.2	1.8	2.7	100—120	4 Days
29.VIII, 19.21—30.VIII, 13 hrs	Large	29.VIII, 21—23 hrs	1.25	6.5±0.2	2.3	2.8	100—120	10-12 Days
13.IX, 00.45—14.IX, 19 hrs	Very large	—	—	(1—1.5)±0.2	0.8	1.2—2.0	170—300	—
21.IX, 10.10—25.IX, 17 hrs	Very large	—	—	4.5±0.2	2.2	2.0	150—180	6-8 Days
29.IX, 00.15—1.X, 10 hrs	Very large	29.IX, 6—17 hrs	0.20	4.0±0.2	1.5—2.0	2.0—2.7	120—170	3-5 Days
21.X, 22.41—23.X, 14 hrs	Moderate	22.X, 00—20 hrs	0.20	9.0±0.2	2.5—3.5	2.6—3.6	90—120	6 Days

Columns 5 and 6 in Table 1 show the greatest drop in mean diurnal readings in the neutron monitor corrected for pressure/barometric factor $K_p = (-0.68 \pm 0.01)\%/mb$, and the ionization chambers corrected for collisions and barometric and temperature effects. The barometric factor for the ASK-1 chamber is $(-0.11 \pm 0.01)\%/mb$ and $(-0.14 \pm 0.01)\%/mb$ for the S-2. The temperature corrections were made by the Feynberg-Dorman method taking into account the atmosphere's temperature section up to a pressure level of 50 mb. The seventh column shows the ratios of the figures contained in the fifth and sixth columns.

Column 8 shows the effective upper limit of the intensity reduction calculated on the assumption that the variation spectrum is in the form given in reference [1]

$$\frac{\delta D(\varepsilon)}{D(\varepsilon)} = \begin{cases} a & \text{at } \varepsilon < \varepsilon_{max} \\ 0 & \text{at } \varepsilon > \varepsilon_{max} \end{cases}$$

It is clear from Table 1 that the difference ϵ_{max} exceeds possible errors in the case of certain storms. Consequently it may be considered that the effective upper limit of the reduction in cosmic ray intensity during August - October 1957, changes from one storm to another within several tens of Bev, remaining above 90.

The ratio $\delta N_p / \delta I_{ipW}$ for the smooth variation in cosmic ray intensity from August 16 - 29 is 2.7 - 3.5, i.e., in this case 80 Bev $\leqslant \epsilon_{max} \leqslant$ 120 Bev.

Thus, from August - October 1957, there were both smooth and sudden changes in intensity in the energy interval with an effective upper limit of at least 80 Bev.

From data contained in [2, 3] the ratio between the variations in the neutron monitor readings in climax and the ionization chamber readings in Freyberg from June - October 1951 was from 4 to 5. If it is considered that these publications quote neutron component data at mountain level, we can see that in 1951 variations in the primary spectrum occurred over an energy interval with an effective upper limit of not more than 80 - 90 Bev.

By comparing ϵ_{max} for variations in 1951 and 1957 we can see that during the period over which solar activity increased, cosmic ray intensity variations occurred over a wider energy

interval than when there is a decrease in solar activity. It should be pointed out, however, that the increase in ϵ_{max} may not be due to an expansion of the energy interval for particles acted on by the mechanism reducing the cosmic ray intensity, but to a variation in the type of primary spectrum in 1957 compared with that in 1951, or to some discrepancy in the coupling factors used to evaluate ϵ_{max}.

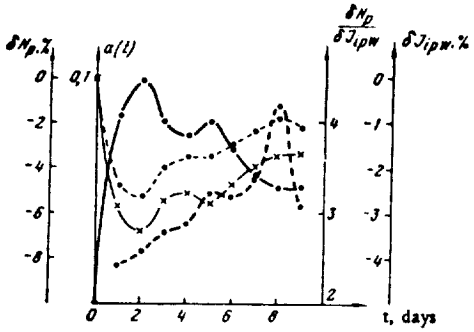

Fig. 2. Variations of various components averaged for the periods of magnetic storms; 3 August, 29 August and 21 October of 1957.

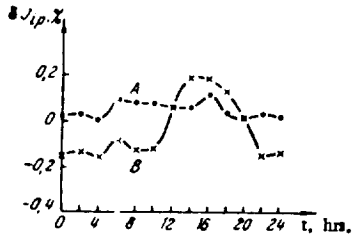

Fig. 3. Diurnal intensity of the hard component, corrected for the barometric effect, averaged for periods: A - slow recovery after magnetic storm, B - during quiet days before the storm.

Figure 2 shows the variation of a, which describes the effectiveness of the mechanism responsible for the intensity reduction, and the ratios of the reduction in the neutron monitor readings to the S-2 chamber readings averaged for three cases of extensive reductions (August 3 and 29, and October 21). As the zero day we chose the day preceeding the commencement of the reduction. It follows from the data in Figure 2 that at the same time as the reduction in the effectiveness of the mechanism responsible for the fall in cosmic ray intensity there is also a reduction in the effective limit of energies of particles experiencing the mechanism.

It is not possible to elucidate the variation in the properties of diurnal variations over the first two or three days after the sudden drop in intensity begins on the basis of data from only one station. But data from one station is enough to draw certain conclusions with regard to the diurnal variations during the period over which the intensity is smoothly restored. Figure 3 shows diurnal variations in hard component intensity measured with an ASK-1 ionization chamber, corrected for ionization collisions, barometric effects and the non-cyclic effect, which was considered linear. The curve A is obtained by averaging data for the periods from January 24 to 27, August 31 to September 2, October 1 to 2, and October 24 to 27, i.e., the periods when the intensity was slowly being restored two to three days after the beginning of the sharp drop. The curve B is obtained by averaging for the periods January 17 - 20, August 26 - 28 and October 15 - 20, i.e., on relatively calm days preceeding the sharp intensity drops.

It is clear from Figure 3 that in these four cases, over the first 2 - 4 days after the intensity had begun to recover, the amplitude of the diurnal variations of global intensity in hard component is smaller by several times than on preceeding calm days. However, during the drop of August 4, during the period August 7 - 10, the diurnal variations in hard component did not decrease in amplitude, but rather there was a sharp change in the maximum time (8 - 10 hours local time instead of 12 - 16 hours). This is also confirmed by the neutron monitor. As a result of the small statistical accuracy of the neutron monitor data, however, a detailed comparison of the variations in the properties of diurnal variations in neutron and hard components cannot be made.

From the five cases considered we can make the following tentative suggestions:

1. For the first two to four days after the intensity of the cosmic rays begins to gradually recover, i.e., two to four days after the sudden drop, the nature of the diurnal variations sharply changes compared with the calm days.

2. The variation in the nature of the diurnal variations may be different for different cases.

Bibliography

1. Dorman, L. I., Cosmic ray variations, Gostekhizdat, 1957.
2. Simpson, J. A., Phys. Rev., 94, p. 2426, 1954.
3. Fonger, W. H., Phys. Rev., 91, p. 351, 1953.

F
6
7

A. I. Kuz'min and G. V. Skripir

REDUCED INTENSITY OF COSMIC RAYS DURING MAGNETIC STORMS

Reports that a reduction in cosmic ray intensity was observed during certain magnetic storms began to come in at the time when the first experimental material had been obtained from continuous recording of the intensity of the μ-meson component in cosmic rays [1, 2]. It was noticed [3, 4] that during effective magnetic storms a sharp reduction was typical, followed by a comparatively slow several-day-long recovery of the normal level.

It was shown in 1937 for the first time [5] that this effect was of a world-wide nature. The magnitude of the effect [3 - 8%] for the neutron and hard components at sea level, and also its world-wide nature show [6, 7] the clearly non-atmospheric origin.

More thorough statistical study of observations in cosmic ray intensity over a period of about 30 years has shown the following interesting statistical regularities in the reduction in intensity during magnetic storms.

1. If the intensity of the cosmic rays changes during magnetic storms, this change is only of the nature of a decrease. The intensity first falls for 15 - 40 hours, after which it recovers its normal level in 4 - 6 days [8].

2. There is no simple connection between variations in the earth's magnetic field and the corresponding changes in cosmic ray intensity [8].

3. Brief magnetic storms normally only cause slight variations in cosmic ray intensity [8].

4. Most magnetic storms during which the variation in cosmic ray intensity was more than 1% at two stations at least can be classed as strong and very strong magnetic storms [7].

5. Most effective magnetic storms have a sudden beginning [9].

6. If a considerable cosmic ray effect is observed during a magnetic storm at any station (let us say 1%), we may fully expect it to be detected at other stations as well, i.e., it will be of a world-wide nature, and the magnitude will not be a function of the geomagnetic latitude [7].

7. Storms accompanied by an appreciable decrease in cosmic ray intensity correlate closely with the passage of a group of sunspots [9] through the central meridian.

8. Most meteorological effects increase the true reduction in the hard component intensity [10].

It should be pointed out that all these regularities have been brought to light on the basis of experimental data on cosmic ray intensity obtained with the aid of instruments at sea level and above at different geomagnetic latitudes and longitudes. Thus, it has only been possible to obtain information on the behavior of primary particles with an energy up to 15 Bev. Until recently the following questions remained open:

1) what was the upper limit and 2) what was the energy spectrum of particles subjected to the cosmic ray effect during magnetic storms.

The first attempt to answer these questions was made by L. I. Dorman [11]. Using coupling factors, it is possible to determine the type of primary particle energy spectrum from the observed variations in secondary component intensity by using the formula

$$\frac{\delta D(\varepsilon)}{D(\varepsilon)} = \begin{cases} -a, & \text{when } \varepsilon \leqslant \varepsilon_1 \sim 40 \text{ Bev} \\ 0, & \text{when } \varepsilon \geqslant \varepsilon_1 \sim 40 \text{ Bev}, \end{cases} \qquad (1)$$

i.e., during effective magnetic storms primary particles with an energy up to 40 Bev are eliminated. This result fits in with Dorman's view that the scattering of the primary particles in the cosmic rays is due to frozen magnetic fields of solar corpuscular streams. In his latest research, Dorman [12] confirms this result on the basis of material from a large number of

stations recording neutron and hard components at sea level.

This evaluation is a rough approximation, since it has been obtained from experimental data for the cosmic ray intensity in the stratosphere and at two different latitudes providing information on the energy spectrum of primary rays in the region less than 15 Bev. Furthermore, as one of the authors of the present article has shown [13], the coupling factors used to obtain this result are unreliable.

The series of observations of cosmic ray intensity over the range of middle energies from 20 to 400 Bev, completed in Yakutsk by the beginning of the IGY, and new coupling factors make it possible to make a more accurate determination of the upper limit and of the energy type of primary particles which have undergone the effect of magnetic storms, and to bring to light certain regularities in the cosmic ray effect during magnetic storms.

Experimental data and analytical method.

In this research use was made of material from continuous recording of the intensity of cosmic rays from November 1957 to September 1958, with a standard neutron monitor, ASK-1 ionization chamber and counter telescopes [14] both at the earth's surface and at 7, 20 and 60 m w.e. below ground. The temperature corrections to the mean diurnal cosmic ray intensities were based on the Feynberg-Dorman system [11]. The barometric effect was calculated using the factors shown in Table 1.

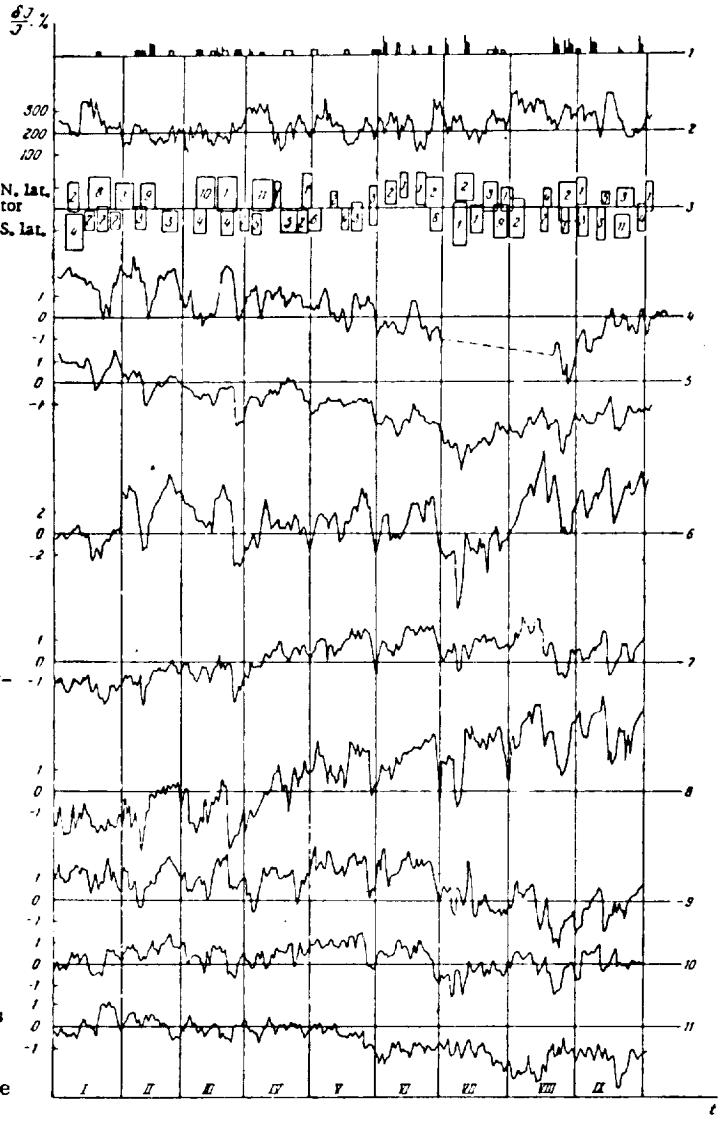

Fig. 1. Mean diurnal intensity of different components of cosmic rays on the earth's surface and below ground, from January 1 to October 1, 1958: 1 - Moment of beginning and end of magnetic storms; 2 - relative number of sunspots on the entire sun-disc; 3 - location of active regions on the sun relative sun's equator and periods of their passage through the central solar meridian. Numbers give duration of existence of active regions in revolutions of the sun; 4 - 11 - cosmic ray intensity: 4 - ASK-1, Moscow, 5 - ASK-11, Tiksi, 6 - neutron component, Yakutsk; 7 - ASK-1, Yakutsk; 8 - counter telescope on the earth's surface, Yakutsk; 9 - counter telescope below ground at 7 m w.e., Yakutsk; 10-20 m w.e., Yakutsk; 11-60 m w.e., Yakutsk.

Data from the whole series of observations of cosmic ray intensity are shown in Figure 1 in the form of mean diurnal

Table 1

Apparatus	Level of observation	Notation for recorders	Mean energy of primary particles, BEV	Barometric coefficient, % /mb	Mean diurnal statistical accuracy, %
Neutron monitor	Sea level	N	27	- 0,67	0,18
Ionization diameter	"	K	60	- 0,11	0,03
Counter telescope	"	T_0	45	- 0,13	0,07
" "	7 m w.e.	T_7	70	- 0,10	0,09
" "	20 m w.e.	T_{20}	150	- 0,08	0,010
" "	60 m w.e.	T_{60}	450	- 0,04	0,14

values corrected for barometric and temperature effects (I_{pW}). For purposes of comparison the same diagram shows the mean diurnal values of I_p in Tiksi and Moscow. The magnetic storms are marked at the top of the diagram in different sized rectangles. The smallest one stands for the slight magnetic storm, and the largest one for a very strong storm. The shaded rectangles represent effective magnetic storms causing a reduction in cosmic ray intensity. The rectangles with a little stroke at the beginning show magnetic storms with a sudden beginning. The storms have been classified by the Yakutsk magnetic observatory. In addition to this, Figure 1 gives a schematic representation of the active regions on the sun by means of rectangles. The sides of the rectangle show the boundaries of the regions in solar latitude and the moments at which the regions pass through the central solar meridian. Mean diurnal figures for solar activity are plotted on the same axis (Wulf number, W). The solar data are taken from Cosmic Ray

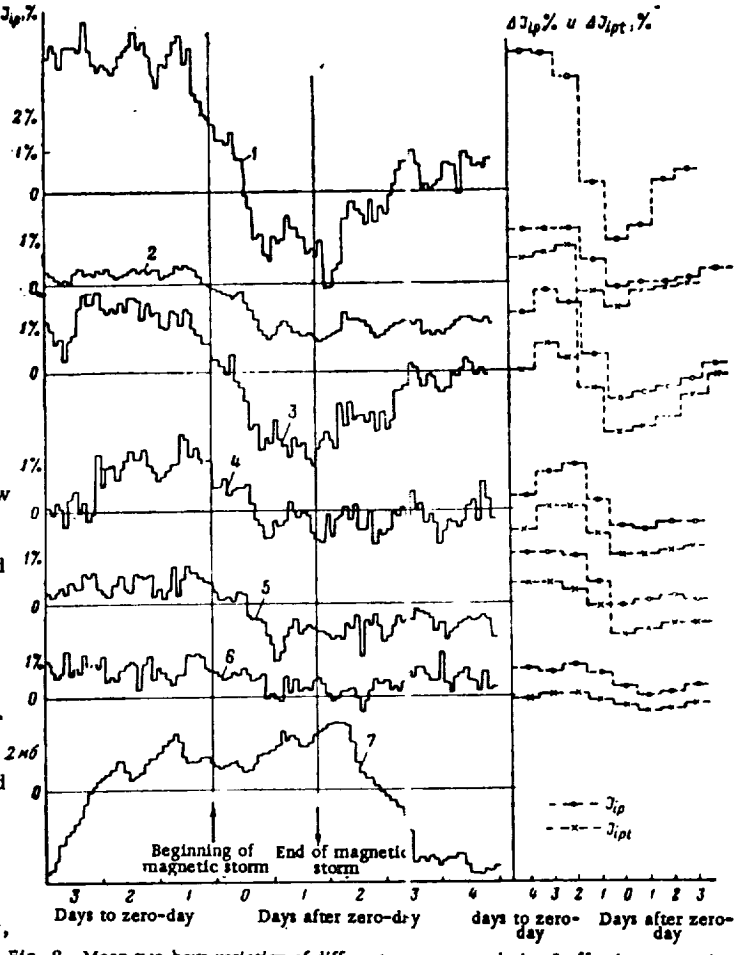

Fig. 2. Mean two-hour variation of different components during 8 effective magnetic storms. 1 - intensity of neutron component at sea level, Yakutsk, 2-6 - cosmic ray intensity, 3 - counter telescope at earth's surface, Yakutsk, 4 - at 7 m w.e., 5-20 m w.e., 6-60 m w.e., 7 - pressure at the earth's surface.

data for 1958.

It is not easy to note the reduction in cosmic ray intensity observed at a depth 60 m w.e. underground during each individual magnetic storm. Hence the mean 2-hour curve for I_p for different components during 8 effective magnetic storms was calculated and is shown in Figure 2. The same diagram shows the mean diurnal curve for I_{pW} for these 8 storms.

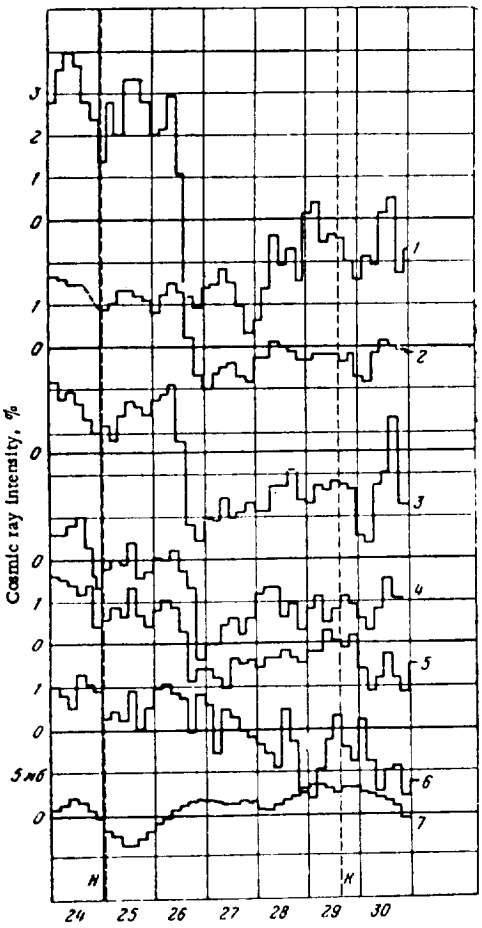

Fig. 3. Change of intensity in different components of cosmic rays during severe magnetic storm: November 24-29, 1957. (Notation same as in Figure 2).

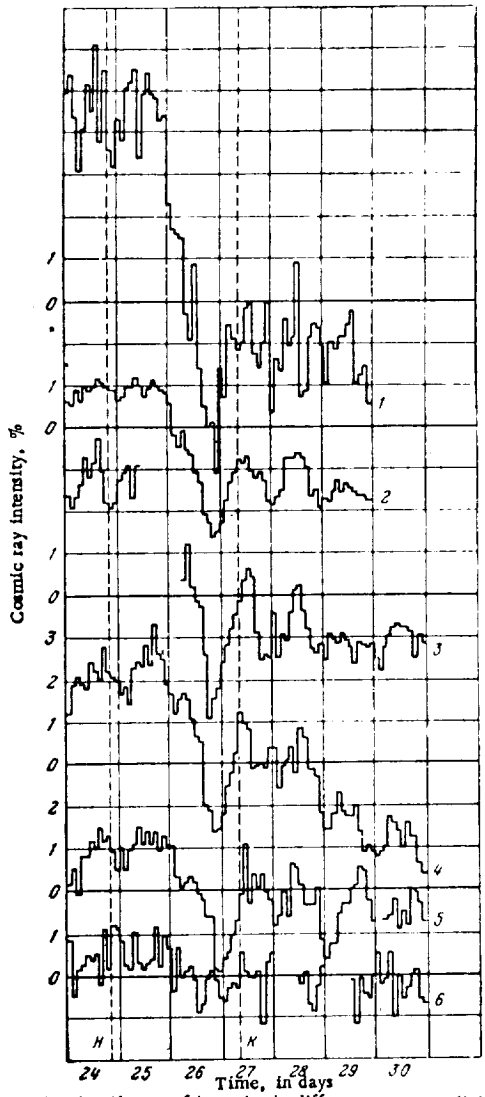

Fig. 4. Change of intensity in different components of cosmic rays during moderate magnetic storm: March 24-26, 1958. (Notation same as in Figure 2).

Figures 3 - 7 show 2-hour variations in the intensity of I_p during several magnetic storms in order to trace its behavior during each one in greater detail.

It is fairly difficult to determine the absolute reduction in I, particularly in underground installations. The snag is that during a magnetic storm there is not only a reduction in I, but also other characteristic variations. For example, there may be diurnal variations, variations just before the storm and statistical fluctuations. We adopted the following procedure to rid ourselves

of them. Then, from the smoothed data, we determined the d fference in mean diurnal I_{pW} corrected for barometric and temperature effects for two days prior to the storm and for two days following it, beginning from minimum intensity. This method clearly improves the statistical accuracy in calculating the absolute value to a considerable extent and eliminates the influence of the diurnal effect.

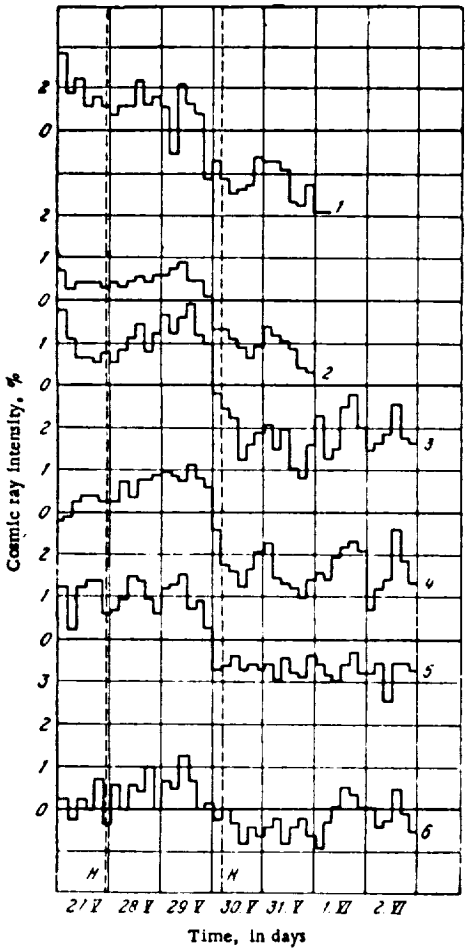

Fig. 5. Change of intensity in different components of cosmic rays during moderate magnetic storm, May 25-29, 1958. (Notation same as in Figure 2).

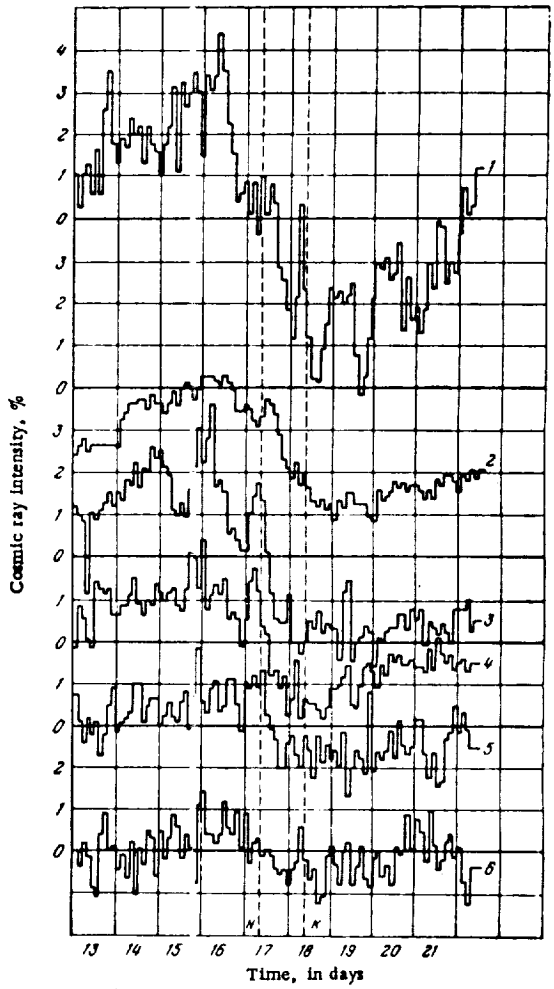

Fig. 6. Change of intensity in different components of cosmic rays during slight magnetic storm, September 16-17, 1958. (Notation same as in Figure 2.)

It is better to use a relative effect to determine the energy spectrum of particles which have undergone a cosmic ray effect during magnetic storms. To do this, we referred the absolute value of the decrease in $\Delta J_p t_i$ during a storm for each component to the absolute value of the decrease observed by a counter telescope on the earth's surface ($\Delta J_p t_{to}$). Normalization with respect to the insulation T_o is due to the fact that its statistical accuracy is comparatively high and the coupling factors (described below) are more reliable. Furthermore, for a more objective evaluation of the relationship between the behavior in the intensity of various components during the reduction for the intervals, shown in Figure 1 in the form of arrows, we derived correlation

factors by linear correlations. The derived absolute and relative values of the reduction in I and correlation factors are given in Table 2. Besides the noted effective magnetic storms (Figure 1), the first line of this table gives information on the storm from November 24 - 29, 1957, which was recorded by a group of Yakutsk installations.

Analysis of data

A considerable number of correlating changes in the intensity of different cosmic ray components of a world-wide nature lasting 5 - 15 days can be observed in Figure 1. There are periods with a pronounced decrease in I_{tw} at all installations, including the apparatus at 60 m w.e. below ground (March 24 - 30, May 28 - June 1, September 3 - 7, September 14 - 20, and August 8 - 20). The mean diurnal values over these periods can be closely correlated (correlation factor between T_0 and T_{60} is more than 50%). Furthermore, there are periods when we observe close correlation (more than 60% at all installations right up to T_{20}, and poor correlation with intensity at 60 m w.e. (T_{60}). Among such are the periods January 13-24, February 8 - 19, March 2 - 10, June 26 - July 5, August 6 - 15, August 20 - September 1. All these periods are characterized by a pronounced reduction in I_{pw} and, as a rule, coincide with magnetic storms. From now on the storms accompanied by an appreciable decrease in I_{pw} are most of the installations in the Yakutsk network and at other stations will be called effective storms.

Table 2. Absolute and relative values of decreasing intensity of cosmic rays during magnetic storms and correlation coefficients, r.

Beginning of magnetic storm	Neutron component			Hard component on the earth's surface						μ-meson component below ground											
				Ionization chamber			Counter telescope			7 m w.e. (T_7)			20 m w.e. (T_{20})			60 m w.e. (T_{60})					
	ΔN_p	$\frac{\Delta N_p}{\Delta T_{0pW}}$	r	ΔI_{pW}	$\frac{\Delta I_{pW}}{\Delta T_{0pW}}$	r	ΔT_{0pW}	ΔT_{7pW}	$\frac{\Delta T_{7pW}}{\Delta I_{0pW}}$	r	ΔT_{20pW}	$\frac{\Delta T_{20pW}}{\Delta T_{0pW}}$	r	ΔT_{60pW}	$\frac{\Delta T_{60pW}}{\Delta T_{0pW}}$	r					
24 XI 1957	4,7	1,9		1,6	0,61		2,5	1,5	0,6		1,4	0,56		0,2	0,08						
17 I 1958	2,2	2,45		0,6	0,67		0,9	0,7	0,78		0,5	0,56		0,3	0,33						
8 II & 11 II 1958	5,7	3,40	0,81	1,1	0,69	0,82	1,6	0,8	0,5	0,86	0,5	0,31	0,5	0,4	0,25	0,4					
15 III 1958	1,3	1,44	0,72	0,6	0,67	0,77	0,9	0,5	0,55	0,67	0,1	0,56	0,17	0	0	0					
24 III 1958	6,0	2,07	0,93	1,9	0,66	0,93	2,9	1,5	0,52	0,87	1,0	0,35	0,92	0,3	0,10	0,57					
6 V & 31 V 1958	5,8	3,06	0,89	1,6	0,84	0,90	1,9	1,6	0,85	0,87	1,5	0,70	0,92	0,6	0,31	0,61					
28 VI 1958	5,0	2,5	0,88	1,6	0,8	0,88	2,0	1,6	0,8	0,90	1,5	0,7	0,92	0,2	0,10	0,60					
8 VII 1958	5,0	2,5	0,93	1,1	0,55	0,57	2,0	1,2	0,6	0,38	1,0	0,5	0,40	0,4	0,20	0,33					
17 VIII 1958	4,4	2,45	0,77	1,4	0,78	0,82	1,8	1,6	0,89	0,79	0,7	0,39	0,72	0,5	0,28	0,55					
22 VIII, 24 VIII & 27 VIII 1958	5,0	2,5	0,69	1,7	0,85	0,88	2,0	1,5	0,75	0,83	1,3	0,65	0,95	0,2	0,10	0,20					
3 IX 1958	2,4	2,7	0,83	0,7	0,78	0,84	0,9	0,7	0,78	1,0	0,7	0,78	0,8	0,3	0,33	0,40					
16 IX 1958	5,0	1,86	0,86	0,2	0,82	0,76	2,7	1,8	0,67	0,74	1,2	0,44	0,81	0,4	0,15	0,13					
25 IX 1958	1,4	1,3		1,0	0,91		1,1	0,5	0,45		0,7	0,64		0,5	0,44						
Average.....	4,15	2,56±0,4		1,32	0,74±0,1		1,8	1,2	0,67±0,14		0,95	0,55±0,18		0,33	0,21±0,13						

Table 3 gives data for effective magnetic storms. It follows from the table that all the strong and very strong magnetic storms with a sudden beginning are effective. At the same time no appreciable variation in I was observed during either of the two strong and very strong storms with

a gradual beginning. Thus, generally speaking, there is an appreciable decrease in cosmic ray intensity during strong and very strong magnetic storms with a sudden beginning.

Of the mild storms only 44% were accompanied by a marked fall in I. Of these 7 effective magnetic storms, 6 had a gradual beginning. It is clear from this that the overall effectiveness of moderate storms, compared with the strong and very strong type, is reduced, and we can no longer speak of the predominant effectiveness of storms with a sudden beginning. Effectiveness of slight storms, compared with the other types, is smaller by a factor of 3 or 4.

It can be pointed out that storms with a sudden beginning show slightly greater probability of being effective than those with a gradual beginning (of 16 effective storms, 6 have a gradual beginning). Thus the results show that the more intensive the storm, the greater the probability of a decrease in cosmic ray intensity.

Table 3

Magnetic storm	Total number of magnetic storms		Number of effective magnetic storms		Number of effective magnetic storms, as % of total number of magnetic storms
	with sudden beginning	with gradual begin.	with sudden begin.	with gradual begin.	
Very strong & strong..	8	2	8	—	80
Moderate.....	3	13	1	6	44
Slight.....	4	1	1	—	20
Total.....	15	16	10	6	52

It follows from Figure 1 that in the case of some magnetic storms there is a surge in intensity at practically all installations a couple days before the intensity begins to drop. As an example we can point out the considerable upsurge 3 - 6 days before storms on January 17, February 8, March 24, May 26, August 17 and September 16. Slight magnetic storms are rarely effective. Hence the short-lived slight storm with a sudden beginning on September 16 is very interesting. Five days before this storm there began a sharp increase in intensity. Two days before the storm the cosmic ray intensity reached a maximum and then a minimum in one or two days. Intensity was restored after three or four days. Thus, a curiously symmetrical wave occurred, rise - fall - rise. This was of a world-wide nature, since it was recorded at all installations in Moscow and Tiksi. It was apparently due to high energy particles up to 200 Bev, since the underground installations in Yakutsk detected it. Two active regions with a decomposing spot groups and a large number of chromospheric flares were passing across the central meridian at this time. It should be pointed out, generally speaking, that all effective magnetic storms coincided in time with increased solar activity, and are evidently linked with the passage of active solar regions with a high degree of chromospheric and photospheric excitation across the central meridian.

A more detailed analysis of the reduction effect can be cited from examination of the 2-hour curve for intensity I_p of different components. The beginning and end of the sharp drop in intensity at all installations in our network can be observed in Figures 3-6 with an accuracy of 3 - 6 hours. In most cases the beginning of the reduction in I_p is 5 - 30 hours behind the beginning of the effective magnetic storm. The duration of the sharp drop varies with storms and ranges from 12 - 40 hours. The beginning of the drop and reaching of the minimum coincide at all installations within 2 - 5 hours. In the case of all magnetic storms the intensity recovers its normal level more than four days after the minimum, i.e., after the magnetic storm ends, the intensity does not recover its normal level.

The effect of the temperature on the reduction in cosmic ray intensity can be observed from Figure 2, which gives a mean diurnal curve for intensity during 8 effective magnetic storms. The inclusion of the Feynberg-Dorman temperature correction [11] considerably reduces the fall in intensity during the magnetic storms for all installations except the one measuring the neutron component, where its effect is slight, and was therefore not taken into account by us. Thus, when studying the fall in I during magnetic storms the temperature effect cannot be ignored. On the

other hand, the reduction in I at 60 m w.e. cannot be accounted for by the influence of temperature. Indeed, since a temperature correction in the ground level installations reduces the fall in I during storms, this means that temperature of the atmosphere as an average has increased. An increase in temperature in the upper layers of the atmosphere would have led to an increase in intensity recorded by the installation at 60 m w.e. at the time. So when the temperature correction was made, the reduction in I_{ph} at 60 m w.e. underground would have increased, which is not what was observed.

On the basis of the above described features in the behavior of cosmic ray intensity during effective magnetic storms, the following behavior pattern can be worked out. For several days before a storm the mean diurnal cosmic ray intensity I_{pW} tends to increase; then, having obtained maximum before the storm begins, it starts to fall gradually. A few hours after the storm has begun, I_{pW} drops sharply, attaining its minimum 12 - 40 hours later during the storm's principal phase. Then it slowly recovers the normal level when the magnetic storm is over.

Table 4. Exponents of normal variation of normal intensity with depth (γ_1), sharp intensity with depth deriving magnetic storms (γ_2) and change of the μ-meson spectrum during magnetic storms.

Energy interval for spectrum determination	γ_1	γ_2	$\gamma_2 - \gamma_1$
$T_0 - T_{15}$	−0,76	−1,50	−0,74
$T_0 - T_{30}$	−1,04	−1,62	−0,58
$T_0 - T_{50}$	−1,38	−2,21	−0,82
$T_7 - T_{30}$	−1,49	−1,72	−0,23
$T_7 - T_{50}$	−1,62	−2,48	0,86
$T_0 - T_{70}$	−1,74	−2,97	−1,20
			−0,74±0,2

Consequently, only some of the characteristic variations in intensity, to wit, the reduction effect, can be related to the magnetic storm period. The fact of other variations in the intensity of I_{pW} (increase before the storm and recovery afterwards) indicates that the cosmic ray variations during magnetic storms are complex and not due to oscillations of the geomagnetic field. It can rather be said that both the geomagnetic storm itself and the cosmic ray variations are due to a common cause. And the effect of this cause on cosmic ray intensity begins considerably earlier and ends considerably later than for the geomagnetic field. Clearly, this common cause must be a change in the electromagnetic properties of the environs of the solar system in accordance with solar activity.

It should be stressed that the above noted characteristic features of behavior in cosmic ray intensity during magnetic storms do not only occur in the intensity of different components on the earth's surface, but also underground to a depth of 60 m w.e. It follows directly from this that during effective storms some sort of mechanism is in action which is able to vary the primary particle spectrum right up to energies of 200 - 400 Bev.

The existence of identical installations for recording the μ-meson component at different levels below ground enables us to make a rough approximation of the energy spectrum of primary particles affected by magnetic storms without using the coupling factors. Indeed, if the μ-meson energy spectrum coincides with the primary particle spectrum with an accuracy up to a constant multiple, the μ-meson spectrum derived by the method described below gives an idea of the form of the primary particle spectrum.

Let us assume that the relationship between the intensity of an undisturbed μ-meson stream and disturbed stream and the depth in time of the magnetic storms can be described by formulae of the type

$$I_{impos} = I_o \epsilon^{\gamma_1} \text{ and } I'_{poss} = I_{o\,poss} \epsilon^{\gamma_2} \qquad (2)$$

For each of the six possible intervals we can find the exponents γ_1 and γ_2. The mean

Table 5. Predicted relative values of decrease in the intensity of cosmic rays during magnetic storms for several test-spectra.

Test Spectrum	ε_1	$\frac{\Delta N_p}{\Delta T_{pW}}$	$\frac{\Delta I_{pW}}{\Delta T_{epW}}$	$\frac{\Delta T_{p\mu}}{\Delta T_{epW}}$	$\frac{\Delta T_{epW}}{\Delta T_{epW}}$	$\frac{\Delta T_{epW}}{\Delta T_{epW}}$
I $\frac{\delta D(\varepsilon)}{D(\varepsilon)} = \begin{cases} -a, & \text{at } \varepsilon_1 > \varepsilon \\ 0, & \text{at } \varepsilon_1 < \varepsilon \end{cases}$	30	2,56	0,74	0,67	0,55	0,21
	100	2,1	0,78	0,09	0,01	0,0
	220	1,10	0,90	0,82	0,43	0,0
	260	1,05	0,96	0,96	0,85	0,27
	∞	1,04	0,98	0,97	0,85	0,37
		1,0	1,0	1,0	1,0	1,0
II $\frac{\delta D(\varepsilon)}{D(\varepsilon)} = -a \begin{cases} 1, & \text{at } \varepsilon < \frac{\varepsilon_1}{4} \\ \frac{2}{\pi} \cdot \arcsin\left(\frac{\varepsilon_1}{2\varepsilon} - 1\right), & \text{at } \frac{\varepsilon_1}{4} < \varepsilon < \frac{\varepsilon_1}{2} \\ 0, & \text{at } \varepsilon > \frac{\varepsilon_1}{2} \end{cases}$	30	3,8	0,95	0	0	0
	100	1,50	0,80	0,59	0,16	0
	220	1,09	0,80	0,90	0,67	0,07
	260	1,06	0,81	0,94	0,73	0,13
	300	1,05	0,84	0,95	0,80	0,19
	∞	1,0	1,0	1,0	1,0	1,0
III $\frac{\delta D(\varepsilon)}{D(\varepsilon)} = \begin{cases} -a\varepsilon^{-1}, & \text{at } \varepsilon_1 > \varepsilon \\ -0, & \text{at } \varepsilon_1 < \varepsilon \end{cases}$	60	2,92	0,80	0,37	0,05	0,0
	100	2,76	0,81	0,46	0,17	0,0
	220	2,75	0,81	0,48	0,29	0,05
	260	2,75	0,81	0,48	0,29	0,07
	∞	2,70	0,82	0,49	0,31	0,12
IV $\frac{\delta D(\varepsilon)}{D(\varepsilon)} = \begin{cases} -a\varepsilon^{-0,7}, & \text{at } \varepsilon_1 > \varepsilon \\ -0, & \text{at } \varepsilon_1 < \varepsilon \end{cases}$	100	2,02	0,76	0,55	0,24	0,0
	180	2,00	0,80	0,66	0,39	0,05
	260	2,00	0,81	0,61	0,41	0,12
	∞	2,00	0,84	0,63	0,45	0,23
V $\frac{\delta N(\varepsilon)}{D(\varepsilon)} = \begin{cases} -a\varepsilon^{-0,5}, & \text{at } \varepsilon_1 > \varepsilon \\ -0, & \text{at } \varepsilon_1 < \varepsilon \end{cases}$	100	1,94	0,74	0,62	0,28	0,0
	180	1,02	0,78	0,69	0,48	0,06
	260	1,60	0,80	0,71	0,54	0,16
	∞	1,60	0,83	0,71	0,57	0,35
VI $\frac{\delta D(\varepsilon)}{D(\varepsilon)} = \begin{cases} -a\varepsilon^{-1}, & \text{at } \varepsilon_1 < \varepsilon \\ -a, & \text{at } \varepsilon_1 > \varepsilon \end{cases}$	3	3,23	0,81	0,48	0,31	0,12
	7	6,4	0,90	0,43	0,29	0,11
	11	6,5	0,97	0,27	0,18	0,07
	15	4,6	0,93	0,15	0,10	0,04
VII $\frac{\delta D(\varepsilon)}{D(\varepsilon)} = \begin{cases} -a\varepsilon^{-0,7}, & \text{at } \varepsilon_1 < \varepsilon \\ -a, & \text{at } \varepsilon_1 > \varepsilon \end{cases}$	3	2,16	0,80	0,63	0,45	0,23
	7	3,25	0,78	0,60	0,42	0,22
	11	3,80	0,79	0,51	0,35	0,19
	15	3,40	0,80	0,36	0,25	0,13
VIII $\frac{\delta D(\varepsilon)}{D(\varepsilon)} = \begin{cases} -a\varepsilon^{-0,5}, & \text{at } \varepsilon_1 < \varepsilon \\ -a, & \text{at } \varepsilon_1 > \varepsilon \end{cases}$	3	1,67	0,72	0,71	0,55	0,35
	7	2,08	0,75	0,69	0,53	0,34
	11	2,40	0,75	0,64	0,49	0,31
	15	2,38	0,73	0,54	0,42	0,26

difference γ_2 and γ_1 gives the variations in the exponent γ for the μ-meson spectrum during the reduction in I_{pW} in magnetic storms. The normal intensity-depth trend for the Yakutsk installation network, as shown by experiments, can be expressed by the ratio

$$I_{T_1} : I_{T_2} : I_{T_3} = 1 : 0,67 : 0,304 : 0,064. \qquad (3)$$

The disturbed intensity stream can be obtained from the means (Table 2) for the relative reduction effects in intensity during magnetic storms, by normalizing them with respect to the μ-meson intensity on the earth's surface. From Table 2 and ratio (3) we obtain

$$I'_{T_1} : I'_{T_2} : I'_{T_3} : I'_{T_4} = 1 : 0{,}45 : 0{,}17 : 0{,}0135. \qquad (4)$$

Taking the absorption of μ-mesons in the atmosphere as equivalent to 10 m w.e., Table 1 gives us the ratio between minimum μ-meson energies recorded by the counter telescope:

$$\varepsilon_{T_1}^{\min} : \varepsilon_{T_2}^{\min} : \varepsilon_{T_3}^{\min} : \varepsilon_{T_4}^{\min} = 1 : 1{,}7 : 3{,}9 : 7{,}0. \qquad (5)$$

Table 4 gives γ_1, γ_2 and $\gamma_2 - \gamma_1$ calculated using equations (2) - (5).

It is clear from the data in Table 4 that the variation in the μ-meson spectrum during a reduction in cosmic ray intensity, as a first approximation, is

$$\frac{\delta d(\varepsilon)}{d(\varepsilon)} \sim a\varepsilon^{-0{,}7 \pm 0{,}2},$$

i.e., during magnetic storms there is a softening of the μ-meson spectrum up to 20 - 40 Bev. This gives grounds for expecting the primary particle spectrum to be similarly related to energy, as the μ-mesons, i.e., $\varepsilon D(\varepsilon)/D(\varepsilon) \sim \varepsilon^{-0.7}$, and the maximum energy of particles undergoing this effect to be 400 Bev. This spectrum can be compared with one calculated by the coupling factor method [11]. Variations in the secondary components I_i/I_i are:

$$\frac{\delta I_i}{I_i} = \int_{\varepsilon_{\min}}^{\infty} W(\varepsilon, h_0) \frac{\delta D(\varepsilon)}{D(\varepsilon)} d\varepsilon. \qquad (6)$$

Here $W(\varepsilon, h_0)$ is the coupling factor of the i-th component at the level h_0, $\delta D(\varepsilon)/D(\varepsilon)$ is the variation in the primary energy spectrum, and $\varepsilon_{\min}$ is the minimum energy for particle energies determined by the geomagnetic threshhold or the experimental conditions.

As has been shown above, the relationship of the following kind can be expected for the reduction in I during magnetic storms.

$$\frac{\delta D(\varepsilon)}{D(\varepsilon)} \begin{cases} -a\varepsilon^{-\gamma}, & \text{when } \varepsilon > \varepsilon_1, \\ -b, & \text{when } \varepsilon < \varepsilon_1. \end{cases}$$

Then the expected magnitude of the drop in I for each installation is

$$\frac{\delta I_i}{I_i} = -b \int_{\varepsilon_{\min}}^{\varepsilon_1} W(\varepsilon, h_0)\, d\varepsilon - a \int_{\varepsilon_1}^{\infty} W(\varepsilon, h_0) \varepsilon^{-\gamma} d\varepsilon. \qquad (7)$$

To determine the constants a, b, ε_1 and γ we need data on the reduction in I from at least four different installations. We had at our disposal data from six installations recording cosmic ray intensity over a wide range of minimum primary particle energies at one point. Let us assume as a first approximation that a = kb; then, using the relative values of the reduction in I, we can proceed to solve five equations with two unknowns. Table 4 gives the expected relative values of the reduction in I during magnetic storms for several "trial" primary particle spectrums, calculated by this method.

In the calculation we used the coupling factors $W(\varepsilon, h_0)$ calculated by one of the authors [13]. These factors are very much different from those previously worked out by Dorman [11]. In the primary particle energy region 20 Bev or more the factors have been derived from an experimental relationship between intensity and depth, recorded by the underground installation network in Yakutsk, and from other authors' data [17]. For energies below 15 Bev we took into account the latitude effect in cosmic ray intensity. Moreover, the coupling factors for energies less than minimum energy for the given installation were "blurred" on the assumption that in the act of interaction between primary particles and air nuclei, fraction α, of the energy is transferred to the secondary component, obeying the law of normal distribution.

Comparing the calculated values given in Table 5 with experimental ones we can conclude that the spectrum calculated by Dorman on the assumption of the effect on I of the regular frozen magnetic field of corpuscular streams from the sun

$$\frac{\delta D(\epsilon)}{D(\epsilon)} = \begin{cases} -1, & \text{when } \epsilon < \frac{\epsilon_1}{4} \\ -\frac{2}{\pi} \arcsin\left(\frac{\epsilon_1}{2\epsilon} - 1\right), & \text{when } \frac{\epsilon_1}{4} < \epsilon < \frac{\epsilon_1}{2} \\ 0, & \text{when } \epsilon > \frac{\epsilon_1}{2} \end{cases}$$

is n... uitable. Indeed, for the underground installations T_{20} and T_{60} the expected effects at ϵ_1 = 100 Bev are very small and approach the experimental values as ϵ_1 increases. For the neutron component at the same ϵ_1, the value $\Delta N_p/\Delta T_{opW}$ is less than the experimental and diverges still more as ϵ_1 increases.

For the same reasons experimental data are not satisfied by a spectrum of the type $\delta D(\epsilon)/D(\epsilon)$ = const, nor of the type $\epsilon^1\epsilon^2\ldots$ at any limitation of the energy ϵ_1 from above at all. We should point out that if we had set ourselves the task of finding an energy spectrum for primary particles from the cosmic rays given for the neutron and meson components (on the earth's surface) as used to be done, it can be seen from Table 4 that the spectrum would have been described by the formula

$$\frac{\delta D(\epsilon)}{D(\epsilon)} = \begin{cases} a, & \text{when } \epsilon < \epsilon_1, \\ 0, & \text{when } \epsilon > \epsilon_1, \end{cases}$$

where ϵ_1 is in the range from 20 and 50 Bev. Thus, we would have obtained Dorman's spectrum. This reaffirms once more that we were right in concluding that without the given underground installations it is hard to determine the primary particle energy spectrum accurately.

It is also clear that spectra of the type ϵ^{-1}, and all the more so ϵ^{-2} and ϵ^{-3} deviate considerably from experimental values since the relative effect in two of the lowest installations is very small, even when they are not cut from above, i.e., when ϵ_1

The most suitable of the "test" spectra given in Table 4 is

$$\frac{\delta D(\epsilon)}{D(\epsilon)} = \begin{cases} -b, & \text{when } \epsilon < \epsilon_1, \\ -a\epsilon^{-0.7\pm0.2}, & \text{when } \epsilon > \epsilon_1, \end{cases}$$

where ϵ_1 = from 5 - 10 Bev and b = 0.5a. This means that dur ng magnetic storms the primary particle intensity is influenced by a mechanism which prevents primary particles with an energy less than 10 Bev reaching the ground. At the same time the primary particle spectrum greater than 5 - 10 Bev is softened by this mechanism, i.e., it falls more sharply than the normal spectrum by a multiple of $\epsilon^{-0.7\pm0.2}$. The strength of the source of mechanism for energies below 10 Bev (b) is less than for high energy particles (a). The strength of the source, a, causing the reduction in I during magnetic storms can be found from underground installation data:

$$a = \frac{\Delta T_{1pW} / \Delta T_{0pW}}{\int_{\epsilon_1}^{\infty} W(\epsilon, h_{T_*}) \cdot \epsilon^{-0.7} d\epsilon}.$$

Derived in this way it is: a = 0.22 ± 0.05, from which b = 0.111± 0.03.

Thus, in its final form the spectrum for primary particles which have experienced the effect of magnetic storms can be represented as

$$\frac{\delta D(\epsilon)}{D(\epsilon)} = \begin{cases} -0{,}11 \pm 0{,}03, & \text{when } \epsilon_1 < 7 \pm 2 \\ -(0{,}22 \pm 0{,}05) \cdot \epsilon^{-0.7\pm0.2}, & \text{when } \epsilon_1 > 7 \pm 2 \end{cases} \qquad (10)$$

Analyzing the data in Table 2 for each magnetic storm separately, we can conclude that a spectrum of type (10) can explain the reduction in I_{pt} during each magnetic storm. Here the parameters a, b, γ and ϵ_1 vary between the errors given for these values in expression (10).

Thus, the variation in the primary cosmic ray stream energy spectrum during the reduced intensity for higher energy particles, when derived by the coupling factor method, coincides with the result of direct calculations from μ -meson component data. This coincidence shows that the energy spectrum for μ -meson at sea level actually coincides with the primary particle spectrum with an accuracy up to a constant multiple, and that when particles with energy 10^9 - 10^{11} ev interact, there are no appreciable changes in the fraction of energy transferred by the primary particle to the hard component.

Using the above described method it is also possible to calculate the energy spectrum of primary particles at different moments of recovery in cosmic ray intensity to the normal level after the storm is over. To do this we use data from mean diurnal I_{pt} during eight magnetic storms (Figure 2).

Table 6 gives relative values for the reduction in intensity on various days after the beginning of the reduction in I, derived from mean diurnal intensity curve during eight magnetic storms. Here, the data for the first, second and third days after the reduction begins show the behavior of cosmic ray intensity after the end of the magnetic storm.

Table 6

Day after beginning of decrease in cosmic-ray intensity	Relative magnitude of the decrease				
	$\frac{\Delta N_p}{\Delta T_{0PW}}$	$\frac{\Delta I_{PW}}{\Delta T_{0PW}}$	$\frac{\Delta T_{7PW}}{\Delta T_{0PW}}$	$\frac{\Delta T_{20PW}}{\Delta T_{0PW}}$	$\frac{\Delta T_{60PW}}{\Delta T_{0PW}}$
First	2,40±0,2	0,70±0,05	0,60±0,08	0,60±0,10	0,20±0,10
Second	2,00±0,2	0,50±0,05	0,60±0,08	0,60±0,10	0,20±0,10
Third	1,80±0,2	0,60±0,05	0,70±0,08	0,60±0,1	0,20±0,10

F 6 7

It is clear from Table 6 and Figure 2 that the neutron component intensity which falls fairly sharply during a storm undergoes a sudden "spurt" towards recovery after the storm, whereas the hard component intensity on the ground and below it does not. This suggests that magnetic storms are due to two independent mechanisms. One mechanism is connected with the moment of commencement and ending of the storm, while the other has no appreciable connection with these moments. The first of these mechanisms can be identified with the influence of the magnetic field, while the second can be identified with the effect of the electric field. Indeed, the magnetic field does not alter the energy spectrum of the primary stream, hence the variation spectrum may be

$$\frac{\delta D(\varepsilon)}{D(\varepsilon)} = \begin{cases} \text{const}, & \text{when } \varepsilon < \varepsilon_1, \\ 0, & \text{when } \varepsilon > \varepsilon_1, \end{cases}$$

or in the case of a frozen magnetic field within the solar corpuscular streams

$$\frac{\delta D(\varepsilon)}{D(\varepsilon)} = a \begin{cases} -1, & \text{when } \varepsilon < \frac{\varepsilon_1}{4}, \\ -\frac{2}{\pi} \arcsin\left(\frac{\varepsilon_1}{2\varepsilon} - 1\right), & \text{when } \frac{\varepsilon_1}{4} < \varepsilon \leqslant \frac{\varepsilon_1}{4}, \\ 0, & \text{when } \varepsilon > \frac{\varepsilon_1}{2}, \end{cases}$$

Since it is only small energy particles, $\epsilon < 9$ Bev, which are substantially scattered, it can be said that either the intensity (potential) of the frozen magnetic field is considerably less than thought [11], or that the frozen field is extremely non-uniform. The second mechanism may be identified with the electric field effect. Indeed, as we have seen, during a storm there is a considerable transformation of the primary spectrum throughout the energy range. This transformation takes the form

$$\frac{\delta D(\varepsilon)}{D(\varepsilon)} = \begin{cases} -b, & \text{when } \varepsilon < \varepsilon_1, \\ -a\varepsilon^{-\gamma}, & \text{when } \varepsilon > \varepsilon_1, \end{cases}$$

where $\gamma = 0.7 + 0.2$, a = 0.22 and b = 0.11; beginning at $\alpha = 9$ Bev, the variations can only be described by the term $\alpha\epsilon\gamma$. A substantial transformation of this kind in the primary cosmic ray stream may evidently be due to the effect of the electric field [5]. Hence it can be considered that in the production of the effect in cosmic ray intensity during magnetic storms the part played by the electric field is appreciable, in addition to that played by the magnetic field.

Conclusions

The most important results of this research can be formulated as follows:

1. Characteristic variations in cosmic ray intensity are observed during magnetic storms both in the case of low energy particles as well as those with very high energies up to ϵ = 400 Bev. The primary variation spectrum, determined both from measurements of μ-meson intensity over a wide range of energies as well as by the coupling factor method, takes the form

$$\frac{\delta D(\epsilon)}{D(\epsilon)} = \begin{cases} -0{,}11 \pm 0{,}03, & \text{when } \epsilon \leqslant 7 \pm 2 \\ (-0{,}22 \pm 0{,}03)\epsilon^{-0.7 \pm 0.3}, & \text{when } \epsilon \geqslant 7 \pm 2 \end{cases}$$

This spectrum contradicts the expected spectrum [11] because of particles being scattered by a frozen magnetic field with an intensity of $\sim 10^4$ gauss in the earth s orbit.

2. Variations in cosmic rays during magnetic storms are due to two mechanisms, one of them reflecting the effect of the magnetic field, the other reflecting the effect of an electric field. Particles with energy ϵ > 9 Bev undergo the effect of both a magnetic and electric field. Here the part played by the magnetic field in scattering primary particles with high energies is small. The time over which this mechanism acts is limited to the moment that the magnetic storm begins and ends. This fits in with the assumption regarding the occurrence of a magnetic storm when the earth comes in the way of a solar corpuscular stream.

During a magnetic storm in the atmosphere there are characteristic changes which reduce the intensity of the μ-meson component to such a degree that the effect cannot be disregarded.

In conclusion the authors would like to express their gratitude to G. A. Akisheva and T. P. Shelekhova for assistance in processing data and to G. V. Shafer who was kind enough to make certain unpublished data available.

F
6
7

Bibliography

1. Meseerschmidt, N., Zs. Phys., 85, p. 332, 1933.
2. Steinmaurer, R., and H. T. Graziadei, Sitzungberichte Acad. Wiss. Wien, 22, p. 672, 1933.
3. Hogg, A. R., Memoirs of the Commonwealth Observatory, Canbury, No. 10, 1949.
4. Lange, J. and S. E. Forbush, Carnegie Institution of Washington Publication, p. 175, 1948.
5. Hess, V. F. and A. Demmelais, Nature, 140, p. 316, 1937.
6. Glokova, Ye. S., L. I. Dorman, N. S. Kaminer, and G. V. Tyanutova, NIIZM Report, 1955.
7. Glokova, Ye. S., Trudy NIIZM, 8, p. 59, 1952.
8. Trumpy, V, Physica, 19, p. 645, 1953.
9. Sekido, J. and N. Wada, Report Ionos. Res. Japan, 9, p. 1974, 1955.
10. Kuz'min, A. I. and G. V. Skripin, Trudy YaFAN, SSSR, Issue 2, p. 107, 1958.
11. Dorman, L. I., Cosmic ray intensity variations, Gostekhizdat, 1957.
12. Dorman, L. I., present collection, p. 159.
13. Kuz'min, A. I., Determining the connection between primary and secondary components in cosmic rays (in print).
14. Kuz'min, A. I., G. V. Skripin, and A. V. Yarygin, Trudy YaFAN SSSR, Issue 2, p. 34, 1958.
15. Al'fven, Kh., Cosmic electrodynamics, Foreign Literature Press, 1952.
16. Bauenberg, E. A., and A. Dattner, Tellus, 6, p. 254, 1954.
17. Dzhorgzh, Ye., Cosmic ray observations below ground and their explanation. Contained in book: "Cosmic Ray Physics", edited by J. Wilson, v. 1, Foreign Literature Press, 1954.

T. M. Berdichevskaya and N. A. Zhukovskaya

ON THE PROBLEM OF EXISTENCE OF SIDEREAL-DIURNAL VARIATIONS IN MESON INTENSITY OF COSMIC RAYS

In their recently published work Conforto and Simpson [1] have made a study of solar-diurnal and sidereal-diurnal variations in different cosmic ray components.

The authors studied the solar-diurnal variation over the period 1953 - 1955 at the following stations:

Huancayo φ = 12° 02' South lat, λ = 75° 20' West (Neutron monitor),
Climax φ = 32° 22' North lat., λ = 106° 11' West (neutron monitor),
Freiberg φ = 47° 55' North lat., λ = 07° 45' East (ionization chamber), and
Rome φ = 41° 48' North lat., λ = 12° 36' East (counter telescope).

This period proved to be particularly interesting since it was observed that the phase of the 24-hour variation underwent considerable shifts during the solar activity minimum. This had been descovered before by Possener and Van Heerden [2].

Konforto and Simpson have represented the 24-hour variation in cosmic ray intensity in the following way. The amplitude of the diurnal variation for each day was defined as the ratio of the sum of deviations for 12 consecutive hourly intervals during which the intensity was greater than average to the standard deviation; the standard deviation was considered constant for each station and equal to the square root of the number of readings per unit of time.

The phase was defined as the central moment of the selected 12-hour period.

It was found that in 1953 and 1955 the diurnal variation phase remained more or less constant (with the exclusion of a few short periods), if the intensity variation was determined from solar time. In 1954 the phase of the diurnal variation vector shifted on the harmonic hour plate counter-clockwise and formed a closed loop.

This effect was first detected for the equatorial station Huancayo, where there are probably no meteorological effects at all.

To confirm what had been found, the same investigation was made for the stations at medium latitudes (Climax, Rome and Freiburg). It was discovered that in the case of all these stations the diurnal variation vector phase from solar time also shifts counter-clockwise, but does not describe a closed loop as in the case of Huancayo. This is evidently due to meteorological effects. The authors think that this regular variation in phase may indicate the presence of a diurnal variation in sidereal time. In order to test this hypothesis, Konforto and Simpson calculated the diurnal variation is cosmic ray intensity for sidereal time. All the vector phases were converted to sidereal time on the assumption that on March 21 solar and sidereal time are identical. It was found that the amplitude and phase of the vectors remained almost constant in 1954 and hardly differed from the amplitudes and phases in 1953 and 1955. The authors assume that the existence of a sidereal-diurnal variation is apparently due to anisotropy of primary cosmic radiation outside the earth's atmosphere and geomagnetic field.

We carried out a similar study of the sidereal-diurnal effect in the intensity of the meson component in cosmic rays from data obtained by middle-latitude stations at Moscow, Yakutsk, Tokyo, Freiburg and the high altitude station at Tikhaya Bay. We plotted a harmonic diagram of the mean monthly diurnal variation vectors for solar time for 1953 - 1955 for all stations (and also for 1956 and 1957 for Moscow and Yakutsk). The amplitude and phase of the diurnal variation for each month for all stations was determined by harmonic analysis.

It came to light when the plotted diagrams were examined that in 1953 and 1955 the phases of

the mean monthly diurnal variation vectors uncorrected for temperature effect showed a wide spread. The solar-diurnal variation phases for Moscow and Yakutsk in 1956 - 1957 are the most constant.

When the temperature correction had been made, which was possible for Moscow from June 1955 to October 1956 and for Yakutsk for 1956, the constancy of the phases became more pronounced, as can be seen from Figures 1 and 2. The phases in 1954 showed a particularly wide and curious spread.

Figure 3 gives the phases and amplitudes of the solar-diurnal variation for the station Tikhaya Bay and Yakutsk for the months January - September 1954. It can be seen that the direction of the diurnal variation vector shifted during this time interval in a counter-clockwise direction (at Tikhaya Bay for example, the vector changed direction by more than 180°, which coincides with Konforto and Simpson's results).

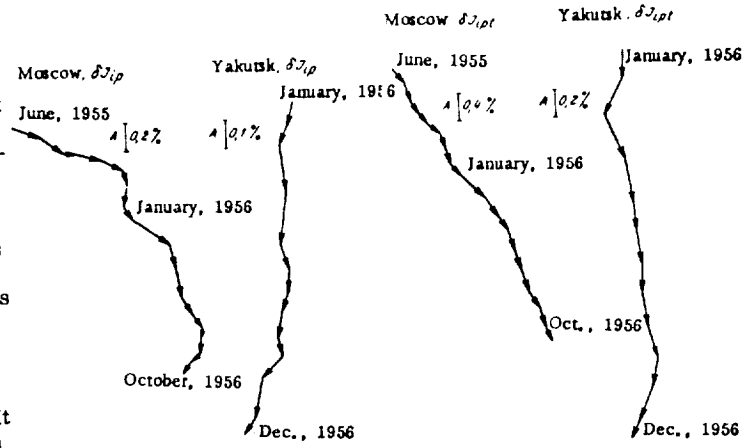

Fig. 1. Solar diurnal variation of meson intensity in cosmic rays, not corrected for the temperature effect.

Fig. 2. Solar diurnal variation of meson intensity in cosmic rays, corrected for the temperature effect.

Table 1
Moscow, 1954

MONTHS	Solar time		Sidereal time I	Sidereal Time, II	
	A, %	φ^h	A, %	φ^h	φ^h
January	0,09	11,3	0,08	7,4	7,0
February	0,10	11,0	0,09	9,0	9,0
March	0,09	9,3	0,13	8,4	9,0
April	0,12	9,0	0,13	10,2	11,0
May	0,11	7,4	0,11	10,8	11,5
June	0,13	6,0	0,13	11,2	12,0
July	0,16	6,8	0,17	14,5	14,8
August	0,21	5,2	0,20	14,6	15,0
September	0,17	4,9	0,18	17,1	17,0
October	0,12	2,0	0,05	16,5	16,0
November	0,04	12,5	0,05	4,5	4,5
December	0,16	12,6	0,16	5,8	6,5

Further, to test the hypothesis of the existence of sidereal-diurnal variation in the meson component intensity we determined the mean monthly amplitudes and phases of the diurnal variation vector for sidereal time for the mentioned stations. The transition from solar to sidereal time was accomplished on the assumption that in the second half of March solar and sidereal time were identical. For the next 15 days they were then shifted one hour, taking it into consideration that sidereal time overtakes solar time. The results were totaled separately for each month, averaged and analyzed harmonically.

This method produced amplitudes and phases for Moscow over the period January - December, 1954. The results are given in Table 1 (columns 3 and 4, sidereal time I).

The same results, however, can be obtained by a simpler, but slightly less accurate method. If it is assumed that sidereal and solar time coincide in March, and it is remembered that a sidereal month is two hours shorter than a solar one, the correction for sidereal time for April

will be two hours, for May four hours, and so on. Corrections for sidereal time in hours for each month are given below.

January..... 20	July..... 8
February.....22	August.....10
March..... 0	September..... 12
April..... 2	October.....14
May..... 4	November 16
June.....6	December.....18

In this way we obtained sidereal-diurnal variation phases for Moscow over the same period (January - December, 1954). The results are given for comparison in Table 1, (column 5, sidereal time II) from which it is clear that they differ only slightly from the earlier results. Hence the sidereal effect for Tikhaya Bay and Yakutsk in 1954 was determined by this, simpler method. The results are given in Figure 4, from which it follows that the sidereal-diurnal variation phases in 1954 are more constant than the solar-diurnal variations. This supports the view expressed by Konforto and Simpson regarding the predominant part played by sidereal-solar variations in cosmic ray intensity during the solar activity minimum.

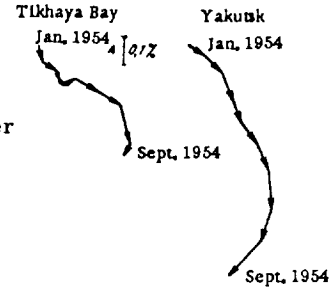

Fig. 3. Solar-diurnal variation of meson intensity in cosmic rays, not corrected for the temperature effect.

We then calculated the mean annual variation in cosmic ray intensity in solar and sidereal time for all stations. The amplitude and phase of the mean annual diurnal variation for different years for all stations were also determined by harmonic analysis.

The results are given in Table 2. An analysis of them suggests that there evidently exist at the same time both a solar-diurnal variation and a diurnal variation with respect to sidereal time. The amplitudes with respect to sidereal time, however, are small in 1953, 1955 and 1956. During these years they were smaller than the solar-diurnal variations by a factor of 2 or 3. In 1954 (a year of minimum solar activity) the variation amplitudes with respect to the sidereal time increased appreciably, and equal or become greater than the solar-diurnal variations for the same year.

Table 2

Station	Year	Solar time		Sidereal time	
		A. %	φ^h	A. %	φ^h
Mowcow	1953	0,09	9,8	0,05	12,5
	1954	0,08	10,6	0,07	11,3
	1955	0,16	8,8	0,07	11,3
	1956	0,12	11,0	0,05	8,5
	1957	0,09	12,3	0,03	7,7
Yakutsk	1954	0,05	6,5	0,06	11,6
	1955	0,07	10,1	0,04	12,0
	1956	0,10	13,1	0,03	12,0
	1957	0,08	14,0	0,02	3,0
Tikhaya Bay	1953	0,03	14,5	0,02	10,7
	1954	0,03	4,0	0,03	9,5
	1955	0,04	9,9	0,04	11,5
Freiburg	1952	0,15	11,6	0,02	11,0
	1953	0,09	10,6	0,03	9,4
	1954	0,04	7,7	0,05	8,4

A similar conclusion may be drawn on the basis of Konforto and Simpson's results. By adding the mean monthly factors in the diagrams in [1] and dividing their total by 12 we obtained mean annual amplitudes for the diurnal variation vector for the stations at Huancayo, Climax and Rome;

they are given in Table 3.

Table 3

Station	1953		1954				1955	
	Solar time		Solar time		Sidereal time		Solar time	
	A, %	φ^h	A, %	φ^h	A, %	φ^h	A, %	φ^h
Huancayo.....	0,17	4,3	0,02	16,9	0,06	7,2	0,16	5,9
Climax.....	0,34	13,0	0,16	16,1	0,39	9,6	0,41	14,3
Rome.....			0,06	5,0	0,11	8,9	0,09	12,1

Our assumption with regard to the simultaneous existence of both types of variation was confirmed by verification of the non-random nature of diurnal variations with respect to sidereal time. We found that the sidereal variation at Tikhaya Bay, even in 1953 when its amplitude was only 0.02%, was genuine, since the error in amplitude was 0.006%; the sidereal variation in Yakutsk in 1957 was also 0.02% and showed an error of 0.004%, i.e., in this case, too, the amplitude of the sidereal-diurnal variation proved genuine. Errors in amplitudes greater than 0.02% do not exceed thousandths of a percent (for example, the variation in Yakutsk in 1954 was 0.06%, and the error 0.003%). All the results obtained suggest the insignificantly small part played by the sun as a source of solar-diurnal variations during the years of solar activity minima, when the principal part in producing the diurnal effect belongs to anisotropy of the primary cosmic particles outside the solar system. Clearly, as the solar activity increases, the number of corpuscular streams causing diurnal variations in cosmic radiation on the earth also increases. The role of the sidereal effect at this time is insignificant.

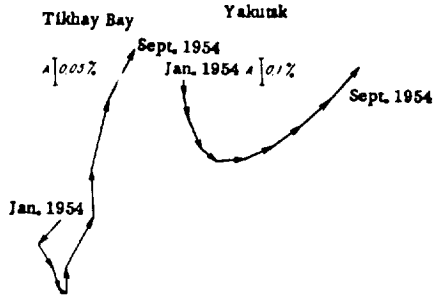

Fig. 4. Sidereal diurnal variation of meson intensity in cosmic rays, not corrected for the temperature effect.

We feel that the results obtained, so far, even those which tally with Konforto and Simpson, are not yet sufficient for final proof of the existence of a sidereal effect in cosmic ray intensity. Further investigation with the use of more extensive material is essential before the question is finally solved.

Bibliography

1. Konforto, A. M. and J. A. Simpson. Nuovo Cimento, 6, No. 5, p. 1052, 1957.
2. Possener, M., and I. I. Van Heerden, Phil. Mag., 1, No. 3, p. 253, 1956.

L. I. Dorman

ENERGY SPECTRUM AND DURATION OF INCREASE IN COSMIC RAY INTENSITY ON EARTH DUE TO CORPUSCULAR STREAM SHOCK WAVE

Publication [1] describes a slight increase in cosmic ray intensity a few hours before the magnetic storm on August 29, 1957. Distribution of the amplitude of the increase over geomagnetic latitude as recorded by seventy instruments located at almost fifty different points on the globe (see Figure 1 taken from [1]) showed that the increase was due to fairly hard particles and, in any event, could not be associated with the effects of solar flares (which have a considerably softer spectrum, (see [2], Chapter XI). The hypothesis has been put forward [3, 1] that the observed increase in cosmic ray intensity is caused by the shock wave from the sharp leading front of the corpuscular stream carrying the frozen magnetic field. In this article we evaluate the prime variation in energy spectrum expected during this process, and compare it with that observed. By this method we hope to test the hypothesis regarding the nature

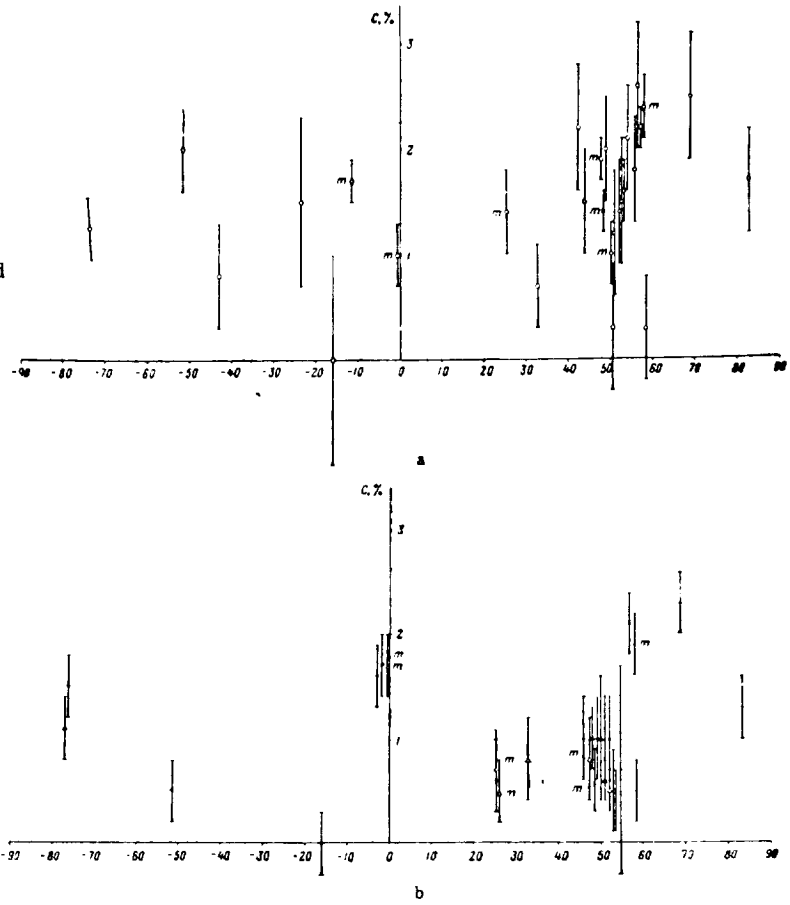

Fig. 1. Dependence of increase amplitude in cosmic-ray intensity immediately prior to the beginning of the magnetic storm on August 29, 1957.

a - neuton monitor; b - counter telescopes (+) and ionization chambers (Δ) (m - stations located in high mountains).

of the phenomenon observed in [1].

The acceleration of charged particles when the shock wave front passes through magnetized plasma was considered in [4]. It was assumed that the frozen magnetic field was perpendicular to the direction of propagation of the wave. It was shown in [4] that in a head-on collision with the shock wave the relative change in energy for relativistic particles is

$$\frac{\Delta\epsilon}{\epsilon} \approx \left(\frac{p_{0\perp}}{p_0}\right)^2 \frac{4}{\pi}\frac{\varkappa-1}{\varkappa+1}, \qquad (1)$$

where $p_{0\perp}$ is the transverse component of the particle pulse (with respect to the magnetic field), and $\varkappa = H_2/H_1$ is the compressibility of the medium. For interplanetary gas in our case $\varkappa = 4$.

Since the mean value $\left(\frac{p_{0\perp}}{p_0}\right)^2 \approx \frac{2}{3}$, then $\frac{\Delta\epsilon}{\epsilon} \approx \frac{1}{2}$.

Applying the results of the research described in [4] to our case, we can make the following comments.

Formula (1) was derived on the assumption of infinite width of the front, and its validity was therefore not limited by high energy increments. But in our case, with a front half-width of $\sim 5 \cdot 10^{12}$ cm, velocity of $\sim 10^8$ cm/sec and field intensity of $\sim 10^{-5}$ oersted, the total energy increment is $\Delta\epsilon \leqslant \frac{n}{c} Hl \sim 5 \cdot 10^7$ ev. Hence, high energy particles with $\epsilon_k \gg 5 \cdot 10^7$ ev will not increase their energy by more than $\Delta\epsilon_{max} \approx 5 \cdot 10^7$ ev before striking the earth.

Second, if the kinetic energy of the particles is $\epsilon_k \lesssim 5 \cdot 10^7$ ev, the variation in energy will be determined from equation (15) in [4] for relativistic particles:

$$\frac{\Delta\epsilon}{\epsilon_k} = \left(\frac{v_{0\perp}}{v_0}\right)^2 \cdot \frac{8}{\pi}\frac{\varkappa-1}{\varkappa+1} + \left(\frac{u_1-u_2}{v_0}\right)^2 \sim 1 \qquad (2)$$

for particles with $v_0 \gg u_1 - u_2$.

Thus, if the differential spectrum of the undisturbed primary component in the cosmic ray takes the form $D(\epsilon_k) \sim \epsilon_k^{-\gamma}$ ($\gamma \sim 2$) then (see [2], Section 29, par. 2) we obtain for the shock wave effect

$$\frac{\delta D(\epsilon_k)}{D(\epsilon_k)} \approx \begin{cases} 1+\gamma, & \text{when } \epsilon_k \leqslant \Delta\epsilon_{max}, \\ (1+\gamma)\dfrac{\Delta\epsilon_{max}}{\epsilon_k}, & \text{when } \Delta\epsilon_{max} < \epsilon_k. \end{cases} \qquad (3)$$

In the case of the magnetic storm on August 29, 1957, the stream velocity was about $2 \cdot 10^8$ cm/sec [1], and consequently, the velocity of the front attained $3 \cdot 10^8$ cm/sec. At $l \sim 5 \cdot 10^{12}$ cm and $H \sim 10^{-5}$ ev (it follows from [1] that the corpuscular stream responsible for this storm moved in a wide slow stream with this field intensity), this gives $\Delta\epsilon_{max} \approx 0.15$ Bev, and

$$\frac{\delta D(\epsilon_k)}{D(\epsilon_k)} \approx \begin{cases} 3, & \text{when } \epsilon_k \leqslant 0{,}15 \text{ Bev} \\ \dfrac{0{,}45}{\epsilon_k}, & \text{when } \epsilon_k \geqslant 0{,}15 \text{ Bev} \end{cases} \qquad (4)$$

Using the data in [2] (see Figure 37 in this publication, which gives $\int_{\epsilon_{min}}^{\infty} \frac{W_\lambda^t(\epsilon, h_0)\, d\epsilon}{\epsilon}$ for different components and geomagnetic latitudes), we find that the amplitude of the increase in the hard component at a latitude of 50° will be about 1% (practically the same at the equator and at 30°), and that for the neutron component at latitude 50° it will be about 3 or 4%, and about 1% at the equator. These results coincide satisfactorily with experimental data contained in the figure within experimental limits.

The duration of the increase will be determined by the time taken by the earth to pass through the region with increased energy particles. The dimensions of this region are of the nature of the particle curvature radius, i.e., $L \sim \epsilon/300\,H$. Thus, the time taken by the increase is

$$\tau \sim \frac{L}{v} = \frac{\epsilon}{300\,Hv},$$

where v is the velocity of propagation of the shock wave front. For $v \sim 3 \cdot 10^8$ cm/sec, $H \sim 10^{-5}$ we obtained at $\epsilon \sim 10^{11}$ ev $\tau \sim 10^5$ sec ~ 1 day, $\tau \sim 8$ hours at $\epsilon \sim 3 \cdot 10^{10}$ ev, $\tau \sim 3$ hours at $\epsilon \sim 10^{10}$ ev, and $\tau \sim 1$ hour at $\epsilon \sim 3 \cdot 10^9$ ev. For very low energy particles, for example $\epsilon_k \sim 10^8$ ev, τ will be of the nature of several minutes. Thus, the general behavior the shock wave effect

is as follows: the amplitude increases as the energy decreases, while the duration decreases as the energy increases. It is essential to make a detailed experimental check of the discovered behavior.

Bibliography

1. Blokh, Ya. L., Ye. S. Glokova, and L. I. Dorman. "Transactions of IGY, cosmic ray series", Issue 1, p. 7, 1959. In Russian.
2. Dorman, L. I., Cosmic ray variations, Moscow, Gostekhizdat, 1957.
3. Dorman, L. I., "Transactions of All Union Conference on magnetic hydrodynamics", Riga, 1959.
4. Dorman, L. I. and G. I. Freydman, Ibid.

N. S. Kaminer

EARTH ZONES STRUCK BY SOLAR PARTICLES (1 - 10 Bev)

Introduction

A great deal of attention has been given of late to the study of the effect of chromospheric flares on cosmic ray intensity [1-4]. In certain cases powerful chromospheric flares on the sun are accompanied by a big increase in cosmic ray intensity on the earth [1-3]. This increase attains tens and hundreds of percent in the hard component [3] and several thousands of percent in the neutron components [4]. Analysis of experimental data shows that these "flares" in cosmic ray intensity are the result of the influx on the earth of an additional stream of particles with energies $\epsilon \lesssim 15$ Bev generated in active regions on the sun [5].

Strong chromospheric flares causing high increases in cosmic ray intensity are a rather rare phenomenon. The chromospheric flares observed on the sun are much more frequently weak ones with a power of 1.2 and sometimes 3, associated with slight increases in the intensity of the neutron component (less than 1%) [6].

Study of the 'greater' and 'lesser' bursts of cosmic rays are of great interest. It may provide us with important information on the generation of high energy particles on the sun and the properties of the earth's magnetic field at great distances, and on the characteristic features of the motion of high energy particles in interplanetary space.

Graphs for constructing impact zones

The trajectory of motion of a charged particle in the earth's magnetic field is characterized by the following parameters: particle hardness, pc/Z; geomagnetic latitude of point at which particle arrives on earth, Φ; zenith angle of incidence, ξ, angle Φ_S, between direction of particle's motion in infinity and plane of geomagnetic equator (geomagnetic latitude of source), and also the "drift" angle ϕ, which is the difference between the geomagnetic longitudes of the source and the point of arrival on earth of the particle. These parameters are shown in Figure 1.

Using both the theoretical and experimental results of study of the motion of charged particles in the earth's magnetic field, Firor [6] has plotted easy-to-use graphs for finding the geomagnetic coordinates of arrival points on earth as the function of the particle's energy (over the range 1 - 10 Bev) and the geomagnetic latitude of the point source for $\xi = 0$. The arrival points for the particles on earth are divided into three groups, forming "impact zones": the late morning zone (about 9 AM local time), the early morning zone (about 4 AM local time) and the evening zone (about 8 PM local time). The variation in the geomagnetic latitude of the source (sun) leads to a shift in the position of the impact zones, i.e., to the appearance of a seasonal zone. The source (sun) is not a point source, but has finite angular dimensions, which means that the impact zones are "blurred". Narrowest is the 9-hour zone; the evening zone changes to a "background zone", covering the entire surface of the earth between latitudes 25 - 60°. The relative intensities in the 9-hour, 4-hour and background zones are 7: 2: 1 respectively for a source with angular dimension $\Delta\Phi_S = 15°$, and 7: 3: 1 when $\Delta\Phi_S = 30°$. Analysis of experimental data shows that the latter ratio is apparently closer to reality [6].

Analysis of the cosmic ray intensity distribution over the globe during four large "bursts" has shown fairly satisfactory agreement between theoretical views and experimental data. A similar conclusion may be drawn from study of the lesser bursts in the neutron component [6]. Of the three impact zones - 9-hour, 4-hour and background - the most interesting are the first two. When considering these zones we will assume that the angular dimension of the source is $\Delta\Phi_S \asymp$

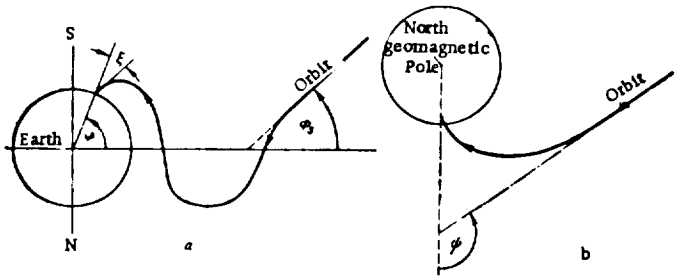

Fig. 1. Parameters determining particle trajectory [6]. a - in meridional plane, b - in geomagnetic equator plane.

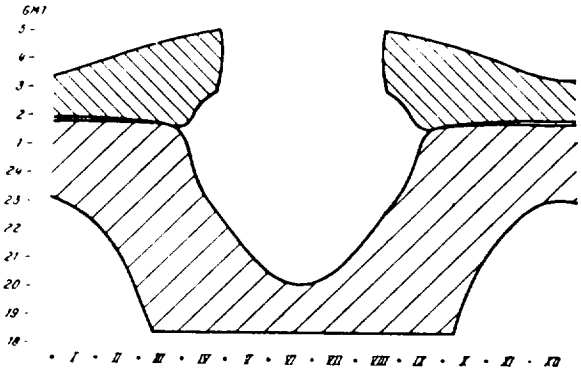

Fig. 6. Moscow (Φ = 50.8° North lat., Λ = 120.5°). Annual variation of time in determining a point in impact zones (world time) $\Delta\Phi_S$ = 30° (± 15°).

30° (± 15° with respect to the earth-sun line). During diurnal and annual motion of the earth the geomagnetic latitude of the sun Φ_S is changing constantly. This variation is the sun's position may be found by using graphs for the transition from geographical to geomagnetic coordinates [7]. The sun's geomagnetic coordinates - latitude Φ_S and longitude Λ_S - were calculated for various values of the sun's inclination $\delta_\odot$ from -23 to +23° (every 5°) and for the geographic longitudes 0, 30, 60, ... 330°.

Making use of these data and also the fact that the angular dimension of the source was $\Delta\Phi_S$ = 30°, on the basis of the graphs in [7] we determined the geomagnetic latitude Φ and drift angle ϕ (towards the west with respect to the earth - sun line) of the impact zone boundaries for various geomagnetic latitudes of the sun Φ_S. The practical application of ϕ is not entirely convenient. Subtracting ϕ from the sun's geomagnetic longitudes Λ_S, we obtain the boundaries of the impact zones in longitude, expressed in degrees of the geomagnetic longitude Λ.

On the basis of the results we plotted graphs for the diurnal and seasonal variation in the position of the 9-hour and 4-hour impact zones on the earth's surface. These graphs are shown in Figures 2 to 5. They are very useful for rapid calculation of the seasonal variation in the location of any point on the earth's surface within an impact zone in the Northern hemisphere. All that needs to be done is to draw a straight line on the graph parallel to the axis of the abscissae and corresponding to the geomagnetic coordinates of the given point. The intersection points between the straight line and curves for various values of the solar inclination $\delta_\odot$ (i.e., for particular calendar dates) are plotted on the graph which has the days of the calendar year along the abscissa and world time along the ordinate.

Thus, we obtain four curves to calculate each impact zone: two of them give the time that the

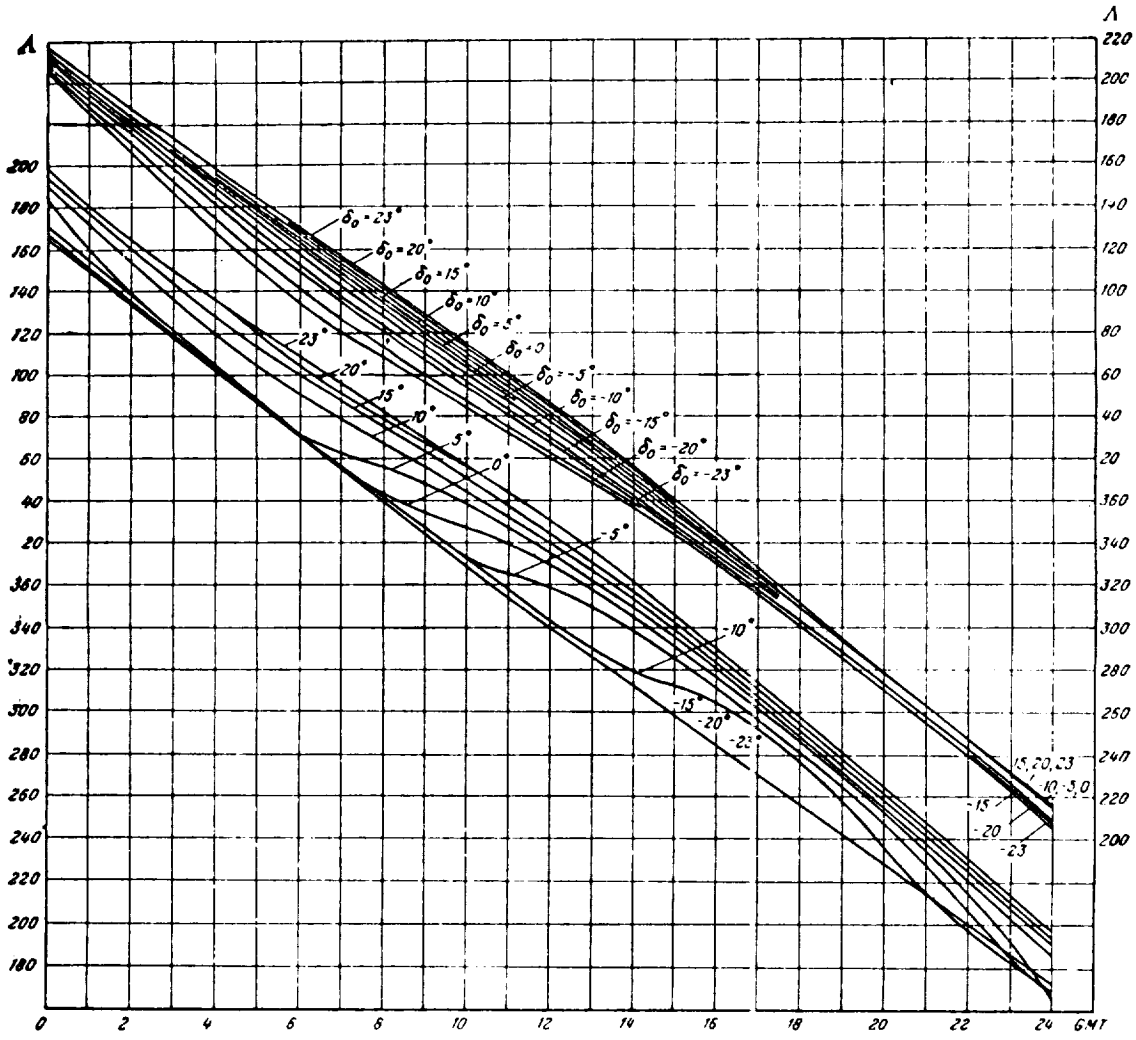

Fig. 2. Seasonal and diurnal changes in latitude in the 9-hour impact zone.
$\Delta\Phi_0 = 30°$. Λ – geomagnetic latitude of observation point. $i_\odot$ – solar inclination.

the zone remains at the given geomagnetic latitude, and the other two show the time zones stay at the geomagnetic longitude. The area on the graph covered by both pairs of curves at the same time shows the annual variation in the time that the point remains in the given impact zone.

Figures 6 - 14 give samples of these graphs for a number of points in the Soviet Union and for Climax (USA).

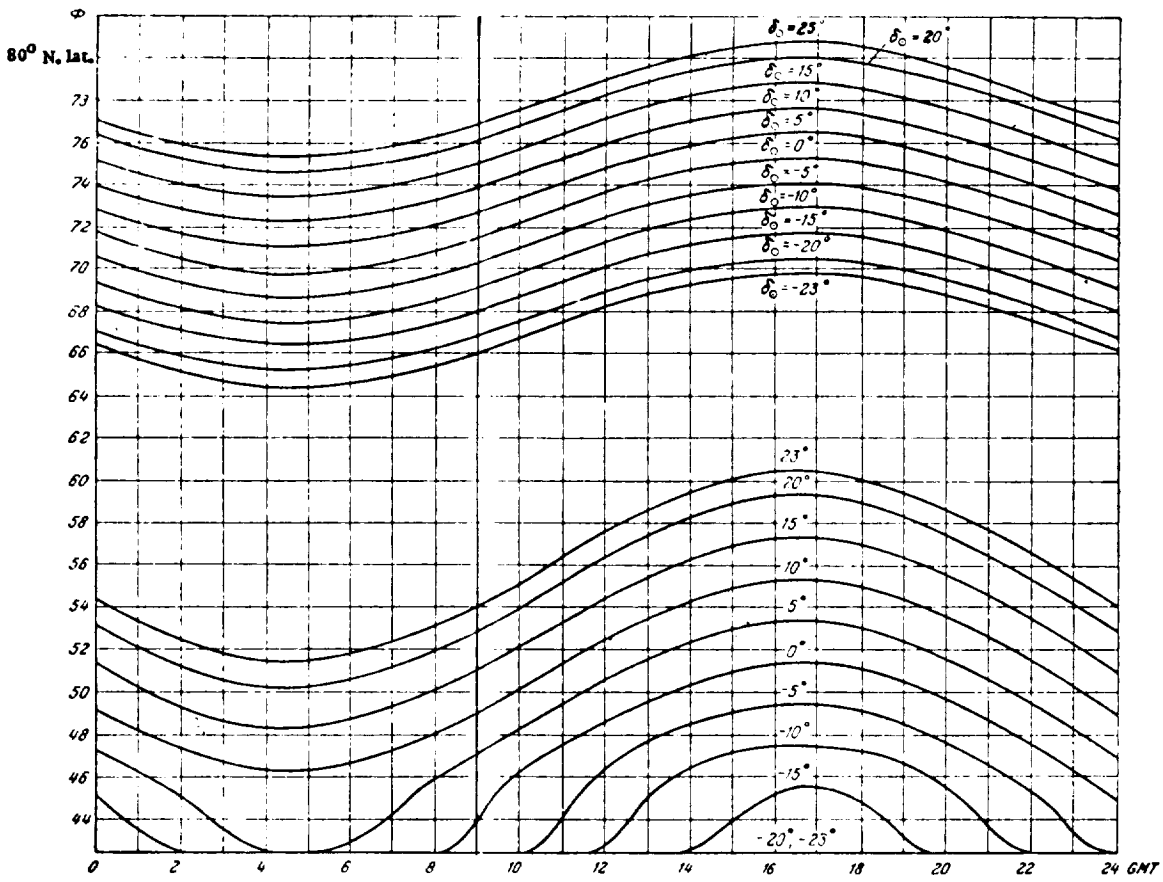

Fig. 3. Seasonal and diurnal changes in latitude in the 9-hour impact zone.
$\Delta\Phi_0 = 30°$. Φ – geomagnetic latitude of observation point. $\delta_\odot$ – solar inclination.

As can be seen from these graphs, the most northerly point, Tikhaya Bay, only comes into the 9-hour zone from April through August. Murmansk and Schmidt Cape are in the 9-hour zone for almost the entire year and in the 4-hour zone for the winter season. The middle-latitude stations - Moscow, Climax, Sverdlovsk, Yakutsk - are in the 4-hour zone for practically the whole of the year and partially in the 9-hour zone. Irkutsk and Tblisi come in the 4-hour zone.

It also follows from these graphs that the width of the impact zone varies appreciably in the course of the year and may achieve 7 - 8 hours, as is the case, for example, for the 4-hour zone in the Fall and the Spring.

Graphs similar to these, plotted at different assumptions with regard to the angular dimensions of the source $\Delta\Phi$ s, make it possible to study the cosmic ray stream of solar origin in more detail, to determine the effective angular dimensions of the source, the energy spectrum of particles, and so on.

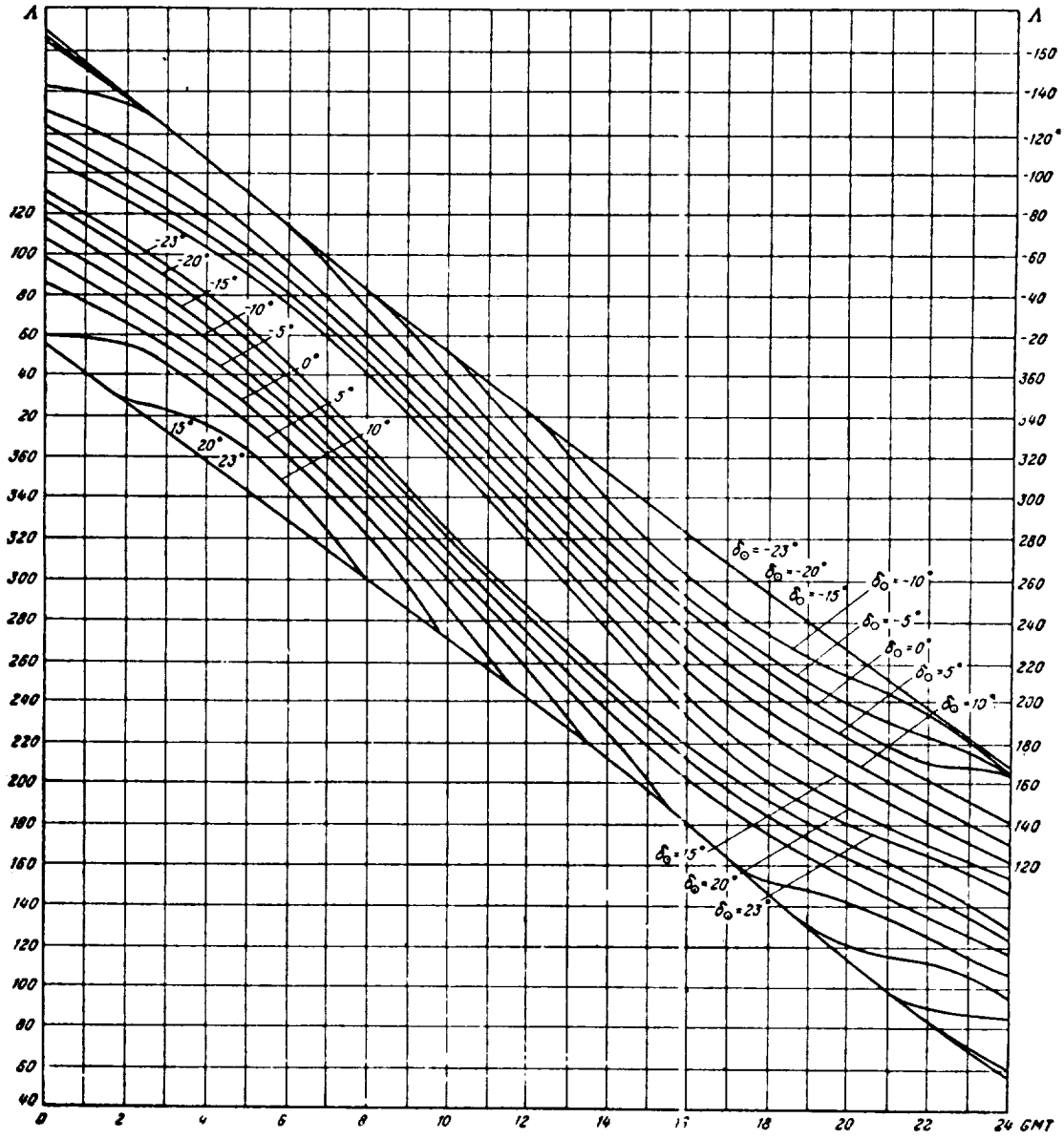

Fig. 4. Seasonal and diurnal changes of latitude in the 4-hour impact zone.
$\Delta\Phi = 30°$, Λ – geomagnetic latitude of observation point, $\delta_\odot$ – solar inclination.

F
6
7

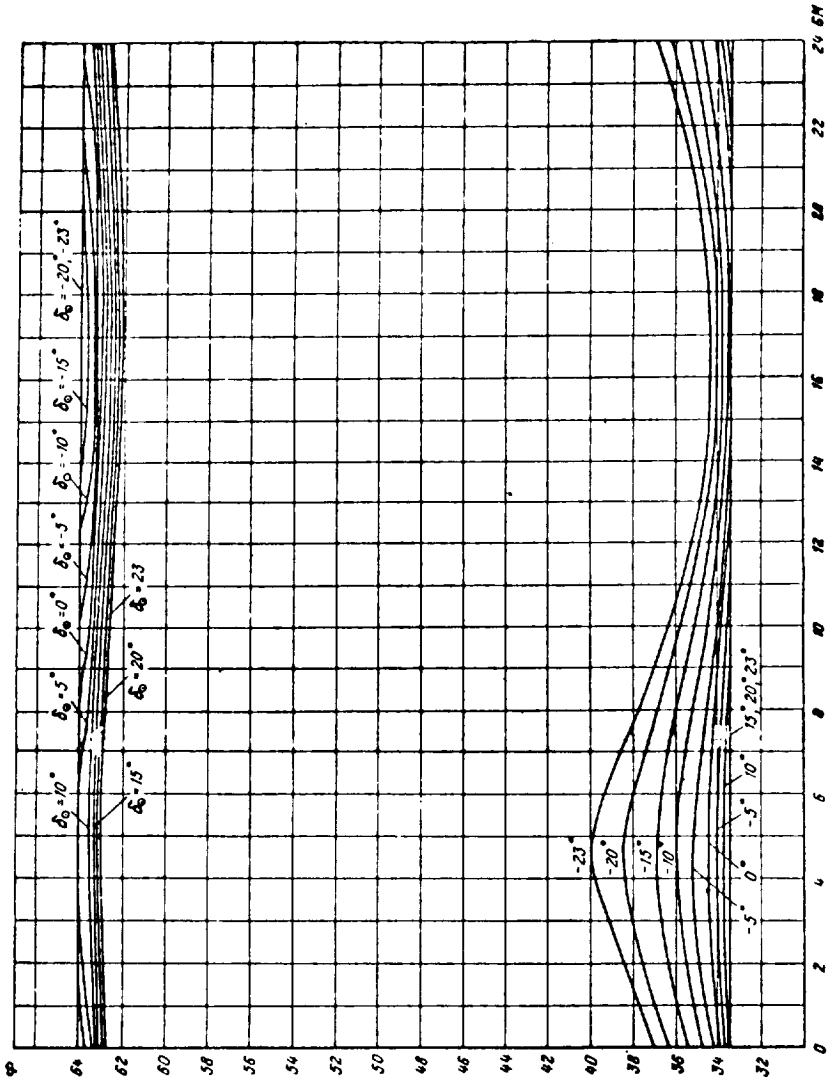

Fig. 5. Seasonal and diurnal changes of latitude in the 9-hour impact zone. $\Delta\Phi = 30°$, Λ — geomagnetic latitude of observation point, $\delta_\odot$ — solar inclination.

Conclusions

It was assumed when plotting the impact zones that the source was narrow in longitude and protracted in latitude.

If we take the longitudinal dimensions of the source into account, the zone boundaries in Figures 6 - 14 have to be widened by $\pm$ Δt (hour) = $\Delta\Lambda_s$ [2·15], where $\Delta\Lambda_s$ is the longitudinal

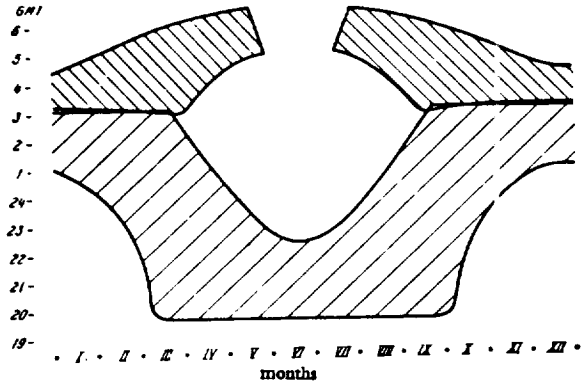

Fig. 7. Sverdlovsk (Φ = 48.1° n. lat., Λ = 140.6°). Annual variation of time in determining a point in impact zones (world time) $\Delta\Phi_S = 30° (\pm 15°)$

F 6 7

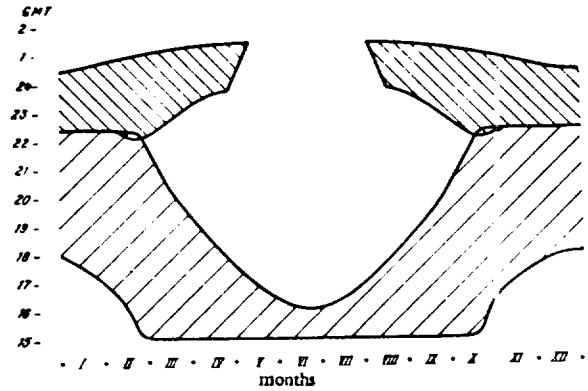

Fig. 8. Yakutsk (Φ = 51.0° n. lat., Λ = 193.8°). Annual variation of time in determining a point in impact zones (world time) $\Delta\Phi_S = 30° (\pm 15°)$

extension of the source (in degrees). Indeed, if this expanse is $\Delta\Lambda_S$ degrees, the observation point is caught in the given impact zone Δt hours earlier and leaves it Δt hours later. Consequently, the time spent in the impact zone is increased by 2 Δt hours. Here, it is only the width of the curves in Figures 6 - 14 which changes, and not their shape. On the basis of the fact that the width of the neutron peaks in the impact zone is about 4 hours, Firor [6] has hypothesized that $\Delta\Lambda_S \approx 60°$. In actual fact the width of the neutron peaks is determined by the both $\Delta\Phi_S$ and $\Delta\Lambda_S$. Since the shape of the graphs in Figures 6 - 14 is solely a function of $\Delta\Phi_S$, and not $\Delta\Lambda_S$, the true value of $\Delta\Lambda_S$ can be determined only when $\Delta\Phi_S$ has been found.

In solving this problem a substantial part must be played by data from points at which the neutron component is recorded, for which the observation conditions for solar originating particles depends considerably on $\Delta\Phi_S$. For example, the burst effect should be absent in the 9-hour zone in Moscow from July to the middle of August, if $\Delta\Phi_S \lesssim 30°$, and should be retained if $\Delta\Phi_S \approx 60°$. In

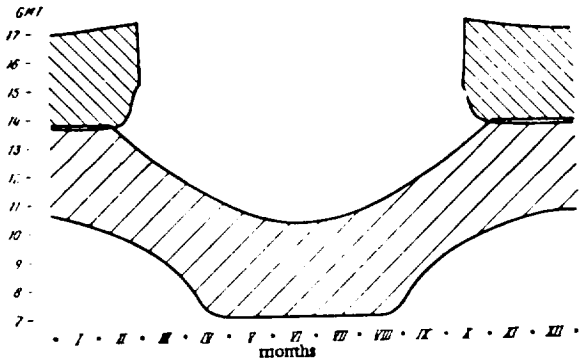

Fig. 9. Climax (φ = 18.1° n. lat. Λ = 315.5°). Annual variation of time in determining a point in impact zones (world time) $\Delta\Phi_S \approx 30°$ (±15°)

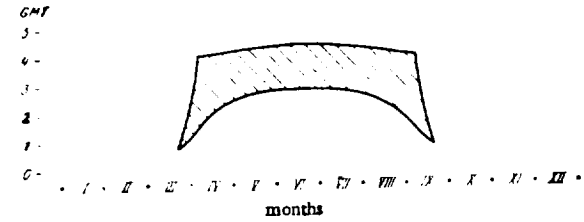

Fig. 10. Tikhaya Bay (φ = 71.5 n. lat. Λ = 153.2°) Annual variation of time in determining a point in impact zones (world time) $\Delta\Phi_S \approx 30°$ (±15°)

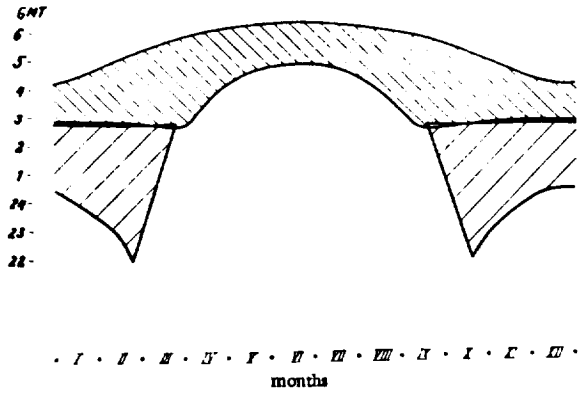

Fig. 11. Murmansk (φ = 64.1° n. lat. Λ = 126.5°). Annual variation of time in determining a point in impact zones (world time) $\Delta\Phi_S \approx 30°$ (±15°)

Yakutsk and Sverdlovsk the pattern should be the same. Schmidt Cape remains in the 4-hour impact zone throughout the year if $\Delta\Phi_S \gtrsim 60°$, and does not come under the 4-hour zone if $\Delta\Phi_S \gtrsim 30°$ [8].

It is only after this type of analysis which makes it possible to find the most probable value

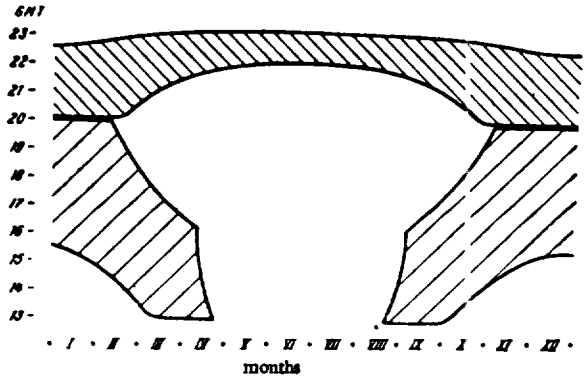

Fig. 12. Schmidt Cape (Φ = 62,8° n. lat. Λ = 227,4°). Annual variation of time in determining a point in impact zones (world time) $\Delta\Phi_S = 30° (\pm 15°)$

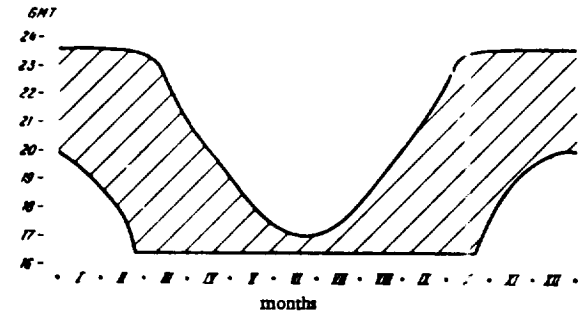

Fig. 13. Irkutsk (Φ = 40,8° n. lat. Λ = 174,5°). Annual variation of time in determining a point in impact zones (world time) $\Delta\Phi_S = 30° (\pm 15°)$

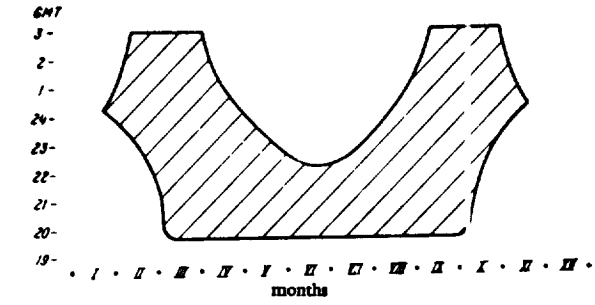

Fig. 14. Tbilisi (Φ = 36,3° n. lat. Λ = 122°). Annual variation of time in determining a point in impact zones (world time) $\Delta\Phi_S = 30° (\pm 15°)$

$\Delta\Phi_S$ that we shall be able to determine the expanse of the source in longitude $\Delta\Lambda_S$.

Firor [6] has studied the effect of chromospheric flares on the diurnal variation in the neutron intensity at Climax. It follows from his results that during the warm six months (April 1 to September 10) Climax evidently does not enter the 9-hour zone. But, unfortunately, we cannot

derive the latitudinal expanse of the source from this, since the absence of the effect in the 9-hour zone must be observed both in the case of $\Delta\Phi_s = 30°$ as well as $\Delta\Phi_s = 60°$. The width of the morning neutron peak (4-hour zone) at climax reaches approximately four hours. If it is assumed that $\Delta\Phi_s \approx 30°$, we can conclude from Figure 9 that the longitudinal expanse of the source $\Delta\Lambda_s$ will be about 15 - 20°, i.e., considerably less than follows from Firor's evaluation (60°).

Bibliography

1. Forbush, S. E., Phys. Rev., 70, p. 771, 1946.
2. Ehmert, A., Zs. Naturforsch, 3a, p. 264, 1948.
3. Dorman, L. I., N. S. Kaminer, V. K. Loiava, and B. F. Shvartsman, Doklady AN SSSR, 108, p. 809, 1958; A. I. Kuz'min, G. V. Skripin, G. V. Chanyutova, and U. G. Shafer, Ibid., 108, p. 66, 1956.
4. Meyer, P., E. Parker, and J. Simpson, Phys. Rev., 104, p. 768, 1956.
5. Dorman, L. I., Cosmic ray variations, Moscow, 1957.
6. Firor, J., Phys. Rev., 94, p. 1017, 1954.
7. McNish, Ter. Mag. Atm. Electr., 41, p. 37, 1936.
8. Kaminer, N. S., NIIZMIR, Report, 1957.

F
6
7

L. I. Dorman

DETERMINING PRIMARY VARIATION IN ENERGY SPECTRUM IN REGION OF VERY LOW ENERGIES FROM DIFFERENCES OF EFFECTS IN EUROPE AND AMERICA

It is very often difficult to determine the energy spectrum of primary variations in the region of low energies. The use of simple variation of the effect with latitude in the high-latitude region, according to [1], page 412, frequently produces a vague result because of low statistical accuracy. On the other hand, a very large number of stations making continuous recordings of cosmic rays are concentrated in Europe and North America, and measurement of the mean difference in effects on these two continents can be made with great accuracy, even when the difference is very slight. Thus, let the amplitude of the type j variation of the type i component in America at the geomagnetic latitude λ at a level h_0 be equal to $\left[\frac{b^j N_\lambda^i(h_0)}{N_\lambda^i(h_0)}\right]_{\text{Amer.}}$ and let it be equal to $\left[\frac{b^j N_\lambda^i(h_0)}{N_\lambda^i(h_0)}\right]_{\text{Europe}}$ in Europe at the same geomagnetic latitude; then, because of

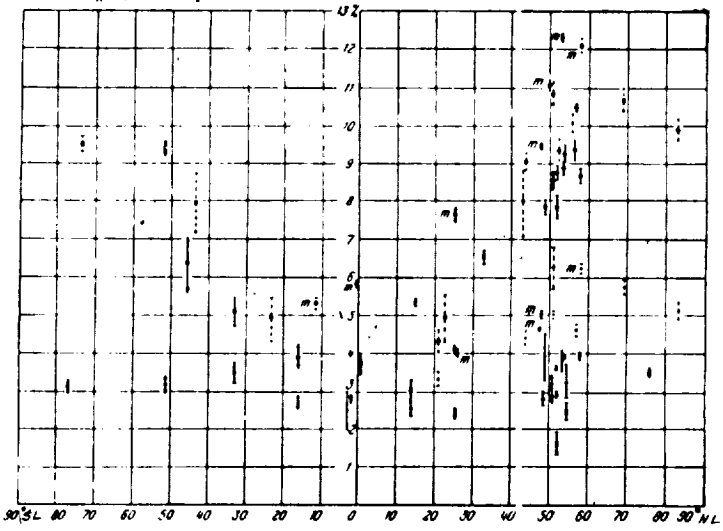

Fig. 1. Decrease in cosmic-ray intensity as a function of geomagnetic latitude and longitude, during magnetic storm of August 29, 1957.

the non-coincidence of the geomagnetic equator with the equator effective with respect to cosmic rays and discovered in the research [2], these two amplitudes will not, generally speaking, coincide. The difference between them can be represented as

$$\left[\frac{\delta^j N_\lambda^i(h_0)}{N_\lambda^i(h_0)}\right]_{\text{Amer.}} - \left[\frac{\delta^j N_\lambda^i(h_0)}{N_\lambda^i(h_0)}\right]_{\text{Eur.}} = \int_{(\epsilon_\lambda^{\min})\text{Amer.}}^{(\epsilon_\lambda^{\min})\text{Eur.}} \frac{\delta^j D}{D}(\epsilon) W_\lambda^i(\epsilon, h_0)\, d\epsilon =$$

$$= \Delta\epsilon_\lambda \frac{\delta^j D}{D}(\bar{\epsilon}) W_\lambda^i(\bar{\epsilon}, h_0), \qquad (1)$$

where

$$\Delta\epsilon_\lambda = (\epsilon_\lambda^{\min})_{\text{Eur.}} - (\epsilon_\lambda^{\min})_{\text{Amer.}}; \quad (\epsilon_\lambda^{\min})_{\text{Amer.}} < \bar{\epsilon} < (\epsilon_\lambda^{\min})_{\text{Eur.}} \qquad (2)$$

From equation (1) it follows that

$$\frac{\delta^j D}{D}(\bar{\epsilon}) = \frac{\left[\frac{\delta^j N_\lambda^i(h_0)}{N_\lambda^i(h_0)}\right]_{\text{Amer.}} - \left[\frac{\delta^j N_\lambda^i(h_0)}{N_\lambda^i(h_0)}\right]_{\text{Eur.}}}{\Delta\epsilon_\lambda W_\lambda^i(\bar{\epsilon}, h_0)}. \qquad (3)$$

As an example of the use of equation (3), we will calculate the energy spectrum of the primary variation in the low-energy region for a reduction in cosmic-ray intensity during the magnetic storm on August 29, 1957. Figure 1 (taken from [3]) shows the latitude-longitude dependence of the amplitude of this effect.

Instrument	Stations		
	American	European	Others
Neutron Minitor	•	•	•
Cubic telescope	+		+
Ionization chamber	·	·	·
m is for high mountainous stations	▲	▲	▲

For the most of the cosmic ray stations located in America at geomagnetic latitudes from 50 to 58°, the mean is $\epsilon \approx 1.5$ Bev. The value $\Delta\epsilon_\lambda$ for these groups of stations was calculated in [1] (see page 420) from data for the increase in cosmic-ray intensity during the great solar flare on April 23, 1956, when the amplitude of the effect in America during isotropic period was practically twice as much as in Europe. The value derived was $\Delta\epsilon_\lambda \approx 0.7 - 0.8$ Bev. It is clear from the data in Figure 30 in [1] that $W_\lambda^i(\bar{\epsilon}, h_0)$ for neutrons at sea level in the region $\bar{\epsilon} \sim 1.5 - 2$ Bev is about 2%/Bev. It is clear from the data in Figure 1 that the difference in effects in America and Europe is about 0.5% for neutrons. Substituting these values into equation (3), we obtain ~ 0.3 for $\bar{\epsilon} \sim 1.5 - 2$ Bev, which is not very much different from the value derived in [3] for some high energies $\left(\frac{\delta D}{D} \sim 0{,}2\right)$. Using the data obtained by stations at still greater latitudes, it is possible, in principle, to find $\delta D/D$ for lower energies.

Bibliography

1. Dorman, L. I., Cosmic ray variations, Moscow, Gostekhizdat, 1957.
2. Simpson, J. A., K. B. Fenton, J. Katzman, and D. C. Rose, Phys. Rev., 102, p. 1648, 1956; D. C. Rose, and J. Katzman, Canadian J. Phys., 34, p. 1, 1956.
3. Blokh, Ya. L., Ye. S. Glokova, and L. I. Dorman, IGY Reports, Cosmic Ray Series, Issue 1, p. 7, 1959.

L. I. Dorman

DETERMINING POINT AT WHICH EARTH ENTERS CORPUSCULAR STREAM, NATURE OF EARTH'S MOTION WITHIN STREAM AND STREAM VELOCITY BY MEANS OF DETAILED STUDY OF VARIATION IN COSMIC RAY INTENSITY DURING MAGNETIC STORMS

When looking at graphs showing the variation in cosmic-ray intensity during magnetic storms, we see that they are only similar as a first approximation. They are all usually marked by a sharp drop in intensity and a gradual recovery. Admittedly, there are a number of cases (Figure 1) where the fall in intensity is almost as gradual as the rise. Thus, we have before us two types of intensity variation in cosmic rays during magnetic storms, which differ sharply from each other. The first question which arises in this connection is what is the reason for this great difference. We will try to show below that the chief reason is not the specific features of any corpuscular streams, but the way in which the earth is seized by the corpuscular stream. We will show that if a stream with a frozen magnetic field seizes the earth with its lateral front, there is a gradual reduction and also a gradual recovery of the cosmic-ray intensity. Indeed, as shown in [2] (see Par. 36), the dimensions of the stream region effective in scattering cosmic-ray particles is determined by the shortest distance between the earth and any of the stream's edges. This statement is evidently valid with great accuracy as long as we ignore the variation in cosmic-ray intensity due to acceleration or retardation of particles by the stream's electric field.* The intensity of the cosmic ray component i can be represented as a first approximation by the expression

$$\frac{\delta N_\lambda^i}{N_\lambda^i} = -\frac{2x}{L} K_\lambda^i, \qquad (1)$$

where x is the shortest distance between the earth and any of the stream's edges, L is the width of the stream round the earth and the coefficient K_λ^i is the maximum reduction in the intensity of the cosmic-ray component i at the latitude λ when the earth is in the middle of the stream (when $x = L/2$). K_λ^i can be found, according to [2] (see Chapter IV), from the formula

$$\left(\frac{\delta N_\lambda^i}{N_\lambda^i}\right)_{max} = K_\lambda^i = \int_{\epsilon_\lambda^{min}}^{\infty} \frac{\delta D}{D}(\varepsilon)\, W_\lambda^i(\varepsilon, h_0)\, d\varepsilon, \qquad (2)$$

where ϵ_λ^{min} is the geomagnetic threshold, h_0, is the pressure at the observation level and w_λ^i (ϵ, h_0) is the coupling factor. According to the theory developed in [2] (see Chapter IX), the primary variations in cosmic rays $\frac{\delta D(\epsilon)}{D(\epsilon)}$ for streams carrying transverse uniform frozen magnetic fields (without taking into account the effect of the induced electric field $E = -\frac{1}{c}[uH]$, where u is the stream velocity, and H is the magnetic field in the stream)

---

* We will attempt to take this variation into account from now on. A preliminary calculation shows that this is most important when determining the variation in anisotropy of the cosmic-ray variation, i.e., in studying disturbances of the solar-diurnal variations in cosmic rays during magnetic storms.

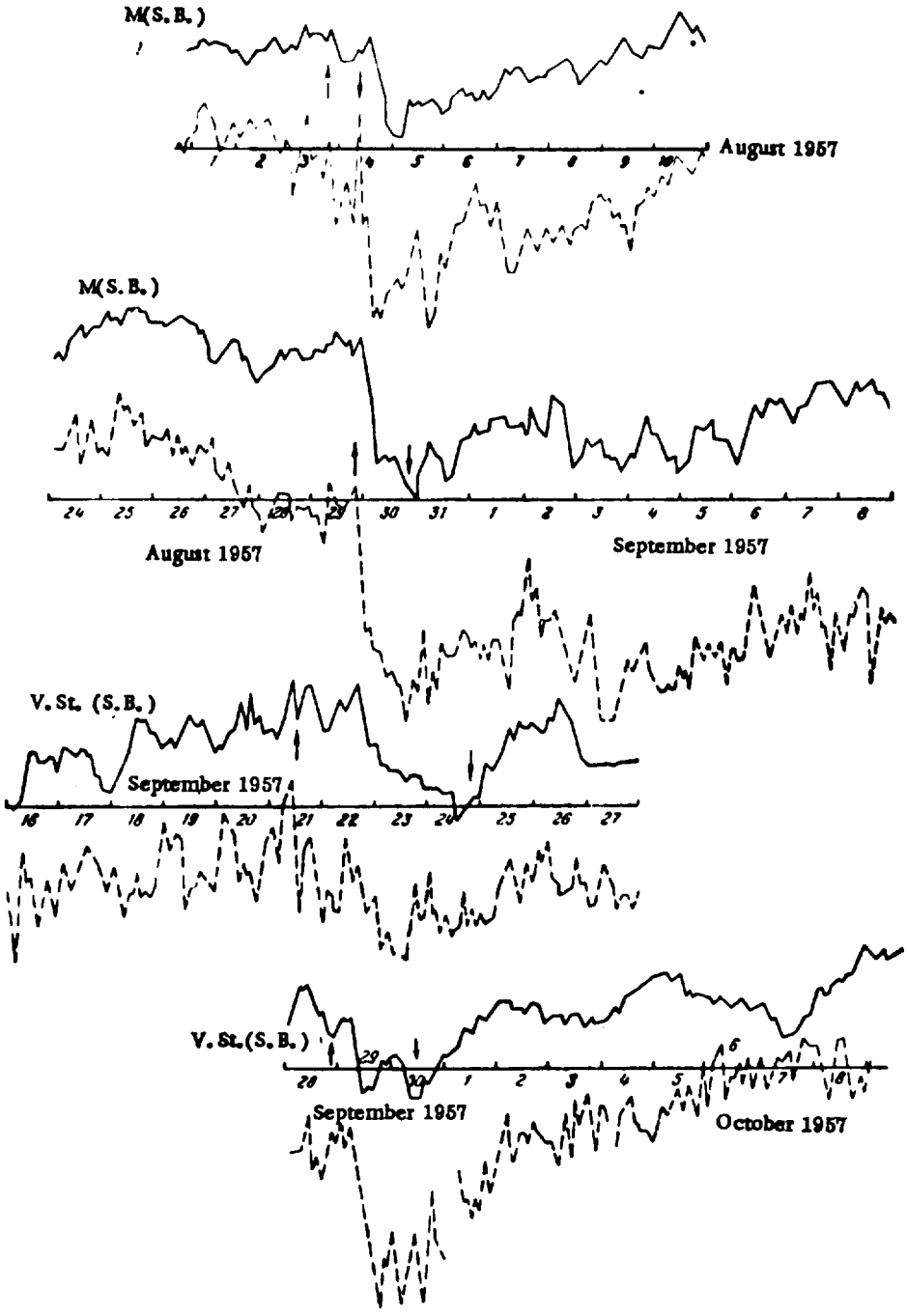

Fig. 1. Change in cosmic-ray intensity during various magnetic storms (1) S - slight storms, St - strong, VS - very stormy, M - moderate, GB - storms with gradual beginning. Solid curves - hard component determined by ASK-1 (Moscow) Dashed curves - neutron component (Yakutsk) ↑ - beginning of magnetic storm ↓ - end of magnetic storm.

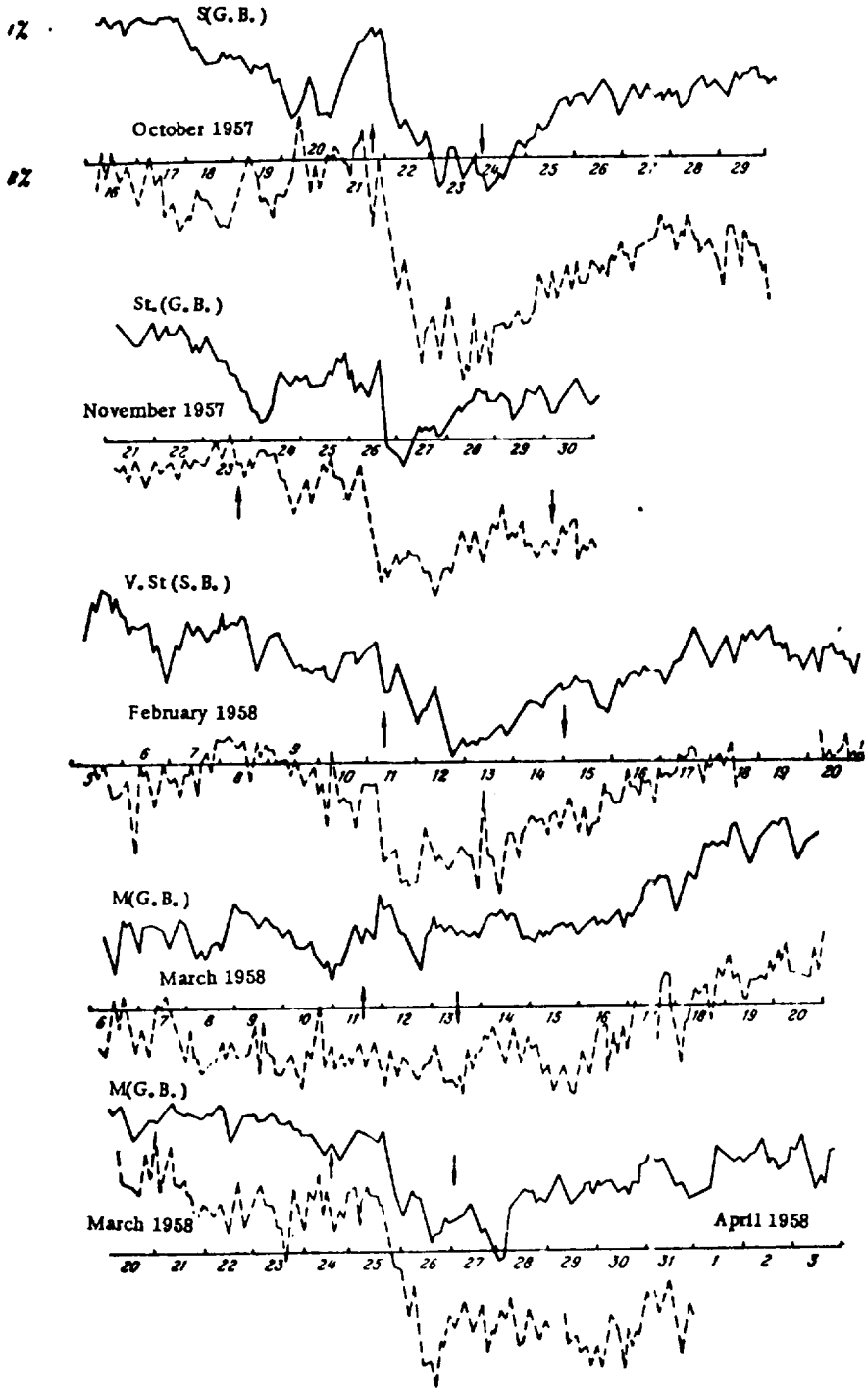

Fig. 1. Continuation.

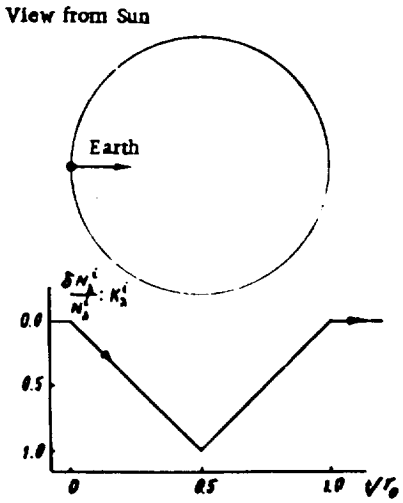

Fig. 2. Predicted change in cosmic-ray intensity during magnetic storm with lateral seizing of the earth by the stream, in the case when the earth moves through the axis of the stream.

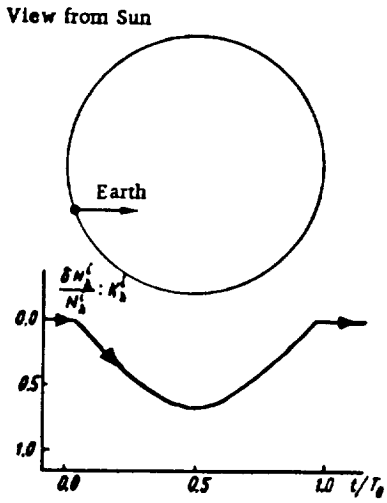

Fig. 3. Same as Fig. 2, except at 1/3 radius away from the stream axis.

Motion of earth within stream (in principal plane).

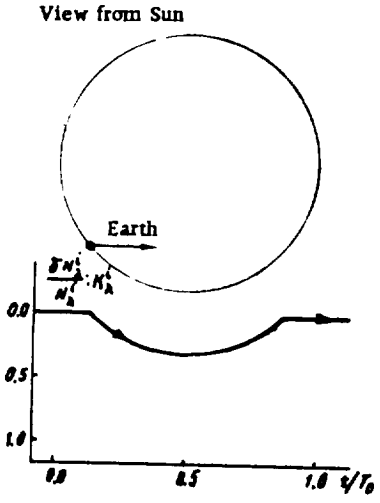

Fig. 4. Same as Fig. 2, except at 2/3 radius away from the stream axis.

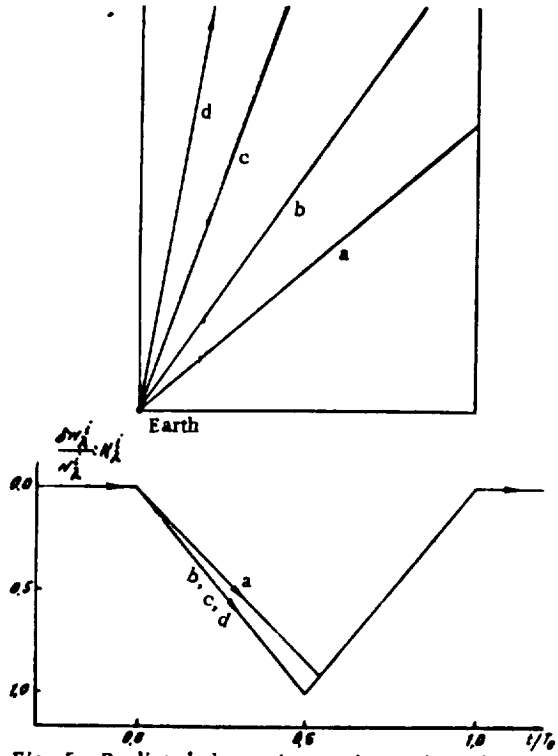

Fig. 5. Predicted change in cosmic-ray intensity during magnetic storm with frontal seizing of the earth by the stream. The earth enters the stream near the frontal lateral surface.

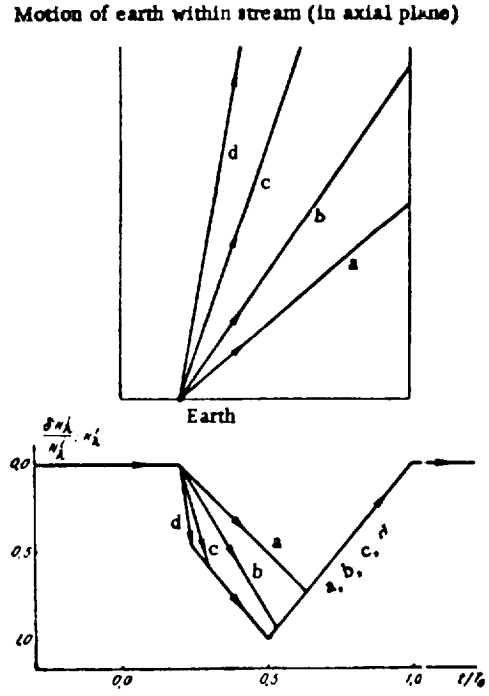

Fig. 6. Same as Fig. 5, except at a distance of 1/5 L from frontal lateral surface.

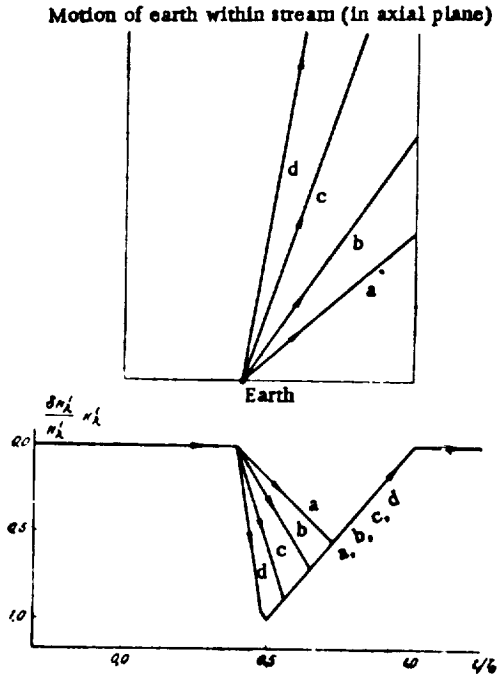

Fig. 7. Same as Fig. 5, except at a distance of 2/5 L from frontal lateral surface.

Motion of earth within stream (in axial plane)

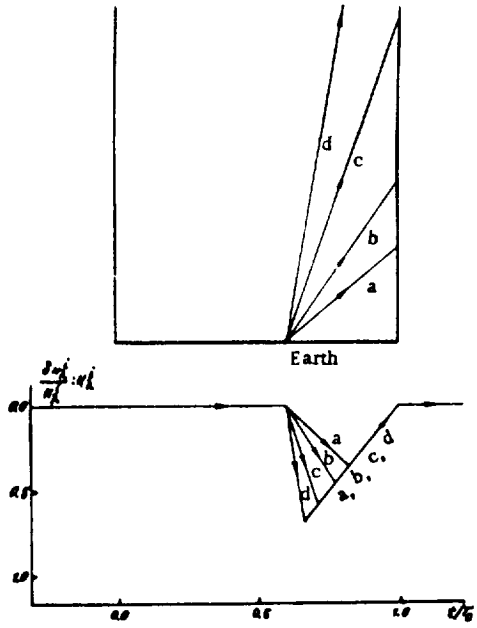

Fig. 8. Same as Fig. 5, except at a distance of 3/5 L from frontal lateral surface.

Motion of earth within stream (in axial plane)

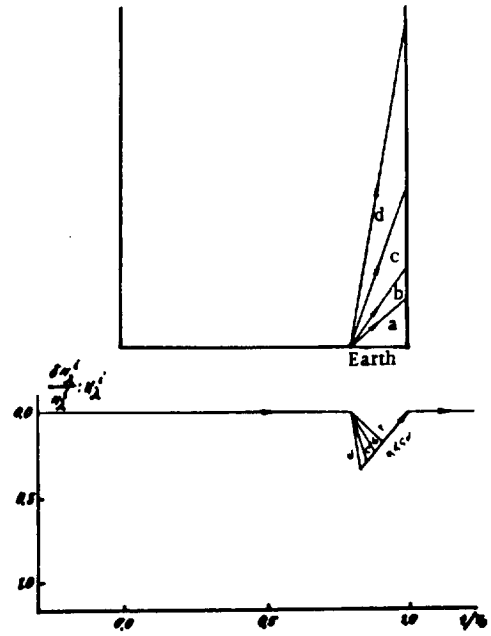

Fig. 9. Same as Fig. 5, except at a distance of 4/5 L from frontal lateral surface.

$$\frac{\delta D(\varepsilon)}{D(\varepsilon)} = f \begin{cases} -1, & \text{when } \varepsilon < \frac{\varepsilon^{\delta}_{\min}}{4}, \\ -\frac{2}{\pi} \arcsin\left(\frac{\varepsilon_{\min}}{2\varepsilon} - 1\right), & \text{when } \frac{\varepsilon^{\delta}_{\min}}{4} < \varepsilon < \frac{\varepsilon^{\delta}_{\min}}{2}, \\ 0, & \text{when } \varepsilon > \frac{\varepsilon^{\delta}_{\min}}{2}. \end{cases} \qquad (3)$$

For the longitudinal magnetic field

$$\frac{\delta D(\varepsilon)}{D(\varepsilon)} = f \begin{cases} -1, \text{ when } \varepsilon < \frac{\varepsilon^{\delta}_{\min}}{4}, \\ 0, \text{ when } \varepsilon > \frac{\varepsilon^{\delta}_{\min}}{4}. \end{cases}$$

Here

$$\varepsilon^{\delta}_{\min} = 300\, HL,$$

where L is the width of the stream around the earth.

Figure 2 represents diagramatically the passage of the earth through the corpuscular stream and the theoretical corresponding variation in cosmic-ray intensity in a case where the corpuscular stream seizes the earth from the side when the earth intersects the stream axis. Figures 3 and 4 show the variation in intensity when the earth, moving on, passes at a distance of correspondingly 1/3 and 2/3 of its radius from the stream axis (it is assumed that the stream has a circular section).

It should be kept in mind that the calculations in Figures 2-4 were based on purely geometrical concepts, valid in essence for any mechanism for reduction in cosmic-ray intensity, in particular, and for the mechanisms suggested by Morrison [3] and Parker [4]. But it stands to reason that the conclusion is only valid as a first approximation. On closer examination there must be some difference from the graphs in Figures 2-4, and also differences between the graphs themselves for different mechanisms.*

In a similar way we can consider the variation in cosmic ray intensity in a case where the corpuscular stream seizes the earth with its leading front. Here the calculation may also be made by Formula (1), and all the terms in it have the same meaning as before. The value x, however, will obey a different law in this case from the one for when the earth is seized by the stream's lateral side. Figures 5-9 show different cases for seizure of the earth by the leading front at four different stream velocities: $3 \cdot 10^7$, $5 \cdot 10^7$, 10^8 and $2 \cdot 10^8$ cm/sec. The calculations make allowance for the lag in stream corpuscles during rotation of the sun (radial propagation is assumed). The remark made above with regard to the general applicability of the geometrical concepts to various mechanisms is still valid for a case in which the earth is seized by the stream's leading front.

By comparing the graphs in Figures 2-9 with the observed variations in cosmic ray intensity, we can determine fairly accurately both the point at which the earth enters the corpuscular stream as well as its motion within the stream and the stream velocity.** Furthermore, knowledge of the point at which the earth enters the corpuscular stream makes it possible to improve considerably the widely-used method of determining stream velocities from the lag in geomagnetic disturbances with respect to the passage of active regions through the sun's central meridian.

F
6
7

* It is planned to make a special study of this question.

** For example, for the storm on August 29, the variation in intensity is similar to the case shown in Figure 6.

Bibliography

1. Blokh, Ya. L., Ye. S. Glokova, and L. I. Dorman, IGY Reports, Cosmic Ray Series, Issue 1, p. 7, 1959.
2. Dorman, L. I., Cosmic Ray Variations, Moscow, Gostekhizdat, 1957.
3. Morrison, P., Phys. Rev., 101, p. 1397, 1956.
4. Parker, E. N., Phys. Rev., 110, p. 1445, 1958.

Translated by Royer and Roger, Inc.,
1000 Vermont Avenue, N. W.,
Washington, D. C.

LAYOUT OF APPARATUS RECORDING COSMIC RAYS AT PHYSICS LABORATORY OF YAKUTSK BRANCH OF SIBERIAN DIVISION OF USSR ACADEMY OF SCIENCES

($\Phi = 51.0°$, $\Lambda = 193.8°$)

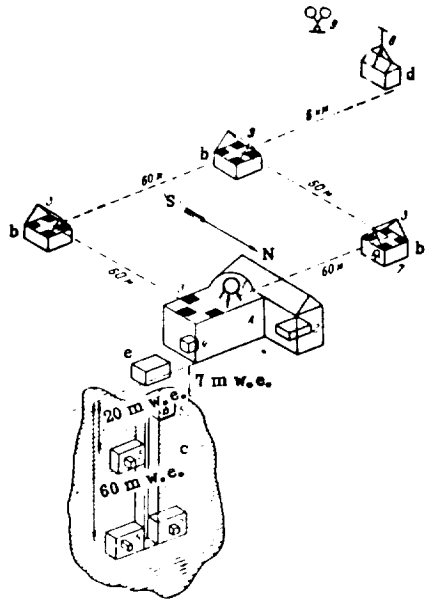

A) Main laboratory building; B) extensive atmospheric shower pavilions; C) underground laboratory; D) stratospheric station; E) building at top of shaft; 1) ASK-1 ionization chamber; 2) neutron monitor; 3) extensive shower apparatus; 4) counter cubic telescope; 5) underground counter telescope; 6) semi-cubic counter telescope; 7) S-2 ionization chamber; 8) USW radio receiver point; 9) stratospheric radiosounding counter telescope.